

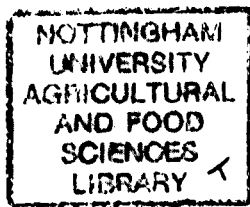
**PUFFED RICE AND THE MOLECULAR CHANGES
THAT DETERMINE ITS STRUCTURE**

by

Thierry Tran

**Thesis submitted to the University of Nottingham
for the degree of Doctor of Philosophy**

March 2003



**Food Sciences Division
School of Biosciences
University of Nottingham
Sutton Bonington campus
Loughborough
Leicestershire LE12 5RD, UK**

*If you don't bump,
They won't puff!*

ACKNOWLEDGEMENTS

I would like to express many, many thanks to Dr. Sandra E. Hill and Pr. John R. Mitchell for their supervision and guidance over these three years of work. Thank you also to Dr. Imad Farhat for many useful discussions.

My thanks also go to the Kellogg Company for the financial support as well as for initiating this project. Thank you for their kind collaboration to the various people I have had the pleasure to meet both in Manchester and in Battle Creek: Peter Booth and David Howling; Gary Day, Joseph George, Tony Gualtieri and Gloria Cagampang.

I would like to acknowledge too the work of the often anonymous technical staff in the various Rice Krispies factories and pilot plants in Manchester, Battle Creek, Omaha and Memphis.

In the Nottingham University (Sutton Bonington) Food Science division, I want to thank Val Street, Phil Glover, Mike Chapman, Lynne Moseley and Kath Brasnett for their assistance and availability throughout the project.

Finally I would like to thank my friends and colleagues who have been involved to various degrees with this project, for the scientific debates, the help with experimental work or simply making the place really enjoyable: Antje, Krim, Mahsa, Olivier, Vanessa, Piyarat, Helen, Elaine, Martin, Linda (you know who you are!), Giusi, Marie-Astrid, Liz, Guy, Javier, Aylin, Lalitha, Asgar, Sarai, Sanya, Suched, Parinda, Carlos, and also Teresa, Jong-Kyung and Danilo, wherever in the world they are.

ABSTRACT

The Rice Krispies™ process consists essentially of the cooking of short or medium rice grains, followed by a mechanical compression between two rolls (bumping), a tempering step and a toasting operation (puffing) which expands the grains into the finished product. The objectives of this project were to clarify which molecular phenomena take place inside the rice grains during the process and to facilitate the improvement and optimisation of the process parameters. The composition and gelatinisation behaviour of seven different raw rice varieties used either in the United States or the United Kingdom were studied. The glass transition of the cooked rice material was determined by dynamic mechanical thermal analysis (DMTA), which allowed each step of the process to be mapped onto a temperature / moisture content state diagram. The bumping step of the process and its effect on the various molecular entities present in the cooked rice were studied in details. Amylose was found to form complexes with the lipids present in the material during cooking, and these reinforced the cooked rice grain structure. One of the roles of the bumping could be to partially dislocate these amylose-lipid complexes to enable the rice grains expansion at the puffing step of the process. The bumping also reduced the molecular weight of amylopectin, which is thought to weaken the rice grains structure and improve the puffed grains expansion. The mill gap between the bumping rolls was the key factor determining the quality of the puffed product. The temperature at which the rice grains are bumped had a secondary influence on the quality of the puffed rice, within the range 26°C to 57°C. The RVA provided a very effective method to categorise post-bumped samples and could be a useful diagnostic tool in case of production problems. Evidence of physical ageing and moisture content equilibration during the tempering step was found. Physical ageing did not have a detectable effect on the expansion of the rice grains, while it was important that moisture content was equilibrated inside the grains to ensure a proper puffing. Finally, correlations were found between the puffed rice grains expansion and the post-bumped grains height recovery, which made it possible to predict the quality of the expanded grains from the characterisation of the post-bumped rice. Overall, the project is a good example of the application of general starch science concepts to the study of a specific industrial process.

TABLE OF CONTENTS

CHAPTER 1: INTRODUCTION	1
1.1 PROJECT BACKGROUND	1
1.2 AIMS AND OBJECTIVES	2
1.3 THESIS OUTLINE	3
CHAPTER 2: LITERATURE REVIEW: MOLECULAR PHENOMENA THAT COULD AFFECT STARCH BEHAVIOUR	4
2.1 INTRODUCTION	4
2.2 THE RICE CROP	4
2.3 RICE GRAIN COMPOSITION AND STRUCTURE.....	6
<i>2.3.1 Polysaccharides.....</i>	<i>6</i>
<i>2.3.1.1 Amylose structure</i>	<i>6</i>
<i>2.3.1.2 Amylopectin structure.....</i>	<i>7</i>
<i>2.3.2 The starch granule.....</i>	<i>9</i>
<i>2.3.3 Proteins.....</i>	<i>11</i>
<i>2.3.4 Lipids</i>	<i>12</i>
2.4 RICE COOKING.....	13
<i>2.4.1 Starch gelatinisation and conversion</i>	<i>13</i>
<i>2.4.2 Amylose-lipid complexes</i>	<i>15</i>
2.5 COOKED RICE MOLECULAR PHENOMENA.....	16
<i>2.5.1 Glass transition.....</i>	<i>16</i>
<i>2.5.2 Physical ageing.....</i>	<i>18</i>
<i>2.5.3 Retrogradation.....</i>	<i>19</i>
<i>2.5.3.1 Amylose</i>	<i>19</i>
<i>2.5.3.2 Amylopectin.....</i>	<i>20</i>
2.6 INDUSTRIAL PROCESSES SPECIFIC TO FLAKED BREAKFAST CEREALS MANUFACTURE	21

2.6.1 Bumping rolls	21
2.6.2 Rice puffing and popping.....	23
2.6.3 Concepts related to the expansion of cereal materials.....	24
2.7 OBJECTIVES OF THE WORK	25
CHAPTER 3: EVALUATION OF THE INDUSTRIAL PROCESS.....	26
3.1 INTRODUCTION.....	26
3.2 INDUSTRIAL BACKGROUND	26
3.3 THE RICE KRISPIES™ PROCESS	27
3.3.1 Process overview	27
3.3.2 Milling and cooking.....	28
3.3.3 After-cooking drying and tempering steps.....	30
3.3.4 Bumping.....	31
3.3.5 Drying and tempering.....	34
3.3.6 Puffing	34
CHAPTER 4: MATERIALS AND METHODS	37
4.1 INTRODUCTION.....	37
4.2 MATERIALS.....	38
4.3 SAMPLE PREPARATION	39
4.3.1 Small scale bumping.....	40
4.3.1.1 Texture analyser.....	40
4.3.1.2. Roller dryer	44
4.3.1.3 Comparison of the three methods to compress the cooked rice.....	45
4.3.2 Small scale post-bumping drying step.....	47
4.3.3 Small scale puffing.....	47
4.3.4 Grinding mills.....	48
4.4 ANALYSIS OF THE RAW RICE	49
4.4.1 Lipid content.....	49
4.4.2 Protein content	49
4.4.3 Amylose content.....	50
4.4.4 Amylopectin branch chain analysis.....	51
4.4.5 Rapid Visco-Analyser (RVA)	52

4.4.6 Differential Scanning Calorimetry (DSC).....	53
4.5 ANALYSIS OF THE COOKED RICE.....	54
4.5.1 Wide angle X-rays diffraction.....	54
4.5.2 Grain damage assessment: Height recovery.....	56
4.5.3 Dynamic Mechanical Thermal Analyser (DMTA).....	56
4.5.4 Differential Scanning Calorimetry (DSC).....	58
4.5.4.1 Method.....	58
4.5.4.2 Amylose lipid complexes.....	59
4.5.4.3 Physical ageing.....	60
4.5.5 Relative and intrinsic viscosities.....	61
4.5.6 Analytical ultracentrifugation (AUC).....	62
4.5.7 Capillary rheometry.....	63
4.5.8 Rapid Visco-Analyser.....	64
4.5.9 Moisture content determinations.....	67
4.6 ASSESSMENT OF THE PUFFED RICE GRAINS EXPANSION QUALITY.....	67
4.6.1 Grain area.....	67
4.6.2 Bulk density.....	68
CHAPTER 5: RAW RICE MATERIAL CHARACTERISATION.....	69
5.1 INTRODUCTION.....	69
5.2 DIMENSIONS AND BULK DENSITY OF THE RAW MATERIAL.....	70
5.2.1 Grain dimensions.....	70
5.2.2 Bulk density.....	72
5.3 MOISTURE CONTENTS.....	73
5.4 STARCH CHARACTERISATION.....	73
5.4.1 Amylose content.....	73
5.4.2 HPLC amylopectin branch chain analysis.....	74
5.4.3 Amylose – amylopectin separation by ultracentrifugation.....	76
5.5 PROTEIN CONTENT.....	78
5.6 CRUDE FAT ANALYSIS.....	79
5.7 RAW RICE GELATINISATION BEHAVIOUR.....	80
5.7.1 RVA profiles.....	80
5.7.2 DSC profiles.....	81
5.8 CONCLUSION.....	85

CHAPTER 6: GLASS TRANSITION OF THE COOKED RICE	86
6.1 INTRODUCTION	86
6.2 PREPARATION OF THE SAMPLES	86
6.3 MEASUREMENT OF THE COOKED RICE GLASS TRANSITION	88
6.3.1 <i>Method for determining the glass transition temperature of each sample</i>	88
6.3.2 <i>Glass transition of the pre-bumped and post-bumped material</i>	89
6.4 ROLE OF THE GLASS TRANSITION IN PROCESSING THE RICE MATERIAL	90
6.4.1 <i>Glass transition and bumping.....</i>	90
6.4.2 <i>Glass transition and puffing</i>	91
6.5 GLASS TRANSITION AND STARCH RETROGRADATION IN THE COOKED RICE ..	93
6.6 CONCLUSION	95
CHAPTER 7: THE BUMPING STEP OF THE RICE KRISPIES™ PROCESS	
.....	96
INTRODUCTION.....	96
7.2 INITIAL OBSERVATIONS: RVA PROFILES	97
7.2.1 <i>Preparation of the samples.....</i>	97
7.2.2 <i>RVA analysis of the series of 13 samples (set A): Identification of three groups of samples</i>	101
7.2.3 <i>RVA analysis of the series of 6 samples (set B): Identification of a fourth group of samples.....</i>	103
7.2.4 <i>Effect of variety, mill gap and bumping temperature: Analysis of the RVA profiles of the Battle Creek factory trials (set C)</i>	107
7.2.5 <i>Summary and interpretations</i>	111
7.2.5.1 <i>Summary</i>	111
7.2.5.2 <i>Hypothetical repartition of the strains in the rice grain structure during the bumping</i>	111
7.2.5.3 <i>Further hypotheses on what is broken inside the rice grain during the bumping</i>	113
7.3 STUDY OF COOKED RICE AMYLOSE-LIPID COMPLEXES.....	114
7.3.1 <i>Evidence of the presence of amylose-lipid complexes in the cooked material.....</i>	114
7.3.1.1 <i>RVA evidence of amylose-lipid complexes.....</i>	114

7.3.1.2 X-rays evidence of amylose-lipid complexes in the cooked rice.....	117
7.3.1.3 DSC evidence of amylose-lipid complexes in the cooked rice.....	119
7.3.2 <i>X-ray study of the effect of the bumping on the amylose-lipid complexes</i>	122
7.3.3 <i>Role of amylose-lipid complexes in reinforcing the structure of the rice grain</i>	125
7.3.3.1 Introduction.....	125
7.3.3.2 Preparation of the samples	126
7.3.3.3 Rice flour cooking without lipids: The effect of amylose content.....	126
7.3.3.4 Rice flour cooking with lipids.....	127
7.3.3.5 DSC evidence of amylose-lipid complexes formation.....	129
7.3.4 <i>Model explaining the strengthening of the rice grain structure by amylose-lipid complexes</i>	131
7.3.4.1 Structure of the cooked rice grain	131
7.3.4.2 Effect of the bumping on the amylose-lipid complexes.....	134
7.4 EVIDENCE OF MOLECULAR WEIGHT REDUCTION	136
7.4.1 <i>Introduction</i>	136
7.4.2 <i>Ultracentrifugation evidence of three populations of polysaccharides in the post-bumped material</i>	137
7.4.2.1 First series of experiments	137
7.4.2.2 Second series of experiments.....	139
7.4.3 <i>Relative viscosity evidence of a molecular weight reduction of the starch material by the bumping</i>	141
7.4.4 <i>Amylopectin branch chain analysis by HPLC</i>	143
7.4.5 <i>Capillary rheometer</i>	145
7.5 CONCLUSION	147
CHAPTER 8: STUDY OF THE TEMPERING STEP	149
8.1 INTRODUCTION.....	149
8.2 EVIDENCE THAT TEMPERED RICE EXPANDS BETTER THAN NON-TEMPERED RICE	149
8.2.1 <i>Protocol</i>	149
8.2.2 <i>Variability of the scanner and image analysis method</i>	150
8.2.3 <i>Variability of the oven conditions</i>	151

8.2.4 Increase in the expansion of the freshly dried grains during tempering.	152
8.3 HYPOTHESES ON THE PHENOMENA OCCURRING DURING THE TEMPERING..	153
8.3.1 Physical ageing.....	153
8.3.2 Gradient of moisture content inside the freshly dried rice grain	153
8.4 EVIDENCE OF PHYSICAL AGEING IN THE TEMPERING RICE	154
8.4.1 Protocol	154
8.4.2 Results.....	155
8.5 EVIDENCE OF A GRADIENT OF MOISTURE CONTENT IN THE FRESHLY DRIED GRAIN.....	157
8.5.1 Protocol	157
8.5.2 Results.....	157
8.6 EVIDENCE THAT THE GRADIENT OF MOISTURE CONTENT HAS MORE INFLUENCE THAN PHYSICAL AGEING ON THE RICE GRAIN EXPANSION	158
8.6.1 Protocol	158
8.6.2 Results.....	159
8.7 CONCLUSION	161
CHAPTER 9: EFFECT OF THE BUMPING PARAMETERS ON THE PUFFED GRAIN DEGREE OF EXPANSION	162
9.1 INTRODUCTION.....	162
9.2 INFLUENCE OF THE MILL GAP AND BUMPING TEMPERATURE ON THE EXPANSION OF THE PUFFED GRAINS.....	163
9.2.1 Description of the samples used.....	163
9.2.2 Influence of the mill gap on the puffed rice grains expansion.....	164
9.2.3 Influence of the bumping temperature on the puffed rice grains expansion	166
9.2.4 Combined effect of mill gap and bumping temperature on the puffed rice grains expansion.....	167
9.3 PREDICTION OF THE PUFFING QUALITY FROM THE POST-BUMPED RICE PARAMETERS	169
9.3.1 Correlation between the post-bumped rice bulk density and the puffed rice degree of expansion.....	169

9.3.2	<i>Correlation between the post-bumped rice grains height recovery and the puffed rice degree of expansion</i>	170
9.3.3	<i>Correlation between the post-bumped rice RVA profile and the puffed rice degree of expansion</i>	172
9.4	CONCLUSION	175
 CHAPTER 10: GENERAL DISCUSSION AND CONCLUSIONS		177
10.1	INTRODUCTION	177
10.2	GLASS TRANSITION AND RELATED PHENOMENA IN THE COOKED MATERIAL	177
10.2.1	<i>Glass transition of the cooked rice</i>	177
10.2.2	<i>Molecular phenomena in the glassy state</i>	179
10.2.3	<i>Molecular phenomena in the rubbery state</i>	179
10.3	EFFECT OF THE BUMPING ON THE COOKED RICE GRAINS STRUCTURE	179
10.3.1	<i>Amylose-lipid complexes</i>	179
10.3.2	<i>Modification of the amylopectin molecular weight</i>	180
10.3.3	<i>Effect of mill gap and bumping temperature on the post-bumped rice grains</i>	181
10.3.4	<i>Correlation between the post-bumped rice characteristics and the puffed product expansion</i>	182
10.3.5	<i>Practical conclusions for factory operations</i>	182
10.3.5.1	<i>Raw material formulation</i>	182
10.3.5.2	<i>Technical specifications</i>	183
10.3.5.3	<i>Process optimisation</i>	183
10.4	SUGGESTIONS FOR FUTURE STUDIES	183
10.4.1	<i>Amylose-lipid complexes</i>	183
10.4.2	<i>Amylopectin molecular weight study</i>	184
10.4.3	<i>Variety study</i>	184
 BIBLIOGRAPHY		186

LIST OF FIGURES

Figure 2.1: Structure of a rough rice grain (Juliano and Bechtel, 1985)	5
Figure 2.2: Linear α -D-(1-4) chain of glucose units	7
Figure 2.3: α -D-(1-6) branching of amylopectin.....	7
Figure 2.4: Diagrammatic representation of the A, B and C amylopectin chains (Hoseney, 1994).....	8
Figure 2.5: Model of amylopectin crystalline (1) and amorphous (2) lamellae (Robin et al., 1974)	9
Figure 2.6: Structural model of a crystalline region in a starch granule (Blanshard, 1987).....	11
Figure 2.7: DSC endotherms of potato starch obtained at various moisture contents (volume fraction of water from 0.28 to 0.81) with a heating rate of $10^{\circ}\text{C}\cdot\text{min}^{-1}$ (Donovan, 1979).....	14
Figure 2.8: Diagrammatic structure of an amylose-lipid complex helix (Godet et al., 1993).....	15
Figure 2.9: DSC midpoint glass transition temperature for pure amylopectin (---) and for an amylopectin-glucose (5:1) mixture (●). The theoretical curve is also shown (—) (Kalichevsky et al., 1993b).....	18
Figure 2.10: Retrogradation mechanism of amylose (Goodfellow and Wilson, 1990)	20
Figure 2.11: Diagrammatic amylopectin retrogradation rate curve at a given moisture content (adapted from Farhat et al., 2000).....	21
Figure 2.12: Diagram of the bumping rolls	22
Figure 3.1: Diagram of the Rice Krispies TM industrial process (Manchester factory)	27
Figure 3.2: Sample of cooked, pre-bumped rice.....	29
Figure 3.3: Examples of the 50 pre-bumped samples RVA profiles taken from the factory at different times and on different days (Swales, 1999).....	30

Figure 3.4: Diagram of the bumping rolls	31
Figure 3.5: Examples of post-bumped rice.....	32
Figure 3.6: Examples of the 50 post-bumped samples RVA profiles taken from the factory at different times and on different days (Swales, 1999).....	33
Figure 3.7: Diagram of the puffing mechanism.....	35
Figure 3.8: Sample of puffed rice (Rice Krispies™).....	35
Figure 4.1: Diagram of the Stable Micro Systems TA-HD texture analyser.....	41
Figure 4.2: Illustration of the bending of the texture analyser load cell under high compression	41
Figure 4.3: Summary of the texture analyser measurements.....	42
Figure 4.4: Example of a Texture Analyser bumping record. The impacting height was set at 0.1mm. The blue and red lines show the first and second impacts respectively	43
Figure 4.5: Example of a Texture Analyser bumping record (zoom of figure 4.4), showing how the measurement of Initial height and Final height was done. The blue and red lines show the first and second impacts respectively.....	44
Figure 4.6: Diagram of the APV Mitchell Dryers Ltd roller drier	45
Figure 4.7: Aluminium shelves for rice puffing in a hot air oven	48
Figure 4.8: RVA profiles of four replications of Balilla rice flour gelatinisation	53
Figure 4.9: Example of DSC endothermic maize starch gelatinisation peak in excess water, showing the onset (T_o), peak (T_p) and end (T_e) temperatures.....	54
Figure 4.10: X-ray spectrum of native semi-crystalline (A-type) Balilla rice flour, cooked amorphous cassava flour and cooked semi-crystalline (V-type) cassava flour (Onyeador, 2002). GMS stands for Glycerol-Mono-Stearate, a lipid which can combine with amylose molecules to form crystalline amylose-lipid complexes	55
Figure 4.11: DMTA measurement head. The liquid nitrogen inlet and outlet constitute the cooling system of the system, while a resistance in the 'temperature enclosure' ensures the heating.....	57
Figure 4.12: Dual cantilever bending geometry of the DMTA head.....	57
Figure 4.13: Example of a DMTA record obtained with a wheat flour extrudate. Moisture content: 24.6% d.w.b. Stimulation frequency: 5 Hz. The variations in	

G', G'' and tan δ at -60°C were interpreted as the melting of the silicon oil coating the sample (Carvalho, 2000).....	58
Figure 4.14: Example of physical ageing endothermic peaks identified by DSC in post-bumped rice. Sample moisture content 11% w.w.b.; tempering times: 0, 1, 2, 4, 6, 8, 10 & 12 hours	61
Figure 4.15: Diagram of the Rosand RH-7 capillary rheometer (Becker, 2001)	63
Figure 4.16: Typical RVA cold paste profiles.....	66
Figure 4.17: Example of a picture of 50 puffed rice grains.....	68
Figure 4.18: Box used for the can weight and bulk density characterisation at the university	68
Figure 5.1: Measurement of raw rice grain dimensions Height x Width x Length (HxWxL)	70
Figure 5.2: Grain dimensions (height, width and length) of the seven rice varieties. The vertical lines show two times the standard deviation	70
Figure 5.3: Ellipsoidal volumes of the seven rice varieties. The vertical lines show two times the standard deviation	71
Figure 5.4: Bulk densities of the seven rice varieties. The vertical lines show two times the standard deviation	72
Figure 5.5: Amylose contents of the seven rice varieties. The two bars represent two replicates of the assay.	74
Figure 5.6: Amylopectin branch chain analysis of the seven raw rice flours.....	75
Figure 5.7: Amylopectin branch chain differential analysis of the seven raw flours.....	76
Figure 5.8: Separation of amylose and amylopectin fractions of the seven raw rice flours by analytical ultracentrifugation	77
Figure 5.9: Ultracentrifugation amylose separation peak of the seven raw rice flours	77
Figure 5.10: Ultracentrifugation amylopectin separation peak of the seven raw rice flours	78
Figure 5.11: Protein contents of the seven rice varieties (single determination).....	78
Figure 5.12: Free lipid contents of the seven rice varieties. When duplicates were done, the +/- figures indicate the variation between the two results.	79
Figure 5.13: Typical RVA gelatinisation profiles of the seven rice varieties	80

Figure 5.14: Relationship between the amylose content and the RVA gelatinisation peak (in blue) and final viscosity (in red) of the seven rice varieties81

Figure 5.15: DSC gelatinisation profiles of the seven raw rice flours. The water : flour ratio was 3:1 (w/w). The profiles were normalised by dividing the heat flow by the weight of dry flour.....82

Figure 5.16: Seven rice varieties average DSC gelatinisation peak characteristics. The +/- figures indicate the variation between the two duplicates.82

Figure 5.17: Seven rice varieties average DSC gelatinisation enthalpies. The +/- figures indicate the variation between the two duplicates.83

Figure 5.18: Relationship between the amylose content and the DSC gelatinisation onset temperature of seven rice varieties.....84

Figure 5.19: Relationship between the amylose content and the DSC gelatinisation enthalpy of seven rice varieties.....84

Figure 6.1: Typical DMTA measurements89

Figure 6.2: $\tan \delta$ glass transition diagram of pre-bumped and post-bumped rice material. The pure amylopectin glass transition curve is also shown (---) (Kalichevsky et al., 1993b).....90

Figure 6.3: Path **(1-2-3-4)** followed by the rice material after the cooking, through the bumping and drying to the tempering step on the theoretical glass transition diagram (\bullet experimental points)91

Figure 6.4: Path **(4-5-6-7)** followed by the rice material during the puffing on the theoretical glass transition diagram (\bullet experimental points)92

Figure 6.5: Diagrammatic retrogradation rate curve in function of temperature for the cooked rice material at 18% moisture content w.w.b (adapted from Farhat et al., 2000)94

Figure 7.1: Diagram of the 13 samples central composite experimental design. The red circles numbered 1 to 13 represent the chosen experimental conditions. Samples number 3 and 5 (dotted circles) are extra-samples added to the original design. The blue lines (labelled 100, 200, 450, 700 and 800) represent the evolution of the mill gap as a function of the roll temperature, for a series of mill gaps initially set to 100, 200, 450, 700 and 800 μ m at room temperature (20°C).....97

Figure 7.2a: Battle Creek 20 trials planned d-optimal experimental design	100
Figure 7.2b: Battle Creek 20 trials actual experimental conditions.....	100
Figure 7.3: RVA cold paste profiles of the central composite experimental design 13 samples	101
Figure 7.4: Diagram showing the link between the 3 groups G1, G2, G3 of samples identified by RVA and the 3 main mill gap levels of the central composite experimental design.....	103
Figure 7.5: RVA cold paste profiles of six Manchester factory Selenio rice samples (set B). F01 is a pre-bumped sample and F02 to F06 were prepared by reducing progressively the gap between the bumping rolls	104
Figure 7.6: Effect of reducing the mill gap on the Manchester Selenio rice RVA profiles.....	105
Figure 7.7: RVA cold paste profiles of the d-optimal experimental design 20 trials	108
Figure 7.8: Diagram showing the correspondence between the four groups and two sub-categories of samples identified by RVA and the d-optimal experimental design actual conditions; ▲△ Medium grain variety, ■□ Short grain variety, ◆◇ Selenio variety. The full and empty symbols for each variety indicate two different days of production.....	109
Figure 7.9: Hypothetical strain field created in the rice grain on the instant of bumping. Fig. 7.9a: Small mill gap; Fig. 7.9b: Wide mill gap.....	112
Figure 7.10: RVA profiles of raw and cooked (15 and 30 minutes) wheat, waxy maize and cassava starches (Becker, 2001).....	115
Figure 7.11: Effect of reducing the mill gap on the RVA profiles of post-bumped Selenio rice	116
Figure 7.12: X-ray spectrum of native and cooked Balilla rice flour (Han and Hill, 1999).....	117
Figure 7.13: X-ray spectra of a series of pre-bumped samples: From top to bottom, three Selenio, two Medium Grain (MGR) and two Short Grain (SGR) varieties. The small letters a, b, and c represent different days of production.....	118
Figure 7.14: DSC evidence of the presence of amylose lipid complexes in pre-bumped rice (arbitrary heat flow scale). The solid : water ratio is 1:3 (w/w) ..	120
Figure 7.15: DSC evidence of the presence of amylose lipid complexes in post-bumped rice (arbitrary heat flow scale). The solid : water ratio is 1:3 (w/w) ..	120

Figure 7.16: DSC assessment of the presence of amylose lipid complexes in six of the 20 samples from the set C d-optimal experimental design - First run (arbitrary heat flow scale). The solid : water ratio is 1:3 (w/w). The profiles were normalised by dividing the heat flow by the weight of dry sample.....121

Figure 7.17: DSC assessment of the presence of amylose lipid complexes in six of the 20 samples from the set C d-optimal experimental design - Second run (arbitrary heat flow scale). The solid : water ratio is 1:3 (w/w). The profiles were normalised by dividing the heat flow by the weight of dry sample.....122

Figure 7.18: Typical X-ray spectra of the four RVA defined groups of cooked samples, using samples from set A and set B series. The bumping severity increases from G1 to G4.....123

Figure 7.19: Typical X-ray spectra of the cooked samples groups defined using the RVA profiles of the 20 trials from the d-optimal experimental design. The bumping severity increases from G2 to G4124

Figure 7.20: Molecular structure of linoleic acid126

Figure 7.21: RVA gelatinisation profiles of Glutinous, Elio and Selenio rice flours127

Figure 7.22: RVA gelatinisation profiles of Glutinous (G), Elio (E) and Selenio (S) rice flours, with (G+L, E+L, S+L) and without lipids added128

Figure 7.23: DSC assessment of the formation of amylose-lipid complexes in mixtures of rice flour and lipids - First run. The solid : water ratio is 1:3 (w/w). The profiles were normalised by dividing the heat flow by the weight of dry sample129

Figure 7.24: DSC assessment of the formation of amylose-lipid complexes in mixtures of rice flour and lipids - Second run. The solid : water ratio is 1:3 (w/w). The profiles were normalised by dividing the heat flow by the weight of dry sample.....130

Figure 7.25: Schematic structure of a raw rice grain and starch granules.....131

Figure 7.26: Schematic structure of an amylose-lipid complex helix (amorphous amylose-lipid complex type)132

Figure 7.27: Schematic structure of a crystalline amylose-lipid complex.....132

Figure 7.28: Schematic structure of a cooked rice grain and its molten starch granules133

Figure 7.29: Hypothetical organisation of amylose-lipid complexes at the edges of the starch granules remnants in the cooked rice	134
Figure 7.30: Hypothetical effect of the bumping on the crystalline order of amylose-lipid complexes in the cooked rice	135
Figure 7.31: Ultracentrifugation evidence of starch molecular weight reduction by the bumping	138
Figure 7.32: Ultracentrifugation of three of the set C d-optimal experimental design 20 samples	140
Figure 7.33: Model of the effect of mill gap and bumping temperature on the relative viscosity of post-bumped rice dilute solutions. The dots indicate the parameters of the actual experiments (set A central composite experimental design) and the shading the level of accuracy of the model.	142
Figure 7.34: HPLC amylopectin branch chain analysis of four pre- and post-bumped samples	144
Figure 7.35: Amylopectin branch chain differential analysis of four pre- and post-bumped samples	145
Figure 7.36: Model of the effect of the mill gap and bumping temperature on the molten post-bumped rice consistency factor. The dots indicate the parameters of the actual experiments (set A central composite experimental design) and the shading the level of accuracy of the model.	146
Figure 8.1: Evaluation of the variability in the measurement of the grain area, using 6 pictures of the same 50 puffed grains, for 2 different samples. The vertical lines indicate one standard deviation	151
Figure 8.2: Evolution of the average grain area of the 'DRIED' sample over 8 hours of tempering. The vertical lines indicate two times the standard deviations of the 50 grains used to take the picture.	152
Figure 8.3: Gradient of moisture contents inside the post-bumped, freshly dried rice grain	154
Figure 8.4: Physical ageing endothermic peak in 11% moisture content w.w.b cooked rice. Tempering times: 0, 1, 2, 4, 6, 8, 10, 12 hours	155
Figure 8.5: Evolution of the area of the physical ageing DSC peak of post-bumped, dried and powdered rice during the tempering	156

Figure 8.6: Evolution of the water activity (A_w) of post-bumped, dried rice during the tempering	157
Figure 8.7: Evolution of the average grain areas of the 'DRIED', 'REFRESHED', 'REFERENCE (1)' and 'REFERENCE (2)' samples over 7 hours of tempering	160
Figure 9.1: Effect of the mill gap on the bulk densities of six puffed samples (set B). The vertical lines represent two times the standard deviation.....	164
Figure 9.2: Effect of the mill gap on the grain areas of six puffed samples (set B). The vertical lines represent two times the standard deviation.....	165
Figure 9.3: Effect of the bumping temperature on the grain areas of three puffed samples. The vertical lines represent two times the standard deviation.....	166
Figure 9.4: Model of the effect of roll gap and bumping temperature on the puffed rice bulk density. The dots indicate the experimental points (set A central composite experimental design), the shading the level of accuracy of the model, and the level curves the predicted bulk density.	167
Figure 9.5: Model of the effect of roll gap and bumping temperature on the puffed grain area. The dots indicate the experimental points (set A central composite experimental design), the shading the level of accuracy of the model, and the level curves the predicted grain area.	168
Figure 9.6: Correlation between the post-bumped rice bulk density and the puffed rice bulk density.....	170
Figure 9.7: Correlation between the post-bumped rice bulk density and the puffed grain area	170
Figure 9.8: Correlation between the post-bumped rice grain height recovery and the bulk density of the puffed material.....	171
Figure 9.9: Correlation between the post-bumped rice grain height recovery and the puffed grain area.....	172
Figure 9.10: Diagram showing the correspondence between the four groups and two sub-categories of samples identified by RVA and the d-optimal experimental design conditions (▲△ Medium grain variety, ■□ Short grain variety, ◆◇ Selenio variety).....	173

Figure 9.11: Average bulk densities of the RVA groups of samples identified with the Battle Creek d-optimal experimental design samples. The vertical lines represent two times the standard deviation.....174

Figure 9.12: Average puffed grain areas of the RVA groups of samples identified with the Battle Creek d-optimal experimental design samples. The vertical lines represent two times the standard deviation.....174

Figure 10.1: Path (**1** → **7**) followed on the theoretical glass transition diagram by the rice material during the bumping, tempering and puffing steps of the Rice Krispies™ process (• experimental points; the line is added as a guide to the eye)178

LIST OF TABLES

Table 2.1: US brown rice crop classification (Tongdang, 2001).....	6
Table 2.2: Comparison of starch granule sizes of various cereals (Tongdang, 2001).....	10
Table 3.1: Manchester factory bumping conditions	33
Table 4.1: List of the rice varieties used during the project	38
Table 4.2: Summary of all the samples received in the course of the project. The numbers in the table refer to the chapters in which the samples are discussed. Blank cells and ✓ indicate that the sample was not sent and was not used respectively	39
Table 4.3: Protocol of the texture analyser experiments	44
Table 4.4: Comparison of texture analyser, roller dryer and bumping mill specifications	46
Table 4.5: Amylopectin branch chain analysis chromatography protocol	51
Table 4.6: Gradient profile for the amylopectin branch chain analysis chromatography	52
Table 4.7: RVA rice flour gelatinisation temperature profile. Total duration of the profile: 18min 30s.....	52
Table 4.8: Specifications for the Rosand RH-7 capillary rheometer.....	64
Table 4.9: RVA cold paste viscosity temperature profile.....	65
Table 4.10: Parameters measured on the RVA cold paste profile.....	66
Table 5.1: List of the rice varieties used during the project	69
Table 5.2: Moisture contents of the seven rice flours varieties	73
Table 5.3: Amylose contents of the seven rice samples	73
Table 5.4: List of the seven rice varieties used during the project	74

Table 6.1: Relative humidities created above saturated salt solutions and resulting moisture contents of cooked rice samples stored under these relative humidities (* adapted from Nyquist, 1983).....	87
Table 7.1: Summary of the central composite design 13 experimental conditions	98
Table 7.2: Summary of the d-optimal experimental design 20 trials conditions. MGR and SGR stand for Medium Grain Rice and Short Grain Rice respectively.	99
Table 7.3: Characteristics of the three groups of RVA profiles	102
Table 7.4: Relationship between the three groups of samples identified by RVA and the mill gap and bumping severity	102
Table 7.5: Average Cold paste, 95°C and Final viscosities for the 4 RVA groups of samples. The standard deviations are indicated in brackets.	104
Table 7.6: Evolution of average Cold paste and 95°C viscosities from RVA groups G1 to G4	106
Table 7.7: Evidence of a decrease in cold paste, 95°C and final viscosities within the RVA group 4, when the mill gap decreases.	106
Table 7.8: Evolution of the RVA parameters when the mill gap decreases among the 4 groups	107
Table 7.9: Repartition of the d-optimal experimental design 20 samples into the four groups and two sub-categories of RVA profiles	108
Table 7.10: Details of the pre-bumped samples used for figure 7.13 X-ray analysis	119
Table 7.11: Characteristics of the V-pattern 20° peak for the 4 groups of samples identified with the set A central composite experimental design and the set B series of 6 varying mill gap factory samples. The figures between brackets indicate the standard deviations.....	124
Table 7.12: Characteristics of the V-pattern 20° peak for the groups of samples identified with the set C d-optimal experimental design. The figures between brackets indicate the standard deviations	125
Table 7.13: Composition of the 6 (flour + lipid) mixes cooked with the RVA.....	126
Table 7.14: Evolution of the amylose content and the RVA final viscosity of Glutinous (G), Selenio (S) and Elio (E) rice flours (single determination).....	127

Table 7.15: Evidence of an increase in RVA final viscosity of medium and high amylose content rice flours (Selenio and Elio) when lipids are added before cooking (single determination).....	128
Table 7.16: Areas of the DSC peaks identified in mixtures of rice flour and lipids (single determination). The enthalpies are expressed in Joules per gram of dry sample	130
Table 7.17: Characteristics of the ultracentrifugation intermediate absorption peak	139
Table 8.1: Summary of the puffed samples produced	150
Table 8.2: Evaluation of the variability of the puffing oven conditions. Evolution of the average grain area of the 'REFERENCE' sample over 8 hours	152
Table 8.3: Water activity of rice samples B and C after 8 hours of tempering	158

CHAPTER 1: INTRODUCTION

1.1 PROJECT BACKGROUND

In the second half of the 19th century, John Harvey and William Keith Kellogg were running a sanatorium in Battle Creek, Michigan, and invented a series of healthy cereal based foods for their patients. The first record of flaked cereals is a patent application for “flaked cereals and process of preparing same” filed by J. H. Kellogg in May 1894. Later on W. K. Kellogg modified the process to make a breakfast cereal product and established in 1906 the Battle Creek Toasted Corn Flake Company, which was renamed the Kellogg Company in 1925 (Fast, 1999). The Rice KrispiesTM process was derived from that of corn flakes in the 1920s and uses similar unit operations. By 1928, the production of Rice KrispiesTM was well established, as indicated by a contract for the supply of raw rice between an Abbeville (Louisiana) based rice grower, Water-Maid Rice, and Kellogg (Dupuy, 2001). Today Kellogg operates two Rice KrispiesTM factories in the United States and one at its European headquarters in Manchester. The rice processed in Manchester is grown in Italy. The current production of the United Kingdom operations is 40 thousand tons a year.

The Rice KrispiesTM process was developed through trial and error over several years and decades. The sheer scale of the current production means that this approach is no longer possible to solve problems arising during the production or to improve the process. This was illustrated in 1994 and 1995, when the rice crops proved very difficult to puff in the United Kingdom, resulting in the disposal of a large proportion of the production. The origins of the project derive from these events, in an effort to improve the understanding of how the process determines the structure of the puffed rice grains.

The project is also part of a company wide research effort to describe on a scientific basis Kellogg’s various processes, with the purpose to facilitate day-to-day operations and factory optimisations. This has become possible with the development of cereal science in the last 20 years. Models of the structure of amylose and

amylopectin have been developed, their interactions with other components of starch systems such as lipids and proteins have been studied, and a better understanding has been gained of the physical phenomena occurring in starch materials, such as gelatinisation, glass transition and physical ageing.

All these developments provide new models and concepts to think about starch, which can be applied to describe more precisely long-existing processes such as the manufacture of Rice Krispies™.

1.2 AIMS AND OBJECTIVES

The production difficulties encountered in 1994 and 1995 led to the hypothesis that the crop quality of these two years was different from usual, and that the right combination of process parameters to compensate for this difference had not been found. Two ways were possible to verify this hypothesis:

- To compare the 1994 and 1995 raw rice composition with a 'normal' crop.
- To identify the molecular phenomena that take place inside the rice grains at each step of the Rice Krispies™ process and investigate their influence on the product structure, so as to determine a range of optimum processing conditions, and how to modify them to solve production problems in the future.

Because the 1994 & 1995 crops were not available any more, the work was based on the second option, and the influence of the process conditions on normal rice crops was chosen as the main theme of study. Two approaches were used in the course of the project:

From a chemical point of view, rice can be seen as a complex assembly of polysaccharides, proteins and lipids, whose amounts, characteristics such as starch molecular weight, organisation and interactions within the rice grain may have an influence on the product quality.

From a polymer science point of view, a rice grain can be described as a composite polymeric material. Raw rice is a semi-crystalline system, while cooked rice can be either amorphous or semi-crystalline, if events such as retrogradation or amylose-

lipid complexation take place. In the amorphous parts of the rice grain, the glass transition has a crucial role in determining the mechanical properties of the material.

1.3 THESIS OUTLINE

In this thesis, chapter 2 reviews relevant work published in the field of starch science and processing of breakfast cereals. Chapter 3 presents in detail the process to manufacture Rice KrispiesTM, while chapter 4 describes the materials and methods that have been used in the course of the project.

The study of raw rice characteristics consisted in analysing the composition, grain dimension and gelatinisation behaviour of seven rice varieties. The results are presented in chapter 5.

The determination of the cooked rice material glass transition described in chapter 6 was a key part of the project, as this allowed each step of the Rice KrispiesTM process to be mapped onto a temperature / moisture content state diagram, and to think out the whole process in terms of glass transition.

The project focused mainly on the bumping step of the Rice KrispiesTM process, which is thought to play a key role in determining the end product quality because of the range of adjustable parameters it offers. Chapter 7 presents the information gathered in the course of the project on this specific step and its effects on the rice grain structure.

Following the bumping, chapter 8 presents a study of the phenomena occurring during the tempering step of the process and their effects on the end product.

Chapter 9 is a summary of how the puffed product quality is affected by the bumping parameters, and suggests some quality control measurements of the post-bumped material that could predict the quality of the final product.

Finally, chapter 10 presents the conclusions of the project and suggests some leads for further studies of the Rice KrispiesTM.

CHAPTER 2: LITERATURE REVIEW: MOLECULAR PHENOMENA THAT COULD AFFECT STARCH BEHAVIOUR

2.1 INTRODUCTION

The breakfast cereals Rice Krispies™ process consists essentially of the cooking of white rice grains, followed by a mechanical compression between two rolls (bumping), a tempering step and a toasting operation (puffing) which expands the grains into the finished product. All these operations can affect the amylose, amylopectin and other molecular components (lipids, proteins) of the rice grains, and therefore determine the grains state and structure.

This chapter presents the structure and composition of raw rice grains (sections 2.2 and 2.3) and reviews the molecular phenomena known to take place in starch materials, during the cooking (section 2.4), such as the formation of crystalline amylose-lipid complexes, and in the cooked material (section 2.5), such as glass transition, physical ageing and retrogradation. A review of the bumping and the puffing, which are unit operations specific to the flaked cereal industrial process, is presented in section 2.6. The aims objectives of the project are detailed in section 2.7.

2.2 THE RICE CROP

The main rice cultivar, *Oryza sativa L.*, is a 'semi-aquatic annual plant member of the *Gramineae* family' (Tongdang, 2001). Nowadays two principal varieties are cultivated: *Indica* is grown in India, Southern China, South-East Asia, Australia, South America, Southern USA and Europe. *Japonica* is grown in Japan, Korea and North China.

Rice grains are harvested with their protective hull (rough rice or paddy). The hull constitutes 20% of the paddy, and the seed (caryopsis) constitutes 80%. Figure 2.1 shows the structure of a rough rice grain.

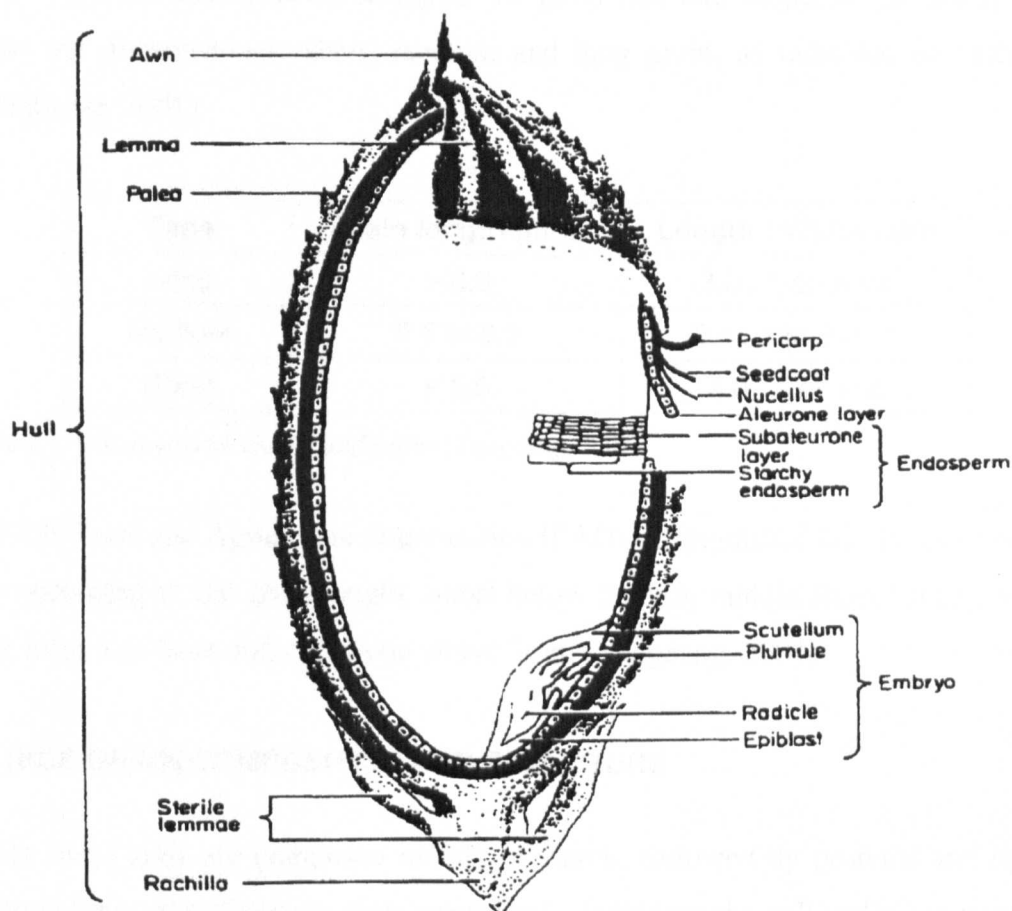


Figure 2.1: Structure of a rough rice grain (Juliano and Bechtel, 1985)

The hull is inedible and composed of the interlocking lemma and palea, two gramineae floral organs analogous to sepals. From the hull to the inner endosperm, three layers are found: The pericarp, the seed coat and the nucellus. The aleurone layer is the outer part of the endosperm. The endosperm is mainly composed of starch material, which is a food reserve for the future growth of the embryo (Juliano and Bechtel, 1985).

Most of the world rice is consumed as white rice. White rice is prepared in two steps: Firstly the rough rice hull is removed (de-hulling), which results in brown rice. Secondly the brown rice is milled to remove the outer layers of the grains and leave only the endosperm and aleurone layer, which constitutes the white rice (Juliano and Bechtel, 1985).

Rice crops are classified according to the grain size and shape. In the USA, three types are distinguished: Short, medium and long grain, as indicated on table 2.1 (Tongdang, 2001).

Type	Grain length (mm)	Length : Width ratio
Long	> 6.6	3.0 : 1 or more
Medium	5.5 to 6.6	2.1 : 1 to 3.0 : 1
Short	< 5.5	2.0 : 1 or less

Table 2.1: US brown rice crop classification (Tongdang, 2001)

The UN Food and Agriculture Organisation (FAO) distinguishes four types of milled rice according to the grain length: Short below 5.0mm, middle from 5.0 to 5.9mm, long from 6 to 7mm and extra long above 7mm (Tongdang, 2001).

2.3 RICE GRAIN COMPOSITION AND STRUCTURE

White rice grains are composed mainly of starch, followed by proteins and lipids. Various ashes and fibres are also constituents, including the cell walls components: Cellulose, hemicellulose, lignin.

2.3.1 Polysaccharides

Polysaccharides are the main component of rice grains. Milled rice typically contains 78% (w.w.b) of starch at 14% moisture content (Juliano and Bechtel, 1985). Starch is constituted of two glucose polymers, amylose and amylopectin, which are, in the native state, tightly packed into granules.

2.3.1.1 Amylose structure

Amylose is an essentially linear chain of glucose units linked through α -D-(1-4) glycosidic bonds (figure 2.2), with some degree of branching through α -D-(1-6) bonds (Buléon et al., 1998).

Amylose molecules are soluble in water and play a key role in increasing the viscosity of starch suspensions during cooking.

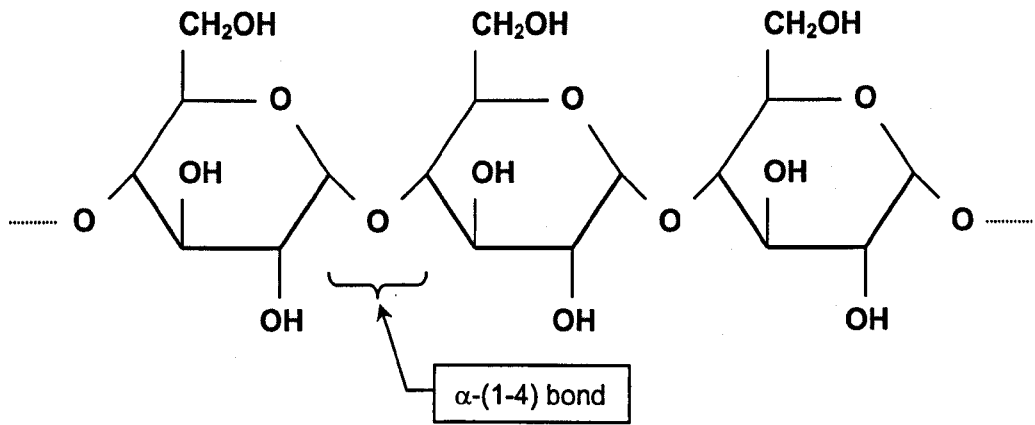


Figure 2.2: Linear α -D-(1-4) chain of glucose units

2.3.1.2 Amylopectin structure

Amylopectin molecules are constituted of linear α -D-(1-4)-branches connected to each other through α -D-(1-6) bonds. Figure 2.3 shows three glucose units connected by α -D-(1-4) bonds, and a fourth glucose unit connected through a α -D-(1-6) bond. The proportion of α -D-(1-6) bonds compared to α -D-(1-4) bonds is estimated between 5 and 6% (Champagne, 1996).

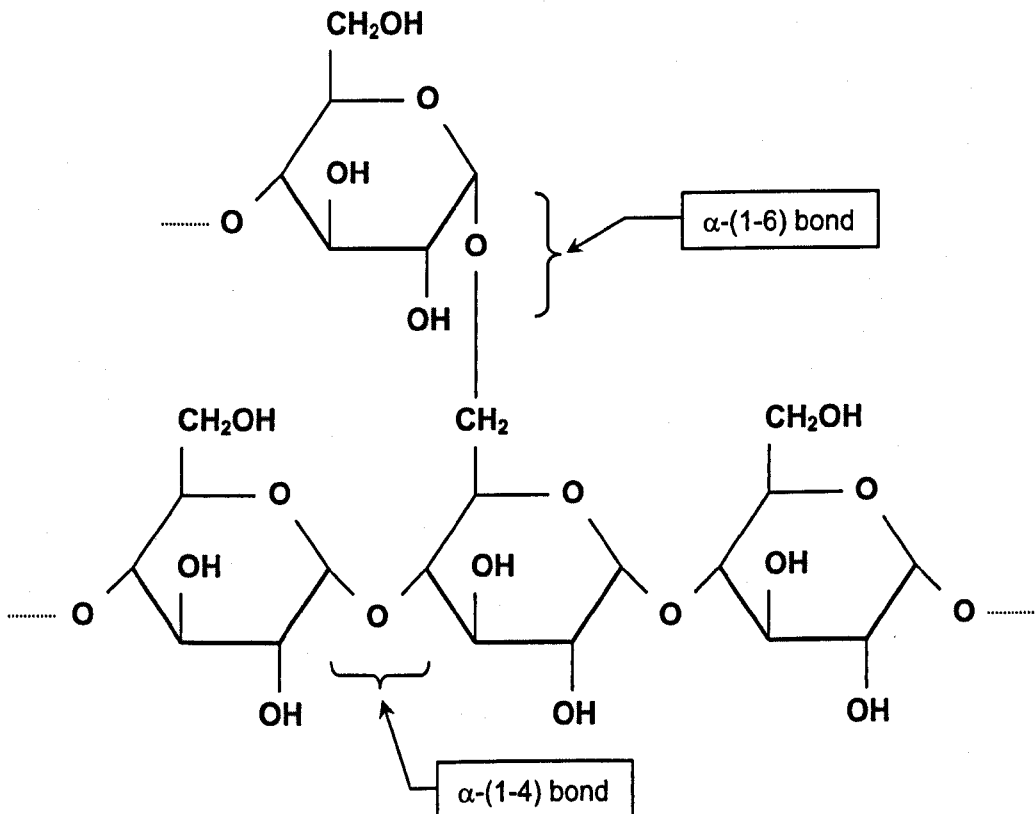


Figure 2.3: α -D-(1-6) branching of amylopectin

Peat *et al.* (1952) defined three types of amylopectin branches: A, B and C. The outermost chains A are linked by their reducing end to C₆ carbons of inner chains B through α -D-(1-6) bonds. The B chains are in turn connected to a central, innermost C chain, also through α -D-(1-6) bonds. Thus one amylopectin molecule has several A and B chains, but only one C chain and only one reducing end, as illustrated on figure 2.4.

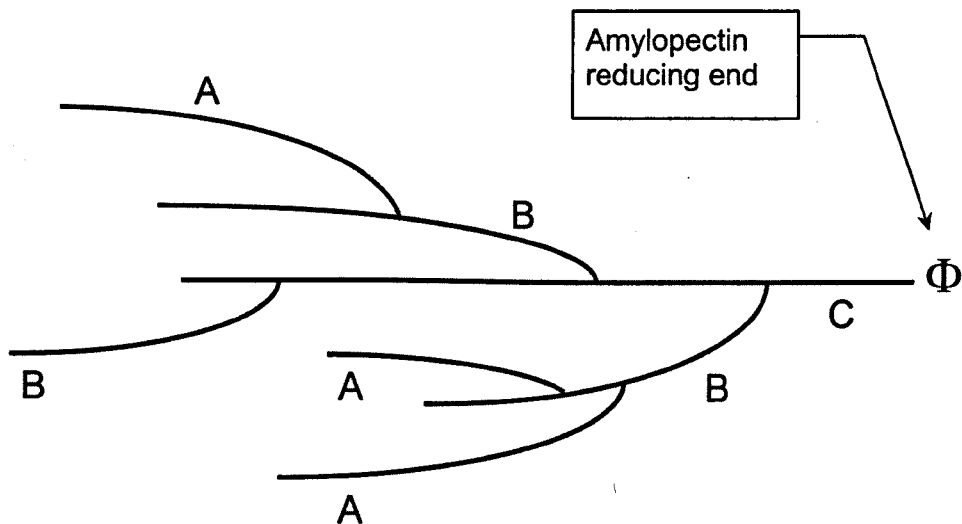


Figure 2.4: Diagrammatic representation of the A, B and C amylopectin chains (Hoseney, 1994)

In its native form, amylopectin is a semi-crystalline structure constituted of alternating crystalline and amorphous lamellae. Figure 2.5 presents a model of this structure.

In the crystalline lamellae, amylopectin branches form double helices arranged in parallel with each other, and in the amorphous lamellae branches are arranged randomly. The crystalline and amorphous lamellae are 6nm and 4nm thick respectively (Robin *et al.*, 1974).

Amylose molecules are found in the amorphous lamellae in between the amylopectin crystallites. Also, it is possible that some amylose molecules can be involved in helices with amylopectin branches and become part of a crystalline lamella (Buléon *et al.*, 1998).

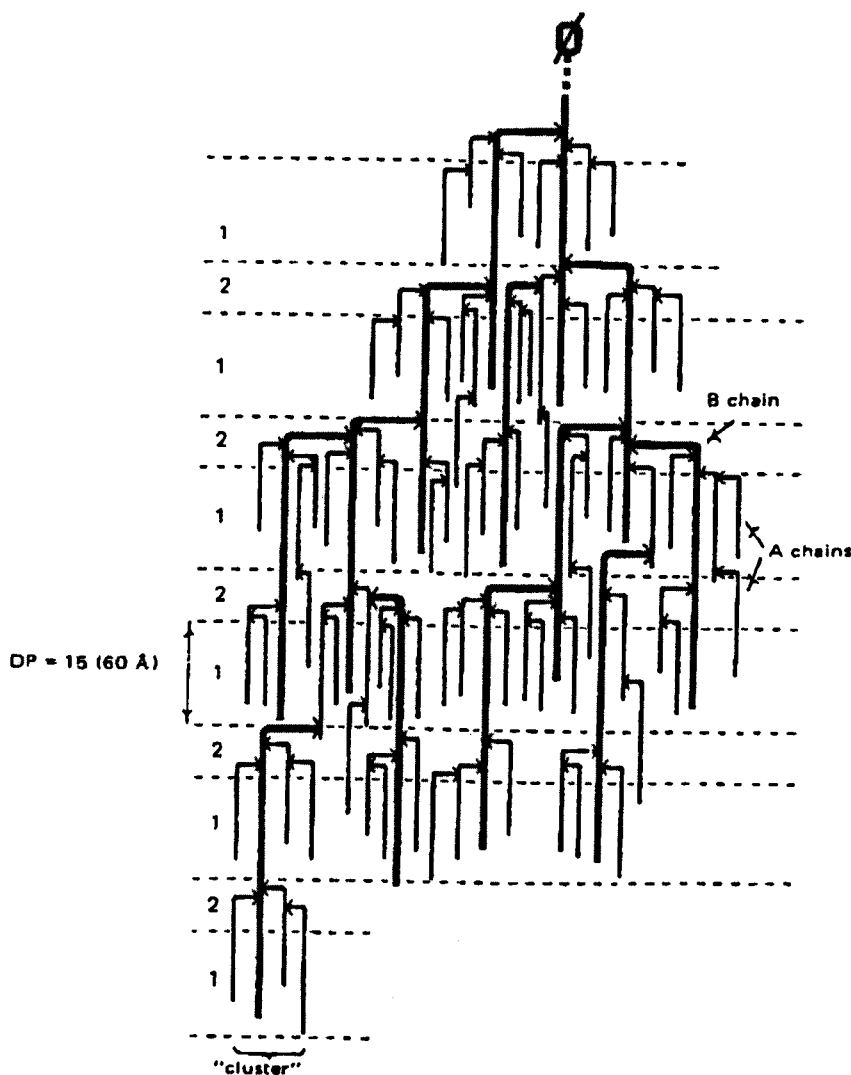


Figure 2.5: Model of amylopectin crystalline (1) and amorphous (2) lamellae (Robin et al., 1974)

Buléon (Buléon et al., 1998) proposed a model to explain the alternation of crystalline and amorphous lamellae. The growing A and B chains of an amylopectin molecule must reach a minimal length to fit in the catalytic site of the branching enzyme. Under that critical length, A and B chains simply grow and form a crystalline lamella. When the critical length is reached, branching takes place, creating an amorphous lamella from which new stems start growing to form the next crystalline lamella.

2.3.2 The starch granule

Amylose and amylopectin are synthesised in the growing seed cells amyloplasts (Buléon et al., 1998). They are packed in polyhedral granules measuring between 3 and 5 μm (Juliano, 1992). The rice granules are among the smallest compared to

other species, as indicated in table 2.2.

Starch	Granule size (μm)
Rice	3-5
Wheat	20-35
Maize	15
Cassava	5-35
Potato	15-100

Table 2.2: Comparison of starch granule sizes of various cereals (Tongdang, 2001)

Amyloplasts dimensions are in the range 7 to 39 μm and contain between 20 and 60 granules. At the end of the rice grain maturation, amyloplasts fill up the cells and take about 90% of the grain volume (Champagne, 1996).

The organisation of molecules in a starch granule is shown on figure 2.6. The amylopectin helices are grouped in the 6nm thick crystalline lamellae, which are connected together by the 4nm thick amorphous lamellae. The amylose can be complexed with lipids to form amylose-lipid complexes, or form helices with amylopectin and be part of a crystalline lamella, or exist as free molecules (Buléon et al., 1998).

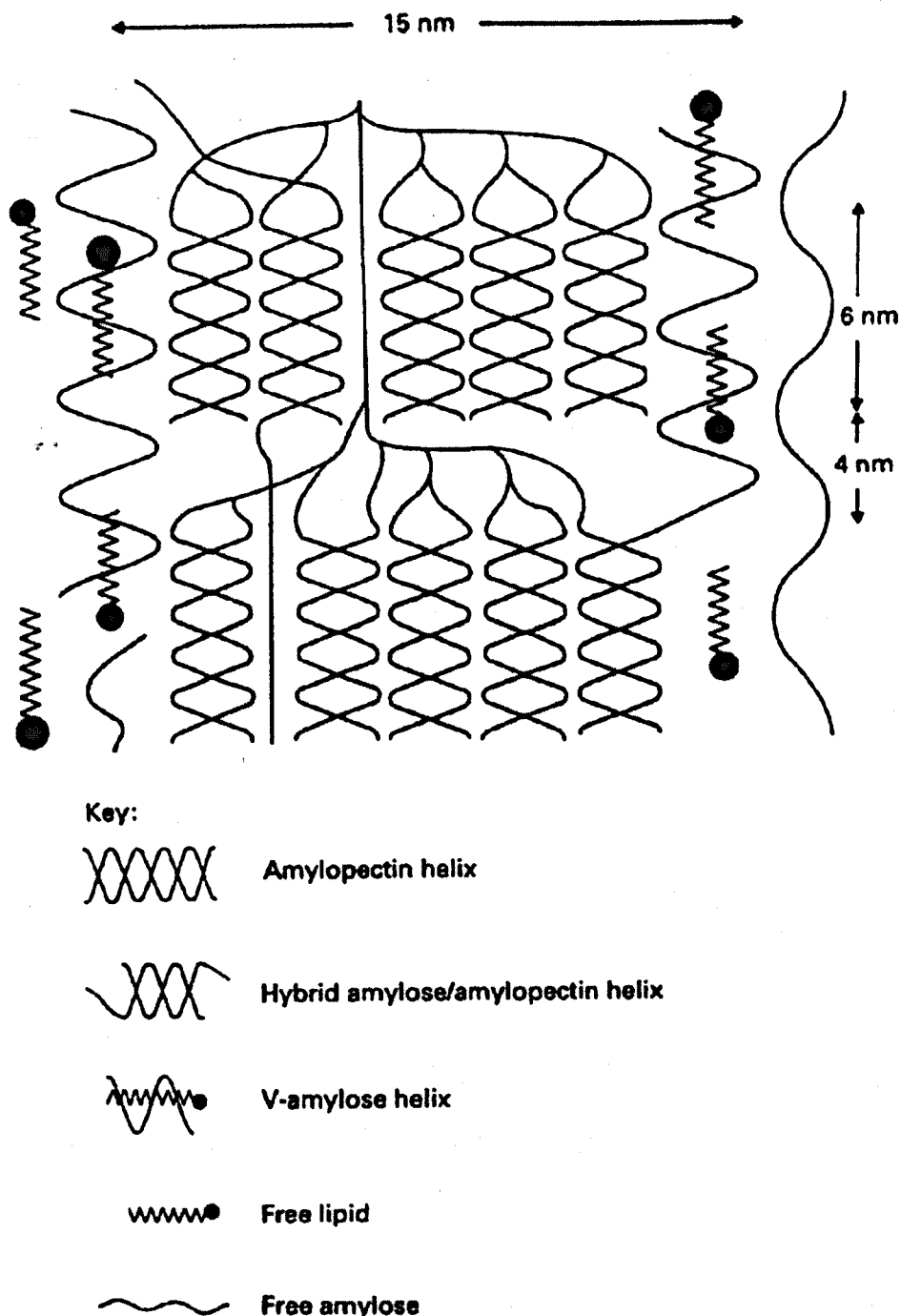


Figure 2.6: Structural model of a crystalline region in a starch granule (Blanshard, 1987)

2.3.3 Proteins

Proteins are the second main component of milled rice with 6 to 7% of the grain weight at 14% moisture content (Juliano, 1985). Approximately 10% of the milled rice proteins can be extracted without granule disruption, while the rest is associated to the starch granules (Buléon et al., 1998).

Mujoo *et al.* (1998) showed that proteins aggregate by formation of disulphide bonds during the cooking and mechanical processing (flaking) of rice.

Hamaker and Griffin (Hamaker and Griffin, 1990) found that cleaving disulfide bonds by adding dithiothreitol during the cooking increased the stickiness and decreased the viscosity of rice pastes. By cooking rice flours at different shear rates (Hamaker and Griffin, 1993), they showed that the addition of dithiothreitol increased the paste viscosity at low shear rate and decreased it at high shear rate. They also found that granules swelled more in absence of disulphide bonds. These studies concluded that the formation of proteins aggregates during the cooking of rice flour limits the swelling of rice granules and reinforces them, thus protecting them from breaking down at high shear rates.

A study of the corn flakes process flaking step (Batterman-Azcona and Hamaker, 1998) concluded that the protein bodies created during the cooking of the corn were deformed but not broken by the flaking.

2.3.4 Lipids

Lipids are contained mainly in the rice grain outer layers: Pericarp, seed coat and nucellus, which are removed during the milling. Therefore there is a marked difference between the brown and white rice lipid contents. Juliano (1985) indicates lipid levels of 1.6 to 2.8% in the brown rice at 14% moisture content, and of 0.3 to 0.5% in the white rice.

Lipids in the aleurone layer, sub-aleurone layer and embryo are found in the form of droplets 0.7 to 1.5 μm in diameter (Juliano, 1983). In the endosperm, lipids are found in increasing concentrations from the centre of the starch granules to their periphery, as is amylose (Buléon *et al.*, 1998). The main lipids in the endosperm of cereals are monoacyl lipids: 0.22 to 0.50% of the total dry weight of purified rice starch are free fatty acids, and 0.41 to 0.86% are lysophospholipids (Buléon *et al.*, 1998).

Lipids may have an important role in the strengthening of the rice grain structure, as they can form a network of amylose-lipid complexes during the cooking (Becker *et al.*, 2001), as discussed in section 2.4.2: Amylose-lipid complexes.

2.4 RICE COOKING

2.4.1 Starch gelatinisation and conversion

The term gelatinisation is used to refer to the series of structural changes that take place in starch granules upon heating in excess water. The term conversion was introduced by Mitchell *et al.* (1997) to describe the structural changes taking place during the processing of starch granules due to heating or mechanical input, and including limited moisture conditions.

Native starch granules dispersed in a solution can absorb only a limited amount of water. Gelatinisation begins when more water moves into the starch granule amorphous parts as temperature increases, which causes the swelling of starch molecules and the beginning of the granule dislocation. The following event is the loss of crystalline order and the melting of the amylopectin crystalline lamellae, which eventually results in the complete dislocation of the starch granule. At the same time free amylose molecules leach out of the granule and increase the viscosity of the solution. Amylose complexation with lipids may also occur following the hydration of the amorphous lamellae. Being insoluble, amylose-lipid complexes tend to remain in the granule and limit its swelling and dislocation (Morrison *et al.*, 1993b).

Han and Hamaker (2001) found that the proportion of amylopectin long chains was negatively correlated to the extent of granule breakdown during gelatinisation, which indicates that amylopectin fine structure also has an influence on the texture of cooked starch.

Levine and Slade (1992) have described the gelatinisation in terms of phase transitions: The first transition to occur is a second-order glass to rubber transition of the amorphous lamellae due to the increase in both moisture content and temperature. The second transition is the first-order melting of the crystalline lamellae, which begins once the amorphous part of the granule is in the rubbery state, making more molecular movements possible.

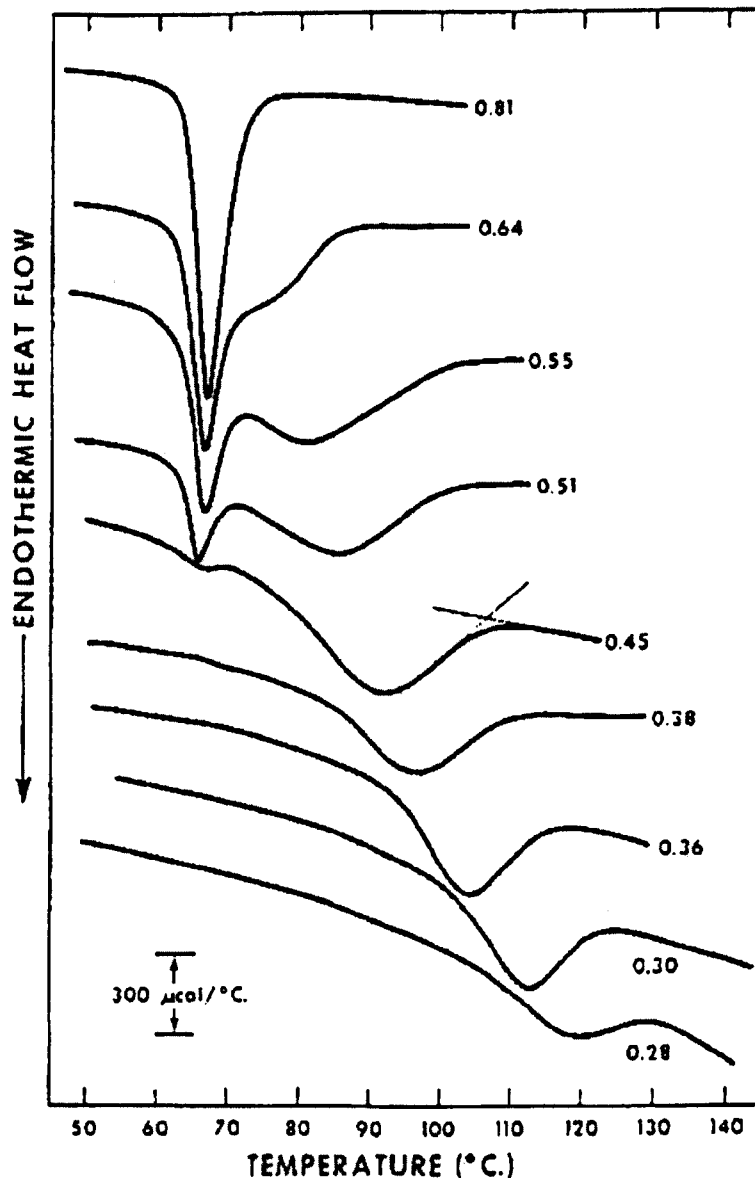


Figure 2.7: DSC endotherms of potato starch obtained at various moisture contents (volume fraction of water from 0.28 to 0.81) with a heating rate of $10^{\circ}\text{C}\cdot\text{min}^{-1}$ (Donovan, 1979)

In starch conversion, the glass to rubber transition of the amorphous lamellae also occurs upon heating, however the low moisture conditions mean that more heating is required to reach the higher glass transition temperature and that only a limited amount of swelling takes place. Consequently, the melting of the crystalline lamellae also takes place at a higher temperature, and the starch granule is only partially dislocated, if at all. Donovan (1979) observed a biphasic starch conversion by DSC for volume fractions of water between 0.45 and 0.55, which he interpreted as the decoupling of the transitions in the starch granule amorphous and crystalline parts. At low moisture contents (water volume fractions between 0.28 and 0.45), only one

endothermic peak whose temperature increased as the moisture content decreased was present, and was attributed to the melting of the crystalline lamellae (figure 2.7)

2.4.2 Amylose-lipid complexes

Amylose molecules can form a left-handed helix around the aliphatic chain of monoacyl lipids present in the starch material, resulting in amylose-lipid complexes (figure 2.8). A turn of the helix is composed of six glucose residues and is between 0.792 and 0.805nm high (Bul on et al., 1998).

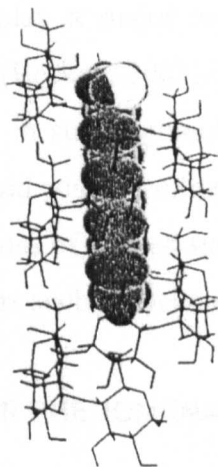


Figure 2.8: Diagrammatic structure of an amylose-lipid complex helix (Godet et al., 1993)

Separate amylose helices around lipids exist in the native starch granule and constitute **type I amylose-lipid complexes**, which are amorphous and dissociate when heated to 94-100°C in water (Raphaelides and Karkalas, 1988). During starch cooking, the type I complexes can form clusters of parallel helices by establishing hydrogen bonds between them. These clusters have a crystalline structure and are referred to as **type II amylose-lipid complexes**. Type II complexes dissociate when heated at 100 to 125°C (Raphaelides and Karkalas, 1988). Also, separate amylose and lipids molecules can be freed from the granule matrix during the cooking and combine to form more type II amylose-lipid complexes. Type II amylose-lipid complexes can be detected by the typical V-pattern on X-rays diffractograms. It is estimated that after gelatinisation, all the monoacyl lipids present in the starch material are in complexed form with amylose.

Amylose-lipid complexes are almost insoluble, therefore they limit or delay the

water migration into the starch granules during the cooking and tend to maintain the granule integrity.

Morrisson *et al.* conducted an extensive study on amylose-lipid complexes (Morrison, 1995; Morrison *et al.*, 1993a; Morrison *et al.*, 1993b). They found that 13 to 22% of the amylose in native maize starch is complexed with lipids (type I complexes), and that upon heating almost all the free amylose could be involved in amylose-lipid complexes.

Amylose-lipid complexes may play a major role in reinforcing the structure of cooked starch systems. Becker (Becker, 2001; Becker *et al.*, 2001) showed that amylose-lipid complexes formed in starch granules cooked under limited moisture and low shear rate prevent the cold paste swelling of wheat flour. Heinemann *et al.* (2001) found that diluted dispersions of cooked starch could form a gel upon addition of amylose-complexing emulsifiers such as lactones.

2.5 COOKED RICE MOLECULAR PHENOMENA

2.5.1 Glass transition

Amorphous polymer materials exist in two states, glassy or rubbery. The transition from one to the other is called the glass transition.

Levine and Slade (1992) defined the glass transition as a ‘temperature-, time- (or frequency-) and composition-dependent, material-specific change in physical state’, corresponding to an increase in the polymer molecular mobility from the glassy to the rubbery state. The glass transition can be detected by its effect on the material mechanical properties, such as the elastic and loss modules G' and G'' , and on the material heat capacity C_p .

Tolstoguzov (2000) published a comprehensive review of the role of the glassy state in food and the factors that control it.

The mechanical properties of a polymer as a function of temperature are described by Arrhenius kinetics in the glassy and rubbery states and by the WLF (Williams –

Landel – Ferry) equation over the glass transition temperature range (Levine and Slade, 1992). Peleg (Peleg, 1996a; Peleg, 1996b) developed a model to describe the mechanical changes in amylopectin and fructose-amylopectin systems in the glass transition temperature range using the Fermi equation. This approach allowed to predict and quantify the effect of additives on the properties of the material.

The evolution of the glass transition temperature as a function of the composition and water content of biopolymers mixtures is usually modelled with the Couchman-Karasz equation (Kalichevsky et al., 1993b). Matveev *et al.* (2000) attempted a more refined modelling using the additive group-contribution technique. They proposed a ‘plasticization function’, taking into account the effect of additives and ‘more precise’ than the Couchman-Karasz equation in the case of dry biopolymers, to predict the T_g of food systems.

The glassy and rubbery states differ most evidently by their mechanical properties: A glass is hard and can be deformed only a little before it shatters, while a rubber is softer and can be deformed to a large extent before it tears. In terms of elastic and loss moduli G' and G'' , a glass has a high elastic modulus and a low loss modulus, and a rubber has a low elastic modulus and a high loss modulus. During the glass transition, large variations in G' and G'' occur, making the mechanical properties of the material very sensitive to the ambient conditions, for instance to temperature or moisture content variations.

Kalichevsky *et al.* (1992) determined the glass transition temperature of amorphous and partially crystalline amylopectin over a range of moisture contents (10 to 22% w.w.b) by nuclear magnetic resonance (NMR), differential scanning calorimetry (DSC) and dynamic mechanical thermal analysis (DMTA). They found the T_g varied from 100°C at 10% moisture content to 18°C at 22% moisture content. A further study (Kalichevsky *et al.*, 1993a; Kalichevsky *et al.*, 1993b) showed that the addition of sugar decreased the glass transition temperature (figure 2.9), which was interpreted as an evidence of the plasticizing effect of sugars on starch systems.

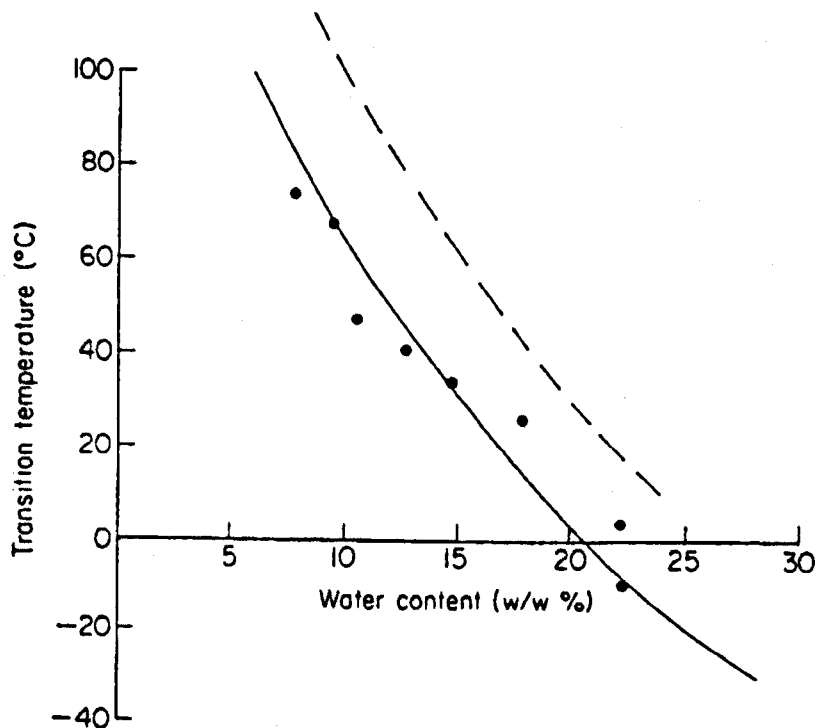


Figure 2.9: DSC midpoint glass transition temperature for pure amylopectin (---) and for an amylopectin-glucose (5:1) mixture (●). The theoretical curve is also shown (—) (Kalichevsky *et al.*, 1993b)

The glass transition is important to control food products shelf life (Levine and Slade, 1992), and in the gelatinisation of starch (section 2.4.1). It controls the mechanical properties of the cooked starch material, and therefore plays a considerable role in the manufacture of breakfast cereals such as corn flakes or rice krispies: Some steps of the process, such as the post-bumping tempering, must be done in the glassy state, while other steps must be done in the rubbery state, such as the bumping of the grains performed slightly above the glass transition temperature (Caldwell *et al.*, 2000; Perdon *et al.*, 2000), or such as the grains final expansion, or puffing. Glass transition is also important in controlling the beginning and the end of the expansion of extruded products (DellaValle *et al.*, 1997).

2.5.2 Physical ageing

Physical ageing consists in small molecular adjustments occurring in a polymer material in its glassy state, tending towards a tighter packing of the molecules. The driving force of physical ageing is the state of non-equilibrium of glassy materials: Structural relaxations can occur so as to minimize the enthalpy of the system (Martinet, 2001).

The phenomenon can be detected by DSC in glassy, aged samples as an endothermic peak roughly half way between the temperature T_A at which the material has been stored and the glass transition temperature T_G . The peak increases and shifts towards T_G when the storage time increases (Shogren, 1992). The closer T_A is to T_G , the bigger the size of the endotherm (Thiewes and Steeneken, 1997; Montserrat *et al.*, 1997). Physical ageing can be removed by heating the material up to its glass transition temperature.

The effects of physical ageing on the mechanical properties are an increase in density and a hardening of the material (Martinet, 2001). This can be of importance for the shelf life of glassy finished products such as crisps, sweets and breakfast cereals, and for processes that involve unit operations on glassy materials. The processing of some breakfast cereals such as Rice KrispiesTM involves a tempering step of up to 24 hours with the material in the glassy state, and hence the physical ageing taking place during that time may have an influence on the following steps of the process.

2.5.3 Retrogradation

2.5.3.1 Amylose

Amylose retrogradation is the crystallisation of free amylose molecules in cooked starch material, as shown on figure 2.10. Goodfellow and Wilson (1990) found that upon cooling of 10% w/w amylose dispersions, amylose molecules form double helices with each other, which creates a gel and increases the viscosity of the system. In the following hours (from 1 to 20 hours), the amylose helices gather together and form crystalline clusters of retrograded amylose. In limited water content conditions (in the rubbery state, below 40% moisture content w.w.b for example), amylose retrogradation also occurs but at a slower rate.

The crystalline amylose clusters modify the mechanical properties of cooked starch materials: The material becomes harder with an increase in the Young's modulus, and sometimes more brittle (Tako and Hizukuri, 2000).

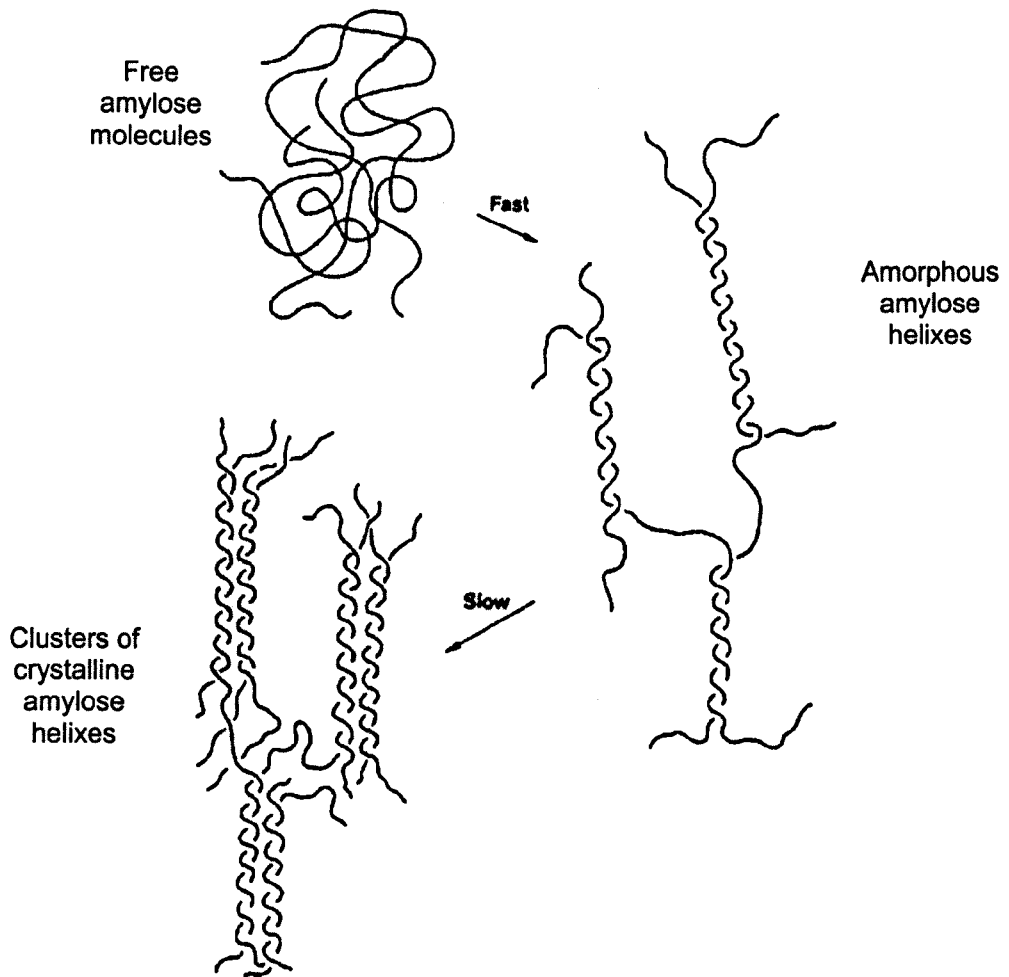


Figure 2.10: Retrogradation mechanism of amylose (Goodfellow and Wilson, 1990)

2.5.3.2 Amylopectin

Amylopectin retrogradation is the crystallisation of amylopectin molecules in the cooked starch material. It occurs in the rubbery state, in the temperature range from T_g to T_m . Below T_g (in the glassy state) and above T_m (in the molten state), the molecular mobility of amylopectin is respectively too low and too high to allow the molecules to combine and form crystallites.

Consequently, the retrogradation rate curve, represented on figure 2.11, is bell shaped, starting as an increasing exponential from the glass transition temperature T_g , passing by a maximum between T_g and T_m , and ending as a decreasing exponential towards the melting temperature T_m . Farhat *et al.* (2000) used the Lauritzen-Hoffman model of polymer crystallisation to predict the effect of water on the retrogradation rate of waxy maize starch. For waxy maize starch, they reported T_g and T_m values of

-12°C and 144°C respectively at 29% moisture content w.w.b, and a maximum retrogradation rate of approximately 6.10^4 s^{-1} (Farhat *et al.*, 2000).

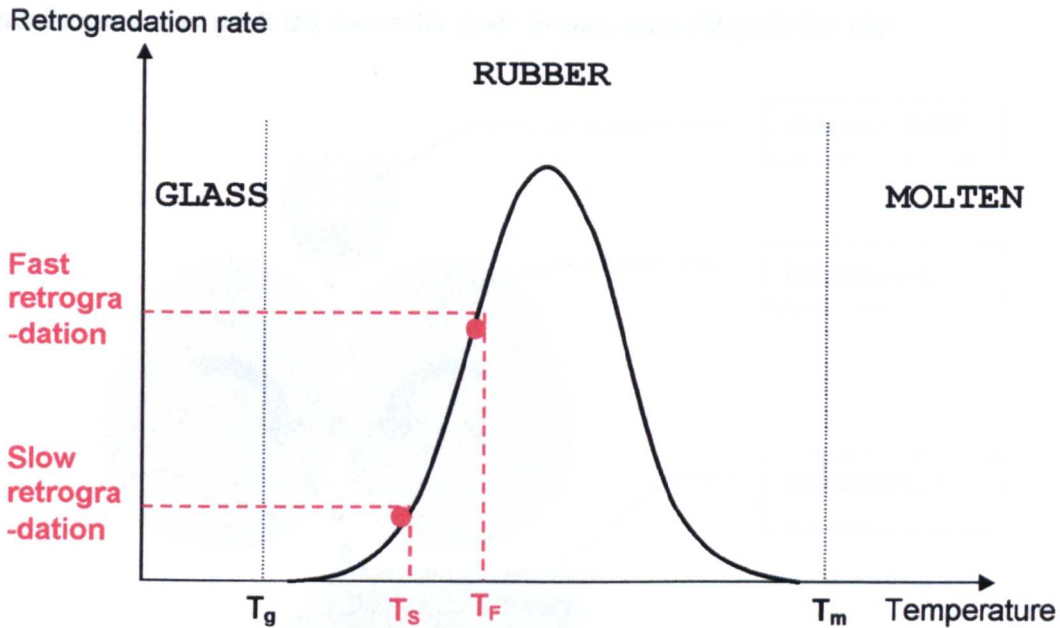


Figure 2.11: Diagrammatic amylopectin retrogradation rate curve at a given moisture content (adapted from Farhat *et al.*, 2000)

Because of its higher molecular weight and branched structure, amylopectin retrogradation takes place over longer periods of time than amylose retrogradation, from several hours in excess water to several days in limited moisture conditions.

2.6 INDUSTRIAL PROCESSES SPECIFIC TO FLAKED BREAKFAST CEREALS MANUFACTURE

The process to produce oven-puffed rice has been described by Juliano and Sakurai (1985). The engineering design and operations of the machines required for the process have been described by Fast and Caldwell (1990). This section reviews two unit operations specific to the manufacture of corn flakes and rice krispies: The bumping and the puffing.

2.6.1 Bumping rolls

Caldwell *et al.* and Fast *et al.* (Caldwell *et al.*, 1990; Fast *et al.*, 1990a) wrote a description of the bumping rolls (figure 2.12) used in the preparation of flaked cereals. The rolls are made of iron or steel. Typical sizes are 50 x 75cm and 65 x 100cm (diameter x width). The mill gap between the rolls is set either by screw jacks

or by hydraulic cylinders. The mill gap is normally set by visual examination of the flakes being produced. The exact value of the mill gap is difficult to determine, because the rolls may undergo a thermal dilation while operating and because the cereal grains may push the two rolls apart as they pass through the gap.

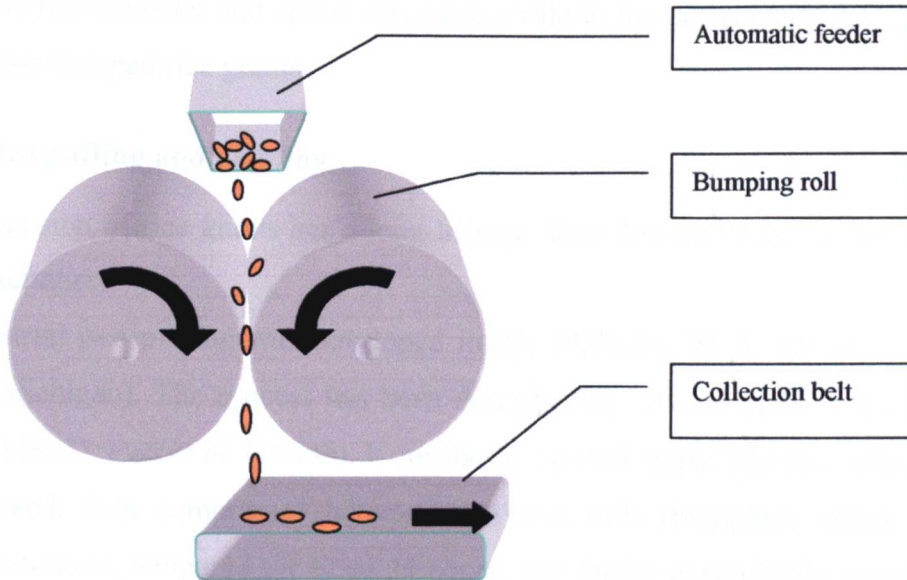


Figure 2.12: Diagram of the bumping rolls

The operating conditions are typically: Roll speeds in the range of 100 to 300rpm and temperatures between 45 and 50°C. In the case of the Rice KrispiesTM, the two rolls have the same speed, which means that no shear is applied to the rice grains.

The mill gap has a direct influence on the force applied to the rice grains as they move between the rolls, and hence on their shape and structural damage after the bumping. Other factors may also be of importance: Using his experience in the sheeting of dough, Levine (Levine, 1993; Levine, 1994; Levine, 1996a; Levine, 1996b; Levine and Levine, 1997) conducted a theoretical and practical study of the influence of the geometry and speed of the rolls on the deformation of cereal pellets. His main conclusions were as follow:

- The normal stress applied on the pellets is proportional to the square root of the roll diameter and to the square root of the roll speed.
- The rolls create a pressure gradient from the inside to the outside of the pellet. This gradient causes the pellet to flatten in both perpendicular and axial directions of the rolls.

- An increase in the roll speed reduces the time spent between the rolls and decreases the axial deformation, leading to more elongated pellets.
- An increase in the roll diameter increases the pressure gradient and hence the axial deformation, leading to less elongated pellets.

Thus, the roll diameter and speed may have a role in the determination of the shape of the post-bumped rice grains.

2.6.2 Rice puffing and popping

The expansion of rice grains has a long history. Two distinct processes are reported in the literature:

(i) Industrial rice puffing was developed in the 1920s by W. K. Kellogg in Battle Creek (Michigan). The process has been described by several authors: Juliano and Sakurai (1985), Fast *et al.* (1990b). It consists of several steps: The raw, white rice is first cooked, then compressed between two iron rolls (bumping), dried to 11% moisture content, tempered for 12 to 24 hours, and finally expanded by toasting in a hot air oven at temperatures between 230°C and 315°C for 60 seconds (puffing).

(ii) Rice popping was described by Juliano and Sakurai (1985) and studied in details by Murugesan and Bhattacharya (Murugesan and Bhattacharya, 1989a; Murugesan and Bhattacharya, 1989b; Murugesan and Bhattacharya, 1991a; Murugesan and Bhattacharya, 1991b) as an Indian recipe to prepare expanded rice. The raw, non de-hulled rice (paddy) is soaked in water to adjust its moisture content to 14% w.w.b., then directly expanded by exposing it to a flow of 225°C hot air for 45 seconds. The process involves no cooking or bumping steps.

The finished product textures are very different: The puffed rice has the structure of a sponge, brittle with many open and relatively big bubbles visible. The popped rice resembles more a foam, with a texture similar to the one of popcorn. Furthermore, when soaked in water (or milk) the popped rice grains tend to shrink while puffed rice grains keep their shape and volume.

Popped and puffed rice have in common their expansion, which is thought to be caused by the formation and growth of water vapour bubbles when the material is heated up. But they differ in their preparation: In popped rice the toasting is done directly with raw, non de-hulled rice, which allows high pressures to build up inside

the rice grain structure. In puffed rice, the preliminary milling and cooking soften the material, resulting in a weaker grain structure, and in lower pressures inside the expanding vapour bubbles during the puffing step. For puffed rice, the bumping is therefore needed before the puffing to further weaken the grain structure and ensure a proper expansion.

Chen and Yeh (2000) found that the optimal moisture content to achieve maximal expansion of extruded rice pellets was 11% w.w.b., and that the expansion temperature T_e increases linearly with the glass transition temperature T_g . Expansion was found to take place in the rubbery state between 20°C and 100°C above T_g .

2.6.3 Concepts related to the expansion of cereal materials

The degree of expansion of cereal products is the result of a balance between two forces (Fan *et al.*, 1996a; Fan *et al.*, 1996b): A force F_E driving the expansion and a force F_C limiting it. At the beginning of the expansion, F_E is bigger than F_C ($F_E > F_C$), so the material expands. As the expansion increases, F_E decreases and / or F_C increases, until the two forces become equal, at which point the expansion stops. If F_C is allowed to become greater than F_E ($F_E < F_C$), the expanded material begins to shrink, which is usually not desirable. Thus there is a need for a mechanism to keep the material maximally expanded.

In bread making, the expansion is driven by the dilation upon heating of CO₂ bubbles produced by fermentation and trapped in the starch-gluten matrix of the dough. The expansion stops when the bubbles break open and let the gas escape. The shrinking of the expanded structure is prevented by the rigidifying of the gluten network. Sevenou *et al.* (2002) described the expanding dough as a foam with independent gas cells, and the end of the expansion as a foam-sponge transition during which cell walls are ruptured and create an open structure.

In expanded extrudates (Fan *et al.*, 1996a; Fan *et al.*, 1996b), the expansion is driven by the dilation of H₂O steam bubbles created in the material by the depressurisation at the exit of the extruder. The force limiting the expansion (F_C) is the elastic modulus of the material. The shrinking of the expanded material is prevented by the loss of moisture and cooling, which take the material through a rubber-to-glass

transition and freezes the system in the expanded state. During the expansion, the breaking of cell walls reaching their elasticity accelerates the loss of water and the beginning of the rubber-to-glass transition, thus limiting the shrinking.

In rice krispies, the expansion is driven by the dilation of H₂O steam bubbles created in the material by the oven toasting. The force limiting the expansion (F_C) is the elastic modulus of the material. The expansion ends when cell walls reach their elasticity limit and break, letting the steam out and bringing the system into the glassy state.

2.7 OBJECTIVES OF THE WORK

Starch materials have been studied in details and the molecular phenomena that determine their properties are now fairly well described and understood. Models of the structure of amylose and amylopectin have been developed, although there is scope for improvement in the description of the amylopectin fine structure. Amylose and amylopectin interactions with lipids and proteins have been studied, and a good understanding has been gained of the physical phenomena occurring in starch materials, such as gelatinisation, retrogradation, glass transition and physical ageing.

Starch is the main staple food around the world, and has been grown and used for thousands of years. Industrial processes to manufacture starch-based products have been developed empirically in the last 100 years, such as extrusion, industrial bread making, and breakfast cereals production. The modern developments of starch science provide new models and concepts to describe the effects of these processes on the starch material structure and properties.

The objectives of this project were to use modern starch science concepts to determine which molecular phenomena take place inside the rice grains during the Rice KrispiesTM process, and what is the influence of the different steps of the process on the product structure and properties, so as to allow the improvement and optimisation of the process parameters.

CHAPTER 3: EVALUATION OF THE INDUSTRIAL PROCESS

3.1 INTRODUCTION

This chapter gives an overview of the manufacturing of Rice Krispies™ (section 3.3.1) and explains in details each unit operation of the process. Section 3.2 presents the industrial background of the project. The rice cooking conditions are presented in section 3.3.2. The drying and tempering steps that precede the bumping are described in section 3.3.3. Section 3.3.4 describes the bumping step conditions. Section 3.3.5 gives the conditions of the drying and tempering steps that follow the bumping. Finally section 3.3.6 describes the puffing step of the process.

The results of early studies conducted by Julie Swales (1999) on the variability of the process are also presented in sections 3.3.2 and 3.3.4 for the pre-bumped and post-bumped rice materials respectively. When starting the work, tempering times, temperatures and moistures contents of the rice as it was processed were not clearly identified, and some effort was spent ascertaining them. The figures given in this chapter are typical processing values at the Manchester factory.

3.2 INDUSTRIAL BACKGROUND

The Rice Krispies™ process was developed in the 1920s by W. K. Kellogg in Battle Creek, Michigan. Today the Kellogg Company operates two factories in the United States and one factory at its United Kingdom headquarters in Manchester. The current production of the United Kingdom operations is 40 000 tons a year.

The origins of the project date back to 1994 and 1995, when the rice crops proved very difficult to puff in the United Kingdom, resulting in the disposal of a large proportion of the production. One of the initial goals of the project was to attempt to understand what went wrong those two years, by examining how the process determines the structure of the puffed rice grains at the molecular level.

By applying the models and concepts of recent cereal science, such as glass

transition and amylose-lipid complexes formation, to describe the Rice Krispies™ process, another objective of the project was to facilitate day-to-day operations and factory process parameters optimisations.

3.3 THE RICE KRISPIES™ PROCESS

This section describes the different steps of the process.

3.3.1 Process overview

Figure 3.1 presents the different steps of the process. The flavour liquor mixed with the rice before the cooking is composed of water, sugar (sucrose), salt, corn syrup and malt.

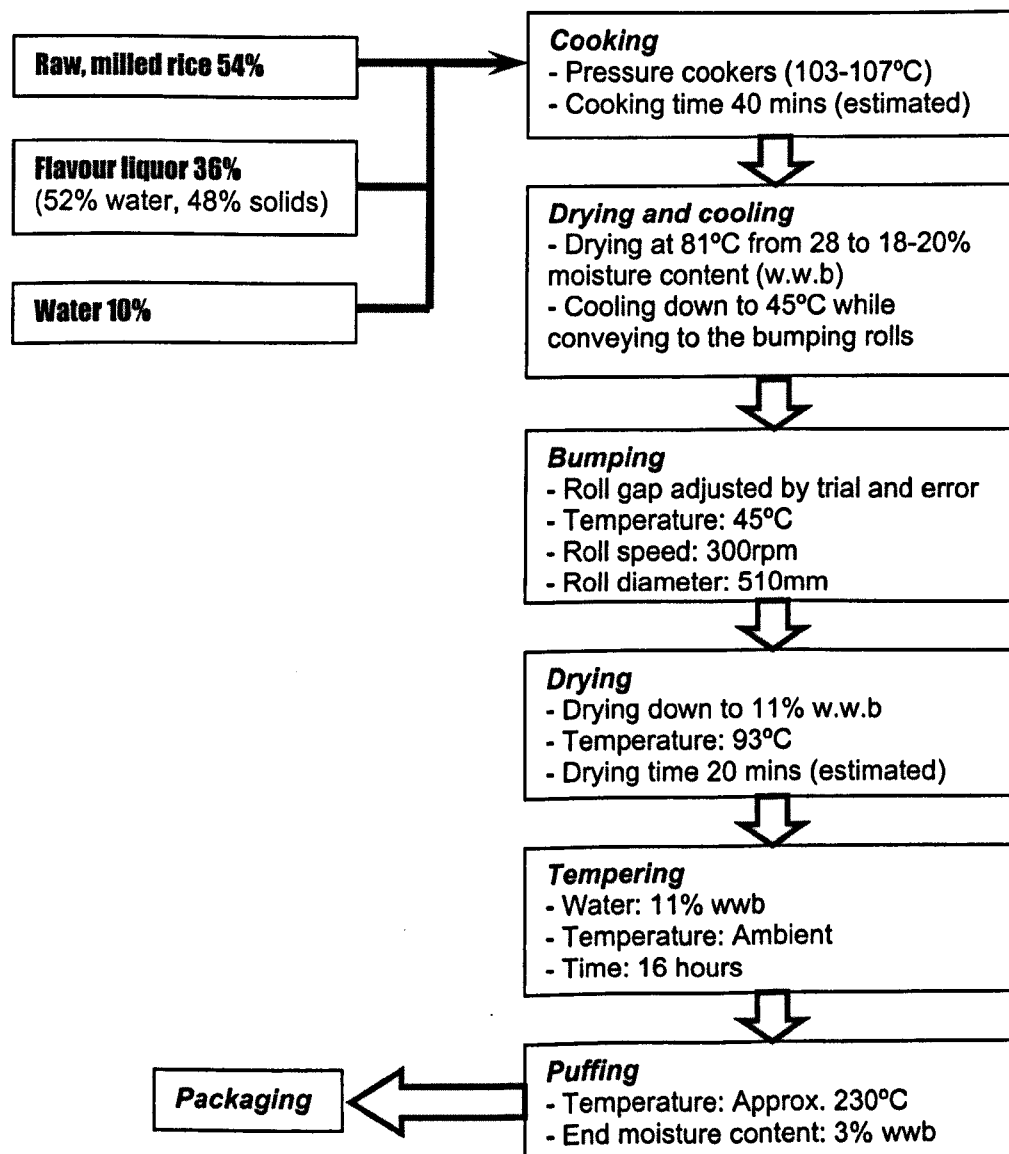


Figure 3.1: Diagram of the Rice Krispies™ industrial process (Manchester factory)

The three important steps in determining the structure of the finished product are outlined below:

- The cooking determines the chemical and mechanical properties of the gelatinised rice grain, particularly the granule structure.
- The bumping consists in compressing the rice grains between two iron rolls and causes mechanical damage to the rice material necessary to achieve a proper expansion of the rice grains.
- The puffing (or toasting) consists in rapidly heating up the material over a 'gas bed' so as to vaporise the water inside the rice grains and force them to expand (puff) through the expansion of the steam bubbles.

In addition, the 16-hour tempering period following the bumping is also known to be of importance, since rice grains puffed straight after the bumping result in less expanded Rice Krispies™.

3.3.2 Milling and cooking

The milling is done on-site at the factory. It consists of the de-hulling and polishing of the rough rice operations (Juliano and Bechtel, 1985).

The cooking is done in rotating batch pressure cookers, at temperatures in the range 103-107°C and under limited water conditions: 28% w.w.b. Before the cooking, the rice is mixed with a 'flavour liquor' containing water (52% w.w.b), sugars (mainly glucose and sucrose) and flavouring agents. More water is added under the form of steam. The proportions of rice, flavour liquor and steam in the batch pressure cookers are 54%, 36% and 10% respectively.

Since the pressure cookers contain no stirring device apart from rotating the cooker itself, the rice grains are subjected to little or no mechanical shear during the cooking stage.

At the end of the cooking all the water is absorbed by the rice grains, which take a translucent, orange aspect due to the added ingredients from the flavour liquor (figure 3.2).



Figure 3.2: Sample of cooked, pre-bumped rice

Microscopic examinations of the cooked rice under both natural and polarised light showed a homogeneous material with no evidence of maltose crosses characteristic of native starch nor of starch granules or granules remnants. It was concluded that the starch was fully cooked and that the starch granules were melted together.

Swales (1999) took a total of 50 samples of pre-bumped rice from the line on different days and at different times in the day. Each sample was ground to a powder and analysed with a standard 12 minutes RVA pasting profile heating the sample from 50°C to 95°C and back to 50°C while stirring at 160rpm. Examples of the profiles, shown on figure 3.3, indicated that some variations occur between batches of cooked rice, in terms of final viscosity.

Another observation on the RVA profile was that the cooked rice samples, although they were cooked and no native granules remained when viewed under the microscope, did not swell in the initial stage of stirring at 50°C, as evidenced by the little increase in viscosity. In other words they had no cold-paste viscosity. Only when temperature reached about 80°C (time 250 seconds on the profile) did the viscosity start to increase significantly, which was interpreted as the hydration (swelling) of starch particles and the release of molecules in the solution. Becker (2001) found similar results when cooking wheat starch in conditions similar to this process rice cooking, and linked the absence of cold paste with the formation of amylose-lipid complexes. Consequently, amylose-lipid complexes became a major

area of investigation in the course of the project.

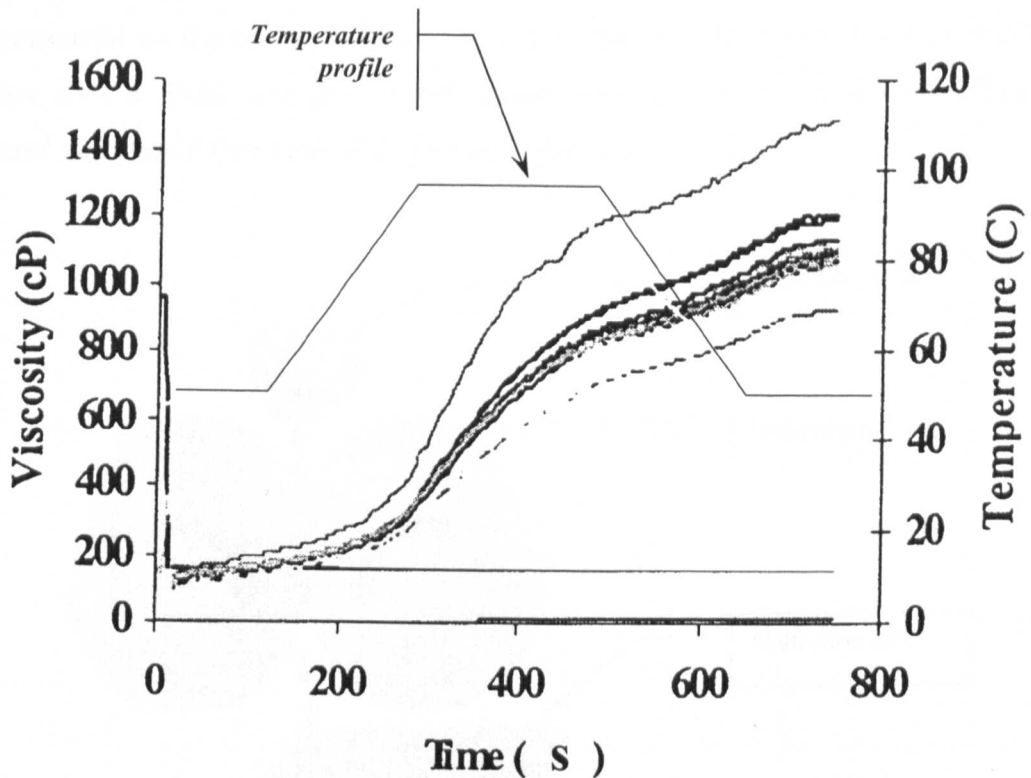


Figure 3.3: Examples of the 50 pre-bumped samples RVA profiles taken from the factory at different times and on different days (Swales, 1999)

3.3.3 After-cooking drying and tempering steps

After cooking, the rice is dried down from 28% to 18-20% moisture content w.w.b, at 81°C.

The rice is then spread on a conveyor belt and slowly moved to the bumping mills. The rice stays on the conveyor belt for approximately 15 minutes, which allows for the tempering of the material and the cooling down to an appropriate bumping temperature, around 45 to 50°C. The main function of the tempering is assumed to be to equilibrate the moisture content inside the rice grains. Some starch retrogradation could also take place at this stage, because the conditions of temperature and moisture content of the material are in the range that allows the phenomenon.

The conditions under which the rice arrives at the bumping step, 18 to 20% moisture content w.w.b and 45 to 50°C, mean that the material is in the rubbery state (cf. chapter 6).

3.3.4 Bumping

The bumping consists in compressing the cooked rice grains between two iron rolls, as represented on figure 3.4. It is similar to the flaking operation of the corn flakes process with a wider roll gap, which means the rice grains are not completely flattened and keep their rounded shape (see figure 3.5).

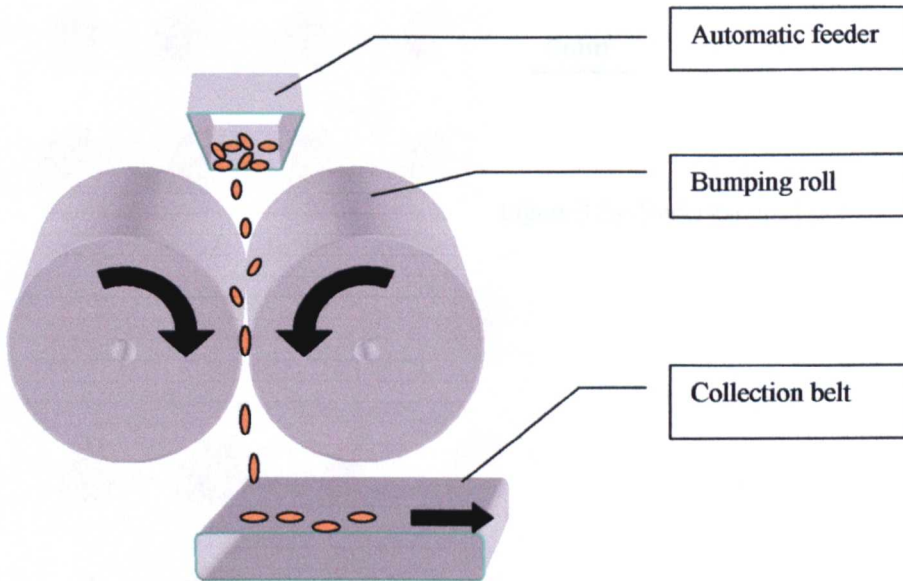


Figure 3.4: Diagram of the bumping rolls

Mill gaps were measured by feeding a solder probe between the rolls at the occasion of a pilot plant trial in Battle Creek and measuring the thickness of the solder coming out of the mill. The normal operating conditions gap was approximately $370\mu\text{m}$. The smallest gap achieved was $250\mu\text{m}$, while the largest was $500\mu\text{m}$.

As a safety feature, one of the pilot plant rolls was spring mounted and therefore was pushed away by the solder as it went through, resulting in an overestimation of the mill gap. By comparing the shapes of pilot plant-bumped rice grains and university-bumped rice grains, for which the mill gap was controlled with a feeler gauge, it was estimated that the gap overestimation with the solder method was between 50 and $100\mu\text{m}$.

Examples of under-bumped, normal bumped and over-bumped samples are shown on figures 3.5a, 3.5b and 3.5c. Factory lore tells that post-bumped grains should be cup-shaped but not squashed (as can be seen on figure 3.5b) for optimal puffing.

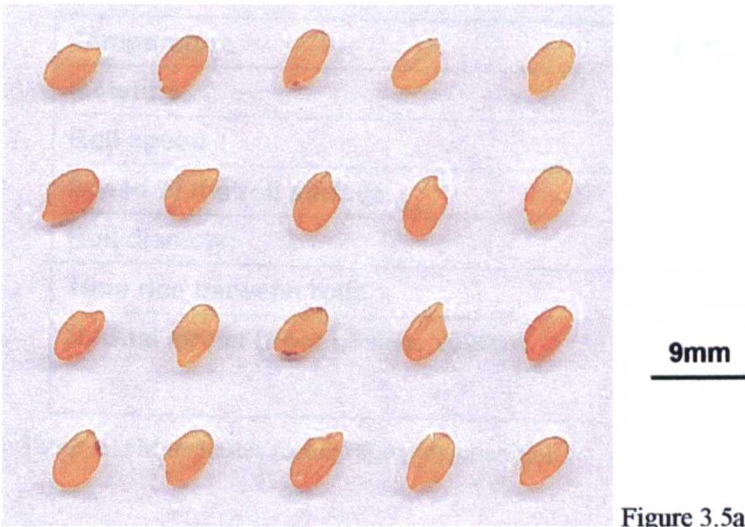


Figure 3.5a: Under-bumped rice

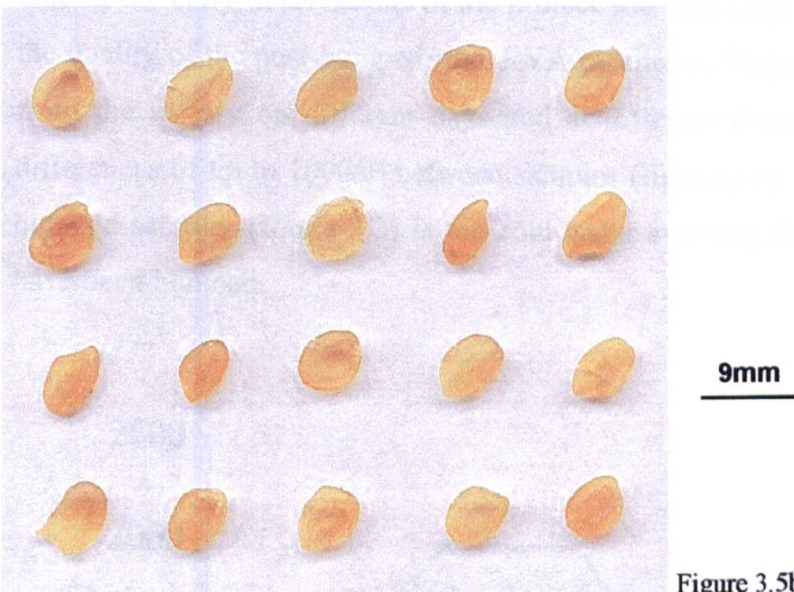


Figure 3.5b: Normal post-bumped rice



Figure 3.5c: Over-bumped rice

Figure 3.5: Examples of post-bumped rice

The bumping conditions at the Manchester factory are summarised in table 3.1.

Temperature	45°C (measured with data logger)
Moisture	18% w.w.b.
Roll speed	300rpm
Speed of the roll surface	8m.s ⁻¹
Roll diameter	510mm
Time rice between rolls	4mm / 8000mm.s ⁻¹ = 5.10 ⁻⁴ s
Normal stress (from Levine, 1996a)	α Roll diameter ^{1/2} α Roll speed ^{1/2}

Table 3.1: Manchester factory bumping conditions

One of the early observations in the project was that large variations could occur in the quality of the post-bumped rice. RVA profiles of 50 post-bumped samples taken from the factory on different days and at different times (Swales, 1999) showed differences of up to 1000cP between samples (figure 3.6). Contrasting with the pre-bumped samples (figure 3.3) is the cold water swelling that occurs after the grains have been bumped.

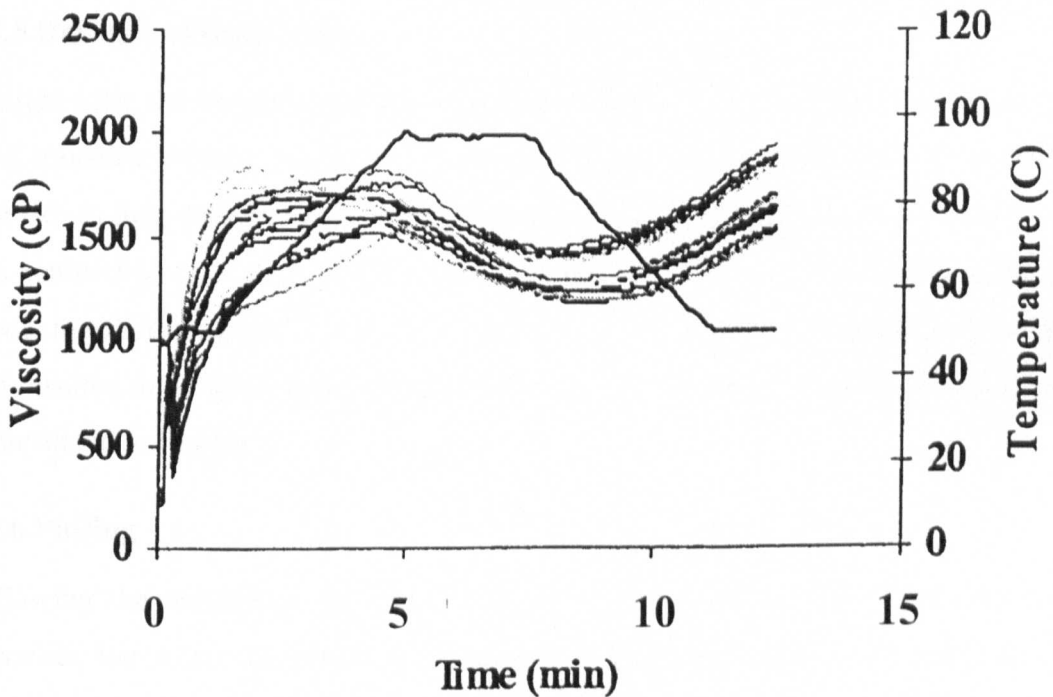


Figure 3.6: Examples of the 50 post-bumped samples RVA profiles taken from the factory at different times and on different days (Swales, 1999)

Consequently, a large part of the work focused on which parameters determine the severity of the bumping and the extent of the post-bumped material damage. Two parameters were thought to have the most direct influence: The mill gap and the bumping temperature. The hypotheses on how they could influence the post-bumped material quality were as follows:

- (i) The severity of the bumping increases when the mill gap decreases, because the force applied on the rice grains becomes higher.
- (ii) The severity of the bumping increases when the temperature decreases, because the rice grains are closer to their glassy state, therefore becoming more brittle and fragile.

The rolls speed could also be of importance, because the glass transition of a polymer also depends on the frequency at which it is measured: The higher the frequency at which the mechanical properties of a material are studied, with a DMTA for instance, the higher the apparent glass transition temperature. Hence, the faster the rolls, the closer to the glassy state the rice material could appear, and thus the more susceptible to damage. The rice variety was also considered.

3.3.5 Drying and tempering

Straight after the bumping the rice material is dried at 93°C down to approximately 11% moisture content w.w.b. The drying process takes approximately 20 minutes. The rice is then tempered, i.e. stored at room temperature for 16 hours. Historically, this tempering step was added to the process a few years after Kellogg began producing Rice KrispiesTM, when the puffing of a batch had to be delayed overnight and resulted in a significantly better product. A detailed study of this tempering step is presented in chapter 8.

3.3.6 Puffing

Following the tempering, the rice is fed by a conveyor belt into a gas bed that vaporises the water contained inside the grains, creating bubbles of steam which force the rice grains to expand. This process is called 'puffing' (figure 3.7).

The puffing conditions are as follows: 230°C for approximately 1 minute. The end moisture content of the rice is between 2 and 3% w.w.b.

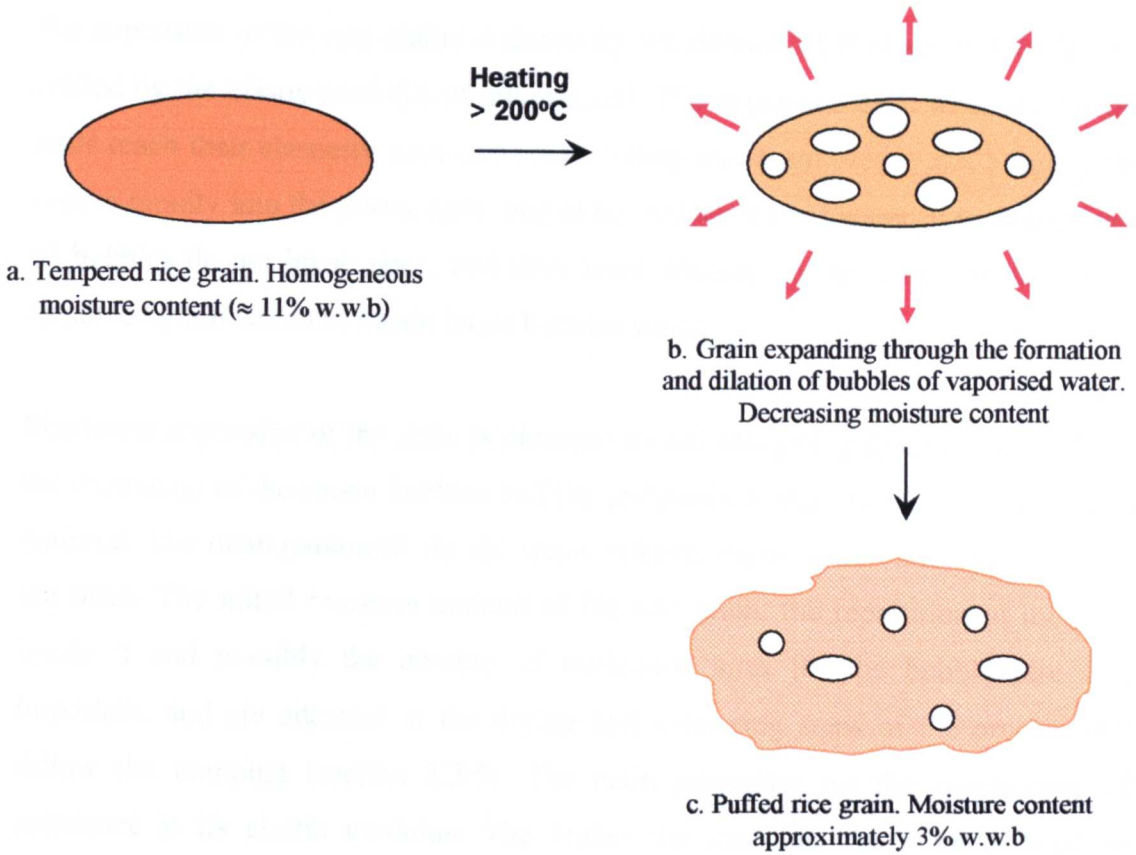


Figure 3.7: Diagram of the puffing mechanism

The result of the puffing is the actual Rice KrispiesTM. Figure 3.8 shows an example of the finished product.



Figure 3.8: Sample of puffed rice (Rice KrispiesTM)

The expansion of the rice grains is driven by the dilation of H₂O steam bubbles and limited by the elastic modulus of the material. The expansion ends when the bubble walls reach their elasticity limit and break, letting the steam escape and bringing the system rapidly into the glassy state, due to the sudden loss of water. It is thought that all bubbles do not break open, and thus some stresses can be stored in the glassy, expanded grain structure inside intact bubbles walls.

Maximum expansion of the grain is obtained by adjusting the parameters controlling the expansion of the steam bubbles and the resistance to the expansion of the starch material. The main parameter for the steam bubbles expansion is the temperature of the oven. The initial moisture content of the rice grain, the repartition of moisture inside it and possibly the amount of nucleation sites for the bubbles are also important, and are adjusted at the drying and tempering steps of the process that follow the bumping (section 3.3.5). The main parameter for the starch material resistance is its elastic modulus: The higher the modulus, the more difficult to expand the material is. It is the role of the bumping (section 3.3.4) to adjust this parameter, by weakening the grain structure and thus decreasing the elastic modulus.

CHAPTER 4: MATERIALS AND METHODS

4.1 INTRODUCTION

This chapter describes the materials used in the course of the project, the methodologies used to prepare the samples, and the techniques used to characterise them.

The different varieties of rice used in the course of the project are summarised in section 4.2.

Several steps of the Rice Krispies™ industrial process have been reproduced on a small scale at the university facilities, and are described in section 4.3. These steps were the bumping, the drying and tempering steps that follow the bumping, and the puffing. The preparation of samples at a small scale allowed a better control of the process conditions, as well as more flexibility than factory trials. The detailed description of the industrial process is covered in chapter 3: Evaluation of the industrial process.

A study of seven raw rice samples was conducted, which involved a series of analytical methods: lipid, protein and amylose contents, amylopectin branch chain analysis by high pressure liquid chromatography (HPLC), separation of amylose and amylopectin by ultracentrifugation, characterisation of the starch gelatinisation by rapid visco-analysis (RVA) and differential scanning calorimetry (DSC). These are presented in section 4.4.

The crystallinity, the degree of gelatinisation, the mechanical properties and the starch average molecular weight in the cooked and post-bumped rice were assessed. The techniques used are detailed in section 4.5: X-rays, rapid visco-analysis (RVA), differential scanning calorimetry (DSC), dynamic mechanical thermal analysis (DMTA), relative viscosity, analytical ultracentrifugation of amylose and amylopectin, capillary rheometry of molten starch and grain damage assessment by

measuring their height recovery.

Finally, two methods were used to characterise the quality of the finished product expansion: Measurement of the expanded grain area and bulk density of the puffed rice (section 4.6).

4.2 MATERIALS

Kellogg provided seven varieties of rice: **Balilla** was the standard variety in use at the UK factory of Manchester at the beginning of the project. It was replaced in year 2000 with the **Selenio (old)** variety. **Elio** is a variety similar to Balilla and Selenio with a higher amylose content. Later in the course of the project, pilot plant scale trials were carried out at the Kellogg WKK research centre in Battle Creek (Michigan), involving **short grain rice (SGR)**, **Bengal medium grain rice (Bengal MGR)** and **Selenio (new)** varieties. Finally, the **medium grain rice (MGR)** standard variety in use at the Omaha and Memphis factories was also provided.

Table 4.1 summarises the seven rice varieties, their codes and origin.

Code	Variety	Origin
RF1	Balilla	Italy
RF2	Elio (high amylose variety)	Italy
RF3	Selenio (old)	Italy
RF4	Selenio (new)	Italy
RF5	Short Grain (SGR)	America
RF6	Bengal Medium Grain (B-MGR)	America
RF7	Medium Grain (MGR)	America

Table 4.1: List of the rice varieties used during the project

The samples were provided at different stages of the industrial process:

- Raw
- Cooked or Pre-bumped
- Post-bumped
- Tempered
- Puffed

Raw, tempered and puffed samples were dry enough to be stored indefinitely at room temperature.

The high moisture content (18-20% w.w.b) of pre-bumped and post-bumped samples meant that they had to be kept in a cold room at 4°C. Later in the project, the necessity to ship samples from the United States to the United Kingdom led to drying the pre-bumped and post-bumped samples down to the moisture content of tempered samples (10% w.w.b), so as to keep them at room temperature without spoilage.

Table 4.2 summarises all the samples received in the course of the project. The numbers refer to the chapters in which work on these samples is discussed.

	Raw	Pre-bumped	Post-bumped	Dried pre-bumped	Dried post-bumped / Tempered	Puffed
Balilla	5	6, 7	6, 7			9
Elio	5, 7					
Selenio (old)	5, 7	6, 7	6, 7		7, 8	9
Selenio (new)	5			7	7	9
SGR	5			7	7	9
Bengal MGR	5			7	7	9
MGR	5			✓	7	9

Table 4.2: Summary of all the samples received in the course of the project. The numbers in the table refer to the chapters in which the samples are discussed. Blank cells and ✓ indicate that the sample was not sent and was not used respectively

Chapter 5 is a summary of the properties of the raw materials. Chapter 6 discusses the role of the glass transition during the Rice KrispiesTM process. Chapter 7 presents the information gathered about the bumping and its effects on the structural and molecular integrity of the rice grain. Chapter 8 examines the phenomena at work during the tempering step. Chapter 9 evaluates the quality of expansion of puffed rice and analyses how the bumping parameters influence it.

4.3 SAMPLE PREPARATION

The samples received from Kellogg (see table 4.2) were prepared with the factory

equipment described in section 3.3 of chapter 3: Evaluation of the industrial process. Experiments conducted in the laboratory were aimed at reproducing under well-controlled conditions the bumping, tempering and puffing steps of the industrial process, using pre-bumped, post-bumped or tempered material received from Kellogg. This section presents the different techniques that were developed for the purpose.

Additionally, a range of analytical techniques such as RVA, X-rays and DSC required the rice samples to be powdered. The protocol and the mills used for that purpose are described in section 4.3.4.

4.3.1 Small scale bumping

Two bumping methods were used:

- The texture analyser allowed a very precise control of the bumping parameters: bumping height, speed of the probe and force exerted on the rice grain. With this method the rice grains were bumped individually to avoid the possibility that the compression force be distributed unevenly between bigger and smaller grains. The drawback was that the method was too slow to produce large amounts of material.
- The roller drier is a kind of miniature model of the factory bumping rolls. It is less precise than the texture analyser but allows larger quantities of samples to be produced.

4.3.1.1 Texture analyser

A texture analyser model TA-HD from Stable Micro Systems (figure 4.1) was used to compress individual rice grains between the flat surface of the instrument base and the flat base of an aluminium cylinder probe (height 40mm, diameter 25mm), and obtain samples for molecular weight analysis. The texture analyser was equipped with a 250kg load cell and operated with the TA-XTRAD software.

The texture analyser recorded the force applied to the probe, the distance of the probe above the base of the instrument and the time since the beginning of the experiment at a rate of 400 points per second (pps).

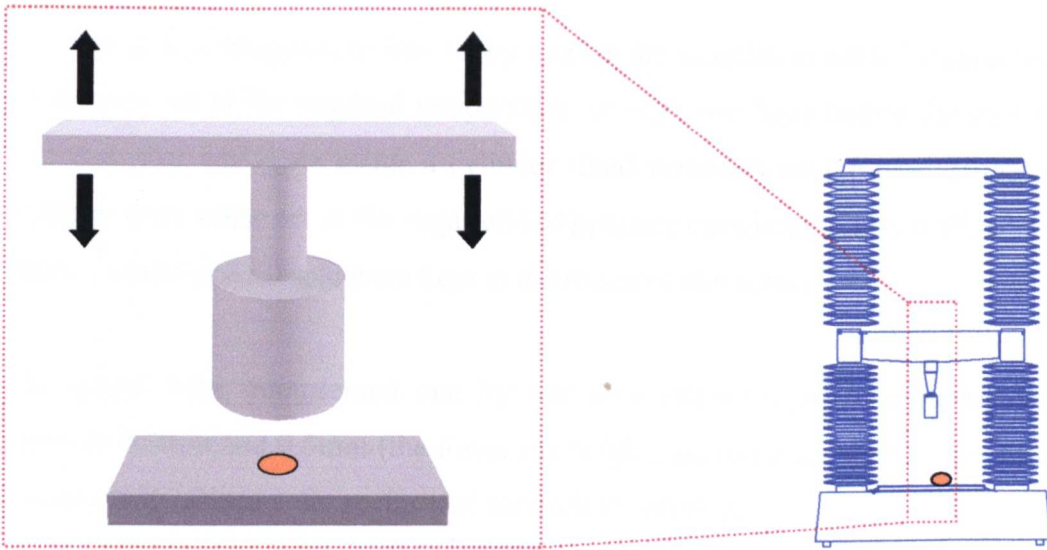


Figure 4.1: Diagram of the Stable Micro Systems TA-HD texture analyser

The horizontal bar ('load cell') holding the probe is not perfectly rigid and bends slightly at high levels of compression (figure 4.2). This means that the recorded compression height can be lower than the actual compression height. Calibration tests performed by pushing the probe against the base in absence of sample showed that under a pressure of 140kg, which was the maximum pressure applied to the rice grains (corresponding to a set compression height of 0.0mm), the load cell deformation was 0.3mm. Because no simple way to measure the actual compression height was found, it appeared preferable to work on the recorded compression height without modifying it, while being aware of the bias.

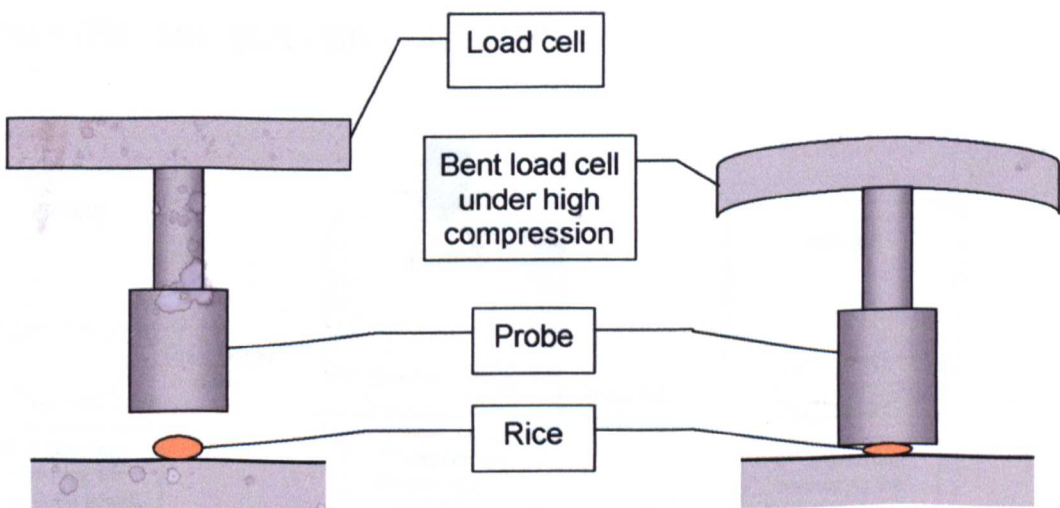


Figure 4.2: Illustration of the bending of the texture analyser load cell under high compression

The rice grains temperature was set by storing the samples in sealed aluminium bags in an oven set at the required temperature, at least one hour before the experiment. The bumping was done inside a cylinder fitted vertically on the base of the texture analyser with water set at the required temperature circulating in its wall, so that the probe and the rice sample were kept at the required temperature.

The grains were compressed one by one to a pre-set height ('bumping height') between 0.0mm and 0.5mm (the lower the height, the more severe the compression). Twenty replications were performed for each experiment.

For each measurement, two parameters were recorded:

- The **peak force** was the force needed to compress the grain down to the required bumping height. It gives an indication of the grain hardness.
- The **resilience** was defined as the ratio 'Recovered height / Compressed height' and is calculated with the formula below (Han and Hill, 1999). It is assumed to be representative of the damage dealt to the rice grains: The more the grain springs back after bumping (i.e. the higher the resilience), the less damaged the grain.

Resilience

$$= (\text{Final height} - \text{Impacting height}) / (\text{Grain height} - \text{Impacting height}) \times 100$$

$$R (\%) = (FH - IH) / (GH - IH) \times 100$$

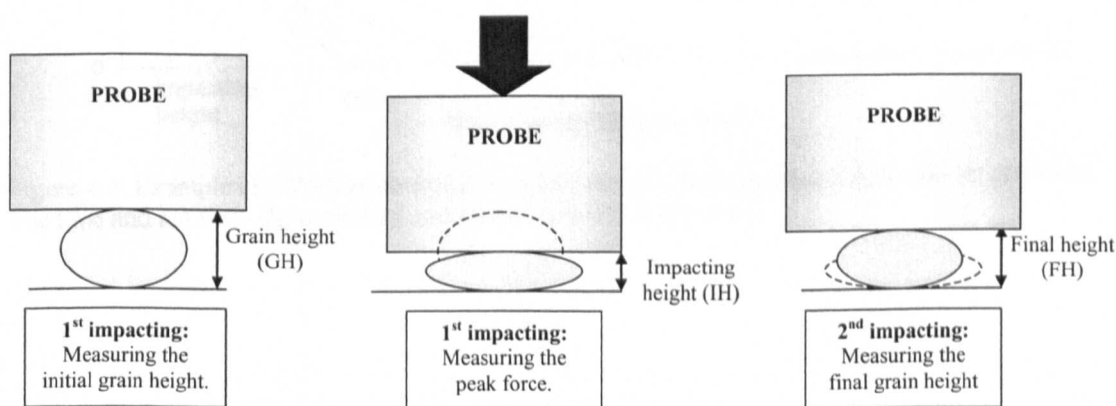


Figure 4.3: Summary of the texture analyser measurements

Figure 4.3 shows how the final height, impacting height and grain height were

measured. These three parameters were defined as follows:

- The impacting height (IH) is fixed by the specifications of each experiment.
- The grain height (GH) is measured at the instant the probe touches the grain on its way down for the impacting. This instant has been arbitrarily defined as the moment the texture analyser detects a force above 50 g.
- The final grain height (FH) is measured after 15 s of relaxation by impacting the grain a second time. The value is recorded when the texture analyser detects a force above 50 g.

Figures 4.4 and 4.5 show a typical measurement, with the Impacting height (IH), Initial grain height (GH), and Final grain height (FH) parameters. The impacting height was set at 0.1mm.

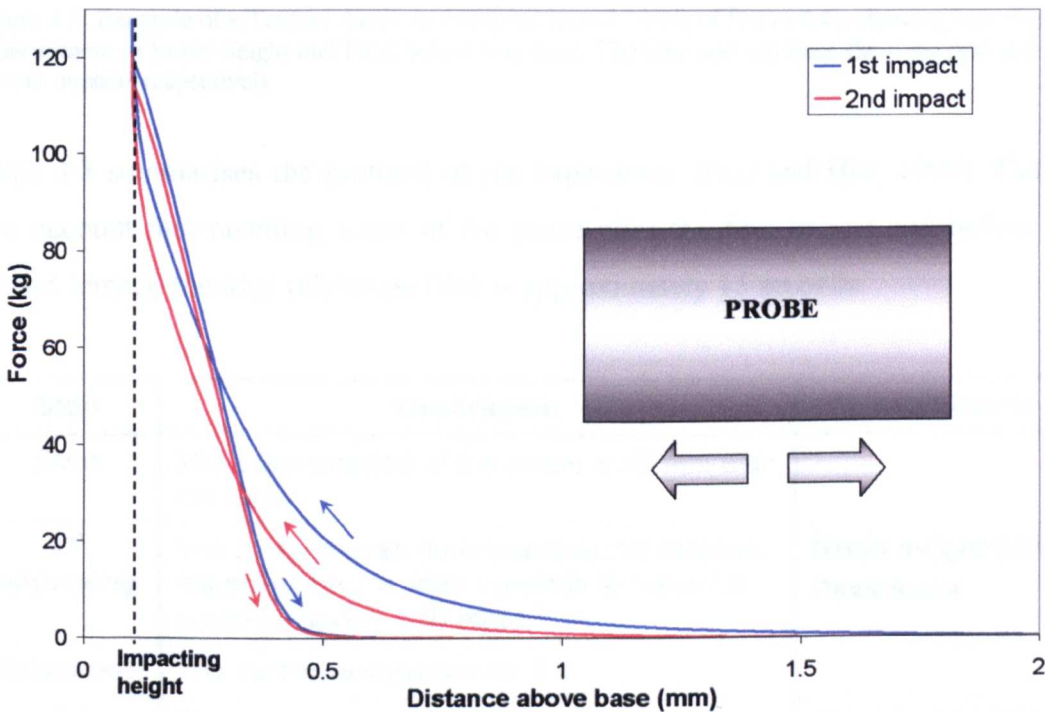


Figure 4.4: Example of a Texture Analyser bumping record. The impacting height was set at 0.1mm. The blue and red lines show the first and second impacts respectively

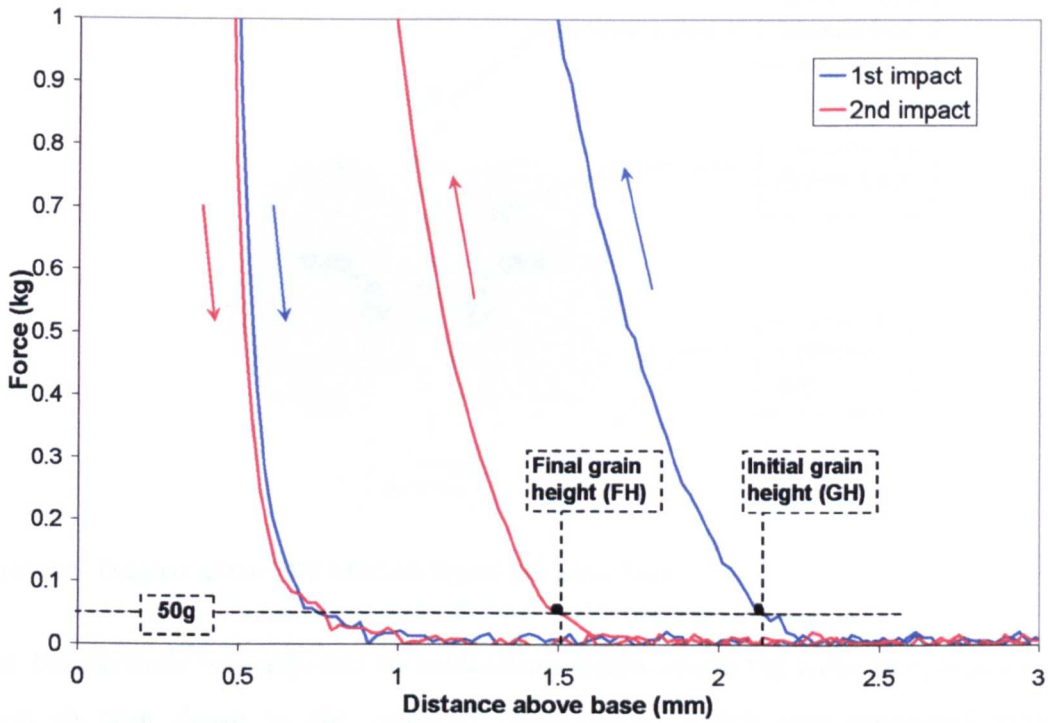


Figure 4.5: Example of a Texture Analyser bumping record (zoom of figure 4.4), showing how the measurement of Initial height and Final height was done. The blue and red lines show the first and second impacts respectively

Table 4.3 summarises the protocol of the experiment (Han and Hill, 1999). Taking into account the travelling times of the probe after the first impact and before the second impact, the total relaxation time is approximately 15 seconds.

Step	Description	Measurements
Start	The initial position of the probe is 50 mm over the base.	
1 st impacting	The probe moves downwards to the required impacting height, then upwards to the initial position. Speed = 10 mm.s ⁻¹ .	Grain height (GH) Peak force
Relaxation	The instrument pauses for 5 s.	
2 nd impacting	The probe moves downwards to the same impacting height, then upwards to the initial position. Speed = 10 mm.s ⁻¹ .	Final height (FH)

Table 4.3: Protocol of the texture analyser experiments

4.3.1.2. Roller dryer

A roller dryer (APV Mitchell Dryers Ltd, series OCD) with the same geometry as the factory mills was used (figure 4.6).

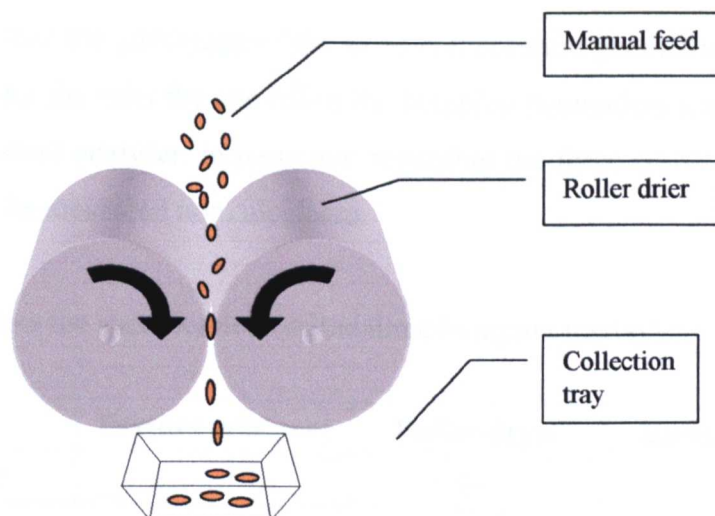


Figure 4.6: Diagram of the APV Mitchell Dryers Ltd roller drier

The temperature was adjusted by circulating steam inside the rolls, then waiting for them to cool down to the required temperature, which was measured with a thermocouple forced into the gap between the rolls. The maximum temperature achievable was 100°C. The roll gap was adjusted with two screws controlling the position of one of the rolls, and measured with a feeler gauge. The range of conditions actually tested was temperatures from 30°C to 80°C and mill gaps from 40 to 700µm.

4.3.1.3 Comparison of the three methods to compress the cooked rice

In the course of the project, three bumping methods were used, each with specific advantages: the texture analyser, the roller dryer and the factory bumping rolls.

When dealing with bumping three elements were considered: the geometry of compression, the compression rate and duration, and the extent of compression.

The texture analyser allowed a precise control of the bumping conditions, in particular the compression height and the force applied to each rice grain. However, the uniaxial compression it exerted on the rice grains (cf. figure 4.2) was considered an approximation of the factory method, where grains are compressed between two rotating rolls (cf. figure 4.6).

The roller dryer had the advantage of the same compression geometry as the factory rolls. However, for the rolls the control of the bumping parameters was less accurate than with the texture analyser, in particular regarding the force applied to the grains which could not be measured nor calculated.

Table 4.4 compares the specifications of the three bumping methods.

	Texture analyser	Roller dryer	Bumping mills
Roll diameter		160mm	510mm
Roll speed		25rpm	300rpm
Compression speed	$10\text{mm}\cdot\text{s}^{-1}$	$160\pi \times 25 / 60$ $= 200\text{mm}\cdot\text{s}^{-1}$	$510\pi \times 300 / 60$ $= 8000\text{mm}\cdot\text{s}^{-1}$
Duration of compression	$< 0.2\text{s}$	$4\text{mm} / 200\text{mm}\cdot\text{s}^{-1}$ $= 2\cdot 10^{-2}\text{s}$	$4\text{mm} / 8000\text{mm}\cdot\text{s}^{-1}$ $= 5\cdot 10^{-4}\text{s}$
Compression height (mill gap)	$0 - 400\mu\text{m}$	$30 - 700\mu\text{m}$	$300 - 500\mu\text{m}$
Force	$< 140\text{kg}$	N/A	N/A
Normal stress (from Levine, 1996a)	$1400\text{N} / 20\cdot 10^{-6}\text{m}^2$ $= 7\cdot 10^7\text{Pa}$	$\propto \text{Diameter}^{1/2}$ $\propto \text{Speed}^{1/2}$	$\propto \text{Diameter}^{1/2}$ $\propto \text{Speed}^{1/2}$

Table 4.4: Comparison of texture analyser, roller dryer and bumping mill specifications

Table 4.4 shows that the compression speed and duration varied widely between the three methods. The compression heights (called mill gaps in the case of the bumping rolls) covered similar ranges for the three bumping methods. However they were measured by different means, such as a feeler gauge or a piece of solder fed between the rolls, and may be incorrect. The texture analyser load cell bent under pressure, which resulted in an underestimation of the compression height (cf. section 3.3.4 of chapter 3: Evaluation of the industrial process). The solder fed between the factory spring loaded rolls pushed them apart, which resulted in an overestimation of the mill gap (cf. section 3.3.4 of chapter 3: Evaluation of the industrial process).

The force applied to the grain was up to 140kg with the texture analyser. The calculation of the force between the two rolls is complex to resolve, in particular because of the difficulty of measuring accurate mill gaps, and was not undertaken. However it is estimated that the force created between the rolls can be much higher than 140kg, due to their larger size and speed. The assessment of starch molecular

weights by ultracentrifugation tended to confirm this, as the amylopectin molecular weight was found to be reduced more by the factory rolls than by the texture analyser. Details of these results are presented in section 7.4.2.1 of chapter 7: The bumping step of the Rice Krispies™ process.

In spite of their differences, all three bumping methods produced puffable post-bumped rice. It was concluded that puffability could be obtained by compressing the material beyond its elasticity limit, which was achieved with the three methods, and that other factors such as the compression rate and force were less important in determining the expansion (cf. chapter 9: Effect of the bumping parameters on the puffed grain quality).

4.3.2 Small scale post-bumping drying step

Knowing the initial moisture content, the initial weight and the required final moisture content of the sample to dry, the weight of sample to attain after drying was calculated with the following equation:

$$W_f = W_i \times (100 - MC_i) / (100 - MC_f)$$

With: W_f Required final weight of the sample

W_i Initial weight of the sample

MC_f Required final moisture content (% w.w.b)

MC_i Initial moisture content (% w.w.b)

A known weight W_i of the post-bumped rice was spread onto a baking tray and kept in an oven at 105°C. The loss of moisture was monitored by weighing the tray at regular intervals, until it reached the required final weight W_f .

Typically, it took approximately 10 minutes to dry 100g of post-bumped rice from 20% to 11% w.w.b moisture content. The corresponding factory drying step takes approximately 20 minutes.

4.3.3 Small scale puffing

Aluminium shelves (figure 4.7) were designed to fit in a hot air oven and resist to the high temperature needed for puffing.

The oven and the shelves were pre-heated to 230°C for at least one hour before the

beginning of the experiment. The rice material was equilibrated at room temperature before puffing.

On each shelf, up to 40g of sample were spread with a wooden spatula and left to toast for 75 seconds. It took about 15 seconds to open the door of the oven, spread the samples and close the door again. This length of time was assumed to be short enough for the temperature of the shelves to be unaltered. At the end of the puffing, the shelves were removed from the oven and the puffed samples were collected and stored at room temperature.

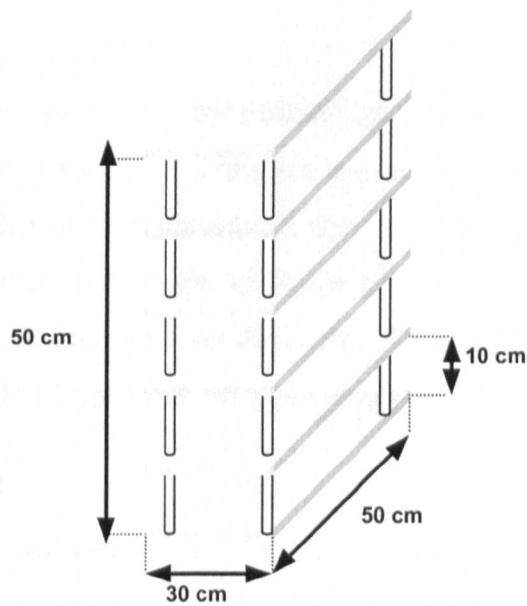


Figure 4.7: Aluminium shelves for rice puffing in a hot air oven

The temperature of 230°C was chosen as the optimal puffing temperature on the university equipment, after a series of tests at temperatures ranging from 200 to 250°C was carried out. Below 230°C the rice grains did not expand fully, while they took a too brown aspect at temperatures above 230°C. Similarly, the time the rice is left in the oven (75 seconds) was chosen as the optimal puffing time, allowing a full grain expansion and avoiding the browning of the material.

4.3.4 Grinding mills

Two mills were used: For large samples, a Retsch mill type ZM1 with a 1mm sieve. For small samples, a Tecator Cyclotec 1093 sample mill with a 1mm sieve.

Samples with 14% w.w.b moisture content or less were hard enough to be ground without further precaution at room temperature. Samples with moisture contents above 14% w.w.b, typically 18-20% w.w.b in the case of the project, became very sticky and formed a paste inside the mill at room temperature. Therefore these samples were frozen at -196°C by dipping them in liquid nitrogen before the milling.

The samples resulting from the milling were used whole, without further sieving to select a specific fraction.

4.4 ANALYSIS OF THE RAW RICE

4.4.1 Lipid content

Crude fat analysis was performed by Soxhlet extraction. A known weight of rice flour (approximately 4g) was put in a thimble and left to reflux in petroleum ether for 18 hours. The lipids dissolved in the solvent were collected in the bottom flask. After evaporation of the ether, the weight of lipids was determined. Unless mentioned otherwise, samples were determined in duplicates. The lipid content was expressed in grams of lipid per 100g of rice flour, on a wet weight basis.

4.4.2 Protein content

Protein analysis was performed by the Dumas method organical elemental analysis (Watson and Galliher, 2001; Wiles *et al.*, 1998). The actual experiments were carried out by a specialist of the university, using a Fisons Instrument NA 2000-N-Protein, automated to load and analyse samples by batches.

A known weight of rice flour (approximately 70mg) was packed in collapsible aluminium trays, heated up to 900°C and burnt out with a burst at 1100°C . The gases resulting from the combustion were eluted with a flow of Helium and trapped on a series of filters, until only the inert gas Nitrogen (N_2) was left in the flow. A final detector recorded the amount of Nitrogen released by the combustion. The percentage of protein in the raw rice was then calculated on a wet weight basis by multiplying the Nitrogen content by the standard conversion factor 6.25. Measurements were calibrated with a standard EDTA sample run before and after the actual samples.

4.4.3 Amylose content

Amylose content was determined with the commercial enzyme-based method Megazyme (Megazyme International Ireland Ltd).

A known weight of rice flour (20 to 25mg) was dissolved by heating at 100°C in 1mL DMSO. Lipids were removed by adding progressively 6mL absolute ethanol to precipitate the starch, which was then recovered by centrifugation at 3000rpm for 5 minutes. The starch was re-dissolved in 1mL DMSO, then diluted to 25mL with a solution of sodium acetate.

In one aliquot (1mL) of the resulting starch solution, amylopectin was precipitated by adding 0.5mL of a 4mg.mL⁻¹ solution of concanavalin A (ConA). Amylose and amylopectin were separated by centrifugation at 13000rpm for 10 minutes. 1mL of the supernatant (containing the amylose fraction) was transferred into a test tube and diluted with 3mL of the sodium acetate solution. The amylose content was determined by digesting it to glucose with 0.1mL of a solution containing amyloglucosidase (3300 U on starch at pH 4.5 and 40°C) and α -amylase (500 U on Ceralpha reagent at pH 5.0 and 40°C). The amount of glucose in the solution was then estimated by adding a solution of glucose oxidase (GOPOD reagent) and measuring the absorbance G_A at 510nm.

A second aliquot (0.5mL) of the DMSO starch solution was diluted with 4mL of sodium acetate. Total starch was determined by digesting both amylose and amylopectin in the aliquot to glucose with 0.1mL of a solution containing amyloglucosidase (3300 U on starch at pH 4.5 and 40°C) and α -amylase (500 U on Ceralpha reagent at pH 5.0 and 40°C). The amount of glucose in the solution was then estimated by adding a solution of glucose oxidase (GOPOD reagent) and measuring the absorbance G_T at 510nm.

The amylose content of the sample was calculated as:

$$\text{Amylose (\%)} = (G_A / G_T) \times (6.15 / 9.2) \times 100$$

Where 6.15 and 9.2 are dilution factors for the Con A and Total starch extract respectively.

4.4.4 Amylopectin branch chain analysis

The distribution of degrees of polymerisation (DP) of amylopectin branch chains was determined by a high-pressure liquid chromatography (HPLC) method developed by Blennow *et al.* (2000). The actual experiments were carried out by Advanced Technologies Ltd (Cambridge).

A known weight of rice flour (150mg) was dispersed in 20mL of a 5mM sodium acetate solution and gelatinised by heating at 100°C in a water bath for 6 minutes, mixing from time to time with a vortex mixer. The sample was cooled down to room temperature and 15µl of isoamylase was added to debranch amylopectin. The sample was incubated in a water bath at 37°C for 4 hours. The enzyme was neutralised by placing the sample in a boiling water bath for 2 minutes. The sample was then cooled down to 4°C and centrifuged at 6000rpm for 2 minutes. The supernatant was collected and diluted five times for injection in the chromatograph.

The details of the chromatography are summarised in table 4.5 and 4.6. The debranched chains of amylopectin are separated in the chromatograph and detected by amperometry as they come out. Their degree of polymerisation is extrapolated from malto-oligosaccharide standard elution times.

Injection volume	5-50µl
Column	Dionex PA 100
Detection	PED - Integrated Amperometry
Flow rate	1.0 ml.min ⁻¹
Solvents	1) 100mM NaOH 2) 100mM NaOH, 0.60M Sodium Acetate
Threshold	1
Area Reject	5000
Peak Width	3.5

Table 4.5: Amylopectin branch chain analysis chromatography protocol

TIME (MIN)	Solvent 1 (%)	Solvent 2 (%)
0.00	100.00	0.00
1.00	100.00	0.00
2.00	100.00	0.00
30.00	0.00	100.00
30.10	100.00	0.00
35.00	100.00	0.00

Table 4.6: Gradient profile for the amylopectin branch chain analysis chromatography

This technique has also been applied to the analysis of cooked rice material, which is discussed in section 7.4.4 of chapter 7: Bumping step of the Rice Krispies™ process.

4.4.5 Rapid Visco-Analyser (RVA)

A Rapid Visco-Analyser (Newport Scientific Ltd, Warriewood, Australia) was used to characterise the pasting properties of raw rice. Rice flour (approximately 4.5g) was dispersed in 25g of distilled water in the RVA canister immediately before starting the measurement. The weight of flour was adjusted to take moisture content into account and disperse exactly 4g of solids. The temperature profile used is indicated in table 4.7.

Step	Temperature (°C)	Duration (s)	Speed (rpm)
Dispersion of the starch powder	50	10	960
Mixing	50	50	160
Warming up	50 to 95	180	160
Holding temperature	95	600	160
Cooling down	95 to 25	180	160
Holding temperature	25	90	160

Table 4.7: RVA rice flour gelatinisation temperature profile. Total duration of the profile: 18min 30s

The results obtained were well reproducible, as illustrated on figure 4.8.

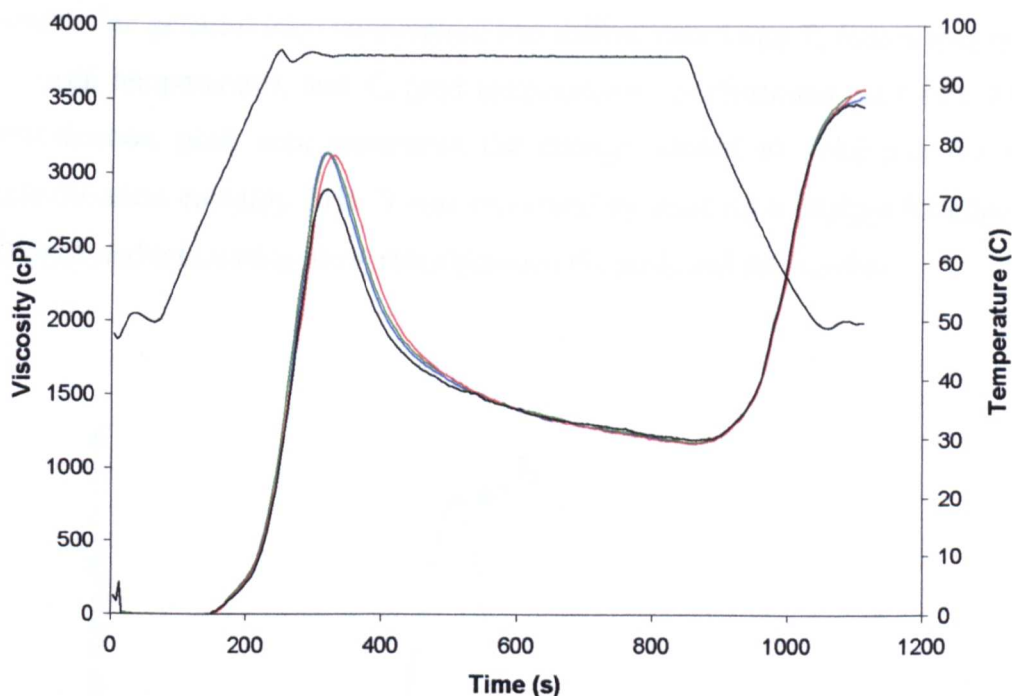


Figure 4.8: RVA profiles of four replications of Balilla rice flour gelatinisation

4.4.6 Differential Scanning Calorimetry (DSC)

Differential scanning calorimetry determines phase changes, such as melting or transition from one crystalline form to another and chemical reactions during which heat is either absorbed or released. The heat gained or lost in these processes is determined by measuring the differential heat flow required to maintain a sample of the material and an inert reference (empty aluminium pan in the reference holder) at the same temperature.

A DSC-7 (Perkin-Elmer, Beaconsfield, UK), calibrated using the melting points of indium (429.8°K) and cyclohexane (279.7°K), was used to analyse the gelatinisation of raw rice flour. About 10mg of flour were weighed in an aluminium DSC pan and mixed with 30mg distilled water, so that the water : flour ratio was 3:1. The sealed pan was scanned at a heating rate of 10°C.min⁻¹, from 0 to 95°C, after overnight storage for equilibration. An empty pan was used as reference during the experiment.

The analysis of the profile consisted in measuring the gelatinisation temperature and peak area. To remove the background effect of the aluminium pan containing the sample, the profile of an empty pan was measured and subtracted from the sample

profile. The gelatinisation temperature was differentiated into T_o (onset temperature), T_p (peak temperature), and T_e (end temperature), as illustrated on figure 4.9. The gelatinisation peak area represents the energy needed to gelatinise the sample (gelatinisation enthalpy ΔH). It was measured by drawing a straight baseline under the peak and integrating the surface between the peak and the baseline.

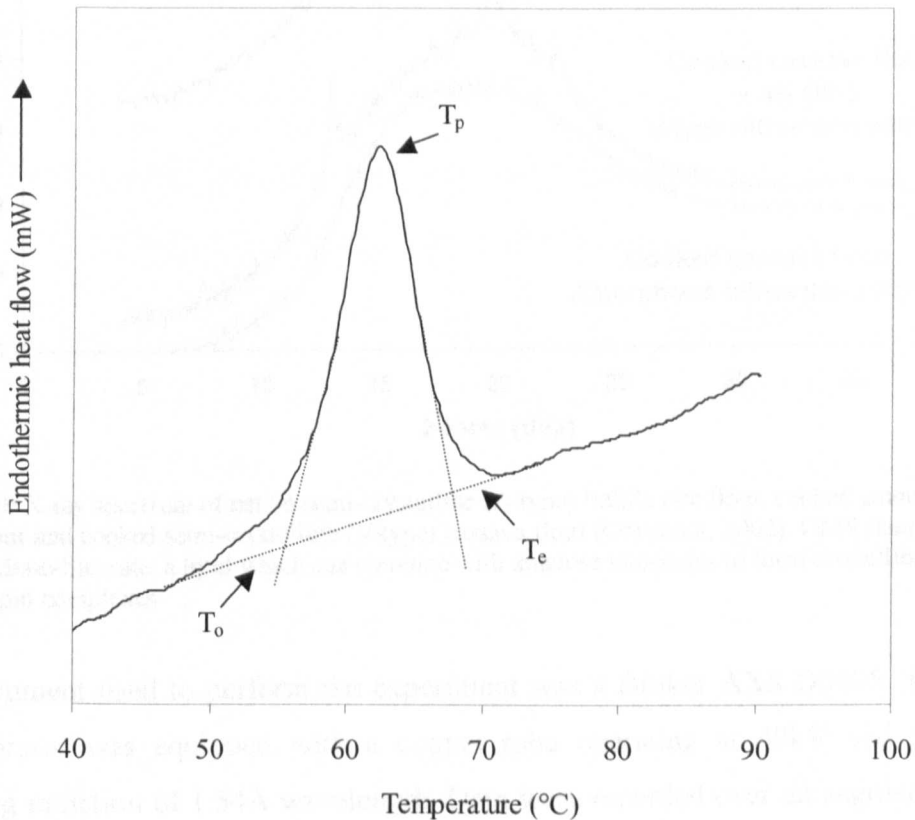


Figure 4.9: Example of DSC endothermic maize starch gelatinisation peak in excess water, showing the onset (T_o), peak (T_p) and end (T_e) temperatures

4.5 ANALYSIS OF THE COOKED RICE

4.5.1 Wide angle X-rays diffraction

X-ray diffraction allows distinguishing between crystalline ordered and amorphous disordered states. Starch material, due to its polymeric nature, can be either completely amorphous, resulting in a diffuse X-ray spectrum, or semi-crystalline, i.e. with parts of the material in a crystalline form, causing the diffraction of X-rays in privileged directions identified by peaks on the X-ray spectrum. Examples of X-rays spectra are given on figure 4.10. 'Wide angle' refers to the specific X-ray technique which analyses the diffraction of rays with large angles of incidence, i.e. above 4° (2θ).

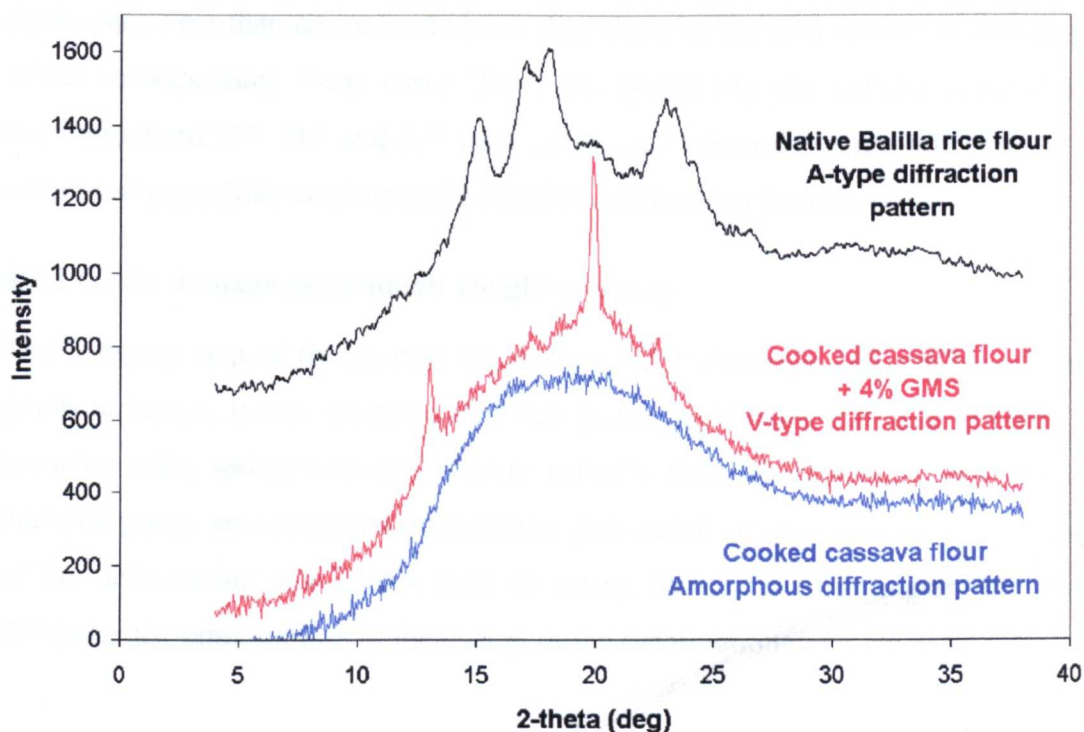


Figure 4.10: X-ray spectrum of native semi-crystalline (A-type) Balilla rice flour, cooked amorphous cassava flour and cooked semi-crystalline (V-type) cassava flour (Onyeador, 2002). GMS stands for Glycerol-Mono-Stearate, a lipid which can combine with amylose molecules to form crystalline amylose-lipid complexes

The instrument used to perform the experiment was a Bruker AXS D5005. The X-ray generator was equipped with a copper tube operating at 40kV and 50mA, producing radiation of 1.54Å wavelength. Data were recorded over an angular range of 4° to 38° (2θ) with an interval of 0.05° and an exposure time of 3 seconds for each angle. The sample was rotated at 60rpm during the measurement in order to reduce the noise created by inhomogeneities within the powder.

The size of the diffraction peaks is sensitive to the hydration level of the crystallites in the material. Hence, before the X-ray analysis, the powdered samples were stored in a dessicator under vacuum over a saturated NaCl solution (relative humidity 75%) at 23°C for one week in order to standardise the moisture content of the samples at about 15% w.w.b.

In the course of the project X-rays were used to assess the amount of crystalline amylose-lipid complexes formed in the cooked rice material. The peak areas were

measured by integrating the X-ray curve between each peak and its baseline. The peak areas were then normalised by dividing them by the area of the amorphous part of the corresponding X-ray curve. The total crystallinity was defined as the sum of the normalised 13°, 20° and 23° peak areas, and was used as an indication of the amount of crystalline amylose-lipid complexes present in the material.

4.5.2 Grain damage assessment: Height recovery

The bumping step of the process (cf. section 3.3.4) damages and weakens the rice grains structure. It was observed that rice grains, after being flattened between the bumping rolls, spring back and recover partially their initial height. This indicates that rice grains are composed of an elastic part which stores a portion of the energy of the deformation and allows them to spring back, and of a fragile part which dissipates the other portion of the energy of the deformation.

Height recovery of the rice grains was used to characterise the amount of damage dealt by the bumping rolls to the grains, and as an estimate of the proportion of elastic and fragile areas inside the material. It was defined as the ratio 'Recovered height / Initial height' and was calculated with the formula below:

$$\text{Height recovery (\%)} = \text{Post-bumped height} / \text{Pre-bumped height} \times 100$$

Measurements were done with a Mitutoyo digital micrometer (precision 0.001mm). Before the measurements, the grains were dried down to 10% moisture content w.w.b at ambient temperature, to ensure they were in a glassy state and were not deformed any further under the pressure of the micrometer. Average heights of 50 pre-bumped and post-bumped rice grains were used to calculate the height recovery.

4.5.3 Dynamic Mechanical Thermal Analyser (DMTA)

The DMTA assesses the structure and properties of solids (mainly polymers) and visco-elastic liquids by measuring their elastic and loss (G' , G'') moduli and the phase angle ($\tan \delta$), as a function of the measurement temperature and of the frequency. The method has a great sensitivity in detecting changes in internal molecular mobility, hence its ability to study glass transition phenomena (T_g) as well as to detect secondary motional transitions.

A DMTA measurement requires bending the sample back and forth and measuring its resistance to the deformation. The DMTA applies a sinusoidal bending whose frequency and amplitude can be chosen in the experimental settings. Figure 4.11 shows a general view of the DMTA and figure 4.12 gives a close-up on how the sample is clamped onto the instrument.

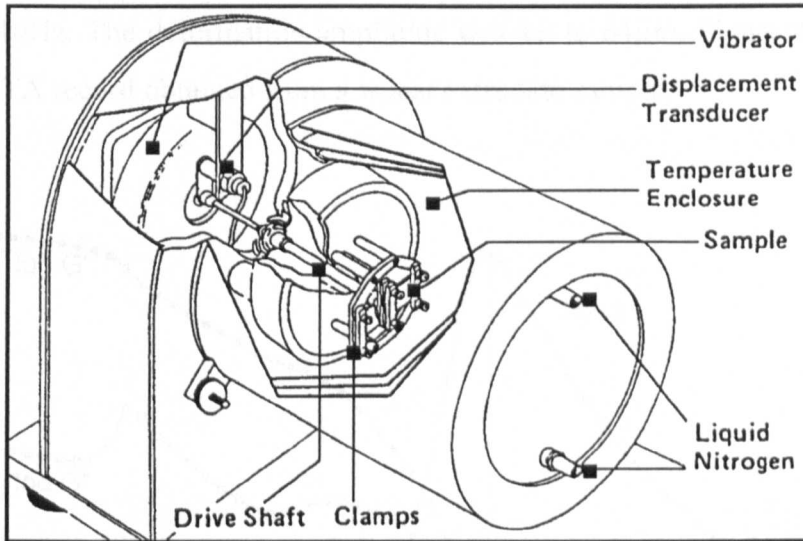


Figure 4.11: DMTA measurement head. The liquid nitrogen inlet and outlet constitute the cooling system of the system, while a resistance in the 'temperature enclosure' ensures the heating.

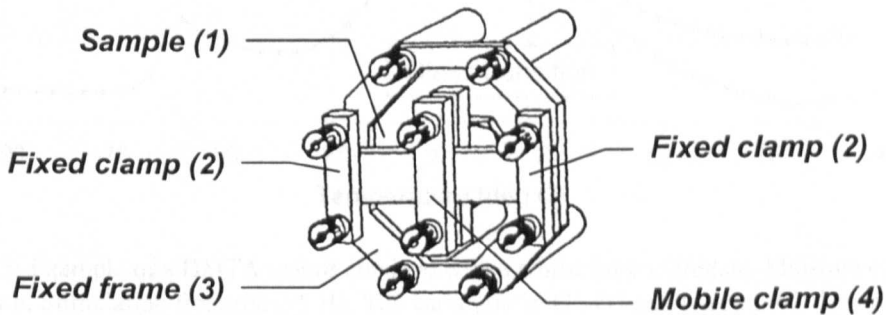


Figure 4.12: Dual cantilever bending geometry of the DMTA head

On figure 4.12 the sample ribbon (1) is clamped (2) along two of its edges on an immobile frame (3), and at its centre on a mobile clamp (4). A sinusoidal stimulation is then applied to the ribbon, through a vibrator attached to the mobile clamp (4). In the course of this project, a single cantilever bending geometry was preferred due to the brittleness of some samples, and thus only one end of the ribbon was clamped on the immobile frame. The sample dimensions were approximately 5.0 x 11.0 x 1.1mm.

The DMTA used was provided by Polymer Laboratories (Loughborough, UK). The sample was covered with silicon oil to limit moisture loss and clamped on the instrument. The sample was cooled down to -100°C with liquid nitrogen, and then warmed up at a rate of $2^{\circ}\text{C}\cdot\text{min}^{-1}$ to 200°C . The elastic modulus G' , loss modulus G'' and $\tan \delta$ were recorded every 4 seconds at three different stimulation frequencies: 0.1, 1 and 10Hz. The deformation amplitude was set to $64\mu\text{m}$. Figure 4.13 shows a typical DMTA record obtained from a wheat extrudate sample.

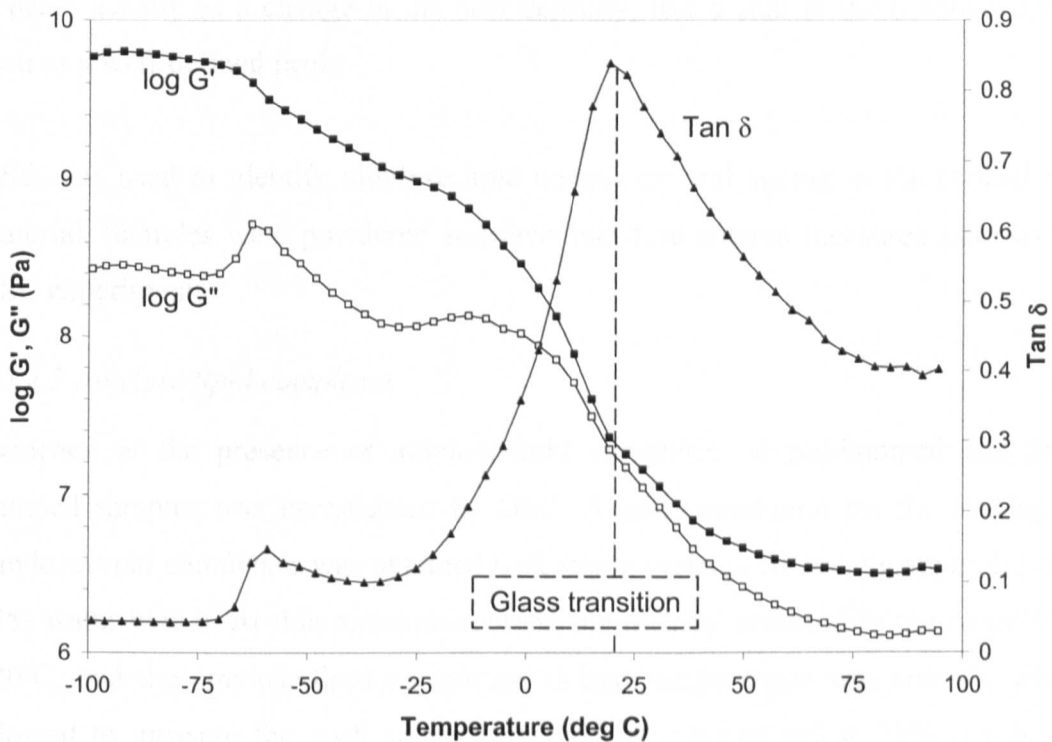


Figure 4.13: Example of a DMTA record obtained with a wheat flour extrudate. Moisture content: 24.6% d.w.b. Stimulation frequency: 5 Hz. The variations in G' , G'' and $\tan \delta$ at -60°C were interpreted as the melting of the silicon oil coating the sample (Carvalho, 2000)

In the course of the project the DMTA was used to determine the glass transition of the cooked rice material. The preparation of the samples for this purpose is described in section 6.3 of chapter 6: Glass transition of the cooked rice.

4.5.4 Differential Scanning Calorimetry (DSC)

4.5.4.1 Method

Differential scanning calorimetry measures the heat flow to or from the studied

sample compared to a reference material, when the sample is subjected to a regular temperature increase.

When a thermal transition occurs in the sample as temperature increases or decreases, a peak in the heat flow is recorded. If the transition requires extra-heat to complete, the peak is qualified of endothermic. A typical example is the melting of ice or the vaporisation of water. If the transition releases heat from the sample, the peak is qualified of exothermic. For example, crystallisation of the sample results in an exothermic peak. A specific case is the glass transition, since this phenomenon appears usually as a change in the heat capacity, like a step in the baseline, rather than as a well-defined peak.

DSC was used to identify amylose-lipid complexes and ageing in the cooked rice material. Samples were powdered and their moisture content measured prior to the DSC experiments.

4.5.4.2 Amylose lipid complexes

Evidence of the presence of amylose-lipid complexes in pre-bumped and post-bumped samples was investigated by DSC. A good resolution for the melting of amylose-lipid complexes was obtained with starch systems containing approximately 75% water w.w.b. At this moisture content, the melting occurred in the range 100-120°C, and the amylose-lipid complexes melting peaks shape was smooth, which allowed to measure the peak areas. For moisture contents below 75% w.w.b, the shape of the amylose-lipid complexes melting peaks was irregular, which made the peak area determination unreliable. For moisture contents above 75% w.w.b, the amylose-lipid complexes melting peaks were smaller than at 75% w.w.b, which decreased the precision of the analysis.

Therefore, for each sample analysis a 1:3 mixture of powdered sample and distilled water was prepared. Approximately 70mg of the mixture were sealed in a stainless steel DSC pan and left to equilibrate at 4°C overnight before the experiment. This caused the retrogradation of the starch material, which appeared as an endothermic peak at 60°C on the DSC profiles. However this peak did not overlap with the amylose-lipid complexes peak that appeared around 100°C, and was not considered a

problem for the experiment.

The DSC protocol consisted in heating up the pan from 20 to 140°C (1st run), cooling down, and heating up again from 20 to 140°C (2nd run). The heating and cooling rates were kept constant and equal to 10°C.min⁻¹. The purpose of the second run was to check the reversibility of the endothermic events observed around 100°C. The melting of amylose-lipid complexes is a rapid reversible phenomenon, which allows to differentiate it from other phenomena observable by DSC such as the gelatinisation or the retrogradation of starch.

The melting enthalpies of the amylose-lipid complexes were measured by drawing a straight baseline under the peak and integrating the surface between the peak and the baseline.

4.5.4.3 Physical ageing

Physical ageing consists in molecular reorganisations occurring in a polymer material in its glassy state, tending towards a tighter packing of the molecules. The phenomenon corresponds to a decrease in the enthalpy of the material, and therefore can be detected by DSC as an endothermic peak, which appears at a temperature roughly half way between the sample storage temperature and the sample glass transition temperature (Martinet, 2001). A second characteristic of the physical ageing endothermic peak is that it increases with the storage time. Physical ageing can be likened to a physical state transition and therefore is completely reversible.

Evidence of physical ageing was investigated in the tempered rice material. To this end, around 50mg of powdered sample, at an approximate moisture content of 11% w.w.b, were packed in a stainless steel pan and analysed. The DSC protocol consisted in heating the sample from -40°C to 90°C at 10°C.min⁻¹.

To study the evolution of physical ageing in the post-bumped, dried rice material a sample with a clear history was produced by running the DSC protocol a first time. Immediately after this first run, a second run was performed to record the profile of the refreshed sample. The DSC measurement was then repeated several times, after increasingly long tempering periods: 1, 2, 3, 4, 6, 8, 10 and 12 hours. The sample

was left to temper in situ inside the DSC instrument at 20°C. Figure 4.14 shows an example of a series of DSC profiles obtained with this method.

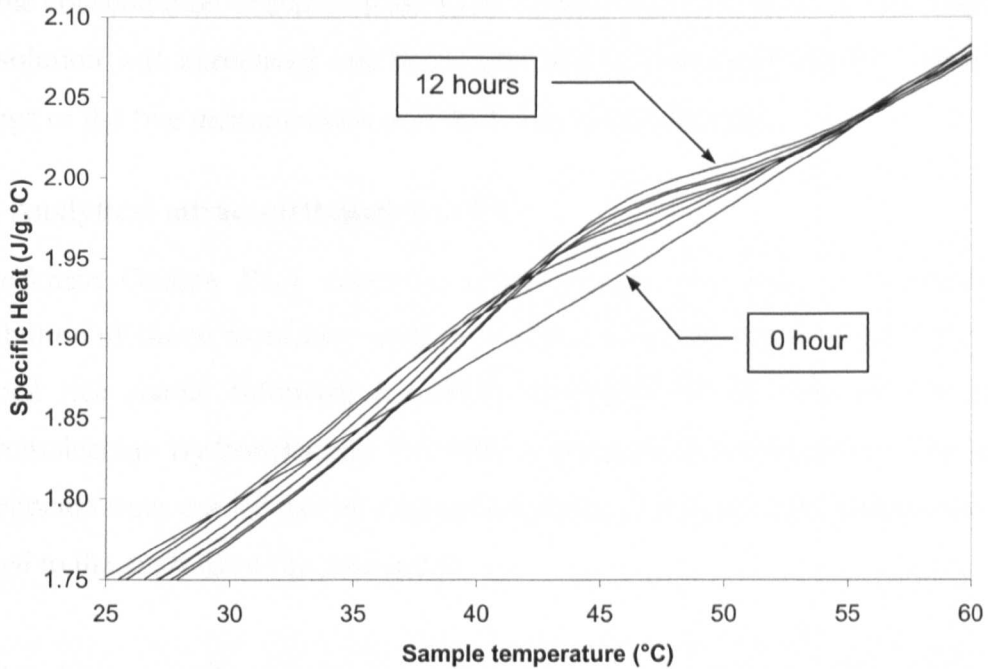


Figure 4.14: Example of physical ageing endothermic peaks identified by DSC in post-bumped rice. Sample moisture content 11% w.w.b.; tempering times: 0, 1, 2, 4, 6, 8, 10 & 12 hours

4.5.5 Relative and intrinsic viscosities

Relative viscosity measurements provide rapid information on the hydrodynamic volume of dissolved starch molecules, which is related to their molecular weight. Harding (1997) wrote a review of the theoretical and practical aspects of intrinsic viscosities measurements of biological macromolecules.

The relative viscosity η_{rel} of a polymer is defined as the viscosity η_p of a dilute solution of polymer divided by the viscosity η_0 of the pure solvent:

$$\eta_{rel} = \eta_p / \eta_0$$

It can be estimated with the following formula:

$$\eta_{rel} \approx t_{sol} / t_0$$

Where t_{sol} is the time needed for a given volume of polymer solution to flow through an Ostwald capillary viscometer (U-tube), and t_0 the time needed for the same volume of pure solvent to flow through the same viscometer.

A 0.3g powdered rice sample was dispersed in 8mL of a 5mol.L⁻¹ potassium hydroxide solution (KOH) and left to solubilise for 20h on a roller mixer, in a 22°C air-conditioned room. The solution was then diluted with 40mL of distilled water, so that the concentration of starch in the final solution was 0.3% w/w. A 2mL aliquot of this solution was introduced into the U-tube and t_{sol} was measured five times. The average of the five measurements was then used to calculate η_{rel} .

4.5.6 Analytical ultracentrifugation (AUC)

A Beckman Optima XL-I analytical ultracentrifuge was used to determine the distribution of starch molecular weights of dilute solutions of pre-bumped and post-bumped rice starch, following a method developed by the National Centre for Macromolecular Hydrodynamics (NCMH, University of Nottingham). The actual experiments were carried out by a specialist of the university. The method was also applied to the analysis of raw rice starch.

Powdered rice starch material was dispersed in 90% DMSO. The starch was solubilised by heating the mixture at 95°C for 15 to 30 minutes in a water bath, then leaving the solution to stir on a roller shaker at room temperature overnight. The starch concentration of the solution was 8.5mg/mL.

A sample of 400 μ L of the solution and 400 μ L of the 90% DMSO solvent were injected in the sample and solvent channels respectively of a 12mm optical path length ultracentrifuge cell, and loaded in the ultracentrifuge. The sample was centrifugated at 50000rpm for 6 hours at 25°C, so that molecules of different molecular weights were separated along the ultracentrifuge cell. The evolution of the sedimentation was followed with a Rayleigh Interference laser cell measuring the difference in refractive index between the sample and solvent solutions. The data was then processed to produce a diagram of the starch solution concentration $g(s^*)$ in function of the sedimentation rate in the ultracentrifuge cell s^* (in Svedbergs). Examples of the results are provided in section 7.4.2 of chapter 7: The bumping step of the Rice KrispiesTM process.

This technique was also applied to the analysis of seven raw rice flours, as discussed in section 5.4.2 of chapter 5: Raw rice material characterisation.

4.5.7 Capillary rheometry

A capillary rheometer was used to measure the viscosity of molten rice starch at a moisture content of 35% w.w.b. The samples used were in the form of powders prepared by grinding post-bumped rice. Moisture contents were adjusted by mixing the powders with the required weight of ground ice and leaving to rest for 24 hours in sealed aluminium bags at 4°C.

Initially the measurement of molten rice starch viscosity at 20% moisture content w.w.b was attempted, so that no water would need to be added to the post-bumped rice material. However the 20% moisture content w.w.b post-bumped rice powder burnt rather than melted with the equipment available in the lab. Hence the moisture content of the material was increased to 35% w.w.b, at which level a proper melt could be achieved.

The instrument used was a Rosand RH-7 (Rosand Precisions Ltd, Stourbridge, UK). Figure 4.15 shows the details of the instrument. The specifications are reported in table 4.8.

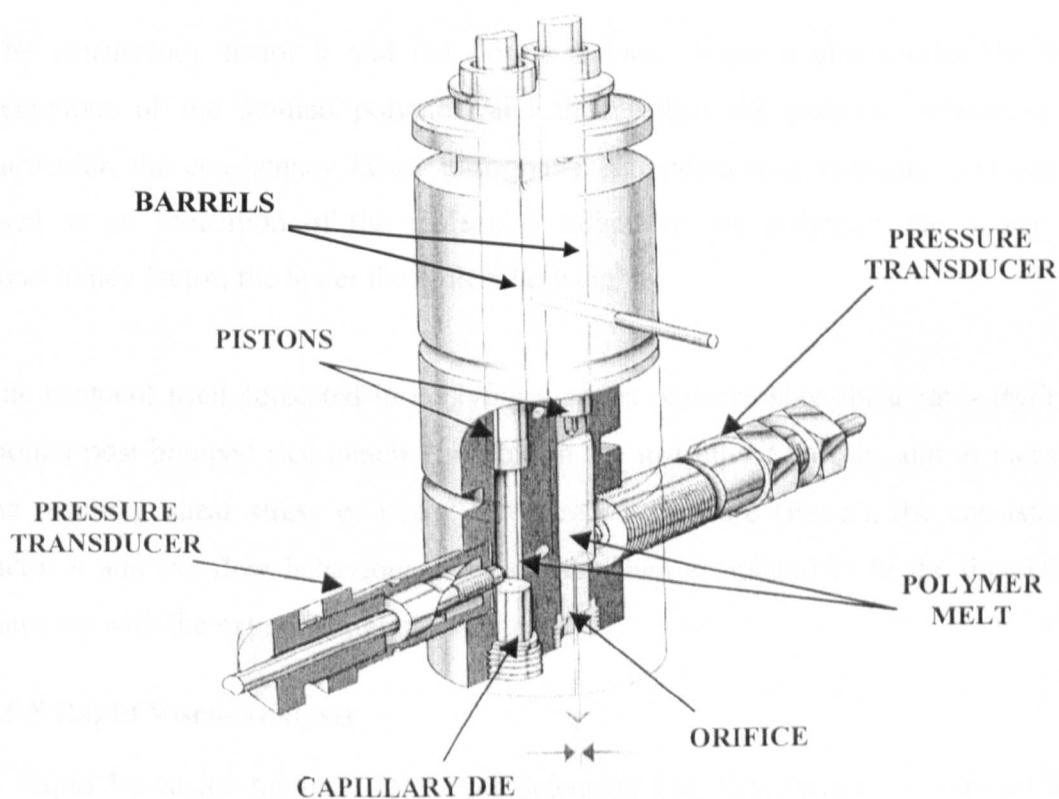


Figure 4.15: Diagram of the Rosand RH-7 capillary rheometer (Becker, 2001)

	Left barrel	Right barrel
Length (mm)	280	280
Diameter (mm)	15	15
Capillary die length (mm)	32	0
Capillary die diameter (mm)	9	9
Capillary die orifice (mm)	2	2
Temperature (°C)	95	95
Pressure transducer max force (psi)	10 000	1500
Maximum pressure build-up (MPa)	58	8

Table 4.8: Specifications for the Rosand RH-7 capillary rheometer

The flow of a molten polymer is described theoretically by the Ostwald - de Waele equation:

$$\sigma = k.(\partial\gamma/\partial t)^n$$

With:

σ : Shear stress (Pa)

$(\partial\gamma/\partial t)$: Shear rate (s^{-1})

k : Consistency factor (Pa.s)

n : Flow behaviour index

The consistency factor k and the flow behaviour index n characterise the flow behaviour of the studied polymer, and thus reflect the polymer properties. In particular, the consistency factor is formally equivalent to a viscosity, and can be used as an indication of the molecular weight of the polymer: The lower the consistency factor, the lower the molecular weight.

The protocol used consisted in applying a series of increasing shear rates $\partial\gamma/\partial t$ on molten post-bumped rice material packed in the instrument barrels, and to measure the resulting shear stress σ . Using a regression software (Excel), the consistency factor k and the flow behaviour index n were then calculated to fit the theoretical equation with the experimental measurements.

4.5.8 Rapid Visco-Analyser

A Rapid Viscosity Analyser (Newport Scientific Ltd, Warriewood, Australia) was used to characterise the rheological behaviour of cooked starch in excess water.

Approximately 5.7g of powdered cooked rice (pre-bumped or post-bumped) were dispersed in 25g of distilled water in the RVA canister immediately before starting the measurement. The weight of powder was adjusted to take the sample moisture content into account and disperse exactly 5g of solids.

Because cooked starch has the ability to partially swell in cold water and thus increase the viscosity of the suspension at room temperature (cold paste viscosity), a temperature profile with a long initial stirring step at 25°C followed by a warming and cooling cycle up to 95°C and back to 25°C was chosen, as shown in table 4.9. The total duration of the profile is 45 minutes.

Step	Temperature (°C)	Duration	Speed (rpm)
Dispersion of the starch powder	25°C	10"	960
Cold paste viscosity	25°C	15' 50"	160
Warming up	25 to 95	7'	160
Holding temperature	95	10'	160
Cooling down	95 to 25	7'	160
Holding temperature	25	5'	160

Table 4.9: RVA cold paste viscosity temperature profile

Figure 4.16 shows two typical RVA profiles obtained using this temperature profile, one with pre-bumped rice, the other with strongly bumped rice.

A first increase in viscosity occurs in the case of the strongly bumped sample at 25°C, and a second one after the beginning of the warming up. The cooling triggers a third increase in viscosity associated with the re-ordering of starch molecules, which leads to the formation of a thick paste or gel. These three increases in viscosity were chosen as parameters to characterise the RVA profiles, and were labelled 'cold paste viscosity' (CP), '95°C viscosity' (95C) and 'final viscosity' (FV) respectively. Table 4.10 summarises these parameters and the times at which they were measured.

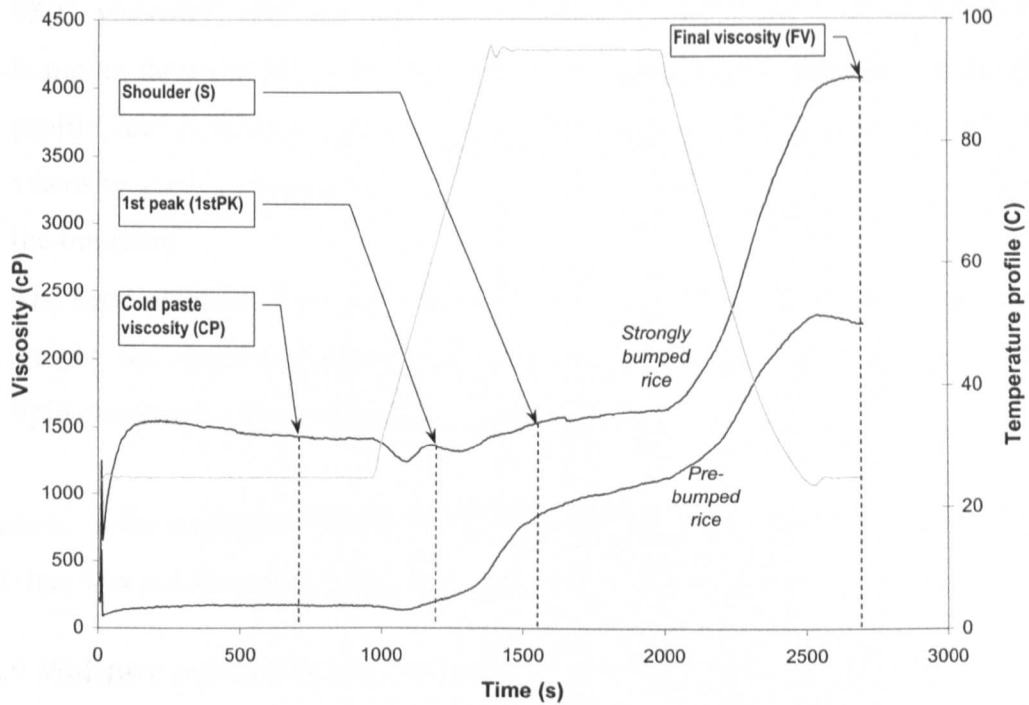


Figure 4.16: Typical RVA cold paste profiles

In the course of the project it was observed that the viscosity at the beginning of the RVA profile seemed to increase more steeply when the sample was more heavily bumped. An attempt to quantify this was made by measuring the ‘initial slope’ (IS) of the RVA curve between the times 20 and 72 seconds, as indicated on table 4.10.

Event	Abbreviation	Time measured (min)
Initial slope ($\text{cP}\cdot\text{s}^{-1}$)	IS	Slope between 20 and 72s
Cold paste viscosity (cP)	CP	12min (720s)
95°C viscosity (cP)	95C	26min (1500s)
Final viscosity (cP)	FV	End of the curve: 45min (2700s)

Table 4.10: Parameters measured on the RVA cold paste profile

Each of the four parameters brings specific information on the state of the starch in the pre-bumped and post-bumped rice samples.

- **Initial slope:** The hypothesis is that this parameter reflects how fast the starch molecules, in particular amylose, can leach out of the material into the solution, and thus gives an idea of the extent of the damage done by the bumping.
- **Cold paste viscosity** also gives an idea of the extent of the damage done to the rice grains: The more damage, the more starch molecules will leak into the solution at room temperature and increase the viscosity.

- **95°C viscosity:** The rice grain starch material that is left undamaged by the bumping does not leach into the solution during the cold paste step of the RVA profile, and is released when the solution is heated to 95°C. Therefore the 95°C viscosity gives complementary indications of the extent of the damage caused by the bumping.
- The **final viscosity** provides information on several factors: The starch molecular weight, the amount of amylose present in the solution, the presence of amylose-lipid complexes, the retrogradation rate of starch molecules.

Remark: In the course of the project the initial slope did not yield useful information, and thus was not discussed in the thesis.

4.5.9 Moisture content determinations

Moisture content determinations were performed by drying 3 to 5g of sample in a 105°C oven for 18 hours. The moisture content (MC) was expressed on a wet weight basis (w.w.b) as:

$$\text{MC (\%)} = (\text{Wet sample weight} - \text{Dry sample weight}) / \text{Wet sample weight} \times 100$$

The measurements were done in three replicates.

4.6 ASSESSMENT OF THE PUFFED RICE GRAINS EXPANSION QUALITY

4.6.1 Grain area

The extent of the expansion of puffed rice was characterised by taking a picture of 50 grains with an office scanner (Acer ScanPrisa 640U, resolution: 200dpi). Figure 4.17 gives an example of such a picture. Using a picture analysis software (Scion Image version beta 3b by Scion Corporation), the picture was converted into pure black and white so that the rice grains appeared as black shapes on a white background. The limit between the white and black domains was adjusted manually. The projected area of each rice grain onto the scanner glass bed was defined as the area of the corresponding black shape and was measured in pixels. The number obtained was then converted in square millimetres using the picture, taken at the same time as the samples, of an object of known dimensions (a penny coin) as a scale. The average grain area of the 50 grains was calculated.



Figure 4.17: Example of a picture of 50 puffed rice grains

4.6.2 Bulk density

Another method, in use at the factory, to characterise the expansion of the puffed grains is to weigh a known volume of sample and to calculate its bulk density.

At the university a square, metallic container of dimensions $L \times l \times h = 75.8 \times 75.5 \times 92.4\text{mm}$ was used to perform this analysis (figure 4.18). The exact volume was determined by filling up the box with distilled water at 25°C : 0.525L.

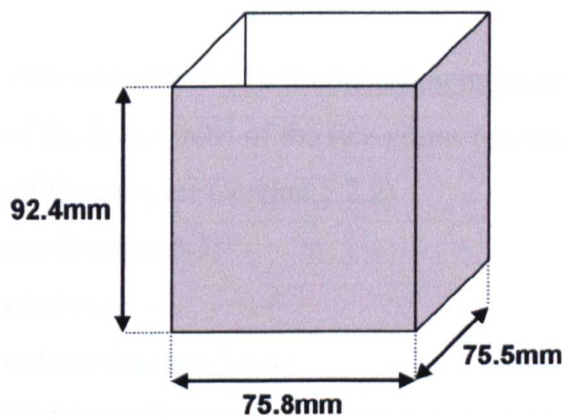


Figure 4.18: Box used for the can weight and bulk density characterisation at the university

To determine the bulk density of a sample, the box was over-filled with the puffed rice sample, then the excess was removed by sweeping a ruler across the top of the box. Three replications were done and the average weight and bulk density, as well as the standard deviation were calculated.

CHAPTER 5: RAW RICE MATERIAL CHARACTERISATION

5.1 INTRODUCTION

This chapter presents the results of a series of characterisations performed on the raw rice material. These characteristics may have an influence on the end product, as will be discussed in the following chapters.

Seven varieties of rice were studied, as shown on table 5.1.

Code	Variety
RF1	Balilla
RF2	Elio (high amylose variety)
RF3	Selenio (old)
RF4	Selenio (new)
RF5	Short Grain (SGR)
RF6	Bengal Medium Grain (B-MGR)
RF7	Medium Grain (MGR)

Table 5.1: List of the rice varieties used during the project

All varieties have been characterised with the following techniques:

- Measurement of the dimensions of the rice grains (section 5.2.1)
- Bulk densities of the samples (section 5.2.2)
- Moisture contents (section 5.3)
- Starch characterisations:
 - Amylose contents (section 5.4.1)
 - Amylopectin debranching and side chain length analysis (section 5.4.2)
 - Amylose and amylopectin separation by ultracentrifugation (section 5.4.3)
- Protein content (section 5.5)
- Crude fat analysis (section 5.6)
- Rice gelatinisation behaviour: RVA and DSC profiles (section 5.7)

Each technique is described in detail in chapter 4: Materials and methods.

5.2 DIMENSIONS AND BULK DENSITY OF THE RAW MATERIAL

5.2.1 Grain dimensions

The height H , width W and length L of ten raw rice grains of each variety were measured in millimetres with a Mitutoyo digital micrometer. Figure 5.1 shows how the measurements were done.

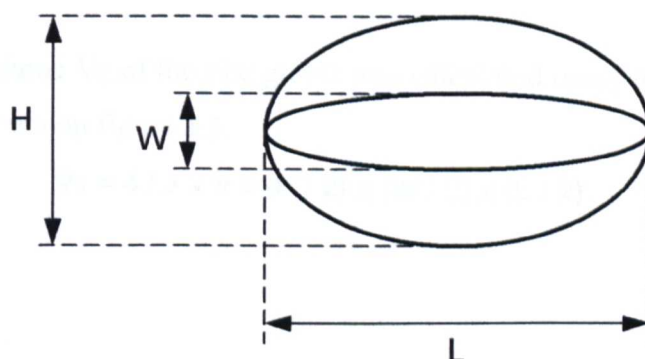


Figure 5.1: Measurement of raw rice grain dimensions Height x Width x Length (HxWxL)

The average dimensions and standard deviations of the ten grains were calculated for each variety. The results are shown on figure 5.2.

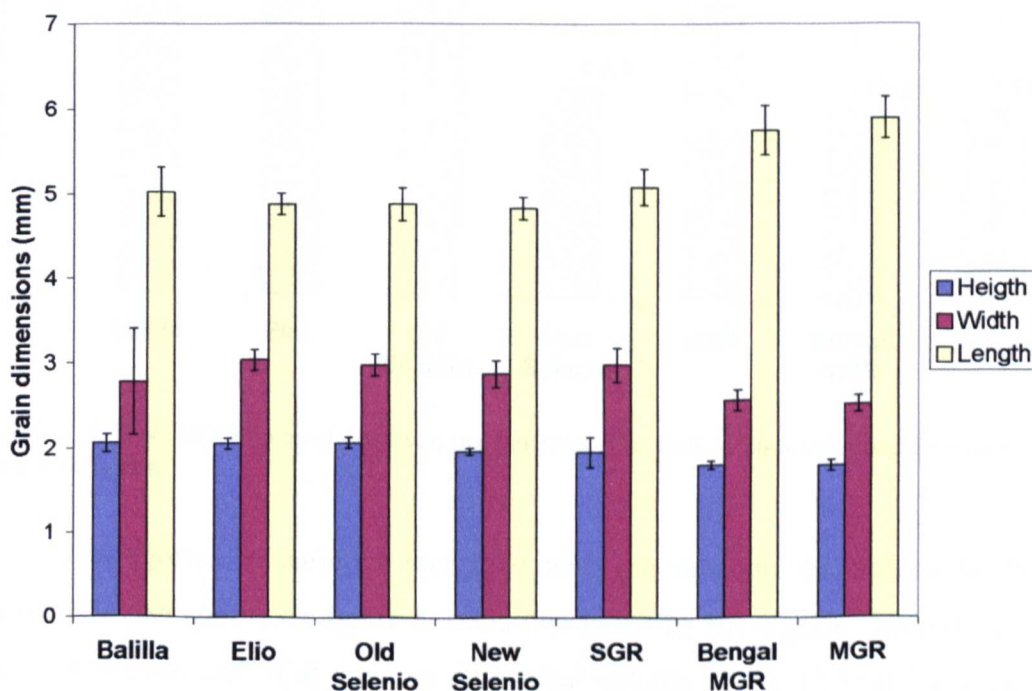


Figure 5.2: Grain dimensions (height, width and length) of the seven rice varieties. The vertical lines show two times the standard deviation

From the histogram, two categories of varieties can be identified:

- (i) The Balilla, Elio, Old Selenio, New Selenio and SGR varieties are shorter and

thicker with the dimensions HxWxL in the range 2.0-2.1 x 2.8-3.0 x 4.8-5.1mm. One way of summarising this is to say that Balilla, Elio, Selenio and SGR are all varieties of the short grain rice family.

(ii) The Bengal MGR and MGR varieties are longer and thinner with the dimensions HxWxL in the range 1.8 x 2.5-2.6 x 5.7-5.9mm. This is expected from medium grain varieties compared to short grain varieties.

The ellipsoidal volume V_E of the rice grains was calculated using the formula below.

The results are shown on figure 5.3.

$$V_E = 4 / 3 \times \pi \times (H / 2) \times (W / 2) \times (L / 2)$$

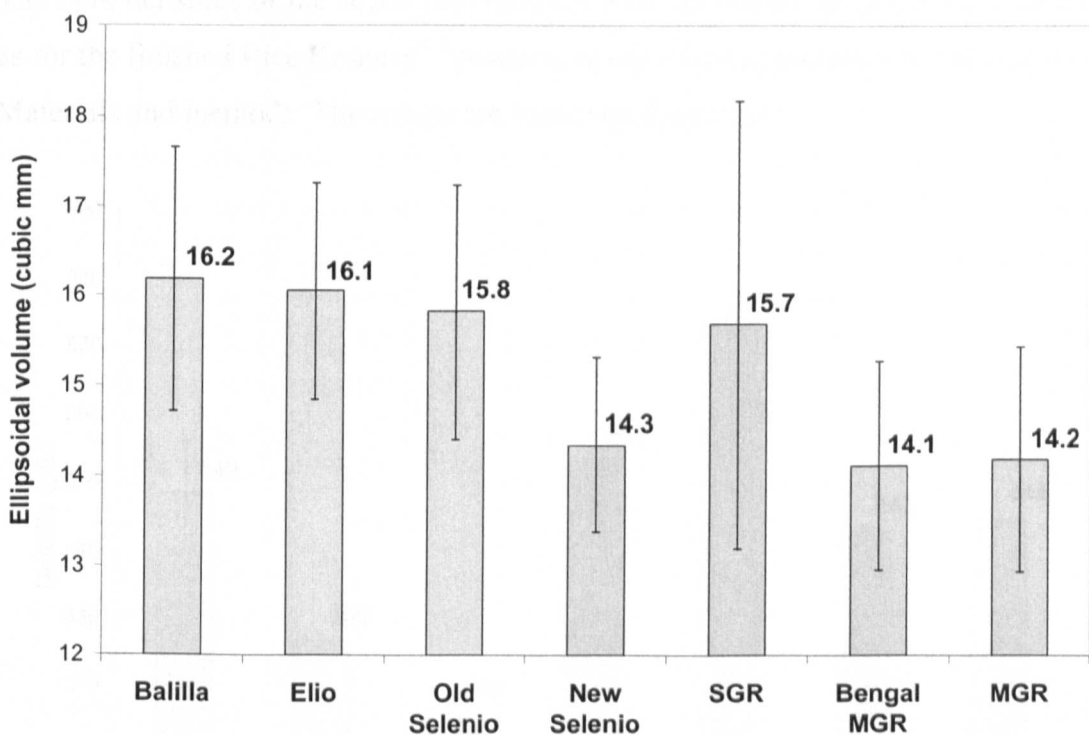


Figure 5.3: Ellipsoidal volumes of the seven rice varieties. The vertical lines show two times the standard deviation

The two categories of varieties identified with the separate dimensions H, W, L (figure 5.2) also appear on figure 5.3: On one hand the short grain varieties Balilla, Elio, Old Selenio and SGR have an ellipsoidal volume above 15.5mm^3 , and on the other hand the medium grain varieties Bengal MGR and MGR have an ellipsoidal volume of approximately 14mm^3 . Although the New Selenio was classified with the short grain varieties, based on its dimensions H, W, L, its ellipsoidal volume (14.3mm^3) is more similar to the ones of medium grain varieties. These volumes figures should be taken with a little caution since assimilating a rice grain to an

ellipsoid is an approximation of its real shape.

The size and shape of the rice grains may be important for the cooking: Rice grains from the short grain variety have a smaller surface area : volume ratio compared to grains from the medium grain variety, which may result in less water migrating into the grains during the cooking. Also, the distance water needs to cover to reach the grain centre is longer in the case of the short grain variety. Thus short grain varieties may need longer cooking times than medium grain varieties.

5.2.2 Bulk density

The bulk densities of the seven rice varieties were measured using the same method as for the finished Rice Krispies™ product, as described in section 4.6.2 of chapter 4: Materials and methods. The results are shown on figure 5.4.

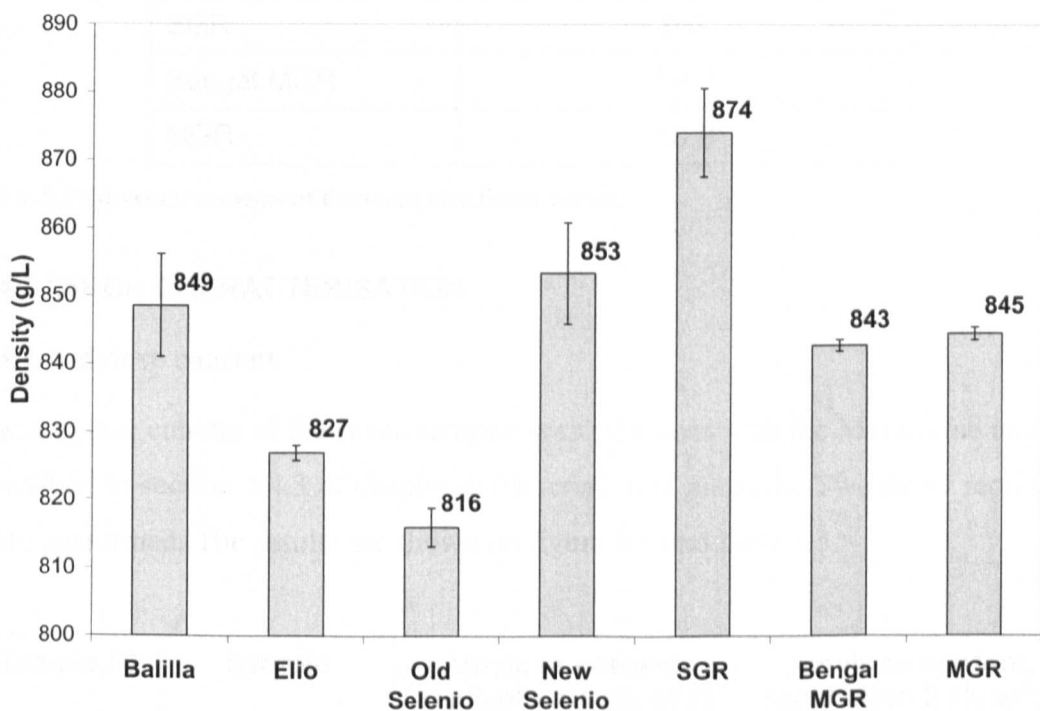


Figure 5.4: Bulk densities of the seven rice varieties. The vertical lines show two times the standard deviation

The histogram indicates that SGR and MGR varieties are different, which may reflect the differences in geometry (see previous section). However Balilla, Elio and Selenio variations are unexplained.

An ANOVA analysis with 5% confidence level indicated that Elio, Selenio (old),

Selenio (new) and SGR varieties were all significantly different from all other varieties. Balilla, Bengal MGR and MGR varieties were not significantly different from each other.

5.3 MOISTURE CONTENTS

The moisture contents of the raw rice flours were determined in triplicates at 105°C for 18 hours. Table 5.2 shows the average results.

Variety	Moisture content (% w.w.b)
Balilla	10.6
Elio	11.1
Old Selenio	11.0
New Selenio	12.1
SGR	9.7
Bengal MGR	10.4
MGR	10.6

Table 5.2: Moisture contents of the seven rice flours varieties

5.4 STARCH CHARACTERISATION

5.4.1 Amylose content

The amylose content of the seven samples was measured with the Megazyme method described in section 4.4.3 of chapter 4: Materials and methods. Two assay replicates were performed. The results are shown on figure 5.5 and table 5.3.

Sample ID	Sample	Amylose content, replication 1 (% w/w)	Amylose content, replication 2 (% w/w)
RF1	Balilla	19.6	20.0
RF2	Elio	22.5	21.4
RF3	Old Selenio	23.3	23.5
RF4	New Selenio	17.8	18.7
RF5	SGR	19.2	19.0
RF6	Bengal MGR	16.5	14.5
RF7	MGR	13.2	13.3

Table 5.3: Amylose contents of the seven rice samples

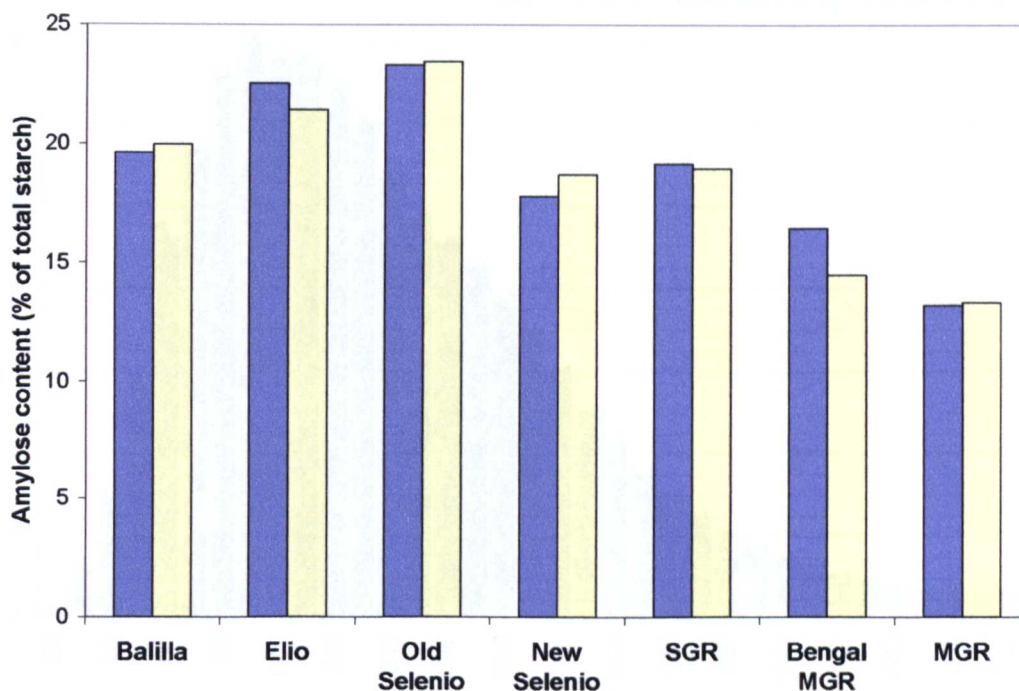


Figure 5.5: Amylose contents of the seven rice varieties. The two bars represent two replicates of the assay.

5.4.2 HPLC amylopectin branch chain analysis

The amylopectin chain length distribution of the seven samples was measured by isoamylase debranching followed by HPLC separation, as detailed in section 4.4.4 of chapter 4: Materials and methods. The results are shown on figure 5.6. The correspondence between the codes and the actual samples is indicated in table 5.4.

Code	Variety
RF1	Balilla
RF2	Elio (high amylose variety)
RF3	Selenio (old)
RF4	Selenio (new)
RF5	Short Grain (SGR)
RF6	Bengal Medium Grain (B-MGR)
RF7	Medium Grain (MGR)

Table 5.4: List of the seven rice varieties used during the project

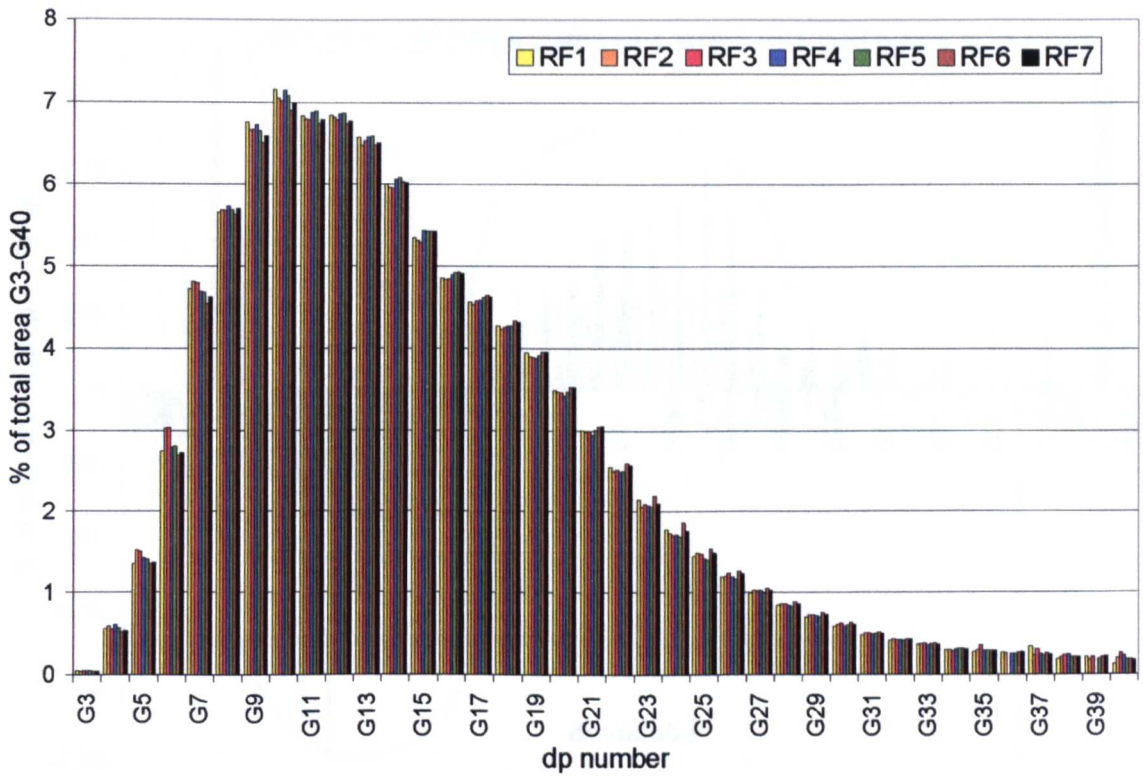


Figure 5.6: Amylopectin branch chain analysis of the seven raw rice flours

Differences between samples were made clearer by choosing the new Selenio variety (RF4) as a reference sample and subtracting it from the other varieties data. This variety was chosen because it appeared to have an intermediate proportion of amylopectin chains for all degrees of polymerisation, compared to the other varieties. The results are shown on figure 5.7: The Elio and Selenio (old) varieties appeared to have a higher proportion of amylopectin chains with a degree of polymerisation (dp number) of 5 to 7 (red circle). The Bengal medium grain and medium grain varieties had a lower proportion of dp 9 to 12 amylopectin chains (blue circle). The short grain, Bengal medium grain and medium grain varieties had a higher proportion of dp 17 to 25 amylopectin chains (green circle).

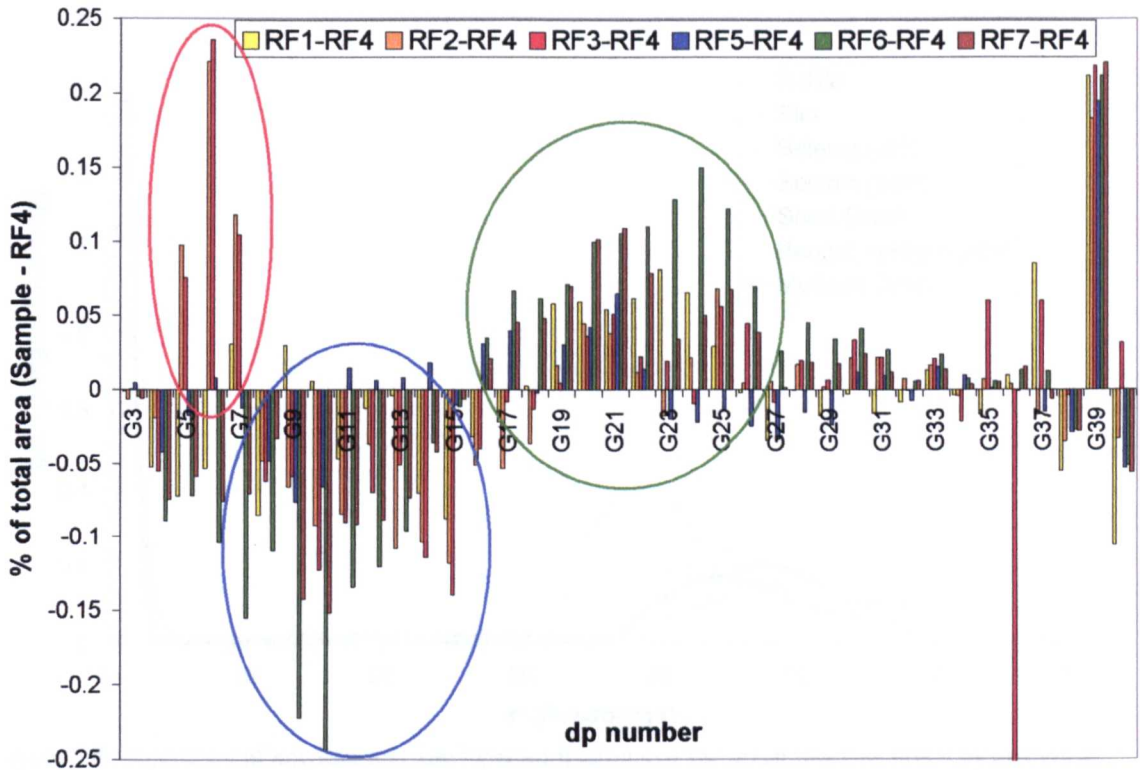


Figure 5.7: Amylopectin branch chain differential analysis of the seven raw flours

5.4.3 Amylose – amylopectin separation by ultracentrifugation

The separation of amylose and amylopectin of the seven samples was done using the ultracentrifugation coupled with laser diffraction method described in section 4.5.6 of chapter 4: Materials and methods.

The technique allowed to separate the amylose and amylopectin fractions of the samples, as shown on figure 5.8: The peaks in the range 1-2 Svedbergs and 30-70 Svedbergs were interpreted as the amylose and amylopectin fractions respectively.

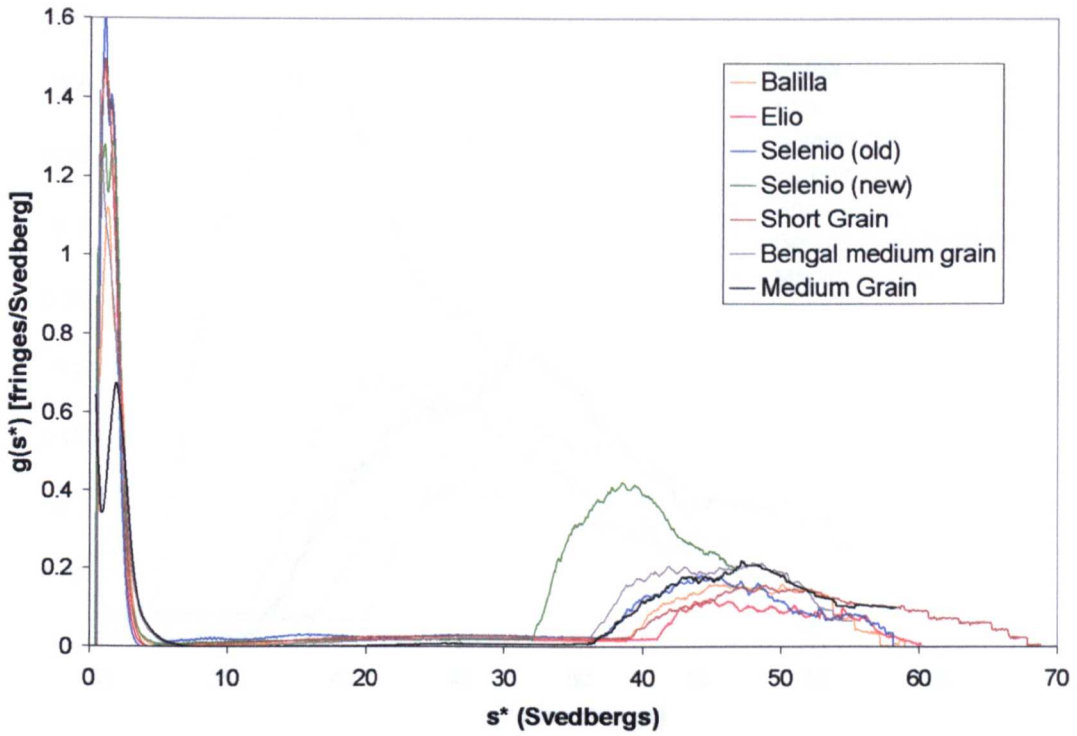


Figure 5.8: Separation of amylose and amylopectin fractions of the seven raw rice flours by analytical ultracentrifugation

Figures 5.9 and 5.10 show a zoom on the amylose and amylopectin peaks respectively, but little difference between the seven varieties could be evidenced with this method. Only the new Selenio variety had a larger amylopectin peak than the others.

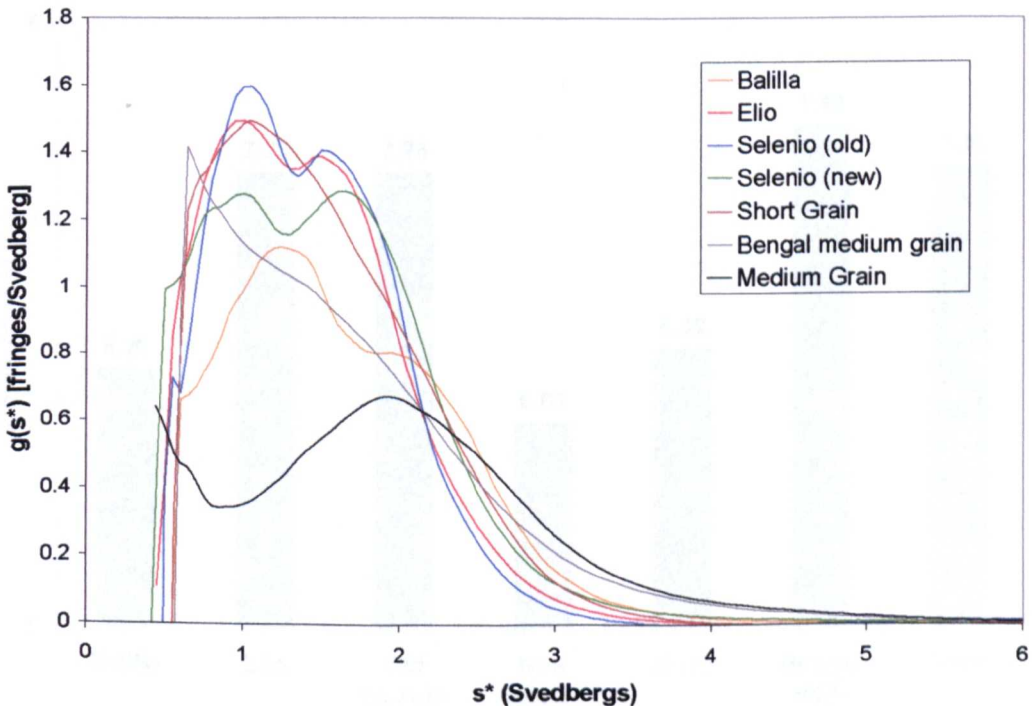


Figure 5.9: Ultracentrifugation amylose separation peak of the seven raw rice flours

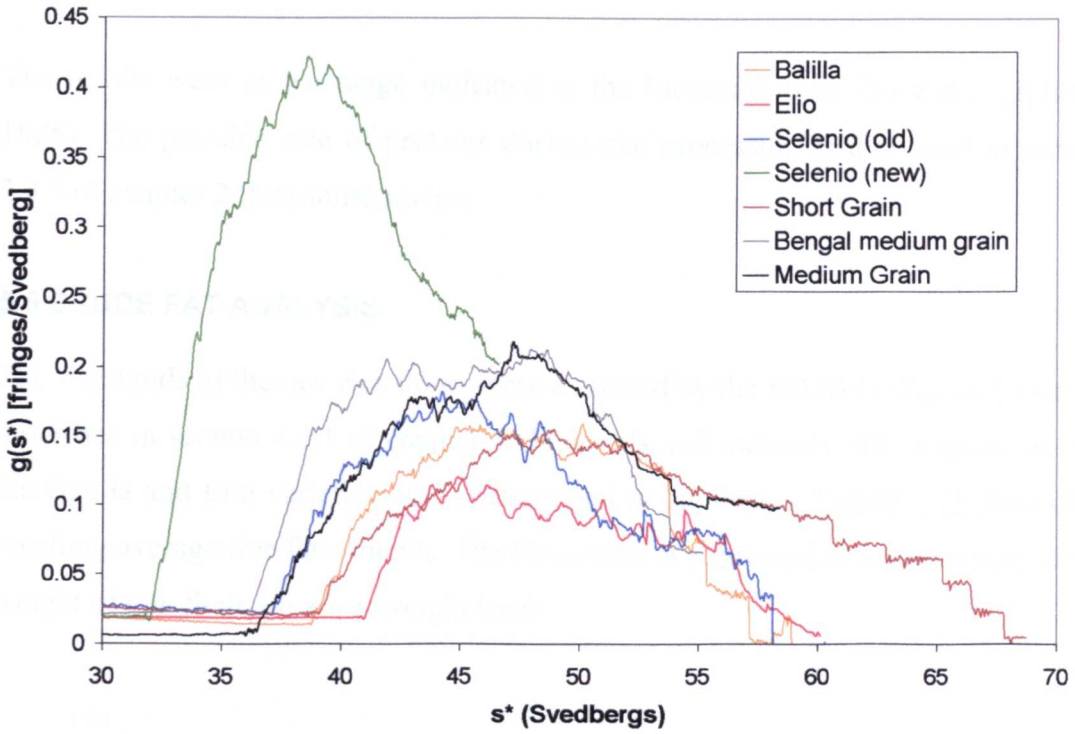


Figure 5.10: Ultracentrifugation amylopectin separation peak of the seven raw rice flours

5.5 PROTEIN CONTENT

The nitrogen content of the seven samples was measured with the organical elemental analysis (Dumas method) described in section 4.4.2 of chapter 4: Materials and methods. The results are presented on figure 5.11. The protein content is expressed as a percentage of the weight of raw flour.

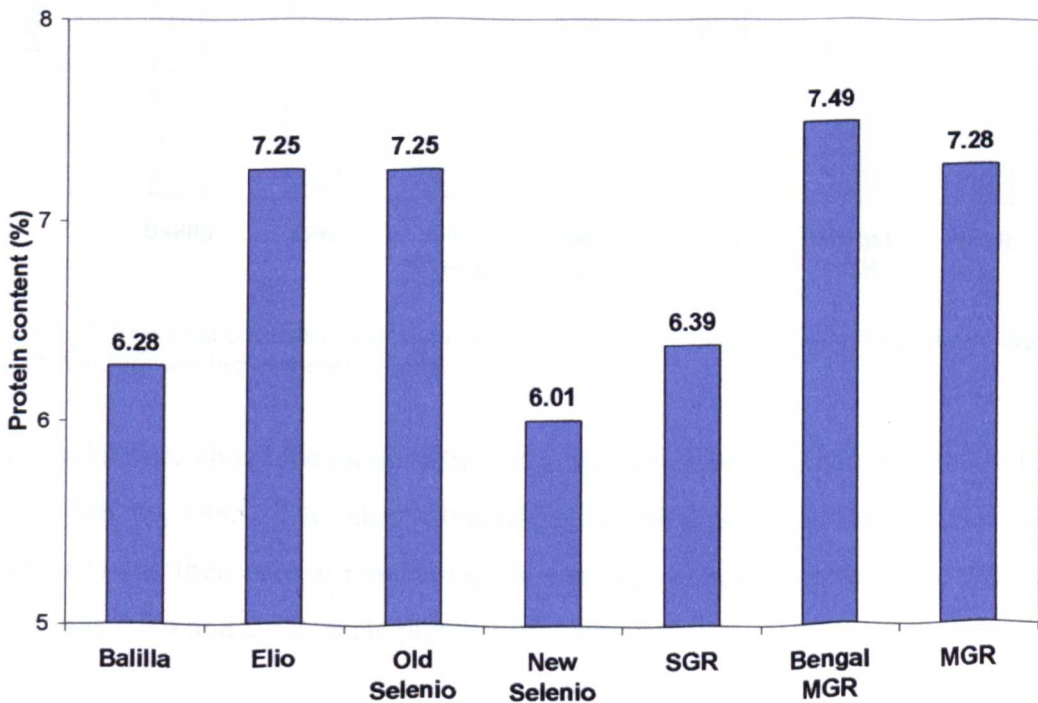


Figure 5.11: Protein contents of the seven rice varieties (single determination)

The results were in the range indicated in the literature, 6 to 7% w.w.b (Juliano, 1985). The possible role of proteins during rice processing is discussed in section 2.3.3 of chapter 2: Literature review.

5.6 CRUDE FAT ANALYSIS

The free lipids of the raw rice flours were extracted by the Soxhlet extraction method described in section 4.4.1 of chapter 4: Materials and methods. All samples, except the Balilla and Elio varieties, were determined in duplicates. Figure 5.12 shows the resulting average free fat contents. The fat content is expressed as a percentage of the weight of raw flour, on a wet weight basis.

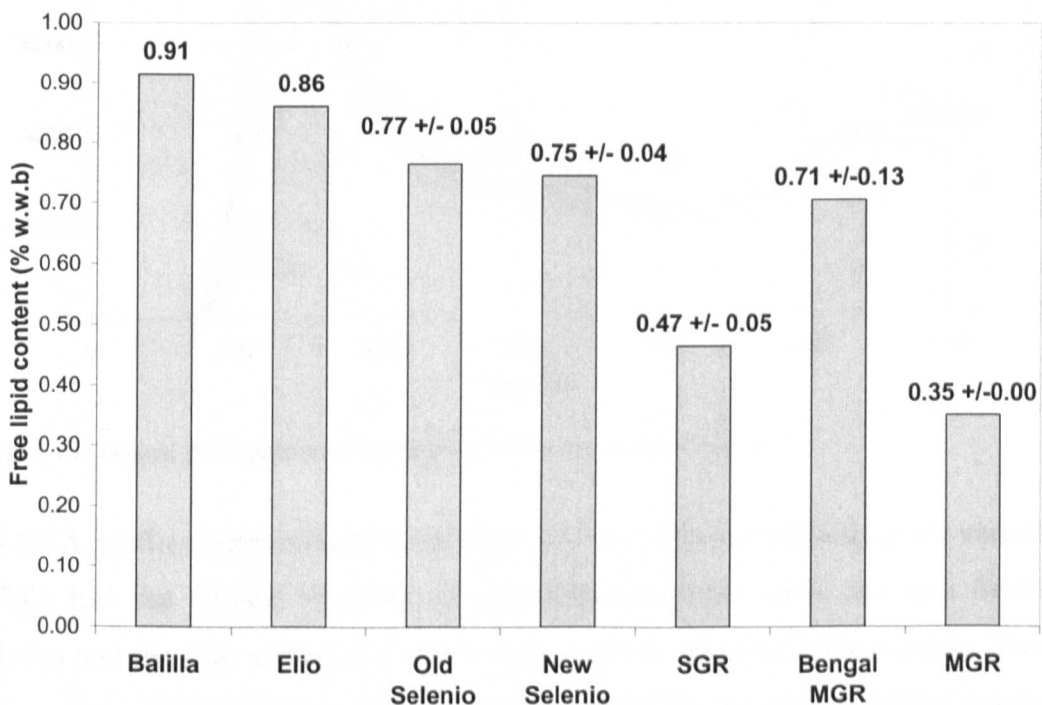


Figure 5.12: Free lipid contents of the seven rice varieties. When duplicates were done, the +/- figures indicate the variation between the two results.

The results were above the range indicated in the literature for white rice, 0.3 to 0.5% w.w.b (Juliano, 1985). The interactions of lipids with amylose to form amylose-lipid complexes and their role in reinforcing the structure of starch systems are discussed in sections 2.3.4 and 2.4.2 of chapter 2: Literature review.

5.7 RAW RICE GELATINISATION BEHAVIOUR

5.7.1 RVA profiles

The gelatinisation of the seven samples was followed by RVA, according to the protocol described in section 4.4.5 of chapter 4: Materials and methods. The RVA profiles are shown on figure 5.13.

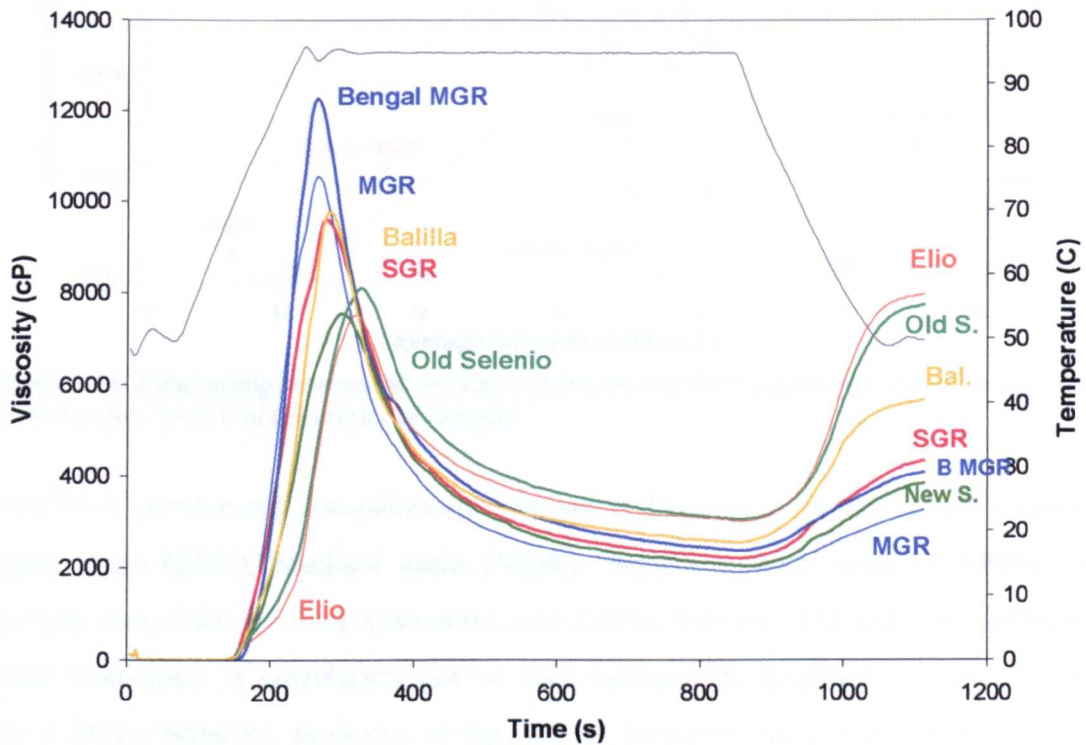


Figure 5.13: Typical RVA gelatinisation profiles of the seven rice varieties

The RVA profiles differentiated some rice varieties: The two medium grain varieties (MGR) had the highest viscosity of gelatinisation peaks while the two Selenio varieties and the Elio variety had the lowest viscosity of gelatinisation peaks. These differences in gelatinisation peak could be related to the rice varieties amylose content. Although the correlation is poor, it appeared that the higher the amylose content, the lower the gelatinisation peak viscosity, as shown on figure 5.14. These observations fitted with the observation that the granules of high amylopectin content starch varieties swell and hence increase the viscosity more during gelatinisation than normal starches.

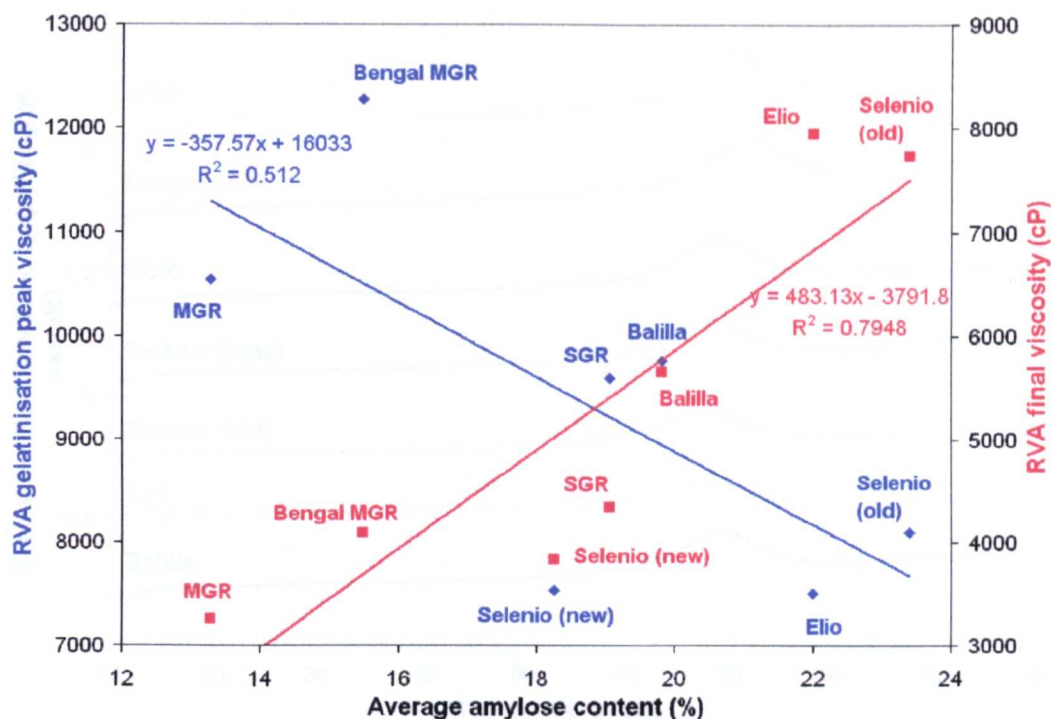


Figure 5.14: Relationship between the amylose content and the RVA gelatinisation peak (in blue) and final viscosity (in red) of the seven rice varieties

The RVA profiles end viscosities also showed differences between the rice varieties: Short grain (SGR), Medium grain (MGR), Bengal medium grain (B-MGR) and Selenio (new) had low final viscosities, and Balilla, Selenio (old) and Elio had higher final viscosities. A correlation can be seen between the amylose contents and the RVA final viscosities, as shown on figure 5.14. However, since SGR, MGR, B-MGR and Selenio (new) varieties were all milled in the United States while Balilla, Selenio (old) and Elio varieties were milled in the United Kingdom, the differences in final viscosities could also be due to a difference in the degree of milling rather than in the rice composition (the US samples appeared to be more milled and polished than the UK samples).

5.7.2 DSC profiles

The gelatinisation of the seven samples was followed by DSC, according to the protocol described in section 4.4.6 of chapter 4: Materials and methods. The experiments were done in duplicates. A typical DSC profile is shown for each sample on figure 5.15. Gelatinisation onset, peak and end temperatures are shown on figure 5.16. The gelatinisation enthalpies (peak areas) are shown on figure 5.17.

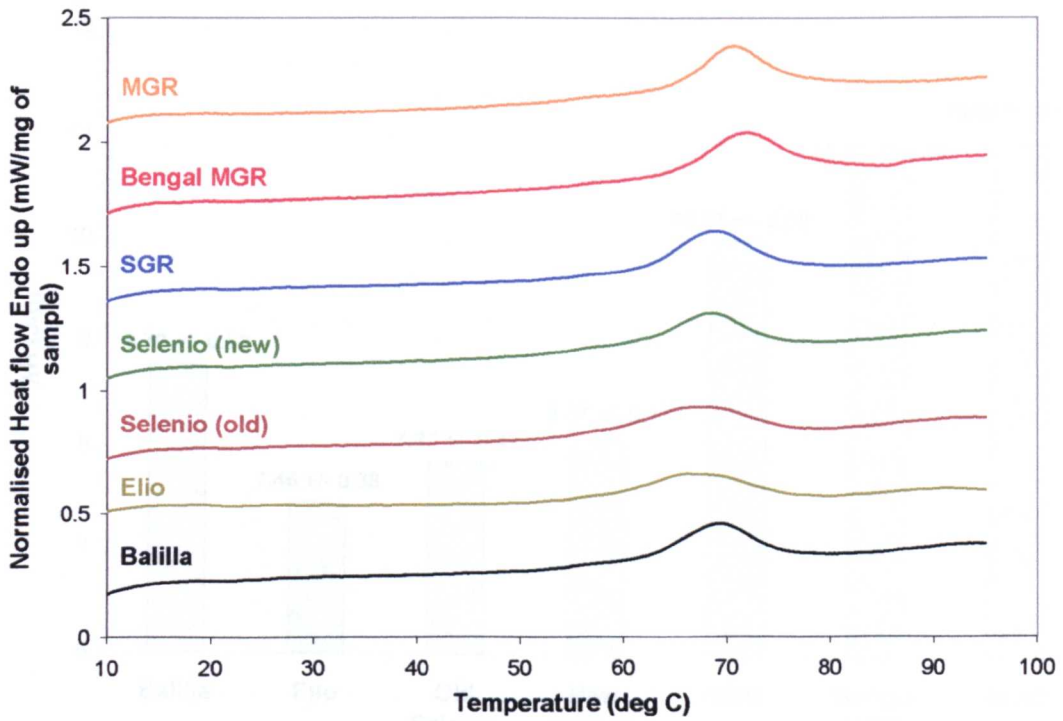


Figure 5.15: DSC gelatinisation profiles of the seven raw rice flours. The water : flour ratio was 3:1 (w/w). The profiles were normalised by dividing the heat flow by the weight of dry flour.

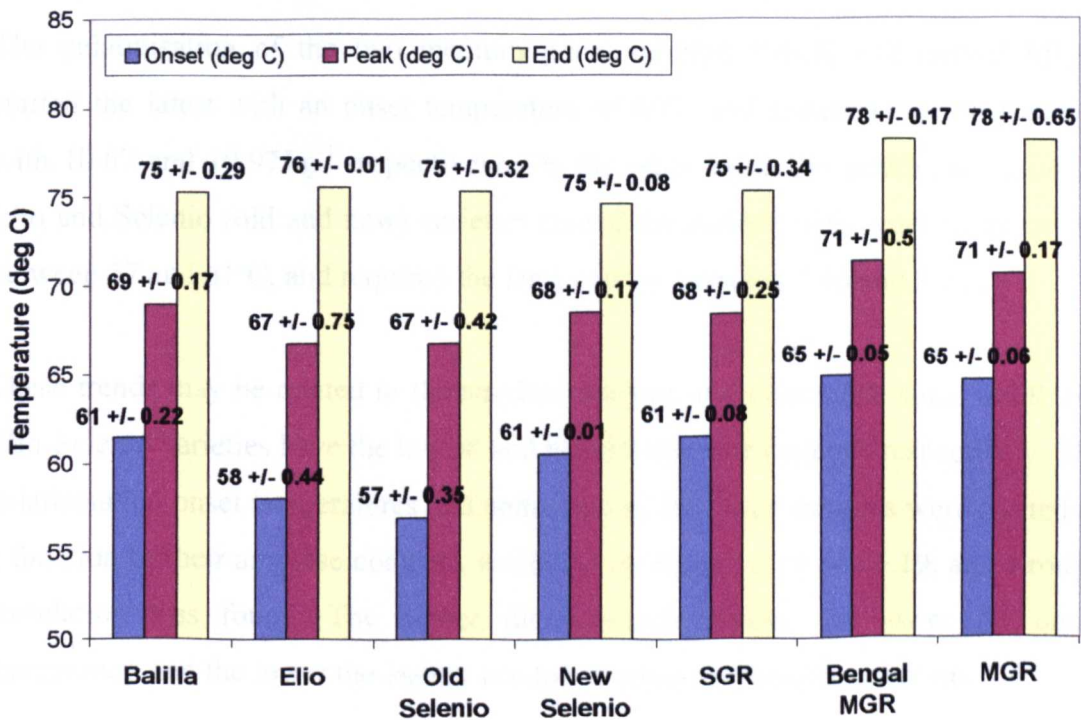


Figure 5.16: Seven rice varieties average DSC gelatinisation peak characteristics. The +/- figures indicate the variation between the two duplicates.

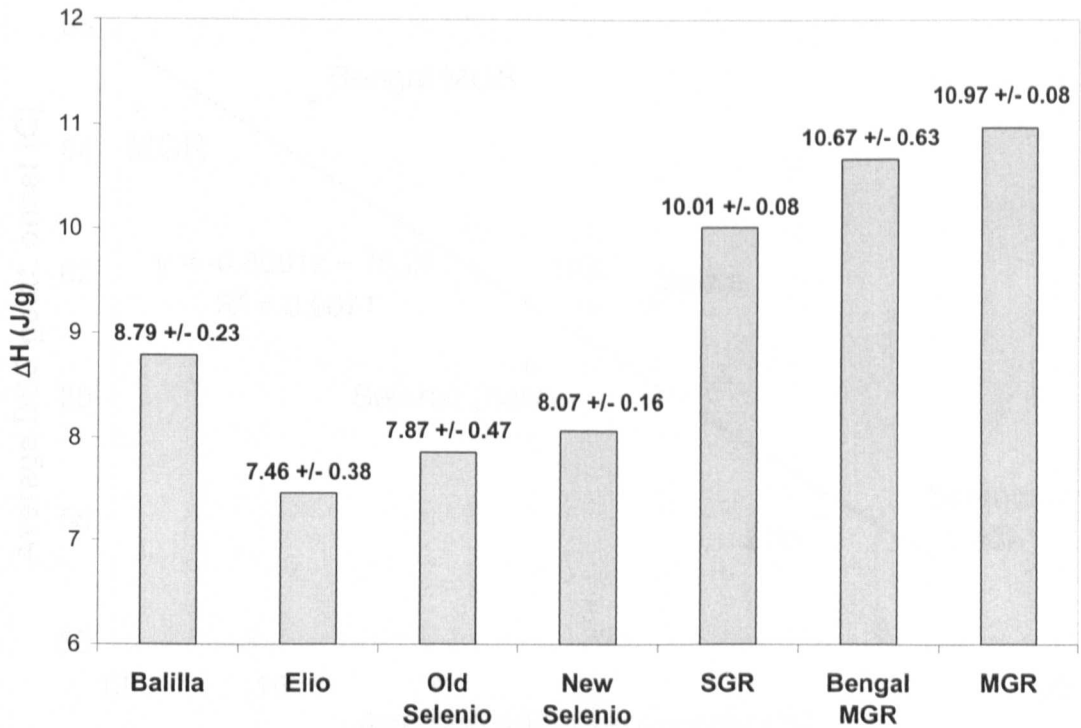


Figure 5.17: Seven rice varieties average DSC gelatinisation enthalpies. The \pm figures indicate the variation between the two duplicates.

The gelatinisation of the two medium grain varieties (MGR and Bengal MGR) started the latest with an onset temperature of 65°C and required the most energy with 10.67 and $10.97\text{J}\cdot\text{g}^{-1}$ respectively. On the other hand, the gelatinisation of the Elio and Selenio (old and new) varieties started the earliest with onset temperatures between 57 and 61°C , and required the least energy, between 7.46 and $8.07\text{J}\cdot\text{g}^{-1}$.

These trends may be related to the amylose content of the samples, since MGR and Elio-Selenio varieties have the lowest and highest amylose contents respectively. The gelatinisation onset temperatures and enthalpies of the seven samples were plotted as a function of their amylose contents, as shown on figures 5.18 and 5.19, and a rough correlation was found: The higher the amylose content, the lower the onset temperature and the lower the energy needed to complete the gelatinisation.

A hypothesis could be that a high amylose content facilitates the penetration of water into the amorphous lamellae of the starch granules, resulting in a decrease in the glass transition temperature of the material, and hence in a lower onset temperature and a less energy consuming gelatinisation.

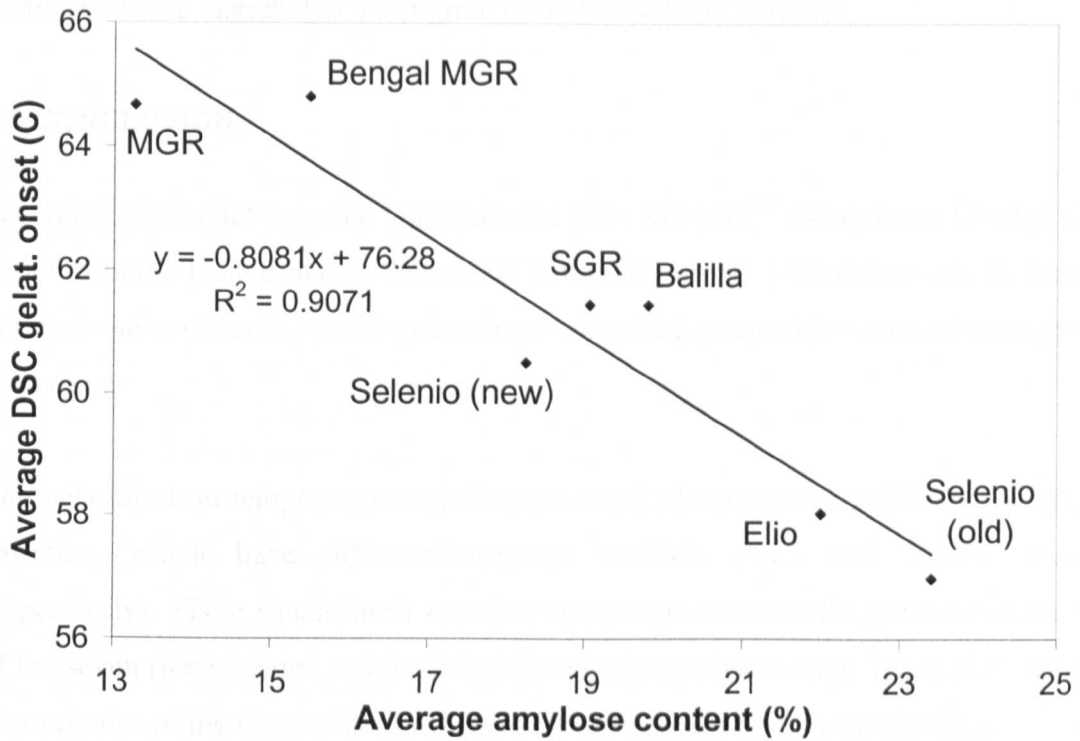


Figure 5.18: Relationship between the amylose content and the DSC gelatinisation onset temperature of seven rice varieties

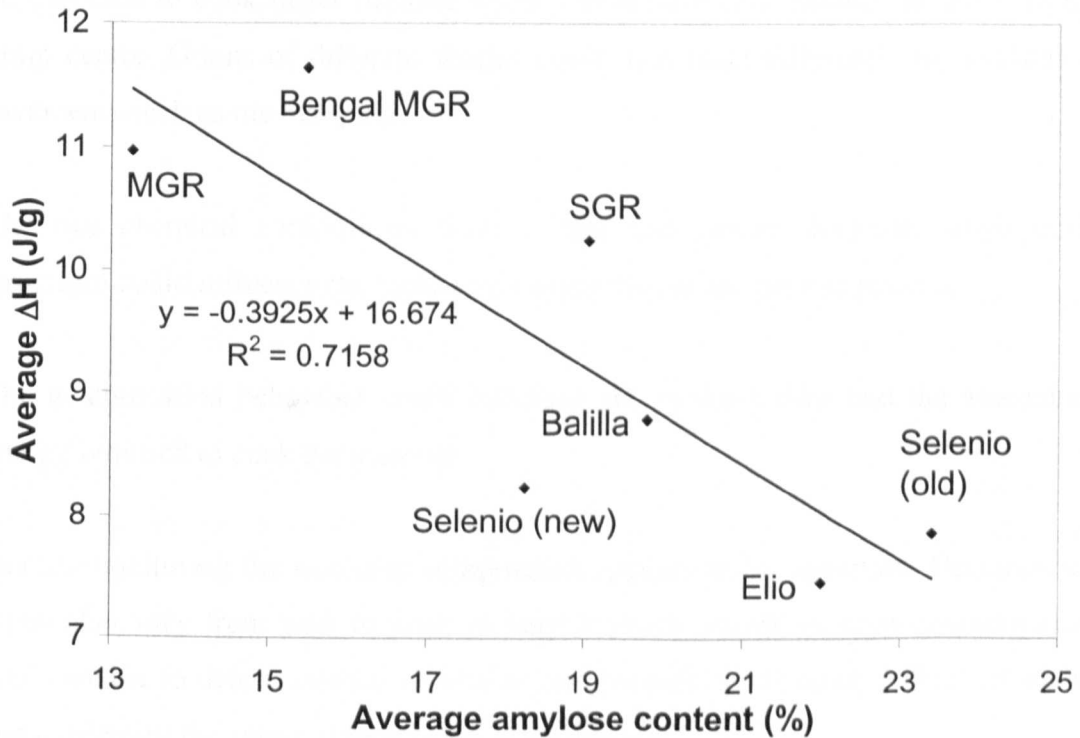


Figure 5.19: Relationship between the amylose content and the DSC gelatinisation enthalpy of seven rice varieties

Process-wise, the higher level of energy needed to complete the gelatinisation of medium grain (MGR) varieties may mean that the cooking MGR varieties could be

more expensive than that of short grain (SGR) or Selenio varieties.

5.8 CONCLUSION

Several rice varieties are used to prepare the Rice KrispiesTM: Medium or Short grain varieties in the United States, Selenio or Balilla in Europe. Differences can be found between these varieties, in the grain shape, chemical composition and gelatinisation behaviour.

The gelatinisation temperature varied by up to 9°C between the MGR and the Elio varieties, which have different amylose contents (13.3 and 21.4% w.w.b respectively). There was a linear negative correlation between the amylose contents of the seven rice varieties and the gelatinisation onset temperature. These differences in properties of the rice varieties can have a major impact on their processing.

The grain shape could influence the cooking time: For instance thinner grains could be expected to cook faster because water would have less distance to travel to the grain centre. Grains of different shapes could also react differently to mechanical treatments such as the bumping.

The rice chemical composition (starch, lipid and protein contents; amylopectin structure) could influence the mechanical properties of the cooked material.

The gelatinisation behaviour could influence the cooking time and the amount of energy required to cook the material.

Hence, monitoring the rice crop composition appears to be important. Because rice crops also vary from year to year, to keep a yearly record of crop characteristics could enable to detect unusual variations and potential processing difficulties early, and to identify the cause of production problems more quickly.

In the following chapters, the influence of some rice components (amylase, lipids) on the rice mechanical properties is discussed, and an indicative range of recommended values for these components is proposed.

CHAPTER 6: GLASS TRANSITION OF THE COOKED RICE

6.1 INTRODUCTION

Kalichevsky *et al.* (1992) showed that the glass transition temperature of amylopectin at 18% moisture content w.w.b is approximately 40°C, as determined by DSC from the midpoint of the heat capacity change observed at a heating rate of 10°C.min⁻¹ and by DMTA from the peak in tan δ . These conditions are very close to the standard bumping conditions: 18% moisture content w.w.b, 45 to 50°C. Since the mechanical properties (elastic and loss modules G' and G'') of polymer materials vary dramatically at and around the glass transition, this means that small variations in the bumping conditions could result in large variations in the post-bumped rice material and inconsistencies in the characteristics of the finished puffed product. Therefore it was important to determine the glass transition state diagram of the cooked rice material specifically. Using a theoretical prediction was not accurate enough because of the addition of sugars and salt during the cooking stage.

This chapter presents the results of a series of experiments aimed at determining the glass transition state diagram of the cooked rice material. The study was conducted on pre-bumped and post-bumped rice material, using the dynamic mechanical thermal analyser (DMTA) described in section 4.5.3 of chapter 4: Materials and methods. The preparation of the samples is described in section 6.2. The measurement of the glass transition is explained in section 6.3. Section 6.4 discusses the role of the glass transition at two key steps of the process: the bumping and the puffing. The probability of starch retrogradation occurring in the cooked rice material in the rubbery state is discussed in section 6.5.

6.2 PREPARATION OF THE SAMPLES

One factory sample of pre-bumped rice (labelled T1) and two factory samples of post-bumped rice (labelled T2 and T3) at 18% w.w.b moisture content were powdered and pressed for 10 minutes at 70°C with a 4 ton hydraulic press into sheets

of material 1.1mm thick. The samples were from the Selenio variety. The sheets were cut into ribbons of dimensions 5.0 x 11.0 x 1.1 mm. The moisture contents of the ribbons were then adjusted by storing them for two weeks at 4°C in 8 RH boxes containing various saturated salt solutions, as shown on table 6.1. The temperature of 4°C was chosen to prevent the samples from getting mouldy. During the moisture equilibration, the ribbons were wrapped in aluminium mesh to keep them flat. The moisture contents of the three samples after two weeks are indicated in the right three columns of the table.

Box	Saturated salt solution	Relative humidity at 20°C (%)	Sample moisture content after 2 weeks (% w.w.b)		
			<i>Samples</i> →	T1 (pre-bumped)	T2 (post-bumped)
RH1	P ₂ O ₅	0	4.9	5.0	4.4
RH2	LiCl	11	5.2	5.6	5.6
RH3	Pot. Acetate	22	6.2	6.4	6.2
RH4	K ₂ CO ₃	44	7.8	7.8	7.6
RH5	NaBr	58	9.8	11.7	10.5
RH6	NaCl	74	12.7	14.6	12.3
RH7	KCl	88	19.2	18.9	18.9
RH8	Distilled water	100	33.0	33.5	33.2

Table 6.1: Relative humidities created above saturated salt solutions and resulting moisture contents of cooked rice samples stored under these relative humidities (* adapted from Nyquist, 1983)

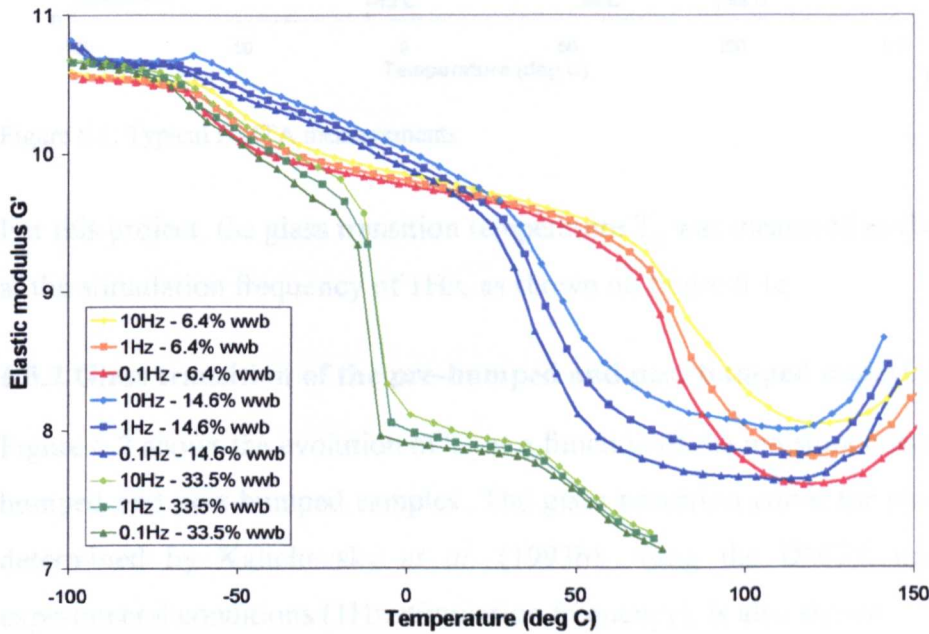
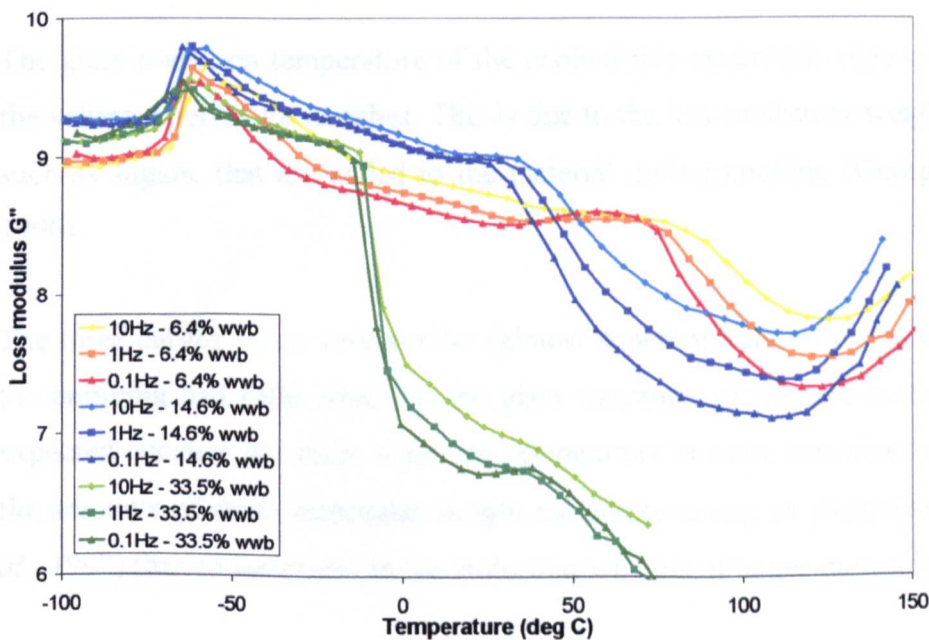
No significant difference in the ability to absorb moisture was observed between the pre-bumped and post-bumped samples.

After the moisture equilibration, the ribbons were covered in silicon oil to limit moisture losses and analysed with the DMTA. The temperature varied from -100 to 200°C at 2°C.min⁻¹. The amplitude of deformation was set to 64µm peak to peak. Three bending frequencies were tested: 0.1, 1 and 10Hz. The advantage of testing various frequencies is to make the difference between frequency dependent and frequency independent transitions, such as glass transition and melting of ice respectively.

6.3 MEASUREMENT OF THE COOKED RICE GLASS TRANSITION

6.3.1 Method for determining the glass transition temperature of each sample

Figure 6.1 shows examples of DMTA measurements. The results presented are for the T2 post-bumped rice sample stored at 22, 74 and 100% relative humidity (6.4%, 14.6% and 33.5% moisture contents w.w.b respectively). Figures 6.1a, 6.1b and 6.1c show respectively the evolution of the elastic modulus G' , the loss modulus G'' and the phase angle $\tan \delta$, which is the ratio G'' / G' , as a function of temperature. The three stimulation frequencies used, 0.1Hz, 1Hz and 10Hz, are also shown.

Fig. 6.1a: G' Fig. 6.1b: G''

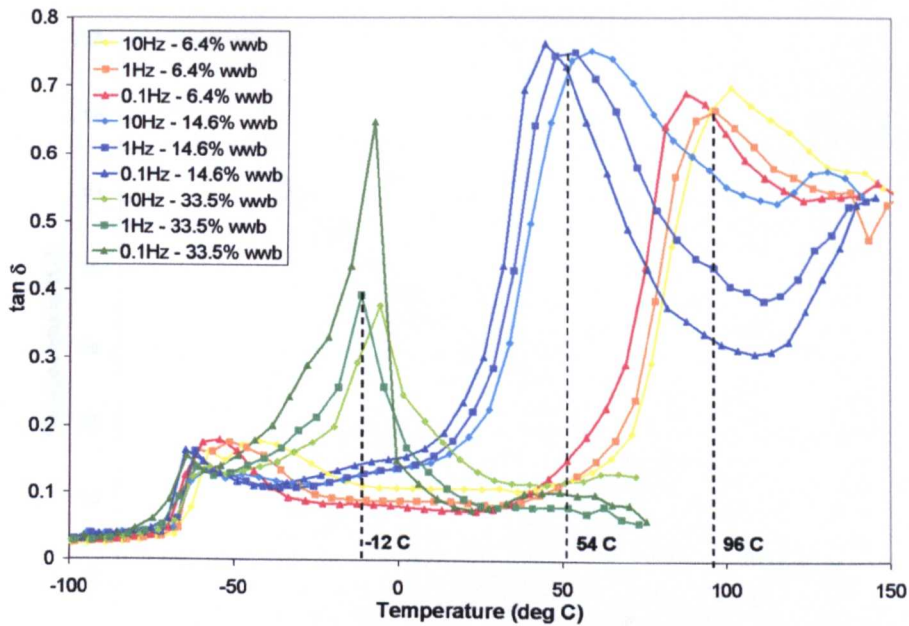
Fig. 6.1c: $\tan \delta$

Figure 6.1: Typical DMTA measurements

For this project, the glass transition temperature T_g was measured as the peak in $\tan \delta$ at the stimulation frequency of 1Hz, as shown on figure 6.1c.

6.3.2 Glass transition of the pre-bumped and post-bumped material

Figure 6.2 shows the evolution of T_g as a function of the moisture content for the pre-bumped and post-bumped samples. The glass transition curve for pure amylopectin determined by Kalichevsky *et al.* (1993b), using the DMTA under the same experimental conditions (1Hz stimulation frequency), is also shown.

The glass transition temperature of the cooked rice material is reduced compared to the values reported for starches. This is due to the low molecular weight plasticizers, such as sugars, that are added to the material during cooking (Georget and Smith, 1996).

The three curves being very similar (almost superimposable), it was concluded that the bumping had little effect on the glass transition of the rice material. This was expected because the glass transition temperature is more sensitive to variations in the amounts of small molecular weight molecules acting as plasticizers (Lourdin *et al.*, 1997) than to variations in the molecular weights of larger molecules.

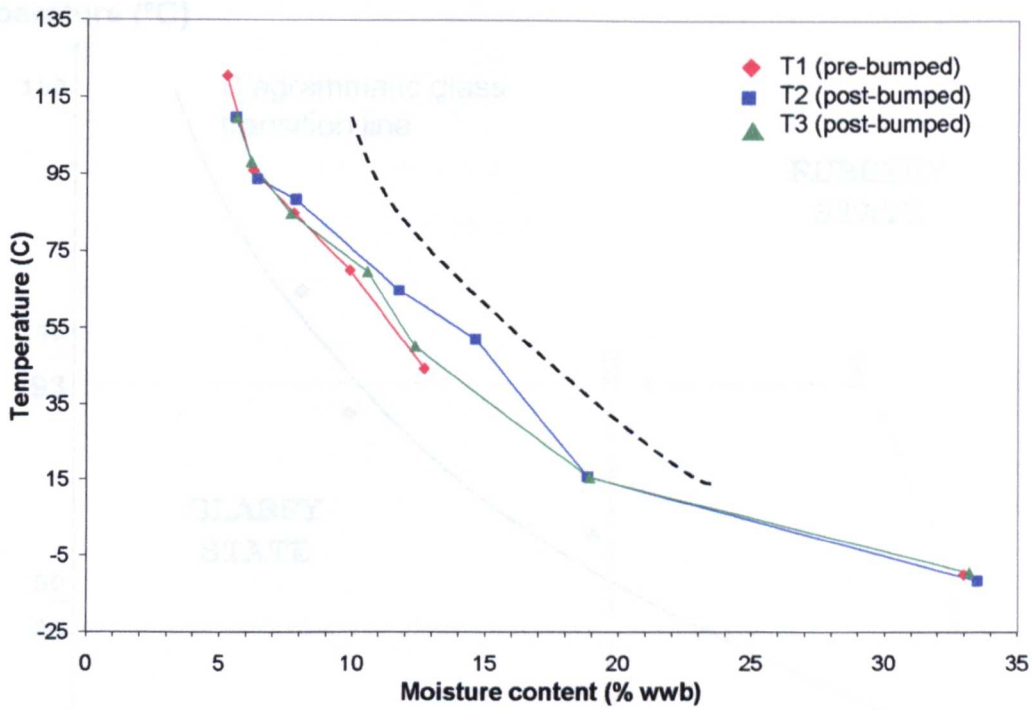


Figure 6.2: $\tan \delta$ glass transition diagram of pre-bumped and post-bumped rice material. The pure amylopectin glass transition curve is also shown (---) (Kalichevsky et al., 1993b)

6.4 ROLE OF THE GLASS TRANSITION IN PROCESSING THE RICE MATERIAL

6.4.1 Glass transition and bumping

Figure 6.3 shows the state diagram of the rice material, and the path the rice follows from its pre-bumped state all the way through the bumping step to the end of the tempering step (just before the puffing).

- **Position 1:** The cooked rice has been dried to 18% moisture content w.w.b and arrives on the bumping roll at a temperature of 45°C. The bumping is carried out at this position with no variation in the temperature or moisture content of the material. Thus, the rice grains are bumped in the rubbery state, although some parts of the grains may be crystalline and therefore rigid and brittle (cf. amylose-lipid complexes model in section 7.3.4.1).
- **Position 2:** The post-bumped rice is warmed up to 93°C and begins to lose water. This corresponds to the after bumping drying step of the process.
- **Position 3:** The rice moisture content decreases to 11% w.w.b. At this point the rice comes out of the drying oven.
- **Position 4:** The rice material is left to cool down to room temperature (20 to 25°C) and to temper for 24 hours.

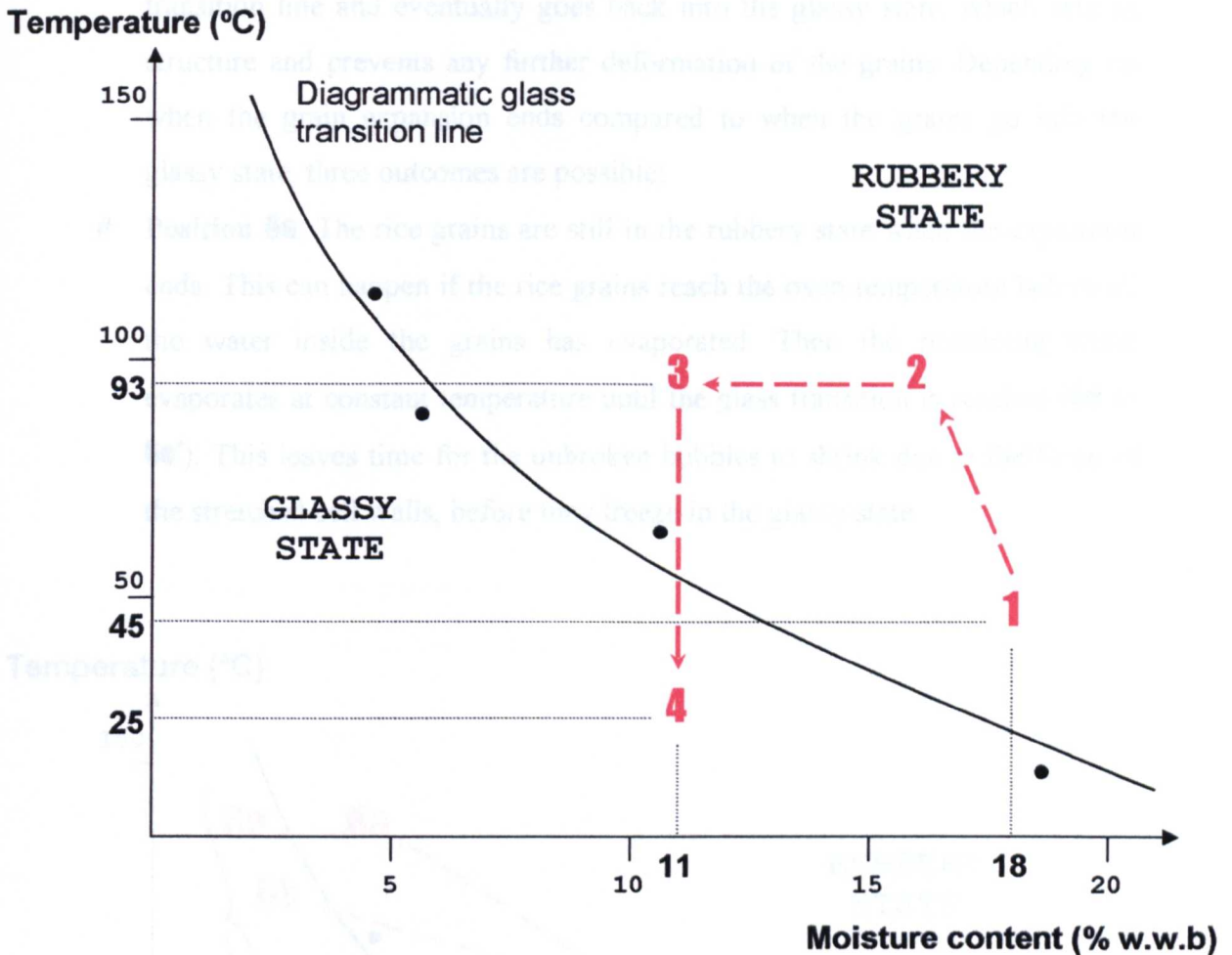


Figure 6.3: Path (1-2-3-4) followed by the rice material after the cooking, through the bumping and drying to the tempering step on the theoretical glass transition diagram (• experimental points)

6.4.2 Glass transition and puffing

Figure 6.4 shows the state diagram of the rice material, and the path the rice follows during the puffing.

- **Position 4:** The tempered rice comes into the oven in the glassy state, and is warmed up through the glass transition to 100°C (position 5).
- **Position 5:** When the rice reaches 100°C (rubbery state), steam bubbles begin to form and expand inside the grains. Starch cell walls are stretched and may break if they reach their elasticity limit, which results in water evaporating from the grains and the slowing down of the expansion. The grains temperature continues increasing towards the 230°C oven temperature.
- **Position 6:** As water evaporates, the material moves towards the glass

transition line and eventually goes back into the glassy state, which sets its structure and prevents any further deformation of the grains. Depending on when the grain expansion ends compared to when the grains go into the glassy state, three outcomes are possible:

- # **Position 6a**: The rice grains are still in the rubbery state when the expansion ends. This can happen if the rice grains reach the oven temperature before all the water inside the grains has evaporated. Then the remaining water evaporates at constant temperature until the glass transition is reached (**6a** to **6a'**). This leaves time for the unbroken bubbles to shrink due to the force of the stretched cell walls, before they freeze in the glassy state.

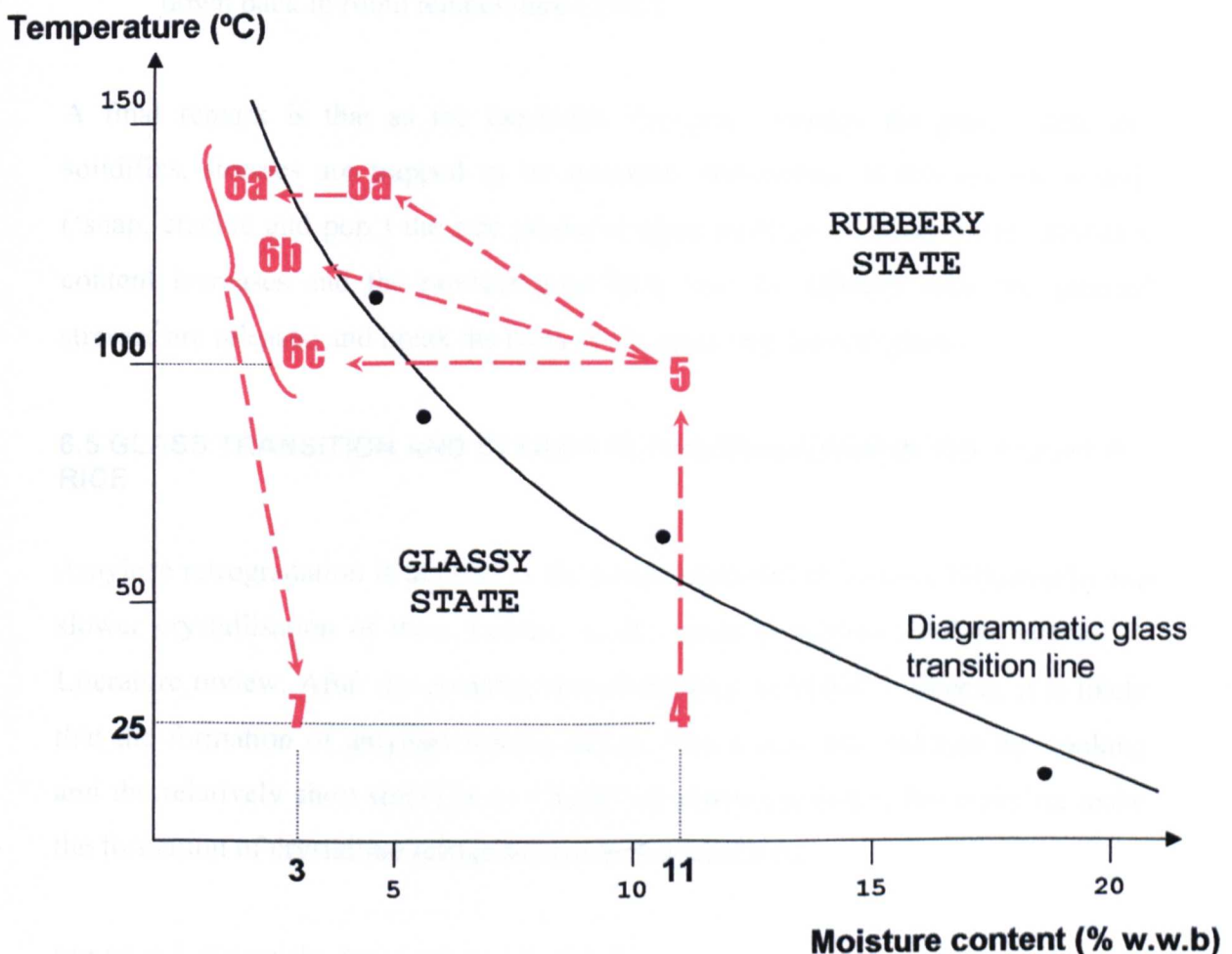


Figure 6.4: Path (4-5-6-7) followed by the rice material during the puffing on the theoretical glass transition diagram (• experimental points)

- # **Position 6b:** The rice grains go into the glassy state, thus ending the expansion, just when they reach their maximum expansion (or very shortly after). This is the desired scenario which keeps the maximally expanded grain structure.
- # **Position 6c:** The rice grains go into the glassy state, thus ending the expansion, before the expansion has reached its maximum. This can happen if the elastic modulus of the material is too high and prevents the expansion of the bubbles, or if the temperature in the oven is too low (the extreme case of an oven temperature of 100°C is represented on the diagram). The result is under-puffed rice.
- **Position 7:** The puffed rice comes out of the oven and is allowed to cool down back to room temperature (25°C).

A final remark is that as the expanded rice grain reaches the glassy state and solidifies, stresses are trapped in its structure. Indications of this are the sounds ('snap, crackle and pop') the rice produces upon addition of milk: As the moisture content increases and the product goes back into the rubbery state, the internal stresses are released and break the parts of the grain that are still glassy.

6.5 GLASS TRANSITION AND STARCH RETROGRADATION IN THE COOKED RICE

Amylose retrogradation is defined as the rapid formation of helices, followed by the slower crystallisation of these helices, as discussed in section 2.5.3 of chapter 2: Literature review. After the cooking step of the Rice Krispies™ process, it is likely that the formation of amylose helices occurs. The drying that follows the cooking and the relatively short time (up to 1 hour) of tempering before the bumping make the formation of crystalline retrograded amylose less likely.

Figure 6.5 shows the theoretical amylopectin retrogradation rate of the cooked rice material at room temperature and 18% moisture content w.w.b. The glass transition temperature indicated ($T_g = 20^\circ\text{C}$) was determined by DMTA. The melting temperature indicated ($T_m = 120^\circ\text{C}$) is a rough estimate inspired from the value determined for waxy maize starch by Farhat *et al.* (2000).

6.1 CONCLUSION

After the cooking step of the Rice Krispies™ process, the rice material is rapidly dried down from 28% to 18% moisture content w.w.b and cooled down to 45°C. Based on an assumed melting temperature around 120°C, this temperature corresponds to a fairly low retrogradation rate $R_{45^\circ\text{C}}$, as indicated on figure 6.5. Therefore amylopectin retrogradation was considered unlikely to take place in the rice material after the cooking and during the bumping step of the Rice Krispies™ process.

The glass transition determination enabled to map the state of the rice material during the bumping step.

The bumping step is shown in the following diagram after the cooking step.

The bumping step is shown in the following diagram after the cooking step.

The bumping step is shown in the following diagram after the cooking step.

The bumping step is shown in the following diagram after the cooking step.

The bumping step is shown in the following diagram after the cooking step.

The bumping step is shown in the following diagram after the cooking step.

The bumping step is shown in the following diagram after the cooking step.

The bumping step is shown in the following diagram after the cooking step.

The bumping step is shown in the following diagram after the cooking step.

The bumping step is shown in the following diagram after the cooking step.

The bumping step is shown in the following diagram after the cooking step.

The bumping step is shown in the following diagram after the cooking step.

The bumping step is shown in the following diagram after the cooking step.

The bumping step is shown in the following diagram after the cooking step.

The bumping step is shown in the following diagram after the cooking step.

The bumping step is shown in the following diagram after the cooking step.

The bumping step is shown in the following diagram after the cooking step.

The bumping step is shown in the following diagram after the cooking step.

The bumping step is shown in the following diagram after the cooking step.

The bumping step is shown in the following diagram after the cooking step.

The bumping step is shown in the following diagram after the cooking step.

The bumping step is shown in the following diagram after the cooking step.

The bumping step is shown in the following diagram after the cooking step.

The bumping step is shown in the following diagram after the cooking step.

The bumping step is shown in the following diagram after the cooking step.

The bumping step is shown in the following diagram after the cooking step.

The bumping step is shown in the following diagram after the cooking step.

The bumping step is shown in the following diagram after the cooking step.

The bumping step is shown in the following diagram after the cooking step.

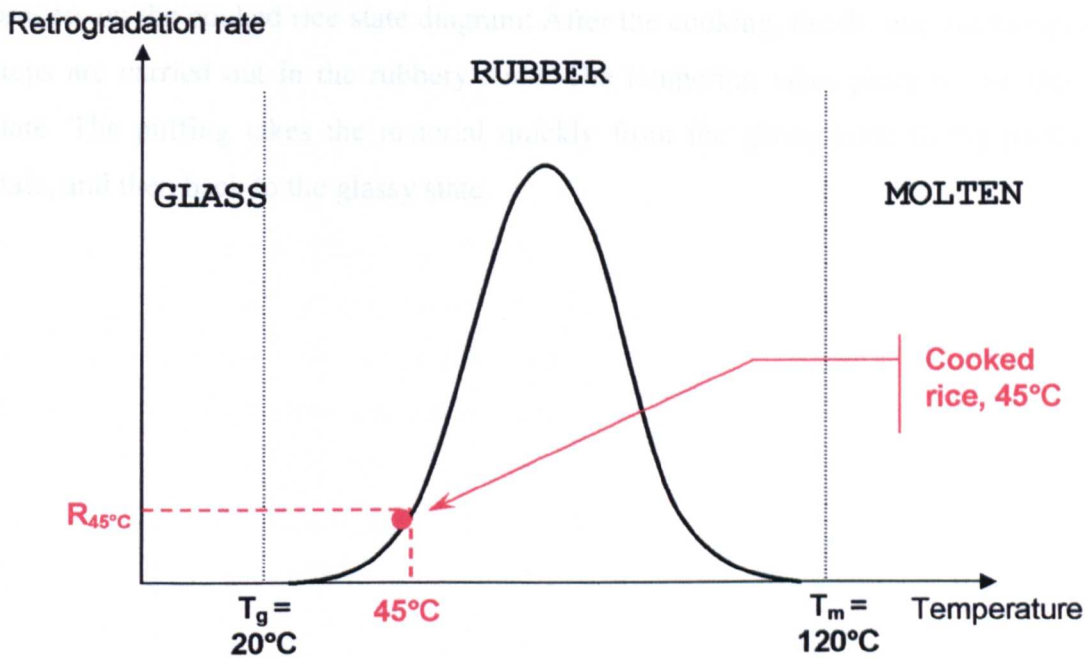


Figure 6.5: Diagrammatic retrogradation rate curve in function of temperature for the cooked rice material at 18% moisture content w.w.b (adapted from Farhat et al., 2000)

After the bumping step, the rice material is dried into the glassy state at 11% moisture content w.w.b, which removes any possibility of retrogradation during the tempering step. The high temperature and the short duration of the puffing step are thought to prevent any possibility of retrogradation at this stage as well.

Thus, starch retrogradation could occur between the cooking and bumping steps of the Rice Krispies™ process, but was thought to be of limited extent and with little influence on the mechanical properties of the rice grains.

6.6 CONCLUSION

The glass transition temperature T_g of the cooked rice material was determined at seven different moisture contents ranging from 5 to 33% w.w.b. It was consistently lower than the T_g of pure amylopectin (as determined by Kalichevsky *et al.* (1992)), which was expected because of the plasticizing sugars added to the rice during the cooking.

The glass transition determination enabled to map the steps of the Rice Krispies™ process on the cooked rice state diagram: After the cooking, the drying and bumping steps are carried out in the rubbery state. The tempering takes place in the glassy state. The puffing takes the material quickly from the glassy state to the rubbery state, and then back to the glassy state.

CHAPTER 7: THE BUMPING STEP OF THE RICE KRISPIES™ PROCESS

INTRODUCTION

The bumping step of the Rice Krispies™ process consists of the compression of the cooked rice between two iron rolls resulting in the flattening of the grains. The bumping has been shown to be a key operation in determining the quality of the puffing: No bumping results in non-expandable grains. Consequently, varying the bumping conditions will alter the quality of the grain expansion. Two of the bumping parameters appear to be of particular importance: the temperature and the roll gap. Several series of trials have been undertaken during the course of the project in order to understand the effect of these two parameters. This chapter presents the results obtained from these trials, and uses them to build up a model of the molecular phenomena taking place during the bumping.

When analysing processed starchy products, the RVA provides a fingerprint of the ability of the starch to hydrate and contribute to viscosity. This gives information on the starch material that relates to the processing conditions. However, because various phenomena occur during the RVA measurement and are superimposed on a single profile, the interpretation of the differences between RVA profiles must be supported with other techniques.

This chapter starts by presenting the series of trials done during the project and the RVA profiles of the resulting bumped samples (section 7.2). Four main categories of samples were identified, and different phenomena are likely to be happening during the bumping.

The following sections (7.3 & 7.4) present separate evidence of two molecular phenomena taking place during the bumping: The dislocation of amylose-lipid complexes and the reduction of starch molecular weight. The techniques used for these studies were the RVA, DSC, X-rays, polymer relative viscosity in dilute

solution measurements, capillary rheometry and chromatography. At the end of section 7.3 is a model of the role amylose-lipid complexes play in reinforcing the cooked rice grain structure, as it is understood at the end of the project.

7.2 INITIAL OBSERVATIONS: RVA PROFILES

7.2.1 Preparation of the samples

Three series of samples were prepared:

(a) Thirteen samples (set A), labelled S01 to S13, were bumped at the university with the roller dryer described in section 4.3.1.2, following a central composite experimental design with two factors: bumping temperature and mill gap. The material used was Selenio rice cooked at the Manchester factory and sent to the university. The transport was done at room temperature (approximately 20°C), then the material was stored at 4°C for two weeks before the experiment. The factory cooking conditions are described in section 3.3.2 of chapter 3: Evaluation of the industrial process. The equipments used to produce the samples at the university are described in section 4.3 of chapter 4: Materials and methods.

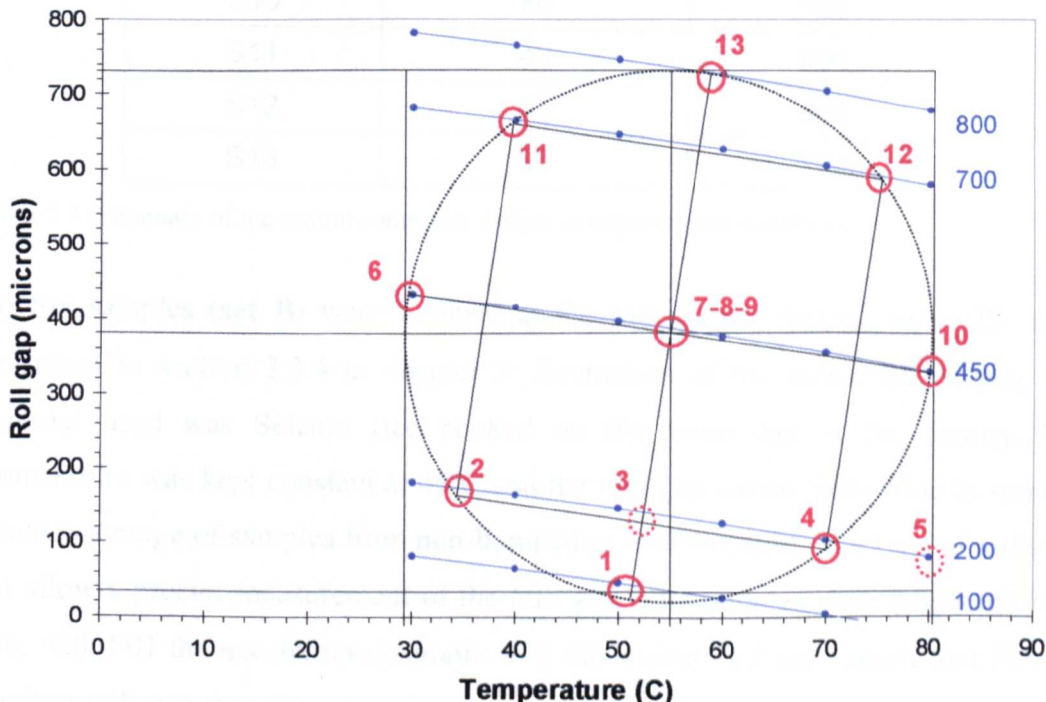


Figure 7.1: Diagram of the 13 samples central composite experimental design. The red circles numbered 1 to 13 represent the chosen experimental conditions. Samples number 3 and 5 (dotted circles) are extra-samples added to the original design. The blue lines (labelled 100, 200, 450, 700 and 800) represent the evolution of the mill gap as a function of the roll temperature, for a series of mill gaps initially set to 100, 200, 450, 700 and 800 μm at room temperature (20°C)

Figure 7.1 and table 7.1 summarise the 13 bumping conditions chosen. The experimental design is tilted so as to reduce the number of mill gap adjustments: Due to the dilation of the rolls, the mill gap decreases as the roll temperature increases (following the blue lines indicated on figure 7.1), and so different mill gaps could be tested without changing the initial gap setting done at room temperature. For example experiments 2, 3, 4 and 5 could all be performed with the mill gap initially set at 200 μm at 20°C.

Experiment	Temperature (°C)	Mill gap (μm)
S01	51	44
S02	35	174
S03	52	142
S04	70	103
S05	82	74
S06	30	431
S07, S08, S09	55	386
S10	80	329
S11	40	664
S12	75	590
S13	59	728

Table 7.1: Summary of the central composite design 13 experimental conditions

(b) Six samples (set B) were bumped at the Manchester factory, using the mills described in section 3.3.4 of chapter 3: Evaluation of the industrial process. The material used was Selenio rice cooked on the same day at the factory. The temperature was kept constant at 45°C and the mill gap varied from wide to small to produce a range of samples from non-bumped to over-bumped. The type of mills did not allow a precise measurement of the mill gap. The samples were labelled F01 to F06, with F01 the non-bumped sample, F02 the widest mill gap sample and F06 the smallest mill gap sample.

(c) Twenty samples (set C), labelled R01 to R20, were prepared at the Battle Creek William Keith Kellogg Institute (WKKI) pilot plant, following a d-optimal experimental design with three factors: bumping temperature, mill gap and rice

variety. Figure 7.2 and table 7.2 summarise the experimental conditions chosen.

Run	Rice variety	Day	Planned temperature		Planned mill gap (μm)	Actual temperature		Actual mill gap (μm)
			(°C)	(°F)		(°C)	(°F)	
R01	MGR	1	26.7	80	100	26.4	79.5	305
R02	MGR	1	54.4	130	300	53.1	127.5	496
R03	MGR	1	54.4	130	100	53.1	127.5	318
R04	SGR	2	54.4	130	100	50.3	122.5	343
R05	SGR	2	26.7	80	100	30.0	86	318
R06	SGR	2	54.4	130	300	51.9	125.5	483
R07	Selenio	3	40.6	105	300	37.2	99	483
R08	Selenio	3	26.7	80	300	28.6	83.5	534
R09	Selenio	3	54.4	130	200	48.1	118.5	369
R10	MGR	4	40.6	105	250	38.6	101.5	394
R11	MGR	4	26.7	80	300	28.1	82.5	508
R12	MGR	4	26.7	80	100	28.1	82.5	318
R13	MGR	4	54.4	130	100	53.1	127.5	369
R14	Selenio	5	40.6	105	100	39.2	102.5	330
R15	Selenio	5	26.7	80	200	26.1	79	407
R16	Selenio	5	26.7	80	100	26.1	79	318
R17	Selenio	5	54.4	130	200	52.2	126	419
R18	SGR	6	40.6	105	200	39.2	102.5	381
R19	SGR	6	26.7	80	300	26.7	80	572
R20	SGR	6	54.4	130	100	53.1	127.5	292

Table 7.2: Summary of the d-optimal experimental design 20 trials conditions. MGR and SGR stand for Medium Grain Rice and Short Grain Rice respectively.

On figures 7.2a and 7.2b, the Medium grain variety is represented as green triangles ($\blacktriangle\triangle$ R01-03, R10-13); the Short grain variety as blue squares ($\blacksquare\blacksquare$ R04-06, R18-20); and the Selenio variety as red diamonds ($\blacklozenge\blacklozenge$ R07-09, R14-17). The full and empty symbols for each variety indicate two different days of production.

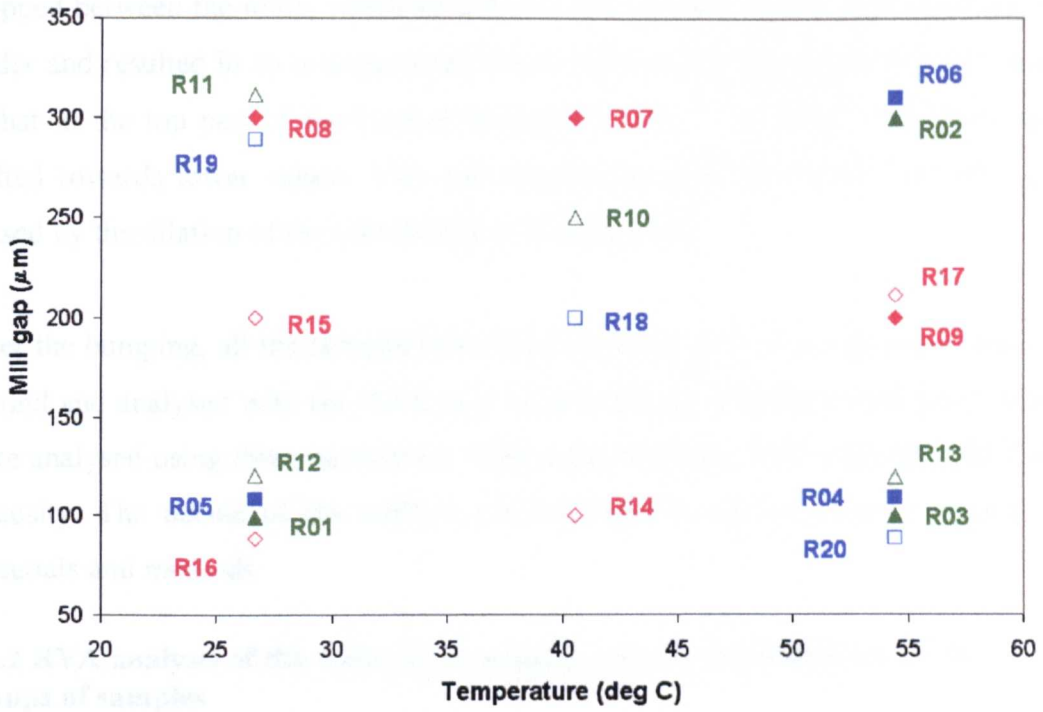


Figure 7.2a: Battle Creek 20 trials planned d-optimal experimental design

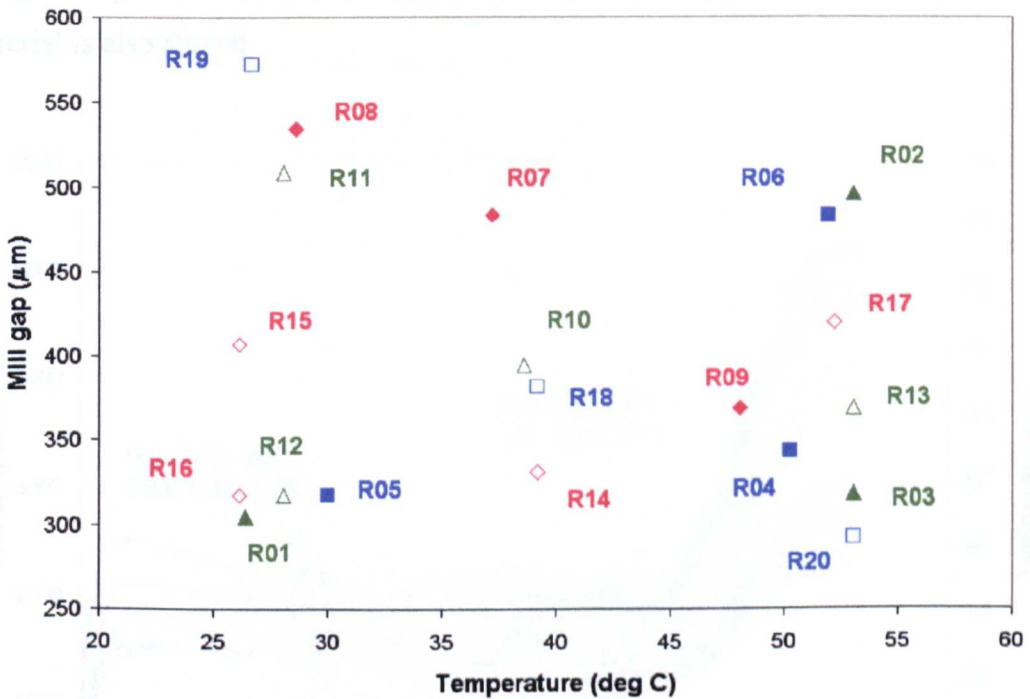


Figure 7.2b: Battle Creek 20 trials actual experimental conditions

As an illustration of the difficulty there can be to control parameters in a factory environment, both planned and actual experimental conditions have been indicated on figure 7.2 (a and b) and in table 7.2. The marked difference between the planned and actual mill gaps is due to the measurement method: A piece of solder was

dropped between the mills, which forced the mills to come apart while crushing the solder and resulted in an overestimated value of the actual gap. Another observation is that in the top part of the studied temperature range, the actual mill gaps were shifted towards lower values. This was interpreted as a reduction in the mill gap caused by the dilation of the rolls at higher temperatures.

After the bumping, all the samples were dried down to 10% w.w.b moisture content, ground and analysed with the RVA cold paste protocol. The RVA profiles obtained were analysed using three parameters: Cold paste viscosity, 95°C viscosity and Final viscosity. The details of the method are described in section 4.5.8 of chapter 4: Materials and methods.

7.2.2 RVA analysis of the series of 13 samples (set A): Identification of three groups of samples

The RVA cold paste profiles of the set A series of 13 central composite experimental design samples are shown on figure 7.3. The RVA profile of the pre-bumped material is also shown.

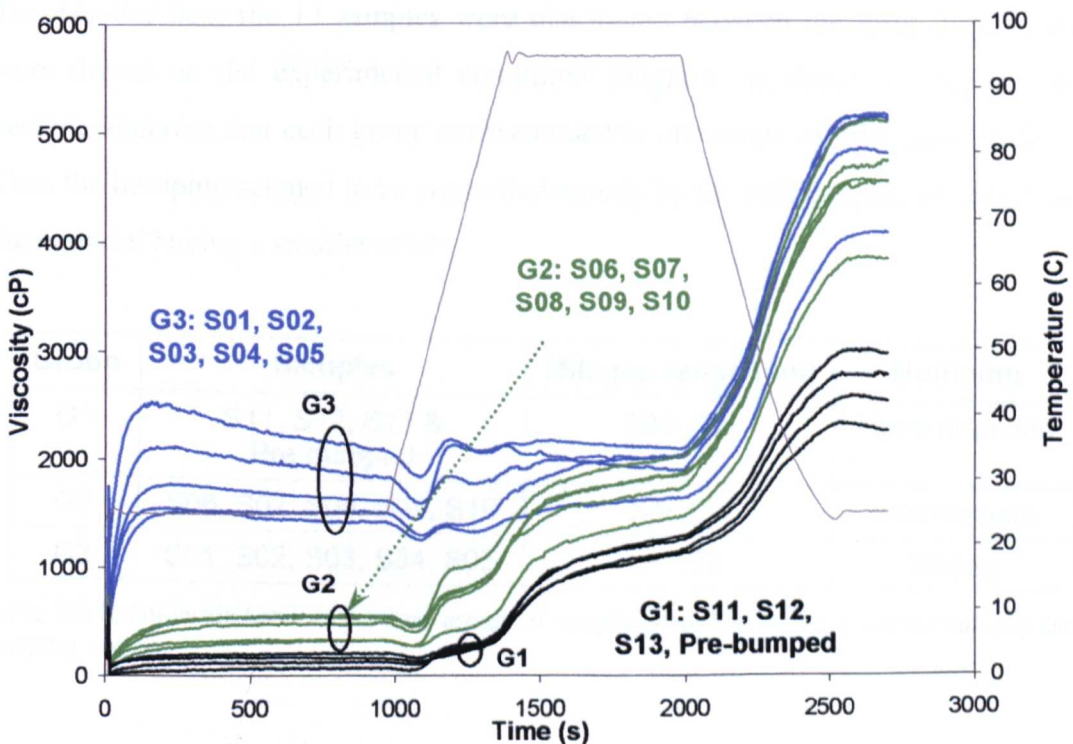


Figure 7.3: RVA cold paste profiles of the central composite experimental design 13 samples

Three groups of samples were identified using the shape of the RVA profiles. They are indicated on figure 7.3 by the black circles G1, G2 and G3. Compared to the other two groups, group 1 samples (G1) have low cold paste viscosities, low 95°C viscosities and low final viscosities. Group 3 samples (G3) have high cold paste viscosities, high 95°C viscosities and high final viscosities. Group 2 samples (G2) are intermediate and have cold paste viscosities comparable to group 1 samples, but 95°C and final viscosities comparable to group 3 samples. The characteristics of the three groups are summarised in table 7.3.

Group	Samples	Cold paste range (cP)	95°C viscosity range (cP)	Final viscosity range (cP)
G1	S11, S12, S13 & Pre-bumped	63 – 211	917 - 1052	2250 - 2948
G2	S06, S07, S08, S09, S10	320 – 553	1240 - 1830	3823 - 5079
G3	S01, S02, S03, S04, S05	1437 – 2187	1580 - 2155	4064 - 5143

Table 7.3: Characteristics of the three groups of RVA profiles

To visualise how the 13 samples were distributed between the three groups, these were drawn on the experimental conditions diagram, as shown on figure 7.4. It became apparent that each group corresponded to one range of mill gaps (table 7.4). Thus the bumping seemed to be controlled mainly by the mill gap, the temperature of the material having a smaller effect.

Group	Samples	Mill gap range (µm)	Bumping
G1	S11, S12, S13 & Pre-bumped	590-728	None or gentle
G2	S06, S07, S08, S09, S10	329-431	Intermediate
G3	S01, S02, S03, S04, S05	44-174	Strong

Table 7.4: Relationship between the three groups of samples identified by RVA and the mill gap and bumping severity

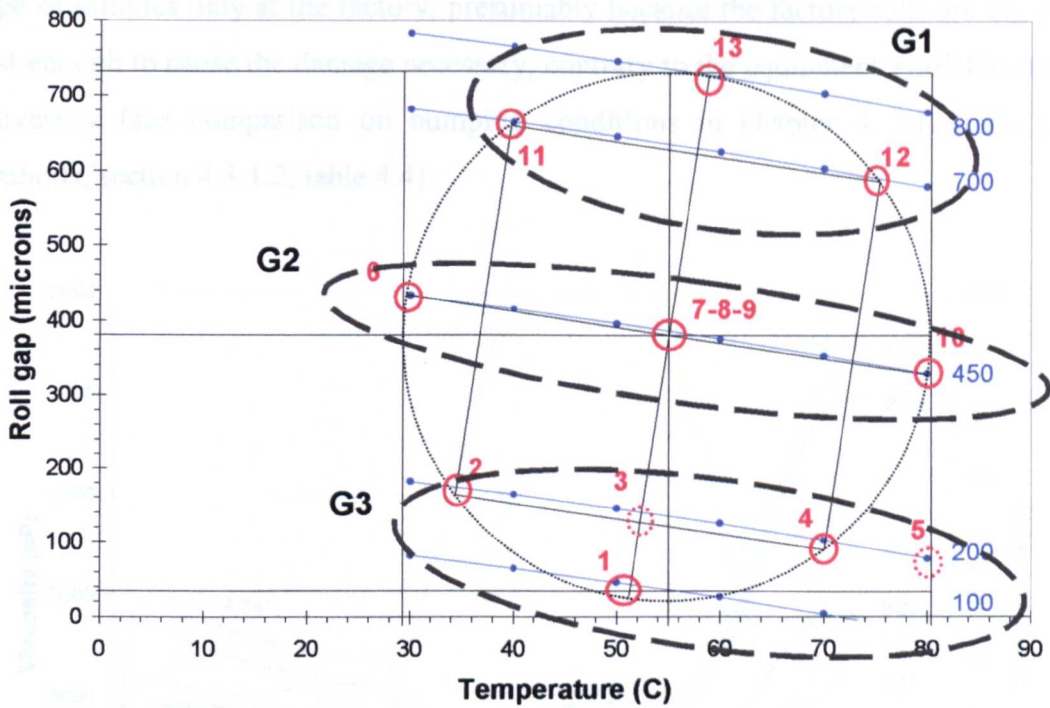


Figure 7.4: Diagram showing the link between the 3 groups G1, G2, G3 of samples identified by RVA and the 3 main mill gap levels of the central composite experimental design

7.2.3 RVA analysis of the series of 6 samples (set B): Identification of a fourth group of samples

The RVA profiles of the set B series of 6 Manchester factory samples are shown on figure 7.5.

The pre-bumped sample (F01) profile matched the corresponding pre-bumped sample presented in section 7.1.2. Similarly, samples F02 and F03 profiles corresponded, by their shape, with the group 3 (G3) category of samples described in section 7.1.2 (figure 7.3), and are shown in blue on figure 7.5.

The profiles of the three smaller mill gaps samples F04, F05 and F06 had a shape not seen before, shown in red and orange on figure 7.5: A high cold paste viscosity, but a low 95°C viscosity and a low final viscosity comparable to the one of the pre-bumped sample. It can be noted that the cold paste, 95°C and final viscosities decrease when the mill gap decreases, contrary to what happens for the other groups of samples (G1, G2 and G3).

This additional group of samples was labelled **G4**. It was possible to produce this

type of samples only at the factory, presumably because the factory rolls are big and fast enough to cause the damage necessary, contrary to the equipment available at the university (see comparison on bumping conditions in chapter 4: Materials and methods, section 4.3.1.2, table 4.4).

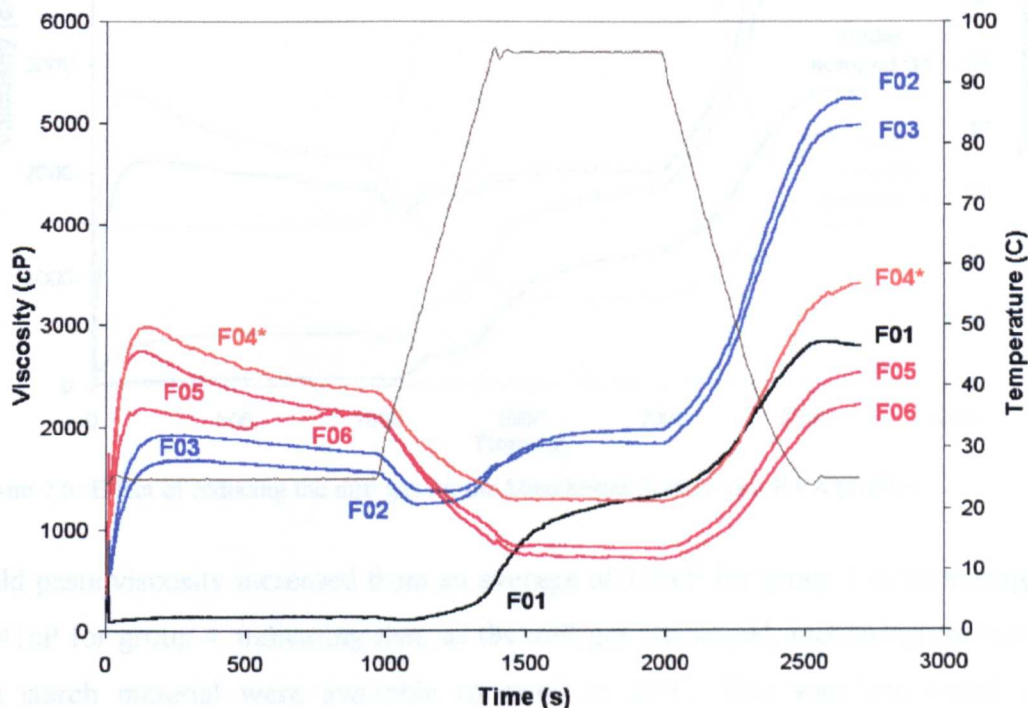


Figure 7.5: RVA cold paste profiles of six Manchester factory Selenio rice samples (set B). F01 is a pre-bumped sample and F02 to F06 were prepared by reducing progressively the gap between the bumping rolls

Figure 7.6 shows a typical RVA profile of each of the four groups of samples. Table 7.5 summarises the average cold paste, 95°C, and final viscosities of the four groups.

Group	Samples	Mill gap	Cold paste (cP)	95°C visc. (cP)	Final visc. (cP)
G1	S11, S12, S13, PRE, F01	Large	139 (53)	832 (62)	2651 (271)
G2	S06, S07, S08, S09, S10	Intermediate	443 (112)	1458 (233)	4540 (458)
G3	S01, S02, S03, S04, S05, F02, F03	Small	1733 (225)	1868 (403)	4919 (1066)
G4	F04, F05, F06	Very small	2240 (294)	955 (617)	2710 (1375)

Table 7.5: Average Cold paste, 95°C and Final viscosities for the 4 RVA groups of samples. The standard deviations are indicated in brackets.

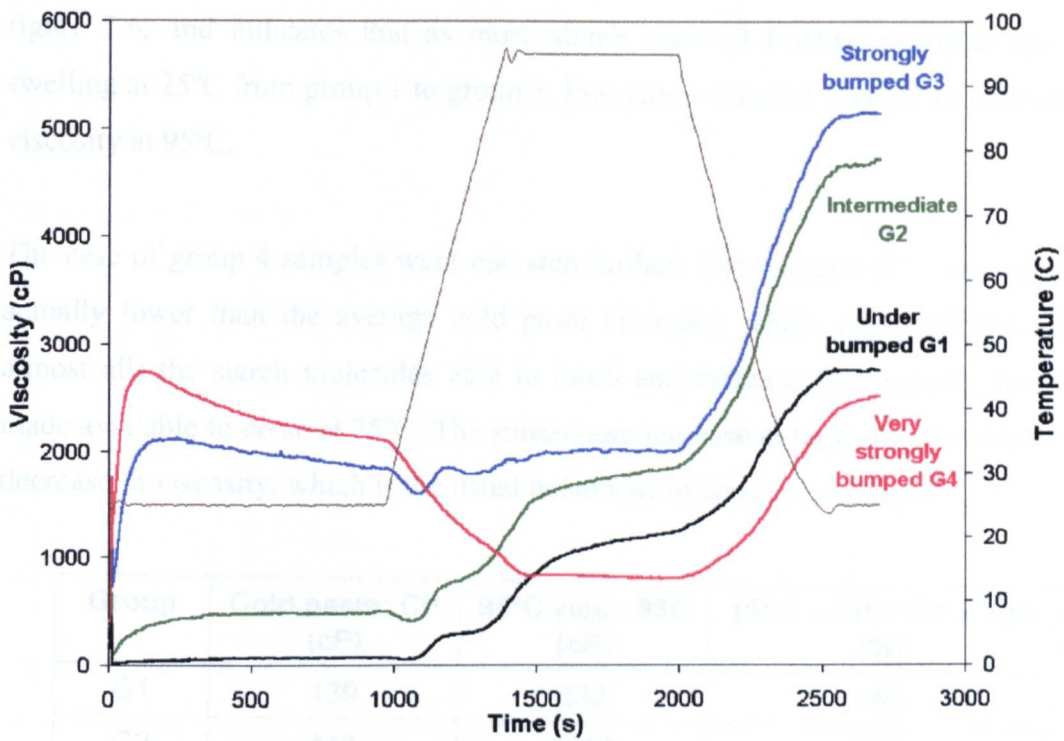


Figure 7.6: Effect of reducing the mill gap on the Manchester Selenio rice RVA profiles

Cold paste viscosity increased from an average of 139cP for group 1 to an average of 2241cP for group 4, indicating that, as the mill gap decreased, increasing amounts of the starch material were available to swell at 25°C. This was interpreted as a confirmation that bumping damages the structure of the rice grains.

This increase in cold paste viscosity when the mill gap decreased was verified for groups 1, 2 and 3. However, among samples of group 4, it was noted that the two smallest mill gap samples, F05 and F06, had lower cold paste viscosities than the preceding sample F04: 2208 and 2076cP against 2435cP respectively.

Similarly, the average 95°C viscosity increased from the group 1 to the group 3 of samples, and decreased in the group 4 of samples to a value comparable to the one of the group 1 (955 and 832cP respectively). However, it proved more interesting to compare the average 95°C and cold paste viscosities within each group of samples: Table 7.6 shows that the bigger the cold paste viscosity among groups 1, 2 and 3, the smaller the subsequent increase in viscosity at 95°C. Hence, for group G1 the increase rate between the cold paste viscosity (CP) and the 95°C viscosity (95C) is 499%, while for group G3, the increase rate is 18%, as indicated in the right hand column of table 7.6. This can also be seen on the RVA profiles of the four groups on

figure 7.6, and indicates that as more starch material became available for cold swelling at 25°C from group 1 to group 3, less starch material was left to increase the viscosity at 95°C.

The case of group 4 samples went one step further: The average 95°C viscosity was actually lower than the average cold paste viscosity, which indicated that all (or almost all) the starch molecules able to swell and increase the viscosity had been made available to do so at 25°C. The subsequent increase in temperature resulted in a decrease in viscosity, which is the usual behaviour of aqueous solutions.

Group	Cold paste: CP (cP)	95°C visc.: 95C (cP)	(95C – CP) / CP x 100 (%)
G1	139	832	499
G2	443	1458	229
G3	1733	1868	18
G4	2240	955	-57

Table 7.6: Evolution of average Cold paste and 95°C viscosities from RVA groups G1 to G4

The average final viscosity followed the same pattern as the average 95°C viscosity: It increased from group 1 to group 3 of samples, and decreased in group 4 of samples to a value comparable to the one of the group 1 (2710 and 2651cP respectively). Also, samples F05 and F06 had lower 95°C and final viscosities than the preceding sample F04, as summarised in table 7.7.

Sample	Mill gap	Cold paste (cP)	95°C visc. (cP)	Final visc. (cP)
F04	Small	2435	1291	3398
F05	Very small	2208	832	2523
F06	Smallest	2076	742	2208

Table 7.7: Evidence of a decrease in cold paste, 95°C and final viscosities within the RVA group 4, when the mill gap decreases.

Table 7.8 summarises the changes in cold paste, 95°C and final viscosities when the mill gap decreases.

Group	G1	G2	G3	G4
Mill gap	→			
Cold paste viscosity	→			→ ↘
95°C viscosity	→		→	↘
Final viscosity	→			↘

Table 7.8: Evolution of the RVA parameters when the mill gap decreases among the 4 groups

These observations showed that the damage done to the rice grains by the bumping is of (at least) two kinds: For relatively large mill gaps, all three viscosities (cold paste, 95°C and final) increased, and for small mill gaps they decreased. This led to the hypothesis that two distinct structure-reinforcing ‘items’ inside the rice grain are broken during the bumping. The hypothesis will be detailed in the conclusion paragraph (§7.2.5) of this section.

7.2.4 Effect of variety, mill gap and bumping temperature: Analysis of the RVA profiles of the Battle Creek factory trials (set C)

The RVA cold paste profiles of the set C 20 Battle Creek d-optimal experimental design samples are shown on figure 7.7. In green, blue and red are figured samples corresponding to groups G2, G3, and G4 respectively. Two G4 samples, R06 and R18, have been drawn in orange to signal an extra shoulder in viscosity appearing at 1200s (group G4’). The three G4 samples with the highest cold paste viscosities (R02, R10, R11) have been drawn in bold red (group G4+).

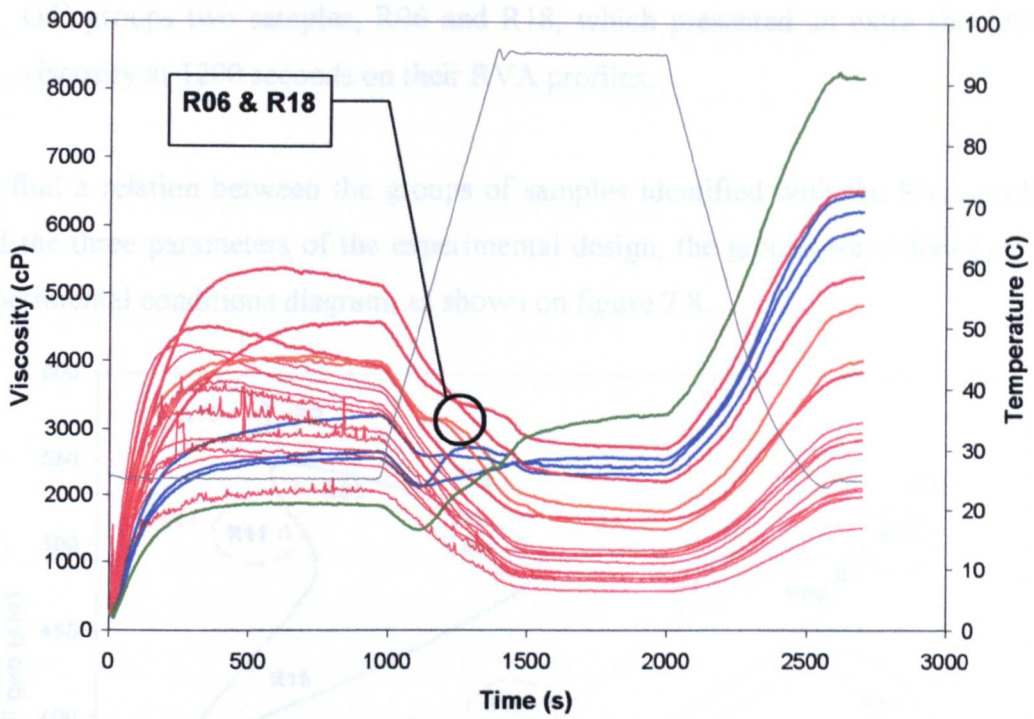


Figure 7.7: RVA cold paste profiles of the d-optimal experimental design 20 trials

Table 7.9 summarises the repartition of the 20 samples between the four groups (G1 to G4) identified in section 7.2.3 (figure 7.6 and table 7.5). The samples were sorted into the four groups visually by considering the shape of the RVA profiles. Samples of the sub-categories G4+ and G4' are also indicated.

Group	Samples	Curve colour code for figure 7.X
G1	None	Black
G2	R19	Green
G3	R07, R08, R15	Blue
G4	All others	Red
G4+	R02, R10, R11	Dotted red
G4'	R06, R18	Orange

Table 7.9: Repartition of the d-optimal experimental design 20 samples into the four groups and two sub-categories of RVA profiles

The two sub-categories G4+ and G4' of group G4 were distinguished as follows:

- G4+ groups the three samples of G4 with the highest cold paste viscosities (R02, R10 and R11), because the RVA profiles of these samples appeared detached above the rest of the lot on figure 7.7.

- G4' groups two samples, R06 and R18, which presented an extra shoulder in viscosity at 1200 seconds on their RVA profiles.

To find a relation between the groups of samples identified with the RVA profiles and the three parameters of the experimental design, the groups were drawn on the experimental conditions diagram, as shown on figure 7.8.

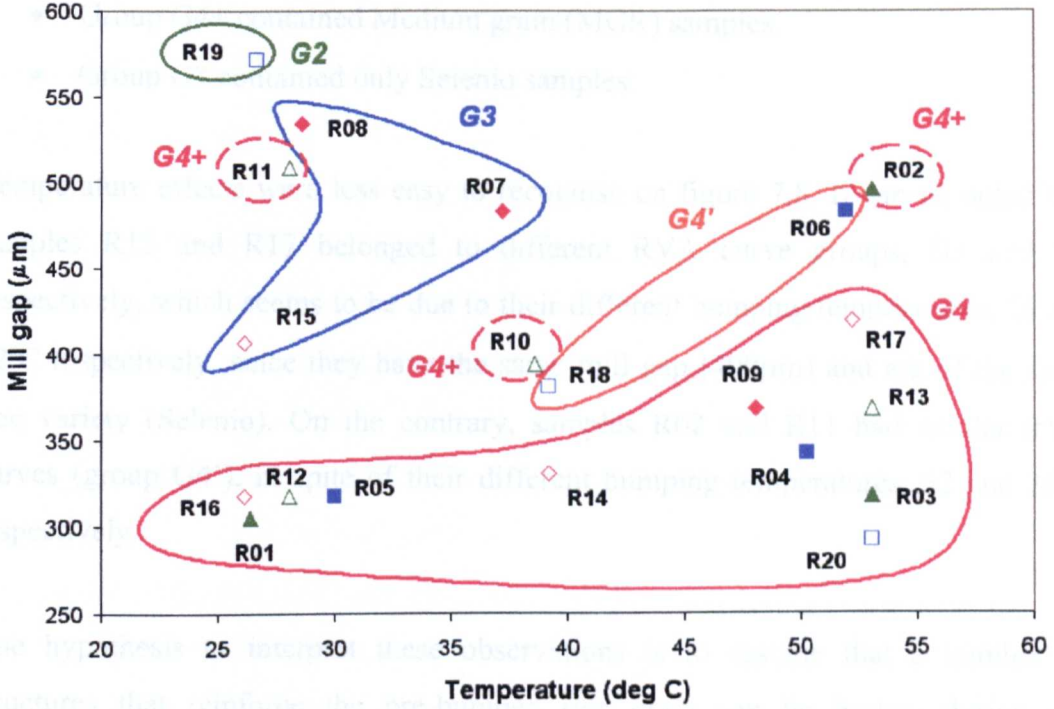


Figure 7.8: Diagram showing the correspondence between the four groups and two sub-categories of samples identified by RVA and the d-optimal experimental design actual conditions; ▲△ Medium grain variety, ■□ Short grain variety, ◆◇ Selenio variety. The full and empty symbols for each variety indicate two different days of production.

Like the results obtained with the set A central composite experimental design 13 samples (section 7.2.2, figure 7.4), the groups could be sorted by mill gaps: G2 corresponded to the bigger mill gap (572µm), G3 to intermediate mill gaps (400-550µm), and G4 to the smaller mill gaps (below 400µm). This confirmed that the mill gap is the main factor in determining the shape of the samples RVA profiles, and hence the quality of the post-bumped samples. The bumping temperature (temperature of the rice grains) and rice variety appeared to have a secondary effect, as their influence could be detected on figure 7.8 for mill gaps above 400µm.

Group G4 occupied the lower part of the diagram (mill gaps below 400µm), covering

the whole range of temperatures tested and grouping samples of all varieties. Thus for small mill gaps the effects of temperature and rice variety were not detectable.

For mill gaps above 400 μm the rice varieties could be distinguished by the shape of the RVA curves:

- Group G4' contained only Short grain (SGR) samples.
- Group G4+ contained Medium grain (MGR) samples.
- Group G3 contained only Selenio samples.

Temperature effects were less easy to recognise on figure 7.8. It can be noted that samples R15 and R17 belonged to different RVA curve groups, G3 and G4 respectively, which seems to be due to their different bumping temperatures, 26 and 52°C respectively, since they have the same mill gap (400 μm) and are of the same rice variety (Selenio). On the contrary, samples R02 and R11 had similar RVA curves (group G4'), in spite of their different bumping temperatures, 52 and 26°C respectively.

One hypothesis to interpret these observations is to assume that a number of structures that reinforce the pre-bumped rice grain can be broken during the bumping.

For mill gaps below 400 μm (when the mill gap is measured with the solder method), everything that can be damaged by the bumping inside the rice grains is entirely broken, which results in samples with RVA profiles belonging to the group G4.

For mill gaps above 400 μm , the rice grains are only partially damaged. The extent and type of damage is then controlled not only by the mill gap, but also by the rice variety and bumping temperature. This explains the diversity of RVA profiles observed (groups G2, G3, G4+, G4').

7.2.5 Summary and interpretations

7.2.5.1 Summary

The RVA analysis of a wide range of post-bumped samples showed that bumping produces four types of samples. These were determined mainly by the size of the mill gap. For mill gaps above 400 μm (as measured with a solder fed between the rolls, cf. section 3.3.3 of chapter 3: Evaluation of the industrial process), rice variety and bumping temperature were found to have a secondary influence on the shape of the RVA profiles.

For mill gaps below 400 μm , only the mill gap had a role in determining the shape of the samples RVA profiles. Rice variety and bumping temperature had little effect. Process wise, this means that bumping the rice with a mill gap smaller than 400 μm should result in less variability in the post-bumped material, which is desirable to achieve a consistent end product and a smoother operation of the production line.

To explain why the bumping resulted in four different types of samples, the hypothesis that cooked rice grains contain various structure-reinforcing 'items' that are damaged by the bumping was introduced. The extent of the damage depends on the mill gap, and also in the case of wide gaps (above 400 μm), of the bumping temperature and rice variety.

7.2.5.2 Hypothetical repartition of the strains in the rice grain structure during the bumping

An attempt to explain the repartition and extent of the damage caused in the rice grain by the bumping is sketched on figure 7.9 for small and wide mill gaps.

The bumping deforms the rice grain, which damages the grain structure, and the structural damage is proportional to the deformation. However, not the whole rice grain is subjected to the same deformations. The centre, where the grain is thickest, is more deformed, and therefore more damaged, than the extremities. This can be modelled by a field of strains created at the instant of the bumping inside the rice grain, as sketched with red arrows on figures 7.9a and 7.9b. At the two ends where the rice grain becomes thinner than the mill gap, it was assumed that no deformation

occurs, and that the strain field is minimal.

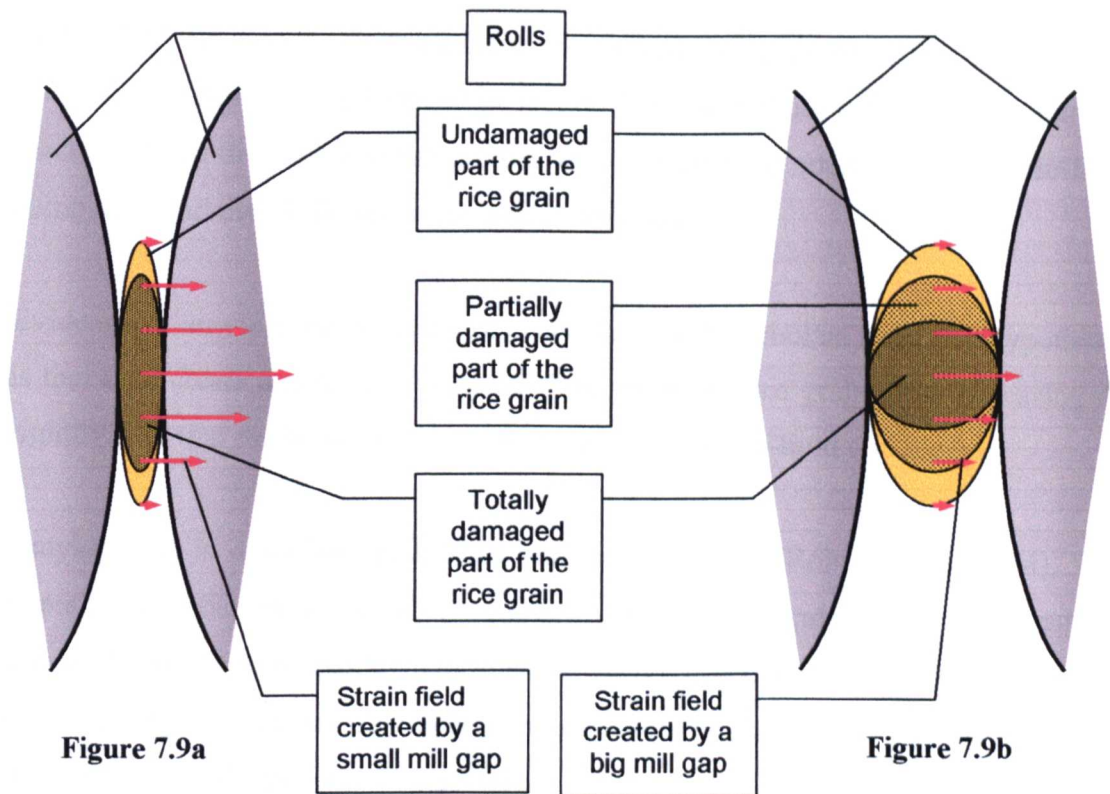


Figure 7.9: Hypothetical strain field created in the rice grain on the instant of bumping. Fig. 7.9a: Small mill gap; Fig. 7.9b: Wide mill gap

The mill gap is as a key parameter to control the extent of the damage to the rice grain. For small mill gaps, important deformations are created in the whole grain except its very edges, thus breaking most of the structure-reinforcing items inside the grain (figure 7.9a). For big mill gaps, the smaller deformation means that the strain field is important enough to damage significantly only the centre of the grain (figure 7.9b). Towards the edges the material is only partially damaged or not damaged at all. The type of damage in this area depends then on others parameters than the mill gap, such as the rice variety and the bumping temperature, which explains the various types of RVA profiles observed.

This description is limited to the strain field perpendicular to the rice grain. However, some longitudinal displacement of starch material from the centre of the grain towards its extremities may also happen at the instant of bumping (Levine, 1997) and cause additional damage at the rice grain extremities.

7.2.5.3 Further hypotheses on what is broken inside the rice grain during the bumping

The hypothesis that bumping weakens the cooked rice grain by breaking ‘structure-reinforcing items’ was introduced in section 7.2.5.1, without detailing the nature of these items. In the course of the project, two of them were identified: Amylose-lipid complexes and the amylopectin molecular structure.

Evidence of amylose-lipid complexes was found in the cooked rice. The hypothesis is that they create a network extending throughout the rice grain, thus increasing its rigidity, and that the bumping partially dislocates amylose-lipid complexes.

Amylopectin is described as a large branched polymer (Robin *et al.*, 1974). The hypothesis is that the bumping decreases its average molecular weight by breaking down amylopectin molecules into smaller polysaccharides. The further hypothesis that bumping debranches amylopectin was considered, however only indications of this, not firm evidence, could be gathered.

The effect of disrupting amylose-lipid complexes and of reducing amylopectin molecular weight is to loosen the rice grain structure to allow a proper expansion at the puffing step of the process. Specifically, the amylose-lipid complexes grain-wide network is thought to lock the whole grain structure and needs to be broken down to allow molecular movements, such as water migration and vaporisation, in the rice grains. The amylopectin molecular weight reduction is thought to decrease the viscosity of the molten starch material, which facilitates the expansion of the water vapour bubbles formed during the puffing.

The next section, 7.3, presents the results of the study of amylose-lipid complexes. Section 7.4 presents the results of the study of amylopectin molecular weight.

7.3 STUDY OF COOKED RICE AMYLOSE-LIPID COMPLEXES

Studies by Morrisson (1995) have shown that amylose-lipid are formed during the cooking of cereals, and that they may affect the mechanical or rheological properties of the cooked material. Therefore they appeared relevant to the rice cooking, and evidence of their presence was investigated (section 7.3.1). The effect of the bumping on the amylose-lipid complexes was studied (section 7.3.2). To assess if amylose-lipid complexes reinforce the structure of cooked starch systems, a study of the cooking of simplified mixtures constituted of rice flours and added lipids was conducted by RVA (section 7.3.3). Finally, an attempt at modelling how amylose-lipid complexes reinforce the structure of the cooked rice grains and are disrupted by the bumping was made (section 7.3.4).

7.3.1 Evidence of the presence of amylose-lipid complexes in the cooked material

7.3.1.1 *RVA evidence of amylose-lipid complexes*

Becker (2001) prepared a series of converted starch samples by quiescent cooking, which consists in cooking the samples in sealed containers with no mechanical input (shear). The moisture content of the samples was 33% w.w.b. The cooking was done at 140°C for up to 30 minutes. These parameters seemed fairly close to those of the rice cooking conditions (see section 3.3.2 of chapter 3: Evaluation of the industrial process), which suggested that the conclusions of her work could be relevant to interpret the RVA profiles of the pre-bumped and post-bumped material.

Becker's conclusions were that when the formation of amylose-lipid complexes was prevented during the cooking, a cold paste viscosity was present on the RVA profile. This is shown on figure 7.10b with waxy maize starch, which contains no amylose, and on figure 7.10c with cassava starch, which contains no lipids. Conversely, when amylose-lipid complexes were allowed to form, no cold paste viscosity appeared on the RVA profiles, as shown on figure 7.10a with wheat starch. Thus, amylose-lipid complexes appeared to prevent the swelling of cooked starch.

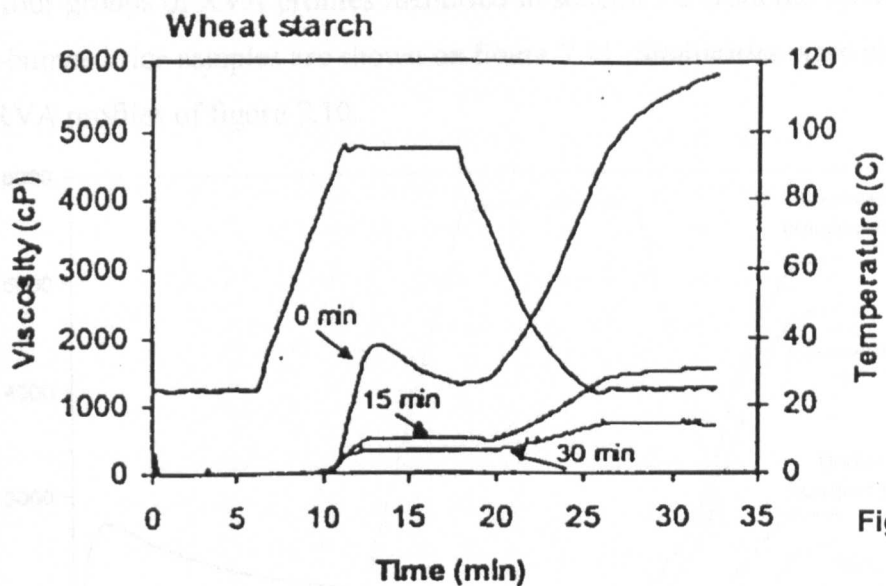


Figure 10a

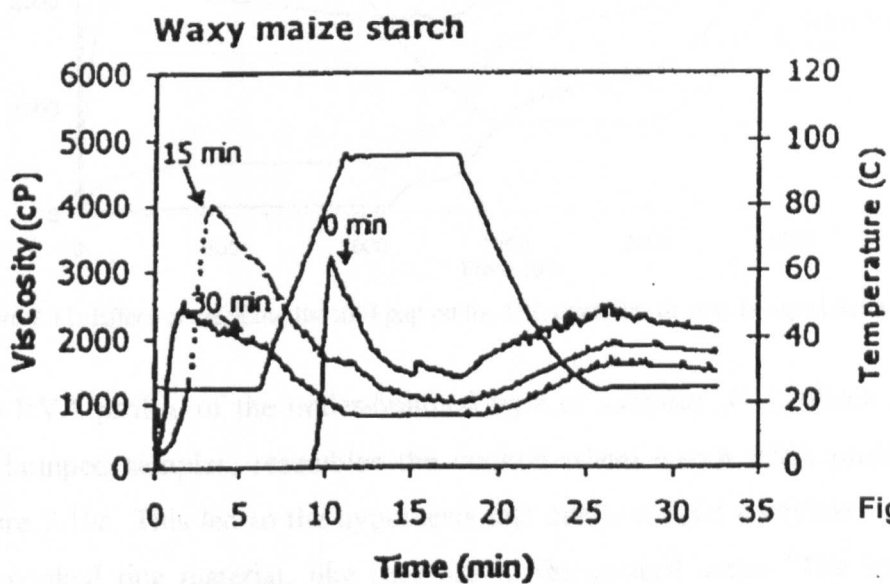


Figure 10b

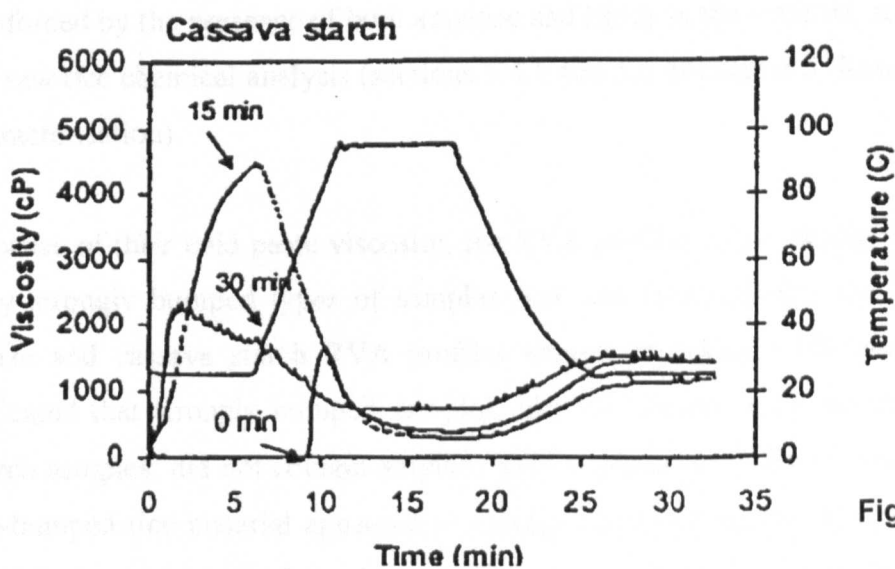


Figure 10c

Figure 7.10: RVA profiles of raw and cooked (15 and 30 minutes) wheat, waxy maize and cassava starches (Becker, 2001)

The four groups of RVA profiles identified in section 7.2 from the series of pre- and post-bumped rice samples are shown on figure 7.11. Similarities were identified with the RVA profiles of figure 7.10.

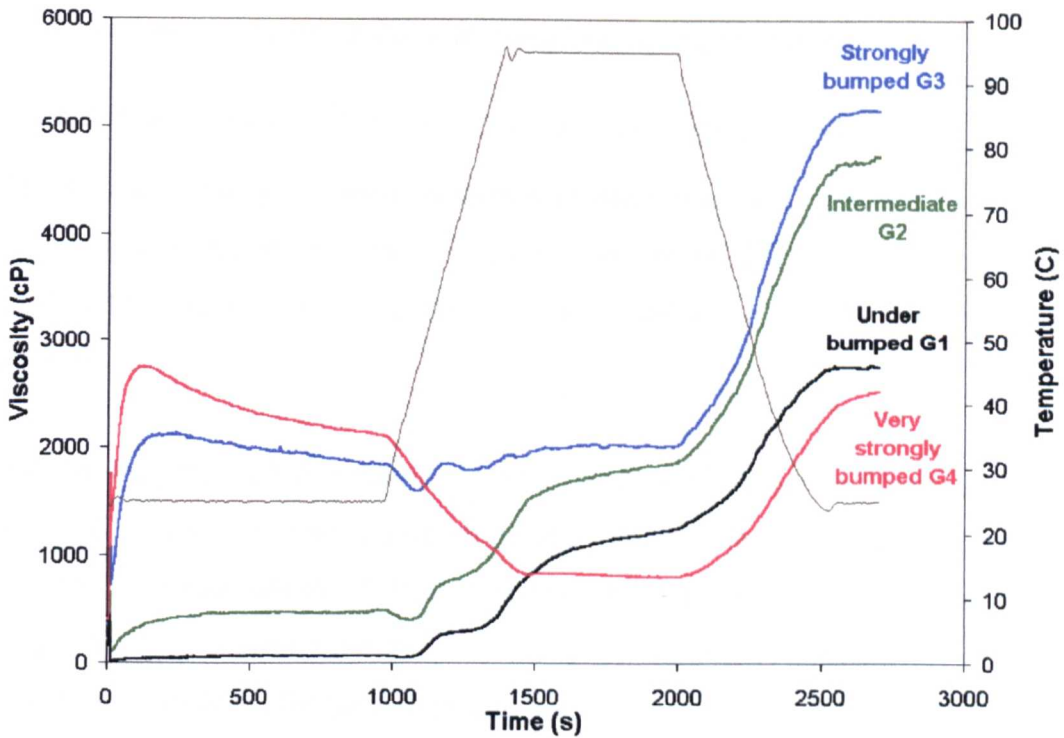


Figure 7.11: Effect of reducing the mill gap on the RVA profiles of post-bumped Selenio rice

The RVA profile of the under-bumped type of samples (G1), which also includes pre-bumped samples, resembles the cooked wheat starch RVA profile shown on figure 7.10a. This led to the hypothesis that amylose-lipid complexes are present in the cooked rice material, like they are in the cooked wheat. The hypothesis was reinforced by the presence of both amylose and lipids in the material, as indicated by the raw rice chemical analysis (sections 5.4.1 and 5.6 of chapter 5: Raw rice material characterisation).

Because of their cold paste viscosity, the RVA profiles of the strongly bumped and very strongly bumped types of samples (G3 and G4) resemble the cooked waxy maize and cassava starch RVA profiles shown on figure 7.10b and 7.10c. This indicated that strongly bumped samples, like the cooked waxy maize and cassava starch samples, did not contain amylose-lipid complexes. More accurately, since the pre-bumped rice material appeared to contain amylose-lipids complexes, the logical hypothesis was that the bumping could disrupt amylose-lipids complexes, allowing starch hydration.

The following section (7.3.1.2) presents evidence confirming the hypothesis that the cooked rice material contains amylose-lipid complexes. Section 7.3.1.3 then examines how the bumping dislocates amylose-lipid complexes.

7.3.1.2 X-rays evidence of amylose-lipid complexes in the cooked rice

The presence of amylose-lipid complexes in starch materials is revealed by a specific X-ray diffraction pattern, referred to as V-type pattern. The characteristics of the V-type pattern are a main diffraction peak at a 2-theta angle of 20°, and a secondary peak at 13°.

Early in the project, X-ray spectra of raw and cooked Balilla rice flours indicated the presence of amylose-lipid complexes in the cooked starch material. On figure 7.12, the raw flour presents the A-type diffraction pattern characteristic of native cereal starch, and the cooked flour presents the amylose-lipid complexes V-type pattern. The diffraction peaks for the A-type and V-type patterns are 15°, 17°, 18° & 23°, and 13°, 20° & 23° respectively (2-theta angles).

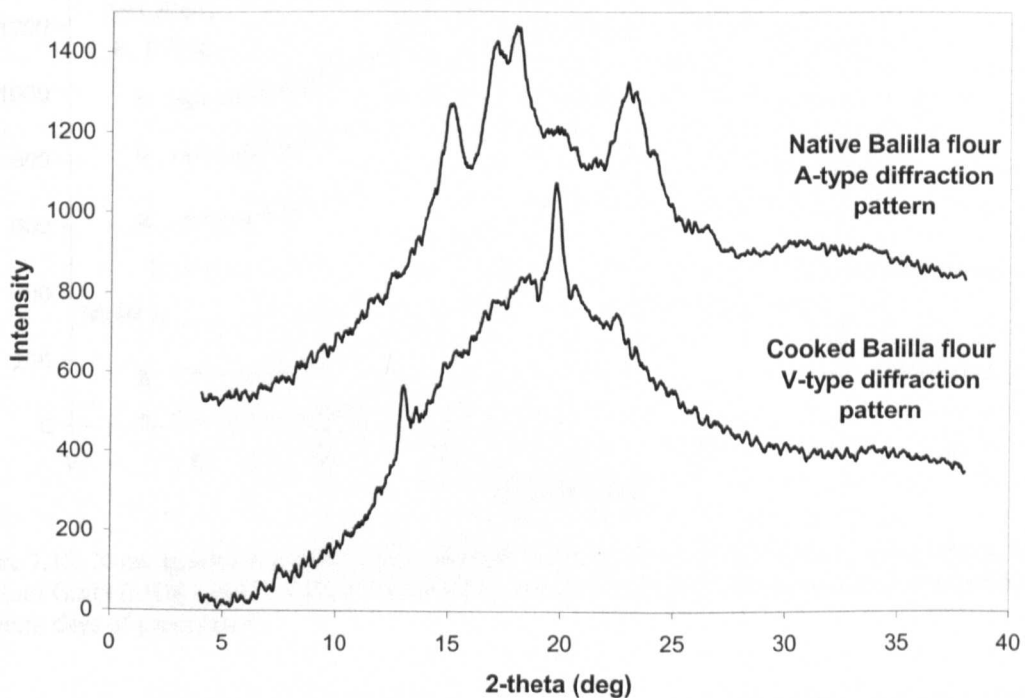


Figure 7.12: X-ray spectrum of native and cooked Balilla rice flour (Han and Hill, 1999)

The Balilla rice was cooked at the university, in a sealed can with 31% moisture

content (w.w.b) and no flavour liquor added. The rice was then dried and milled into flour. The X-ray protocol used is described in section 4.5.1 of chapter 4: Materials and methods.

Later on when the experimental designs described in section 7.2 were performed, several cooked samples of the Short Grain, Medium Grain and Selenio rice varieties were produced at the factory following the normal procedure described in section 3.3.2 of chapter 3: Evaluation of the industrial process. Upon X-ray analysis, all samples presented the amylose-lipid complexes V-type diffraction pattern. Figure 7.13 presents the X-ray spectra of six pre-bumped samples from the d-optimal experimental design (set C), and the X-ray spectrum of the pre-bumped Selenio sample of the central composite experimental design. Table 7.10 gives details of the samples.

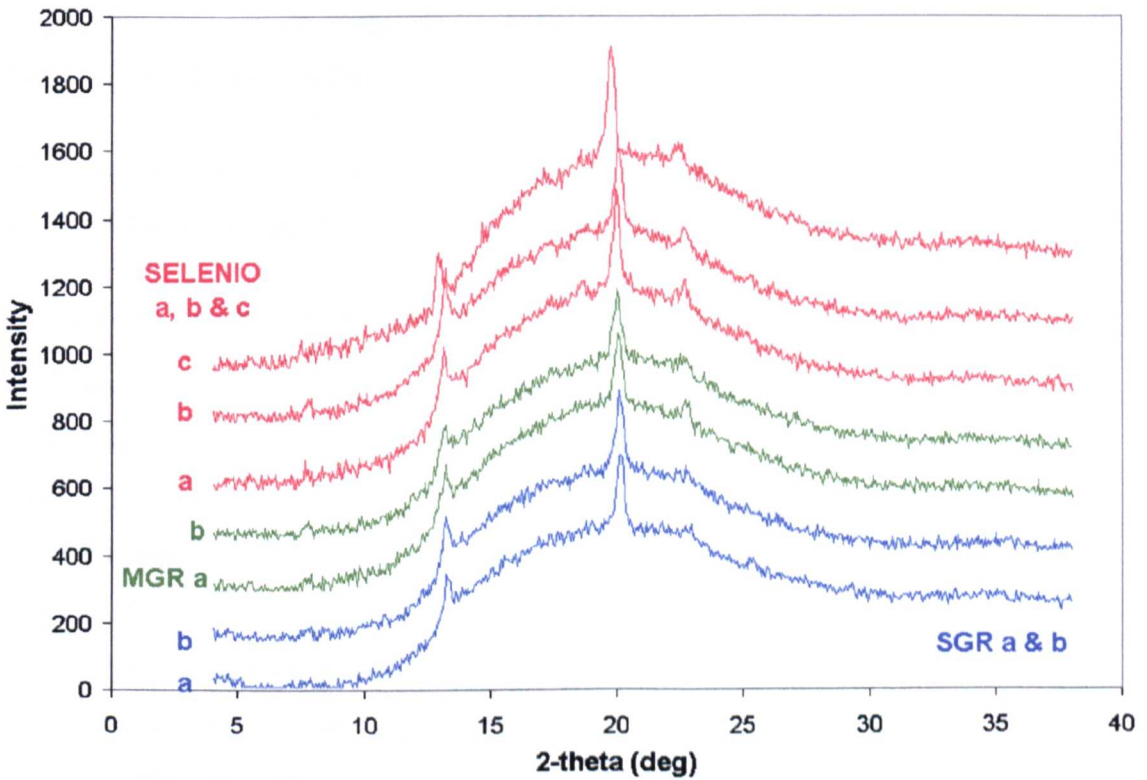


Figure 7.13: X-ray spectra of a series of pre-bumped samples: From top to bottom, three Selenio, two Medium Grain (MGR) and two Short Grain (SGR) varieties. The small letters a, b, and c represent different days of production

Table 7.10 also shows the total crystallinity, i.e. the area of the three V-pattern peaks divided by the amorphous area and expressed as a percentage (cf. section 4.5.1 of chapter 4: Materials and methods), of the set C d-optimal experimental design

samples. The Medium rice grain variety (MGR) appeared to have lower amounts of amylose-lipid complexes than the Short rice grain (SGR) and Selenio varieties, which could be related to the lower amounts of amylose found in the MGR variety (cf. section 5.4.1 of chapter 5: Raw rice material characterisation): 15.5% w.w.b. for the MGR variety against 19.1% w.w.b. and 18.2% w.w.b. for the SGR and Selenio varieties respectively.

Legend	Experimental design	Run	Rice variety	Total crystallinity (%)
SGR a	D-optimal	R05	Short Grain	0.17
SGR b	D-optimal	R19	Short Grain	0.20
MGR a	D-optimal	R11	Medium Grain	0.09
MGR b	D-optimal	R02	Medium Grain	0.12
SELENIO a	D-optimal	R08	Selenio	0.39
SELENIO b	D-optimal	R15	Selenio	0.12
SELENIO c	Central composite	N/A	Selenio	N/A

Table 7.10: Details of the pre-bumped samples used for figure 7.13 X-ray analysis

All these observations led to the conclusion that amylose-lipid complexes are present in the cooked grains of the rice varieties used to produce Rice Krispies™.

7.3.1.3 DSC evidence of amylose-lipid complexes in the cooked rice

The presence of amylose-lipid complexes in starch materials can be detected by DSC as an endothermic peak corresponding to the melting of the complexes in the temperature range 90-140°C. Because the re-crystallisation of amylose-lipid complexes upon cooling is a rapid phenomenon, a second DSC run is usually carried out immediately after the first one, in order to verify that the endothermic peak observed in the 100-140°C range does correspond to amylose-lipid complexes rather than to other phenomena such as starch gelatinisation or retrogradation. The complete DSC protocol is described in section 4.5.4 of chapter 4: Materials and methods.

Two samples from the set A central composite experimental design described in section 7.2 were analysed by DSC: The pre-bumped sample and the sample bumped with the smallest mill gap (sample 5, labelled S05). The pre-bumped sample 1st and 2nd runs are shown on figure 7.14 and the post-bumped sample 1st and 2nd runs on

figure 7.15.

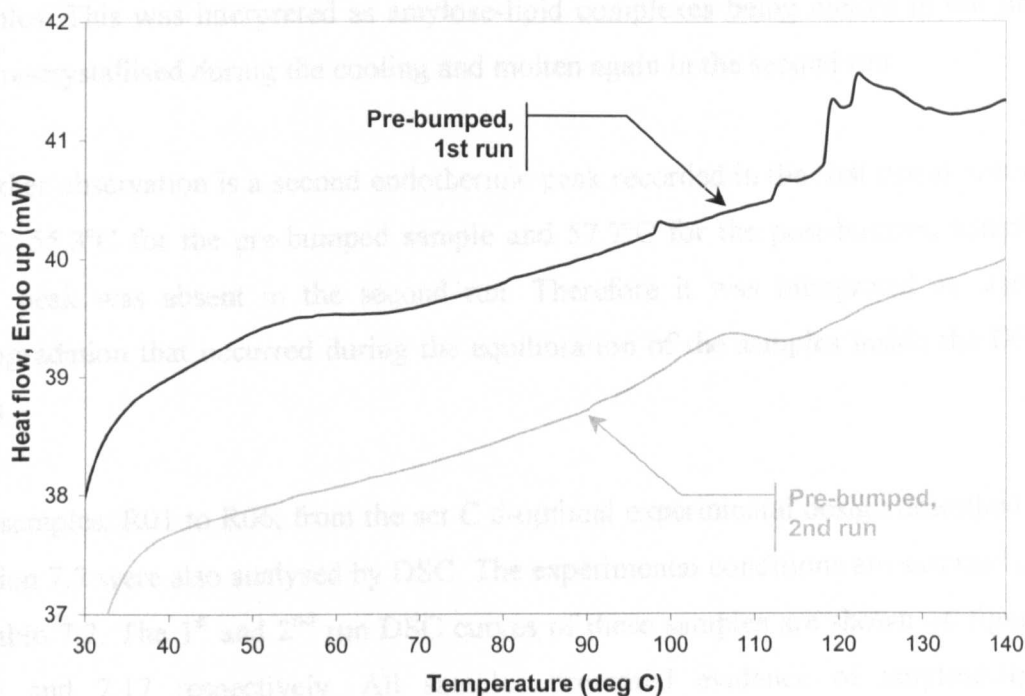


Figure 7.14: DSC evidence of the presence of amylose lipid complexes in pre-bumped rice (arbitrary heat flow scale). The solid : water ratio is 1:3 (w/w)

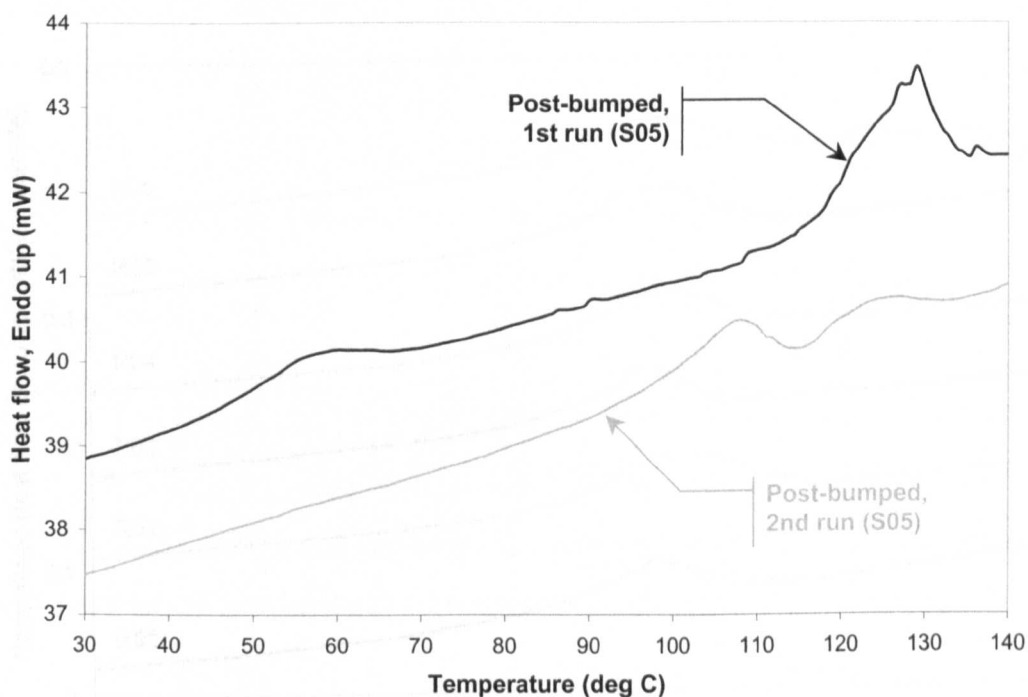


Figure 7.15: DSC evidence of the presence of amylose lipid complexes in post-bumped rice (arbitrary heat flow scale). The solid : water ratio is 1:3 (w/w)

The curves obtained for the pre-bumped and the post-bumped samples were of similar shapes. In the first run, an endothermic event was visible in the temperature

range 110-140°C for both the pre-bumped and post-bumped samples. In the second run, an endothermic event appeared in the temperature range 95-130°C for both samples. This was interpreted as amylose-lipid complexes being melted in the first run, re-crystallised during the cooling and molten again in the second run.

Another observation is a second endothermic peak recorded in the first run at around 56°C: 55.3°C for the pre-bumped sample and 57.7°C for the post-bumped sample. This peak was absent in the second run. Therefore it was interpreted as starch retrogradation that occurred during the equilibration of the samples inside the DSC pans.

Six samples, R01 to R06, from the set C d-optimal experimental design described in section 7.2 were also analysed by DSC. The experimental conditions are summarised in table 7.2. The 1st and 2nd run DSC curves of these samples are shown on figures 7.16 and 7.17 respectively. All samples presented evidence of amylose-lipid complexes in the post-bumped material, with an endothermic peak at approximately 122°C in the first run and at 106°C in the second run.

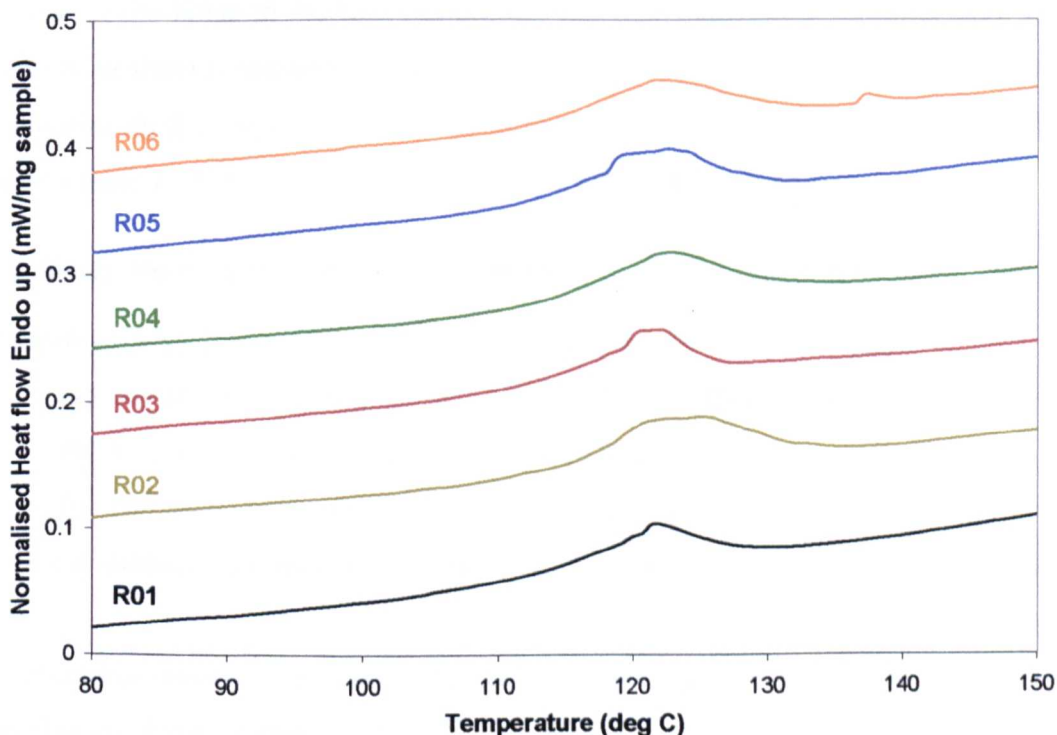


Figure 7.16: DSC assessment of the presence of amylose lipid complexes in six of the 20 samples from the set C d-optimal experimental design - First run (arbitrary heat flow scale). The solid : water ratio is 1:3 (w/w). The profiles were normalised by dividing the heat flow by the weight of dry sample

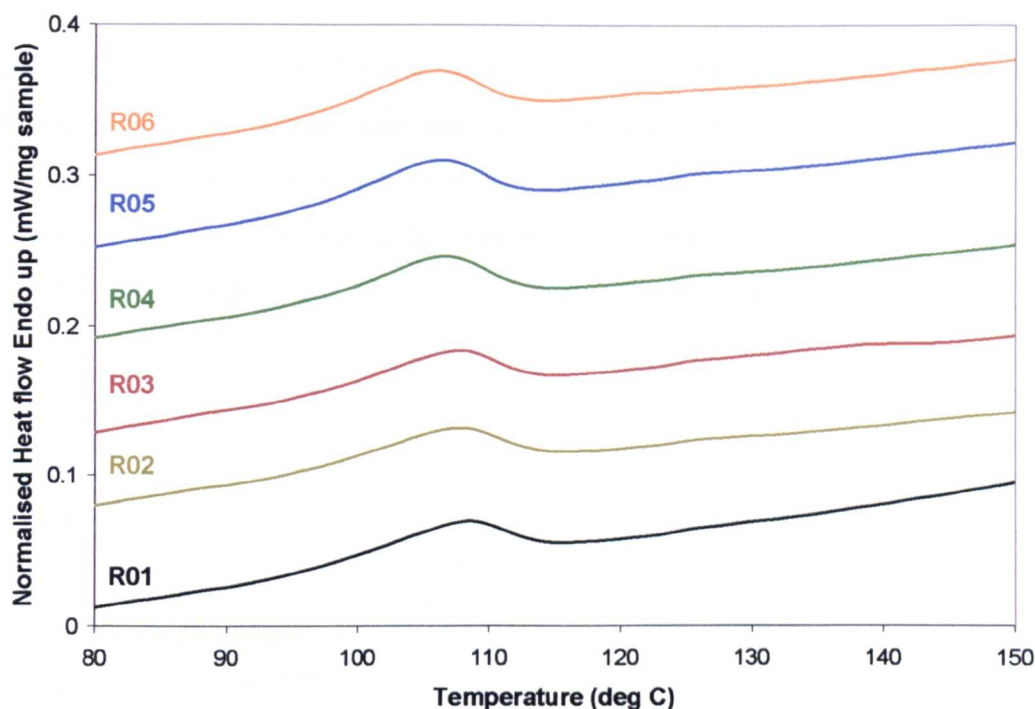


Figure 7.17: DSC assessment of the presence of amylose lipid complexes in six of the 20 samples from the set C d-optimal experimental design - Second run (arbitrary heat flow scale). The solid : water ratio is 1:3 (w/w). The profiles were normalised by dividing the heat flow by the weight of dry sample

Because of the noise in the first run curves, the amylose-lipid complexes peak area could not be determined with accuracy. Thus DSC provided evidence of the presence of amylose-lipid complexes in the cooked rice material, but could not be used to quantify them and analyse the effect of different bumping conditions.

7.3.2 X-ray study of the effect of the bumping on the amylose-lipid complexes

All samples described in section 7.2 were milled and analysed by X-rays:

- (a) The set A 13 central composite experimental design samples (S01 to S13).
- (b) The set B 6 varying mill gap samples (F01 to F06).
- (c) The set C 20 d-optimal experimental design samples (R01 to R20).

The X-ray protocol is described in section 4.5.1 of chapter 4: Materials and methods.

The resulting spectra were sorted between the four groups G1 to G4 of samples identified by RVA (section 7.3), including the two sub-groups G4+ and G4' in the case of the d-optimal experimental design samples. The groups correspond to increasing bumping strengths, from under-bumped samples in G1 to very strongly

bumped samples in G4.

Figure 7.18 shows a typical X-ray spectrum for each of the four groups, as well as a pre-bumped sample spectrum. The samples used were F01, S11, S07, S01, F05 from the central composite experimental design and the varying mill gap samples. All spectra presented the V-type pattern characteristic of amylose-lipid complexes, with a main diffraction peak at 20° 2-theta angle, and secondary peaks at 13° and 23° .

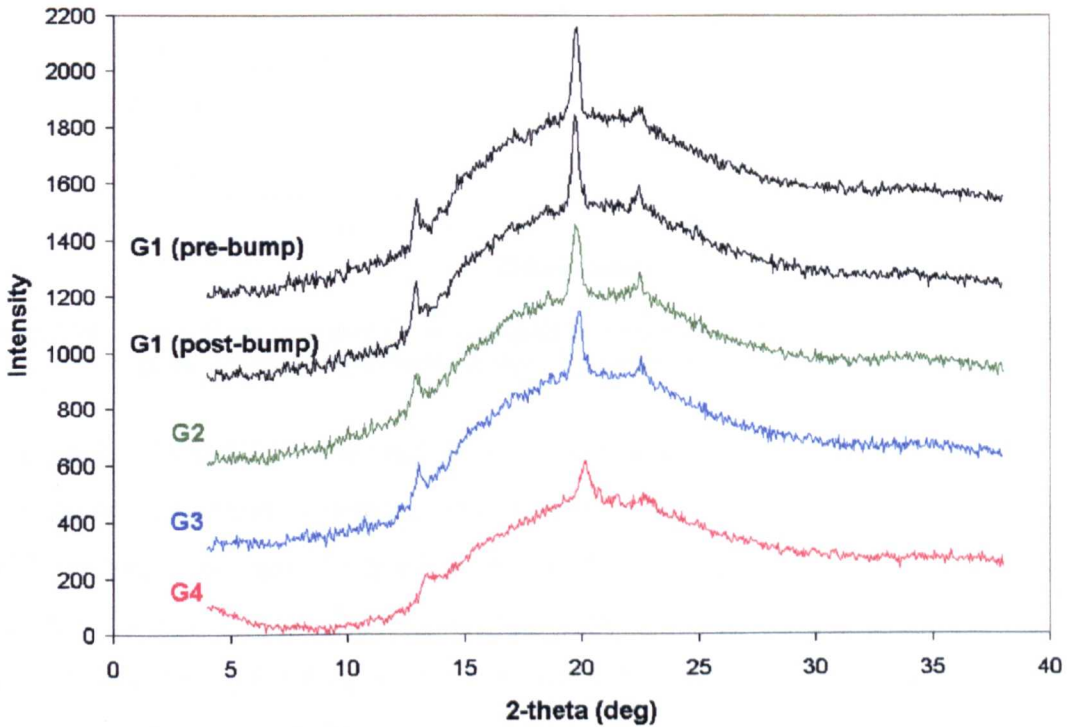


Figure 7.18: Typical X-ray spectra of the four RVA defined groups of cooked samples, using samples from set A and set B series. The bumping severity increases from G1 to G4

Figure 7.19 shows typical X-ray spectra for each of the groups G1, G2, G3, G4 and the sub-categories G4' and G4+ identified in the d-optimal experimental design.

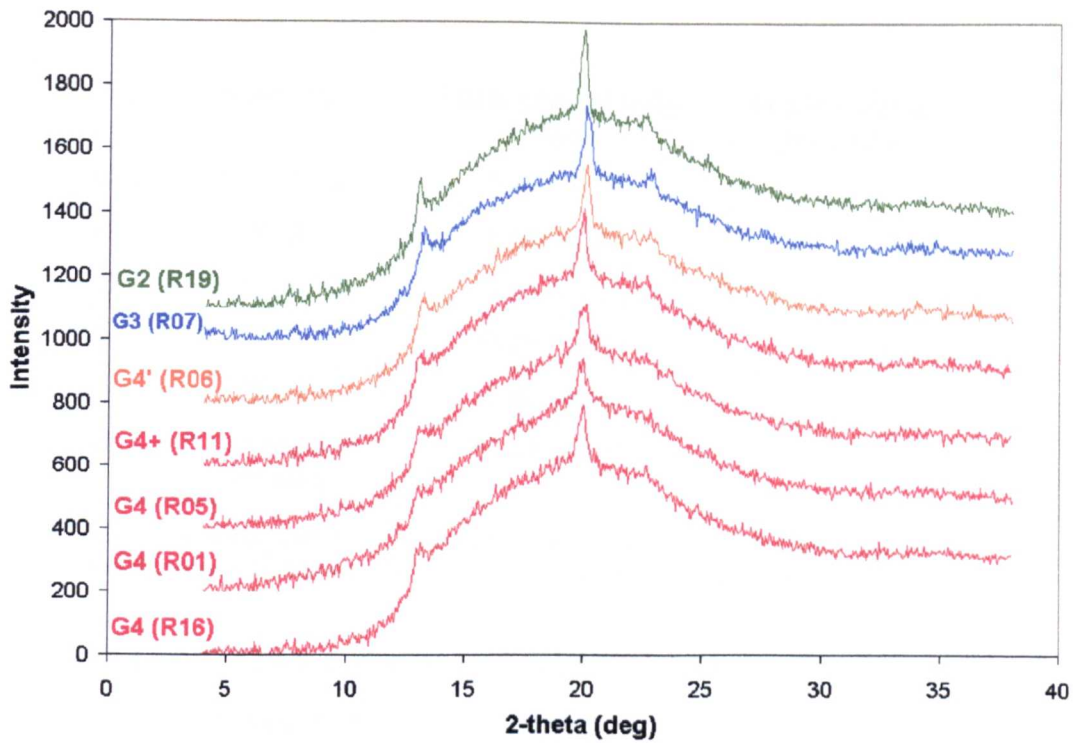


Figure 7.19: Typical X-ray spectra of the cooked samples groups defined using the RVA profiles of the 20 trials from the d-optimal experimental design. The bumping severity increases from G2 to G4

On figures 7.18 and 7.19, the peak areas (in particular the main 20° peak) seemed to decrease as the bumping strength increased from groups G1 to G4. Also, the 20° peak width seemed to increase. To analyse the effect of the bumping on the amylose-lipid complexes, the averages of the total crystallinity and of the 20° peak mid-height width were calculated for each group of samples and the pre-bumped sample, and reported in table 7.11 for the central composite experimental design (set A) and the varying mill gap (set B) series of experiments, and in table 7.12 for the d-optimal experimental design (set C).

Group	Samples	Total crystallinity (%)	Mid-height width of 20° peak (2-theta units)
G1	Pre-bumped, S11, S12, S13	0.76 (0.03)	0.33 (N/A)
G2	S06, S07, S08, S09, S10	0.69 (0.05)	0.32 (0.10)
G3	S01, S02, S03, S04, S05	0.68 (0.04)	0.36 (0.06)
G4	F04, F05, F06	0.67 (0.07)	0.43 (0.05)

Table 7.11: Characteristics of the V-pattern 20° peak for the 4 groups of samples identified with the set A central composite experimental design and the set B series of 6 varying mill gap factory samples. The figures between brackets indicate the standard deviations

Group	Samples	Total crystallinity (%)	Mid-height width of 20° peak (2-theta units)
G1	Pre-bumped	0.97 (0.13)	0.31 (0.03)
G2	R19	0.83 (N/A)	0.33 (N/A)
G3	R07, 08, 15	0.91 (0.15)	0.34 (0.03)
G4+	R02, 10, 11	0.79 (0.09)	0.31 (0.02)
G4'	R06, 18	0.89 (N/A)	0.33 (N/A)
G4	11 remaining samples	0.70 (0.13)	0.37 (0.05)

Table 7.12: Characteristics of the V-pattern 20° peak for the groups of samples identified with the set C d-optimal experimental design. The figures between brackets indicate the standard deviations

Tables 7.11 and 7.12 show that the total crystallinity decreased and the 20° peak mid-height width increased when the bumping strength increased from the pre-bumped sample to the strongly bumped group of samples, with the exception of sub-categories G4+ and G4' mid-height width. These results led to the conclusion that the bumping partially disrupts the crystalline amylose-lipid complexes present in the cooked rice. A model of the dislocation is proposed in the concluding paragraph 7.3.4 of this section.

7.3.3 Role of amylose-lipid complexes in reinforcing the structure of the rice grain

7.3.3.1 Introduction

The X-ray and DSC studies presented in the preceding sections showed that crystalline amylose-lipid complexes are present in the cooked rice material, and that the bumping seems to reduce the amount of complexes detected by X-ray. The effect of this dislocation on the mechanical properties of the rice grains could not be evidenced with the instruments (DMTA and Texture analyser) available at the university. The hypothesis that amylose-lipid complexes reinforce the structure of the rice grains and modifies the behaviour of the structure in water was introduced.

To verify the importance of the amylose-lipid complexes, a series of rice starch / lipid mixtures containing various amounts of amylose and added lipids were prepared with the RVA, so as to create a series of samples containing various

amounts of amylose-lipid complexes. The RVA and DSC analyses of the samples showed that increasing amounts of amylose-lipid complexes result in higher RVA final viscosities.

7.3.3.2 Preparation of the samples

Three varieties of rice flours were studied: Low amylose (glutinous rice), medium amylose Selenio variety and high amylose Elio variety (cf. section 5.4.1 of chapter 5: Raw rice material characterisation). Each variety was cooked with and without lipid added. The lipid used was linoleic acid ($C_{18}H_{32}O_2$, with two unsaturations at carbons 9 and 12).

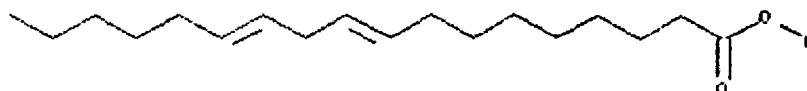


Figure 7.20: Molecular structure of linoleic acid

The RVA was used to cook the samples in excess water. The RVA temperature profile used is detailed in section 4.5.8 of chapter 4: Materials and methods. Six samples were prepared, as shown on table 7.13.

Sample	Sample ID	Flour (g)	Lipid (g)	Distilled water (g)
Glutinous	G	3	0	25
Selenio	S	3	0	25
Elio	E	3	0	25
Glutinous + lipid	G+L	3	0.09	25
Selenio + lipid	S+L	3	0.09	25
Elio + lipid	E+L	3	0.09	25

Table 7.13: Composition of the 6 (flour + lipid) mixes cooked with the RVA

At the end of the cooking, the samples were dried down to 50% w.w.b moisture content (water : solid ratio = 1:1) in an 80°C oven and characterised by DSC to monitor the presence of amylose-lipid complexes. The DSC protocol is detailed in section 4.5.4 of chapter 4: Materials and methods.

7.3.3.3 Rice flour cooking without lipids: The effect of amylose content

The RVA profiles of Glutinous, Selenio and Elio samples (G, S and E) are shown on

figure 7.21. Differences between the samples were evidenced by the gelatinisation peak and by the final viscosity. In particular, the final viscosity increased with the amylose content of the samples, as can be seen on table 7.14.

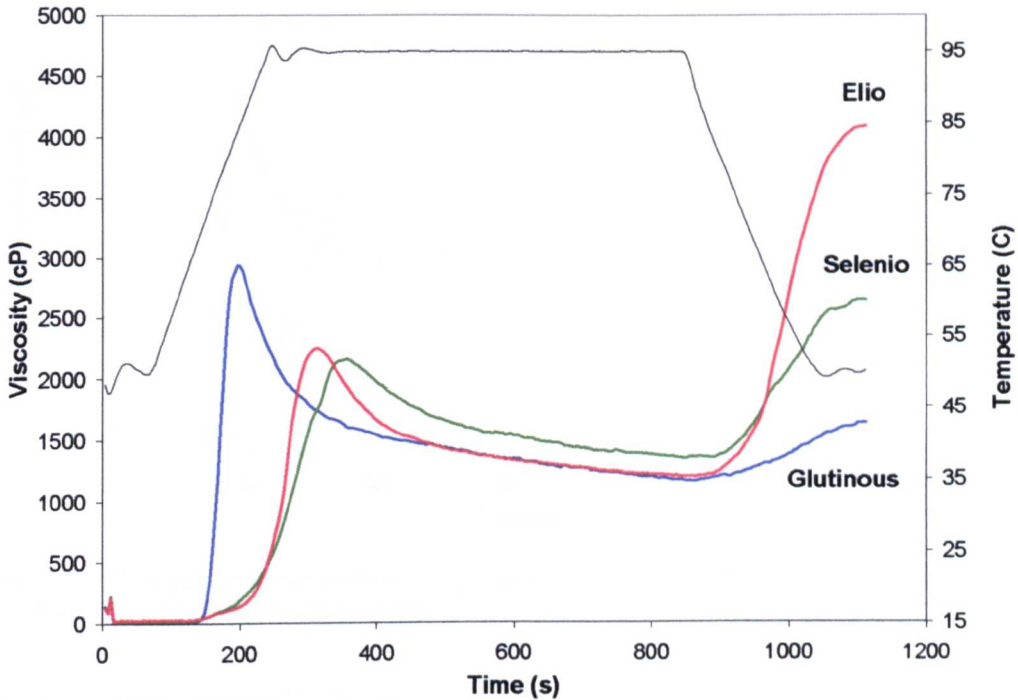


Figure 7.21: RVA gelatinisation profiles of Glutinous, Elio and Selenio rice flours

Sample	Amylose content (% w/w)	Final viscosity (cP)
Glutinous	2.39	1632
Selenio	18.25	2647
Elio	21.99	4086

Table 7.14: Evolution of the amylose content and the RVA final viscosity of Glutinous (G), Selenio (S) and Elio (E) rice flours (single determination)

7.3.3.4 Rice flour cooking with lipids

The RVA profiles of Glutinous, Selenio and Elio samples with lipid added (G+L, S+L and E+L) are shown on figure 7.22. The RVA profiles of Glutinous, Selenio and Elio samples (G, S and E) have also been drawn on the graph for comparison.

The gelatinisation peaks of the ‘lipid added’ samples did not show major differences with the ‘no lipid added’ ones, which was expected because at the gelatinisation stage amylose molecules are not yet completely available to interact with the lipids.

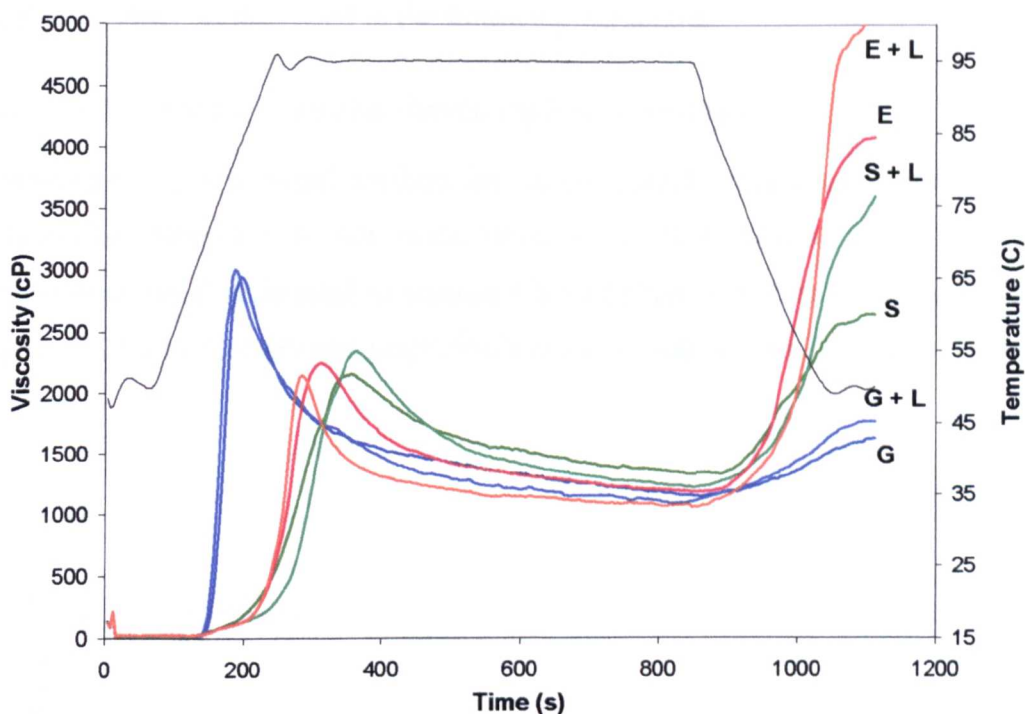


Figure 7.22: RVA gelatinisation profiles of Glutinous (G), Elio (E) and Selenio (S) rice flours, with (G+L, E+L, S+L) and without lipids added

On the contrary, markedly higher final viscosities were obtained with the medium and high amylose samples (Selenio and Elio) when lipids were added to the mixture, as shown on table 7.15. The final viscosity of the low amylose sample (Glutinous) also increased in presence of lipids, but in smaller proportion.

Sample	Final viscosity (cP)	Difference between sample with and without lipid	
		<i>Absolute (cP)</i>	%
Glutinous	1632		
Glutinous + Lip.	1779	147	9.0
Selenio	2647		
Selenio + Lip.	3604	957	36.2
Elio	4086		
Elio + Lip.	5002	916	22.4

Table 7.15: Evidence of an increase in RVA final viscosity of medium and high amylose content rice flours (Selenio and Elio) when lipids are added before cooking (single determination)

These results indicated that amylose and lipids interact during the cooking to strengthen the structure of the system. The way amylose and lipid interact is by

forming amylose-lipid complexes, whose presence in the cooked samples was verified by DSC, as discussed in the following paragraph.

7.3.3.5 DSC evidence of amylose-lipid complexes formation

Following the conventional method for amylose-lipid complexes characterisation, each cooked sample was run twice through the DSC heating cycle. The DSC methodology used is detailed in section 4.5.4 of chapter 4: Materials and methods. Figures 7.23 and 7.24 present respectively the first and second DSC runs for the six samples.

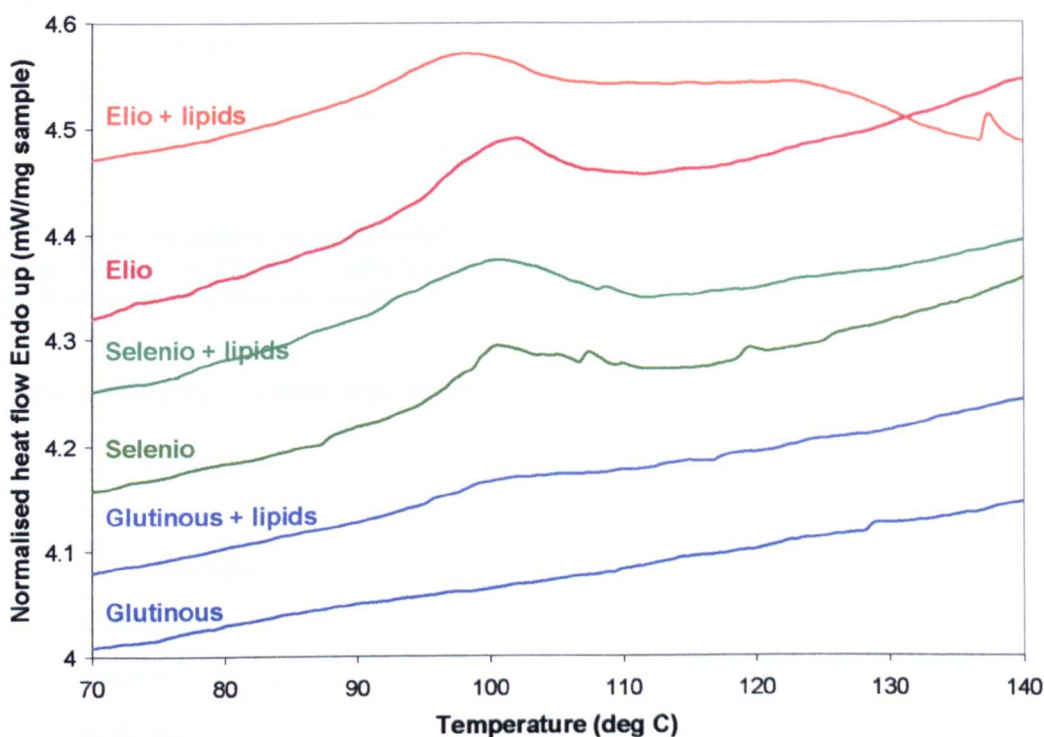


Figure 7.23: DSC assessment of the formation of amylose-lipid complexes in mixtures of rice flour and lipids - First run. The solid : water ratio is 1:3 (w/w). The profiles were normalised by dividing the heat flow by the weight of dry sample

The first run (figure 7.23) showed an endothermic peak in the 90-110°C range, except for the ‘Glutinous’ sample. This was interpreted as the melting of amylose-lipid complexes present in the RVA cooked material. The presence of the same endothermic peak on the second run (figure 7.24) confirmed this interpretation by ruling out gelatinisation and retrogradation, which are other possible endothermic phenomena occurring in cooked starch materials, but do not appear on a second run performed shortly after the first one.

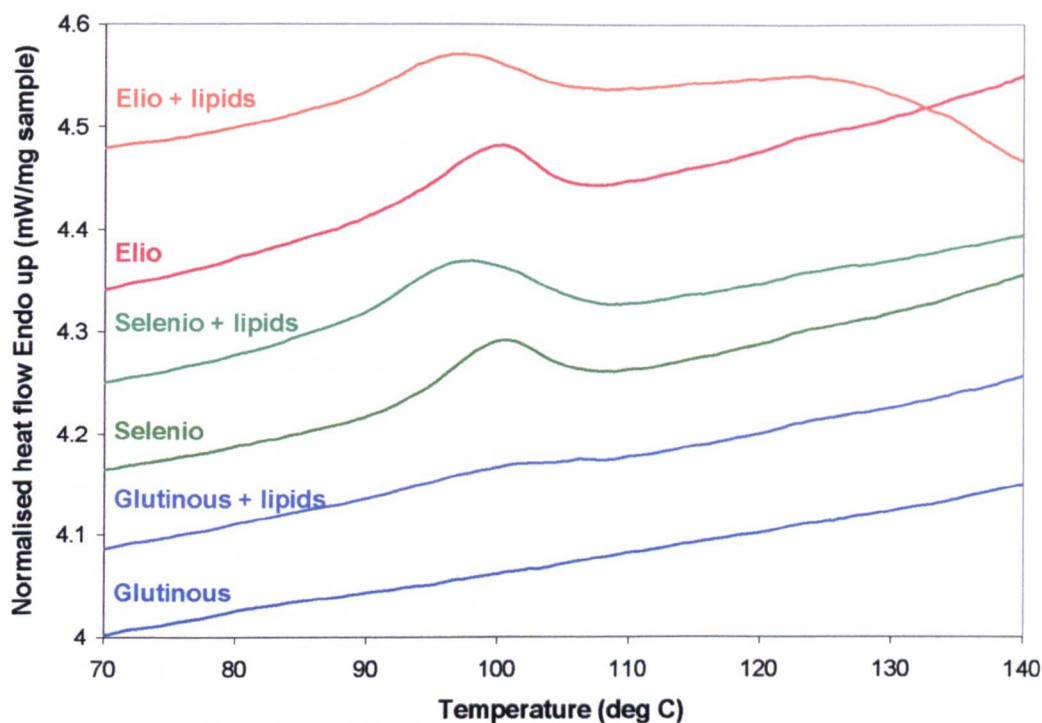


Figure 7.24: DSC assessment of the formation of amylose-lipid complexes in mixtures of rice flour and lipids - Second run. The solid : water ratio is 1:3 (w/w). The profiles were normalised by dividing the heat flow by the weight of dry sample

The peak enthalpies ΔH were measured for each sample and are summarised in table 7.16.

Sample	1 st run ΔH (J.g ⁻¹)	2 nd run ΔH (J.g ⁻¹)
Glutinous	N/A	N/A
Glutinous + Lipids	1.54	1.01
Selenio	4.02	2.94
Selenio + Lipids	6.77	5.94
Elio	6.20	4.24
Elio + Lipids	6.23	4.65

Table 7.16: Areas of the DSC peaks identified in mixtures of rice flour and lipids (single determination). The enthalpies are expressed in Joules per gram of dry sample

Table 7.16 shows that when the amylose content increased among the samples without added lipids, the peak area increased from nil in the Glutinous variety to 4.02J.g⁻¹ in the Selenio variety and 6.20J.g⁻¹ in the Elio variety (1st DSC run). When lipids were added, a small peak appeared in the Glutinous variety (1.54J.g⁻¹), the Selenio variety peak area increased markedly from 4.02 to 6.77J.g⁻¹, while the Elio

variety peak area remained almost unchanged (6.20 to $6.23\text{J}\cdot\text{g}^{-1}$).

This section showed that amylose and lipids interact during the cooking to form amylose-lipid complexes (§7.3.3.5) and strengthen the structure of the system (§7.3.3.4). Using these results, it was assumed that amylose-lipid complexes present in the cooked rice of the Rice Krispies™ process have a similar role of making the rice grain areas containing the complexes more rigid.

7.3.4 Model explaining the strengthening of the rice grain structure by amylose-lipid complexes

Evidence has been gathered that amylose-lipid complexes are formed during the cooking of rice grains (section 7.3.1), that these complexes reinforce the structure of the grains (section 7.3.3), and that they are partially dislocated by the bumping (section 7.3.2). The following section presents a model of the amylose-lipid complexes location and role in the rice grain structure from the cooked to the post-bumped steps of the Rice Krispies™ process, as it has come to be understood in the course of the project.

7.3.4.1 Structure of the cooked rice grain

Figure 7.25 shows a sketch of a raw rice grain, with enlarged starch granules packed together.

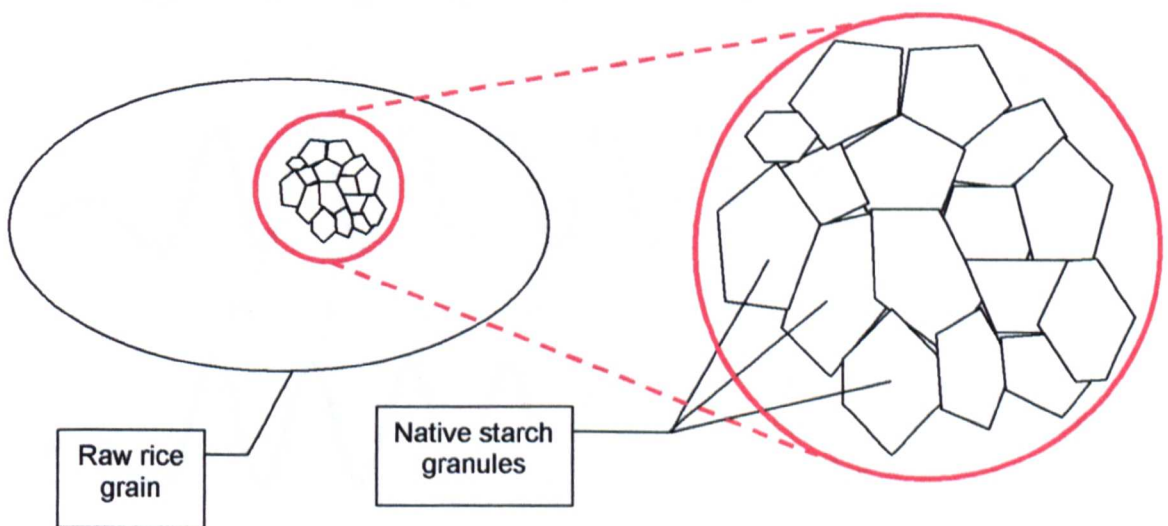


Figure 7.25: Schematic structure of a raw rice grain and starch granules

In the raw starch material and during the cooking, amylose molecules can form

helices around fatty acid molecules, resulting in the amorphous form of amylose-lipid complexes (type I), theoretically detectable by DSC but not by X-rays (Morrison *et al.*, 1993a). Figure 7.26 shows one amylose helix around a fatty acid.

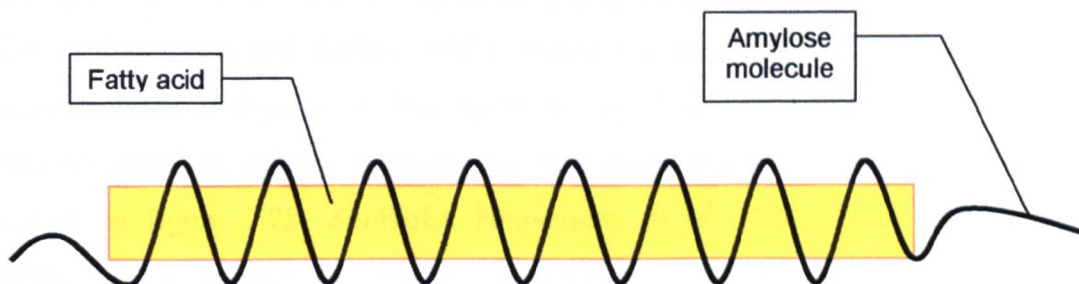


Figure 7.26: Schematic structure of an amylose-lipid complex helix (amorphous amylose-lipid complex type)

Furthermore, these helices can gather by establishing hydrogen bonds between them during the cooking, as shown on figure 7.27. The resulting regular arrangement of parallel helices constitutes the crystalline form of amylose-lipid complexes (type II), responsible for the V-pattern detectable by X-rays.

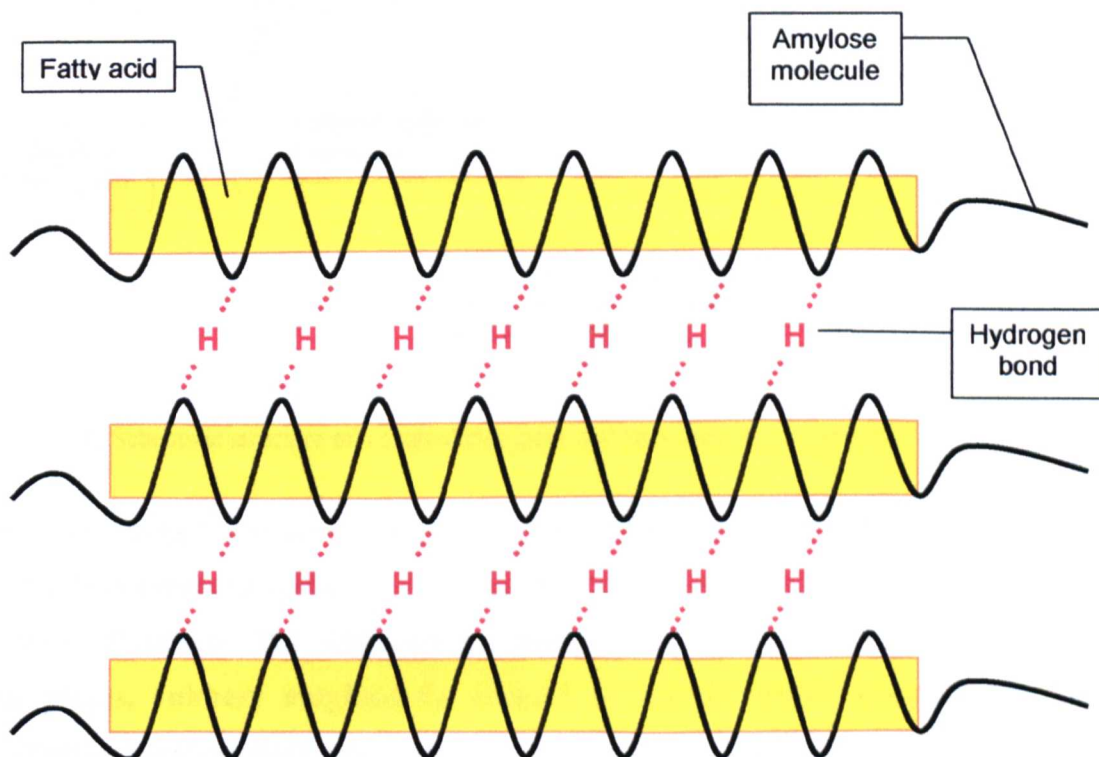


Figure 7.27: Schematic structure of a crystalline amylose-lipid complex

Because several amylose molecules can be involved in the same crystal, the

formation of crystalline amylose-lipid complexes reduces the molecular mobility of the amylose and makes the rice grain structure more rigid.

The concentration of amylose inside starch granules increases from the inside to the periphery (Morrison and Gadan, 1987). Hence the periphery and edges of starch granules cooked in absence of shear constitute amylose-lipid complexes rich zones connected together, which reinforce the rice grain structure (Becker, 2001), as sketched on figure 7.28. Similarly, Heinemann *et al.* (2001) have shown that amylose-lipid complexes can trigger the gelation of dilute starch solutions, thus strengthening the starch system.

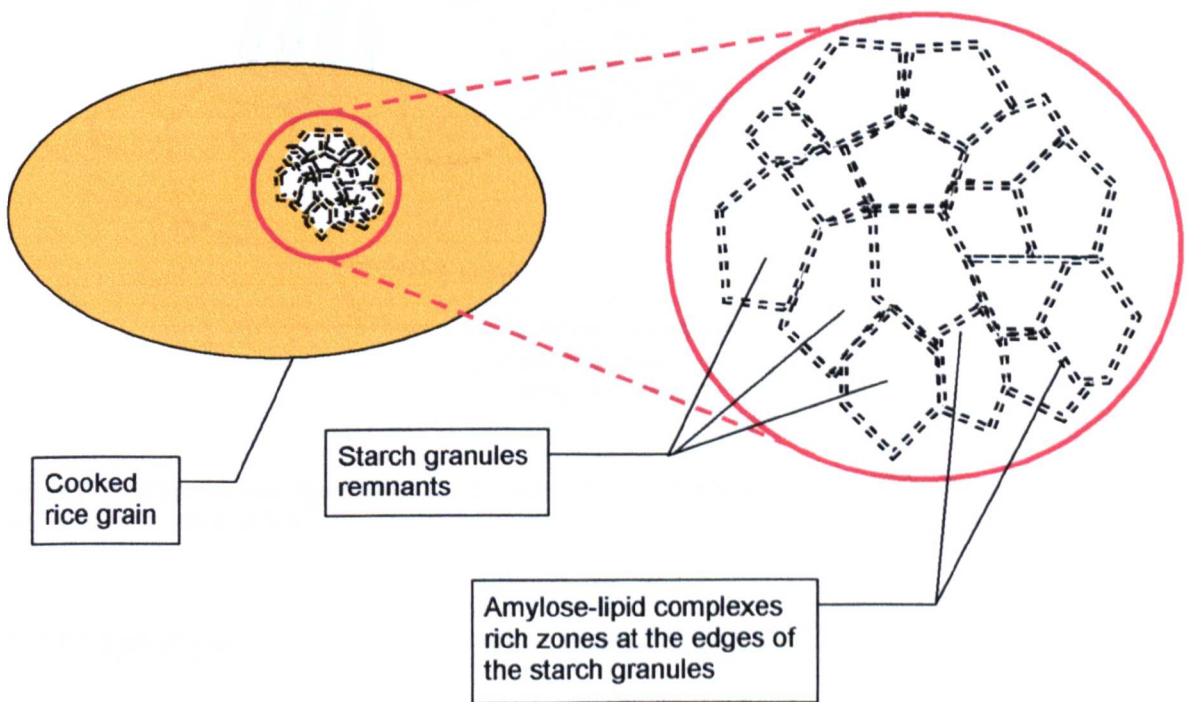


Figure 7.28: Schematic structure of a cooked rice grain and its molten starch granules

Thus, the cooked rice grains at the bumping step of the Rice Krispies™ process (50°C, 18% moisture content w.w.b) can be thought of as being composed of two separate structures: The remnants of the starch granules composed mainly of **amorphous, rubbery amylopectin** encased in a **grain wide network of semi-crystalline amylose-lipid complexes** that follows the edges of the starch granules remnants and makes the grain structure more rigid and less able to swell in cold water.

Finally, a hypothetical arrangement of the amylose-lipid complexes around the cooked starch granules remnants is shown on figure 7.29.

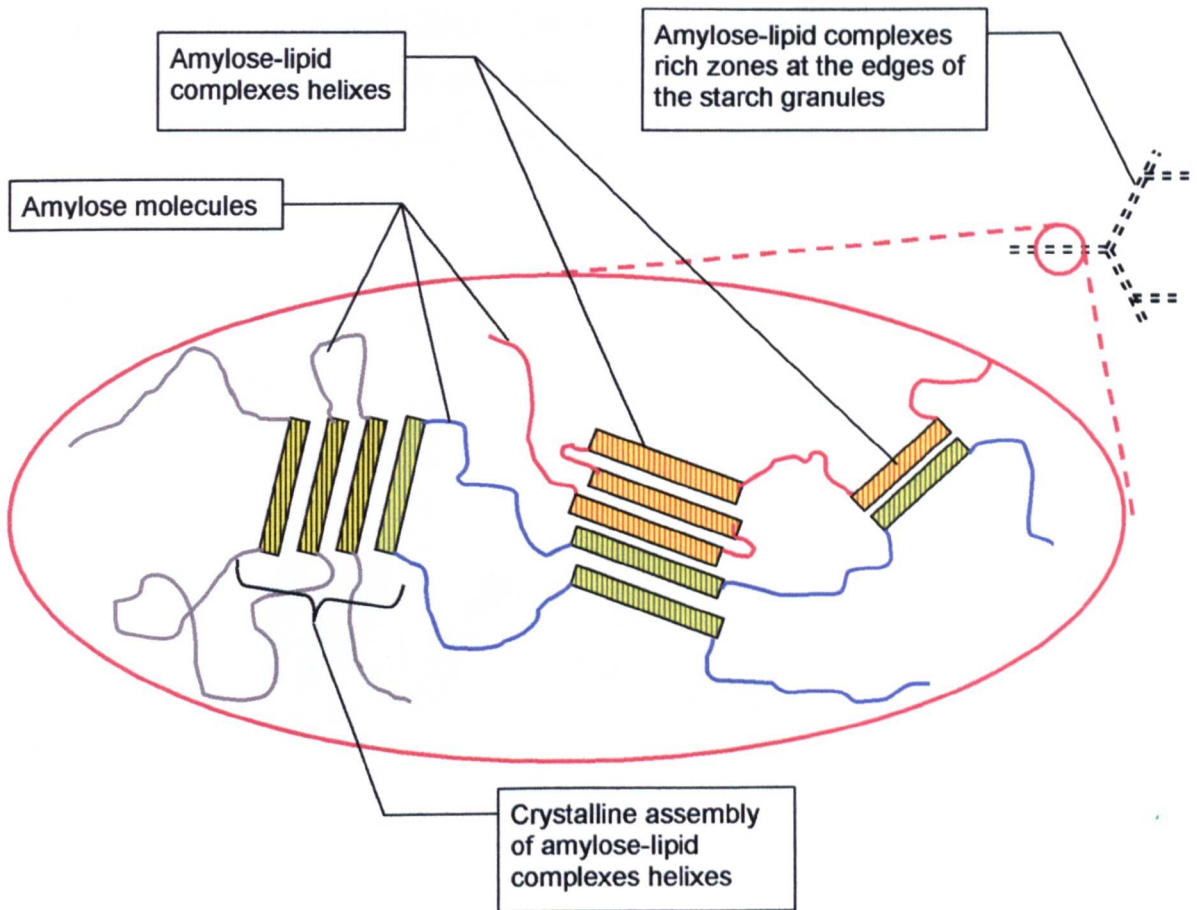


Figure 7.29: Hypothetical organisation of amylose-lipid complexes at the edges of the starch granules remnants in the cooked rice

7.3.4.2 Effect of the bumping on the amylose-lipid complexes

The X-rays analysis of post-bumped samples showed that the V-pattern diffraction peaks became broader and the peak areas decreased when the bumping strength increased (section 7.3.2). This was interpreted as a dislocation of the crystalline amylose-lipid complexes, as sketched on figure 7.30.

After the bumping, the amylose helices involved in the crystalline amylose-lipid complexes are less well aligned, and the crystallites are smaller, which could account for the broadening of the diffraction peaks.

Also, some amylose helices may be detached from the crystalline arrangement, as indicated by the black arrows on figure 7.30, which could account for the decrease in

the diffraction peak area. Consequently, amylose molecules that were linked together in the crystalline arrangement may come apart, with the effect of loosening the amylose network. This weakening of the rice grain structure is thought to have a key role in allowing the formation and growth of vapour bubbles in the material at the puffing step of the Rice Krispies™ process.

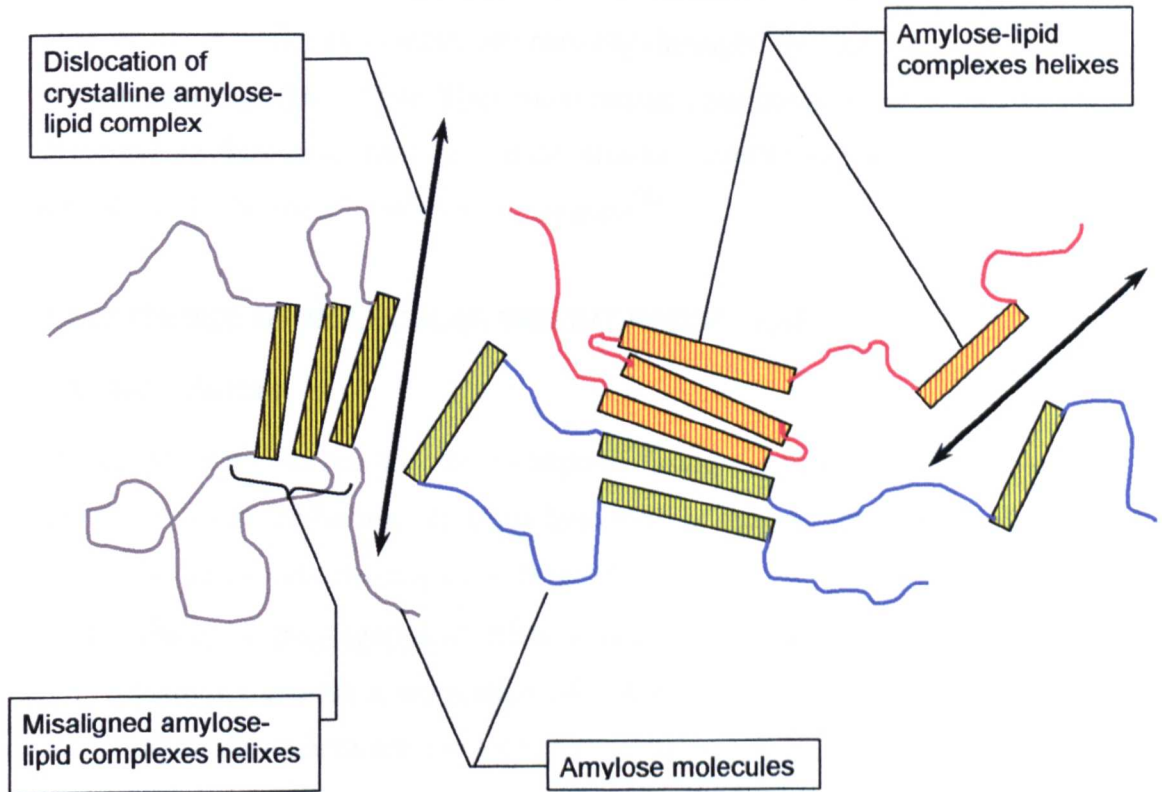


Figure 7.30: Hypothetical effect of the bumping on the crystalline order of amylose-lipid complexes in the cooked rice

One way to summarise the amylose-lipid complexes model is to think about them as a three-level structure, by analogy with the four-level structure of proteins:

- The separate amylose and lipid molecules form the primary structure.
- The amylose helices around the lipid molecules form the secondary structure (figure 7.26).
- The aggregates of parallel helices linked by hydrogen bonds form the third-level structure, which is responsible for the diffraction of X-rays due to its long-range order (figures 7.27 and 7.29).

In this model, the bumping does not affect the primary and secondary structures, and partially dislocates the helix aggregates of the third-level structure (figure 7.30). As a

result several diffraction planes are created without entirely destroying the crystalline structure of the complexes, which could account for the wider and smaller X-rays diffraction peaks (tables 7.11 and 7.12).

Additionally, it has been shown that proteins aggregates formed during the cooking of cereal flour reinforce the granule structure (Hamaker and Griffin, 1993) and, in the case of the corn flakes process, are partially damaged by the bumping (Batterman-Azcona and Hamaker, 1998). Thus some further consideration could be given to rice proteins, as they may have a similar structure-reinforcing role to amylose-lipid complexes in the processing of Rice Krispies™.

7.4 EVIDENCE OF MOLECULAR WEIGHT REDUCTION

7.4.1 Introduction

The second phenomenon thought to happen during the bumping is the amylopectin molecular weight reduction. To study the effect of the bumping on the amylopectin in the rice grains, four techniques were used:

- The ultracentrifugation of dilute solutions of cooked rice starch indicated that bumping creates a population of polysaccharides with a molecular weight intermediate between amylose and amylopectin (section 7.4.2).
- Relative viscosity measurements showed that the cooked rice starch average molecular weight decreases when the bumping severity increases (section 7.4.3).
- The complete debranching of amylopectin by isoamylase treatment followed by the HPLC (high pressure liquid chromatography) separation of the resulting polysaccharides showed that strongly bumped samples have a higher proportion of small polysaccharides than pre-bumped samples (section 7.4.4).
- Capillary rheometer measurements indicated that the viscosity of the molten starch material decreases when the bumping severity increases (section 7.4.5).

Taken altogether, these observations led to the conclusion that bumping does reduce the molecular weight of the amylopectin in the rice grains. At the puffing step of the

process, the molten material reduced viscosity that ensues should allow a better expansion of the rice grain.

7.4.2 Ultracentrifugation evidence of three populations of polysaccharides in the post-bumped material

Ultracentrifugation separates polymer molecules in dilute solution according to their molecular weight: The heavier the molecule, the further towards the tube bottom it travels. Thus, the method can separate the amylose and amylopectin molecules of a dilute starch solution. Furthermore if the amylopectin is damaged, for example debranched, it is possible to observe the smaller polysaccharides resulting from the damage. The ultracentrifugation protocol is detailed in section 4.5.6 of chapter 4: Materials and methods.

7.4.2.1 First series of experiments

Six Balilla samples were analysed by ultracentrifugation:

- A pre-bumped sample, labelled **PRE**.
- Three samples bumped at the university with a texture analyser (see section 4.3.1.1 in chapter 4: Materials and methods), down to three different heights: 0.0, 0.1 and 0.2mm. These samples were labelled **0.0mm**, **0.1mm**, **0.2mm** respectively.
- Two samples bumped at the factory at two different sample temperatures: 31 and 42°C. These samples were labelled **POST 31C** and **POST 42C** respectively.

In terms of bumping severity, the two most strongly bumped samples were those from the factory, where the size and speed of the machinery make bumping conditions more severe than in the laboratory. The pre-bumped sample was the least strongly bumped. The three samples prepared with the texture analyser were intermediate between pre-bumped and factory bumped samples. The bumping severity increased from the '0.2mm' sample to the '0.0mm' sample.

The polymer concentration along the test tube is detected by laser scattering. The results are shown on figure 7.31.

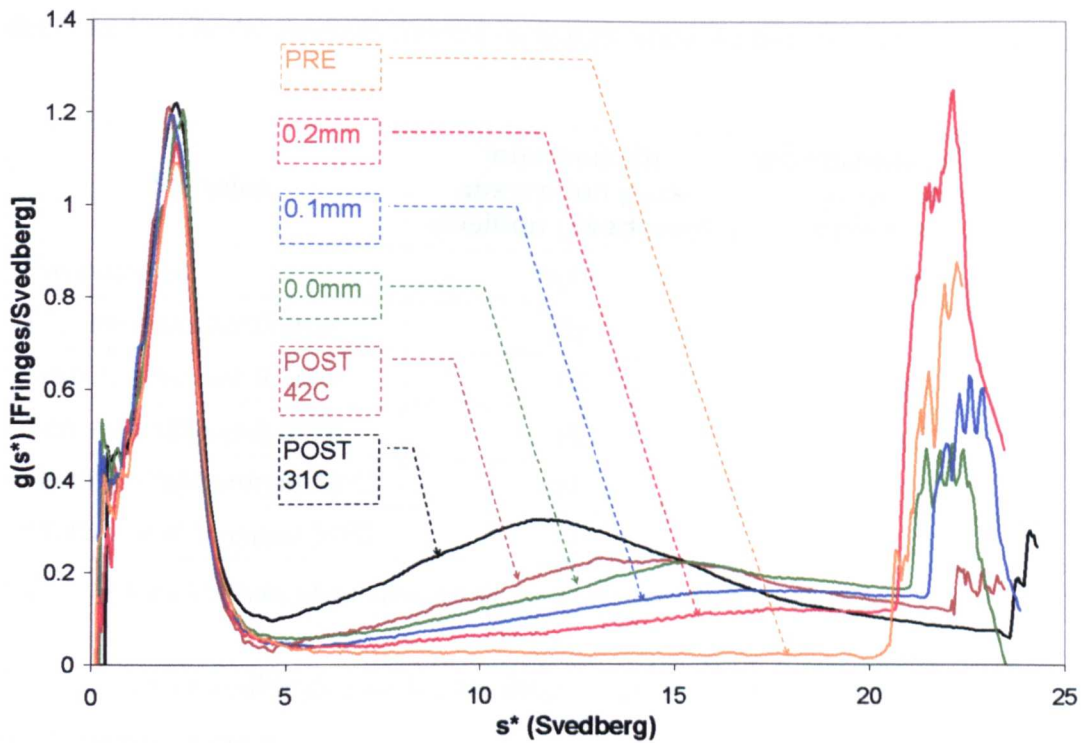


Figure 7.31: Ultracentrifugation evidence of starch molecular weight reduction by the bumping

The pre-bumped sample curve showed two absorption peaks, one at the top and one at the bottom of the test tube (2 and 22 Svedberg respectively). The 2 Svedberg peak corresponds to a low molecular weight fraction of the rice starch, and was interpreted as the amylose fraction. The 22 Svedberg peak corresponds to a high molecular weight fraction, and was interpreted as the undamaged amylopectin fraction.

All the post-bumped samples showed a low molecular weight fraction peak similar to the one of the pre-bumped sample. They also displayed a high molecular weight fraction peak, whose size decreased as the bumping severity increased. Most interestingly, an additional peak appeared between that of the low and high molecular weights. This indicated that the bumping creates a third fraction of starch molecules. The molecular weight of this third fraction is intermediate between the amylose and amylopectin. The characteristics of the intermediate peak are summarised for each sample in table 7.17.

From the pre-bumped sample to the factory post-bumped 31°C sample, the peak shifted towards lower sedimentation values (18 to 12 Svedberg), and its intensity increased. This indicated that the molecular weight of the third starch fraction

decreased while the amounts formed increased when the bumping severity increased.

Samples	Intermediate absorption peak position (Svedberg)	Intermediate absorption peak intensity (arbitrary units)
Pre-bumped	None	None
Texture analyser 0.2mm	18	0.12
Texture analyser 0.1mm	16	0.20
Texture analyser 0.0mm	15	0.23
Factory post-bumped 42°C	14	0.24
Factory post-bumped 31°C	12	0.29

Table 7.17: Characteristics of the ultracentrifugation intermediate absorption peak

There are two possible origins for the third starch fraction: Either the amylose or the amylopectin fractions.

The possibility of the formation during the bumping of ‘amylose clusters’ with a higher molecular weight than individual amylose molecules was considered. However, table 7.17 shows that an increasing bumping strength results in a lower, rather than higher, molecular weight of the third fraction, which contradicts this hypothesis.

More likely is the hypothesis of the formation of the third starch fraction from the breaking down of amylopectin into smaller molecules. This is consistent with the observed decrease in molecular weight when the bumping strength increases, and also can explain the decrease in the intensity of the amylopectin peak when the intensity of the third starch fraction peak increases.

These results led to the conclusion that the bumping decreases the molecular weight of amylopectin.

7.4.2.2 Second series of experiments

Three samples from the Battle Creek d-optimal experimental design described in section 7.2 were powdered and ultracentrifuged. All were of the short grain rice variety (SGR), and were labelled PRE for pre-bumped, R4 for post-bumped run 4

(small mill gap, high temperature), and R5 for post-bumped run 5 (small mill gap, low temperature). The results are shown on figure 7.32.

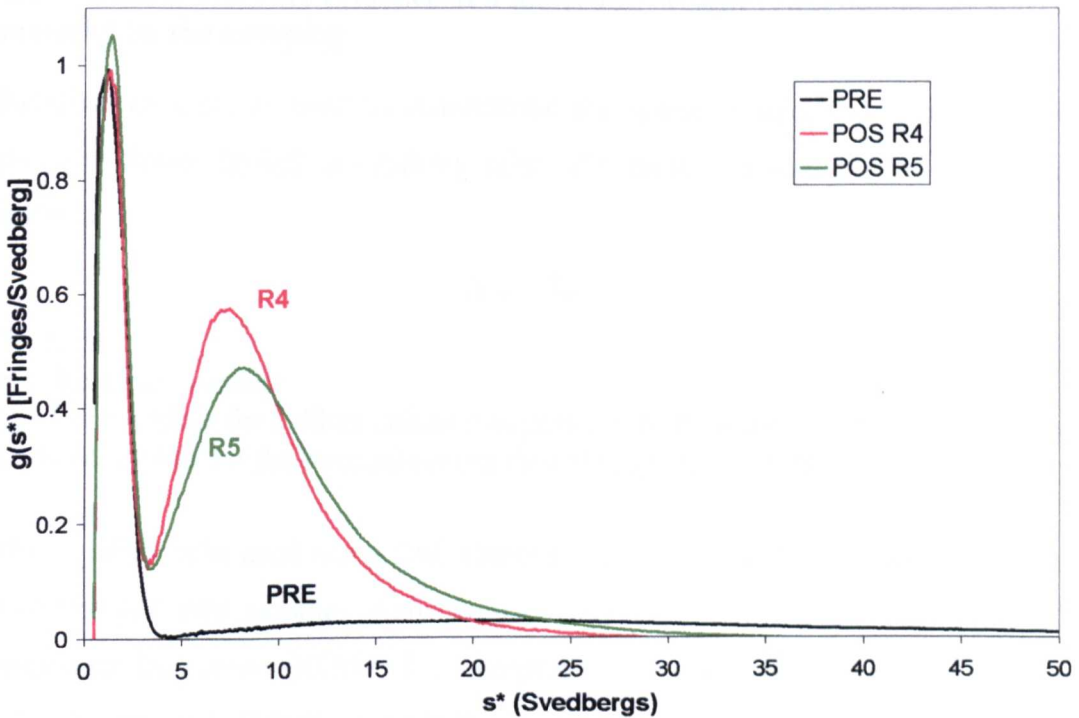


Figure 7.32: Ultracentrifugation of three of the set C d-optimal experimental design 20 samples

The pre-bumped sample curve presents a narrow amylose peak and a wide amylopectin molecular weight distribution. The shape of the curve is more similar to those obtained for raw rice (section 5.4.3 of chapter 5) than to those obtained for post-bumped samples, which is an indication that the cooking does not alter much the molecular weight of amylose and amylopectin.

The two post-bumped samples R4 and R5 showed intermediate amylopectin peaks bigger and of lower molecular weight (lower sedimentation) than the ones presented in the preceding section 7.4.2.1. This may be because the mill gap used to prepare these samples was smaller than the one used to prepare the factory samples from Manchester. However, it may also be because the conditions of the second series of ultracentrifugation experiment were slightly different, having been carried out more than a year after the first series.

The curves for samples R4 and R5 were too similar to draw any conclusion on the effect of the bumping conditions on the amylopectin structure.

7.4.3 Relative viscosity evidence of a molecular weight reduction of the starch material by the bumping

Relative viscosity is used to characterise the speed at which a dilute solution of polymer flows through a capillary tube. The relative viscosity was calculated as follows:

$$\eta_{\text{rel}} = t_{\text{sol}} / t_0$$

With:

η_{rel} : Relative viscosity

t_{sol} : Time it takes for a dilute solution of polymer to flow through the capillary tube

t_0 : Time it takes for the pure solvent to flow through the capillary tube

The capillary tube used was a 2mL Ostwald viscometer (U-tube). Dilute solutions of post-bumped rice samples were prepared by dissolving milled rice material in potassium hydroxide (KOH). The comprehensive protocol is described in section 4.5.5 of chapter 4: Materials and methods.

At a given concentration of polymer (typically 0.3% w/w), the dilute solution flows more slowly if the macromolecules are large and have a big hydrodynamic volume. In other words, the relative viscosity is an indication of the average molecular weight of the fully solubilised polymer.

The relative viscosities of the set A 13 post-bumped samples prepared following the central composite experimental design described in section 7.2 were measured. The results were used to generate a model of the variations of the relative viscosity in function of the bumping temperature and mill gap, as shown on figure 7.32. The software used to compute the model was Design Expert™ (version 6.0). The black arrow on figure 7.32 indicates the direction of increasing bumping severity, from large mill gap and high temperature to small mill gap and low temperature (details of the hypotheses on the direction of bumping severity are given in section 3.3.4 of chapter 3: Evaluation of the industrial process).

The equation of the model is:

U-tube relative viscosity = 1.12

$$+ 7.55 \cdot 10^{-3} \times \text{Temperature } (^\circ\text{C})$$

$$+ 7.00 \cdot 10^{-4} \times \text{Mill gap } (\mu\text{m})$$

$$- 5.47 \cdot 10^{-5} \times \text{Temperature}^2$$

$$- 5.47 \cdot 10^{-7} \times \text{Mill gap}^2$$

$$- 3.61 \cdot 10^{-6} \times \text{Temperature} \times \text{Mill gap}$$

The probability that the model is not significant is 1.35%.

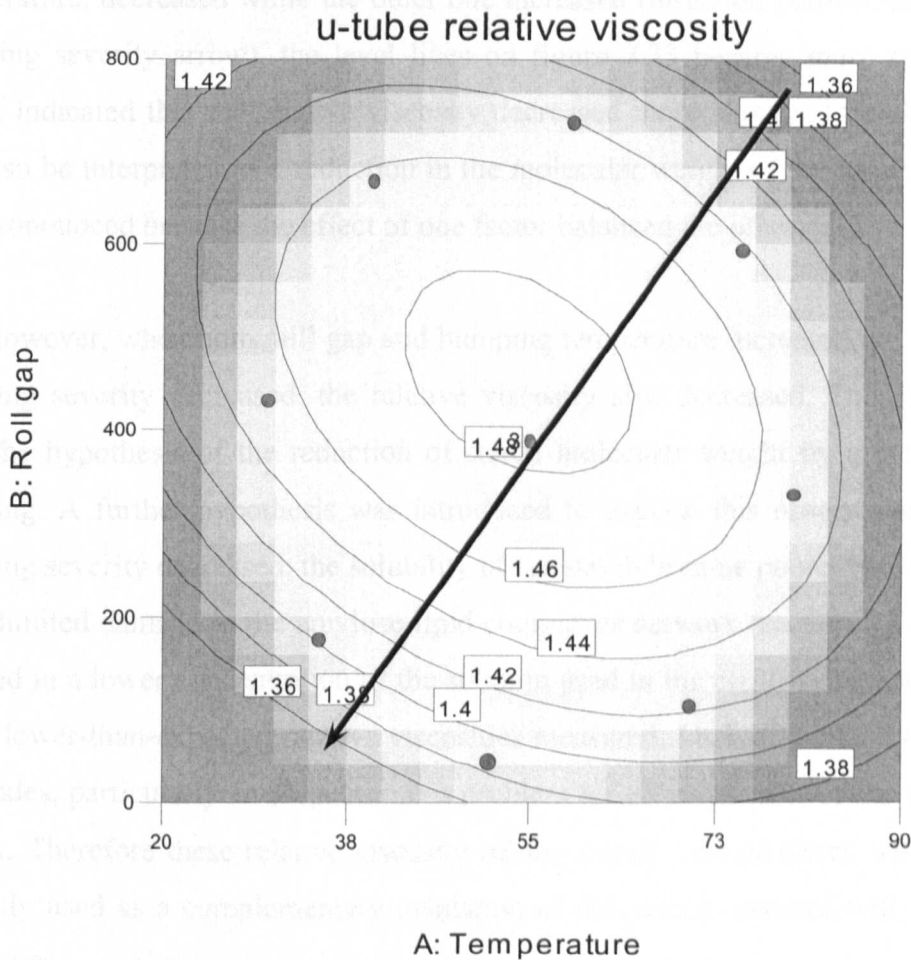


Figure 7.33: Model of the effect of mill gap and bumping temperature on the relative viscosity of post-bumped rice dilute solutions. The dots indicate the parameters of the actual experiments (set A central composite experimental design) and the shading the level of accuracy of the model.

Figure 7.33 shows that the highest relative viscosity was obtained for intermediate values of mill gap and bumping temperature, approximately 500 μm and 55 $^\circ\text{C}$. From this central position, three directions must be considered in turn: (i) Towards increasing bumping severity, (ii) perpendicular to the bumping severity arrow, and

(iii) towards decreasing bumping severity.

(i) When both the mill gap and bumping temperature decreased, i.e. when the bumping severity increased, the relative viscosity decreased fairly sharply, as indicated by the closeness of the level lines on figure 7.32. This observation was interpreted as a reduction in the molecular weight of the starch material.

(ii) When only one of the two factors, either the mill gap or the bumping temperature, decreased while the other one increased (direction perpendicular to the bumping severity arrow), the level lines on figure 7.33 became more spaced out, which indicated that the relative viscosity decreased more slowly. This observation can also be interpreted as a reduction in the molecular weight of the starch material, less pronounced because the effect of one factor balanced the other.

(iii) However, when both mill gap and bumping temperature increased, i.e. when the bumping severity decreased, the relative viscosity also decreased. This did not fit with the hypothesis of the reduction of starch molecular weight by a more severe bumping. A further hypothesis was introduced to explain this observation: As the bumping severity decreased, the solubility of the starch became poorer because of the more limited damage to the amylose-lipid complexes network (section 7.3.1), which resulted in a lower concentration of the solution used in the capillary viscometer and in the lower-than-expected relative viscosities measured. Lack of solubility of starch molecules, particularly amylopectin, is a problem for all measures of their molecular weight. Therefore these relative viscosity results should be considered with caution and only used as a complementary validation of the results obtained with the other techniques.

7.4.4 Amylopectin branch chain analysis by HPLC

Four samples from the Battle Creek d-optimal experimental design (set C) described in section 7.2 were debranched by isoamylase and the chain length distribution analysed by high pressure liquid chromatography (HPLC), following the method described in section 4.4.4 of chapter 4: Materials and methods. All samples were of the short grain rice variety (SGR), and were labelled PRE for pre-bumped, R5 for post-bumped run 5 (small mill gap, low temperature), and R4 and R20 for post-

bumped runs 4 and 20 (small mill gap, high temperature) respectively. The results are shown on figure 7.34. R4 and R20 were bumped under similar conditions on two different days (cf. figure 7.2).

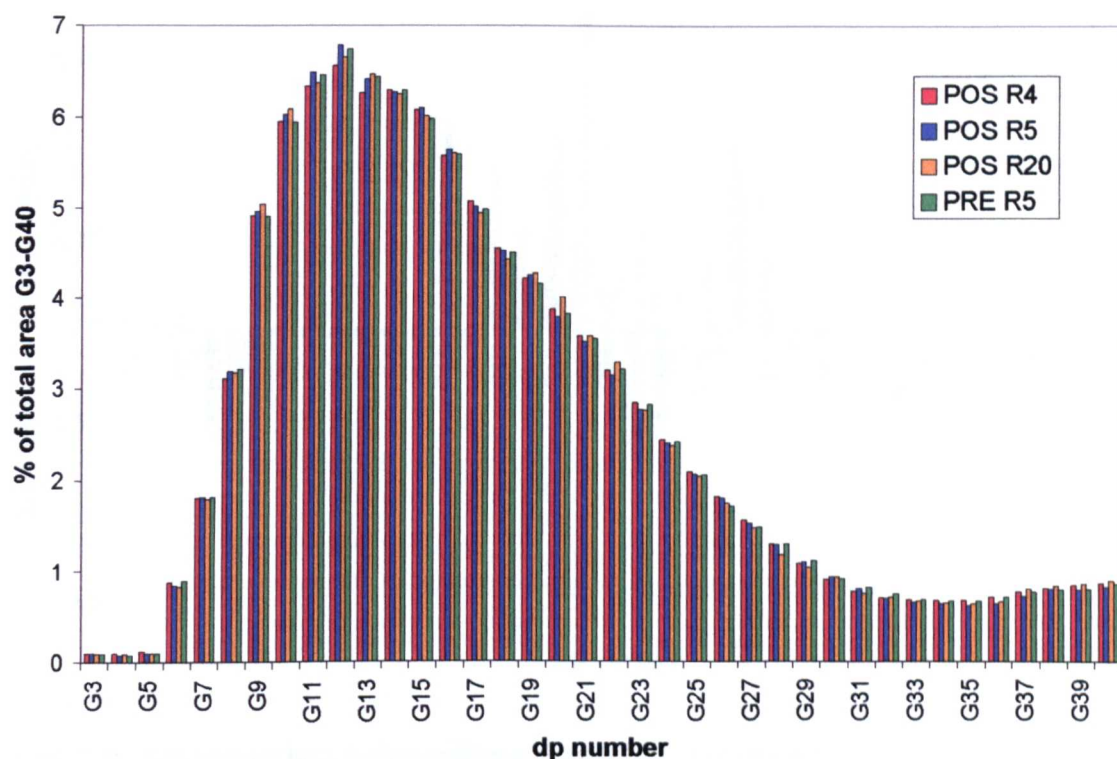


Figure 7.34: HPLC amylopectin branch chain analysis of four pre- and post-bumped samples

To make the differences between samples clearer, the pre-bumped sample data (PRE) were subtracted from the three post-bumped samples (POS R4, POS R5 and POS R20) data. The results are shown on figure 7.35.

If the bumping step of the Rice Krispies™ process decreases the amylopectin molecular weight, then the post-bumped samples should have a higher proportion of short amylopectin branches, and the pre-bumped sample should have a higher proportion of long amylopectin branches.

This expectation is not verified on figure 7.35, where the sign of the difference between the post-bumped samples and the pre-bumped sample does not depend on the degree of polymerisation (dp number). One interpretation is that the bumping, although it decreases the amylopectin molecular weight (as other methods indicate), does not alter markedly the amylopectin chain length distribution. Thus it could be

that the bumping breaks down preferentially a small number of the longer amylopectin B- and C-chains, and leaves the A-chains untouched.

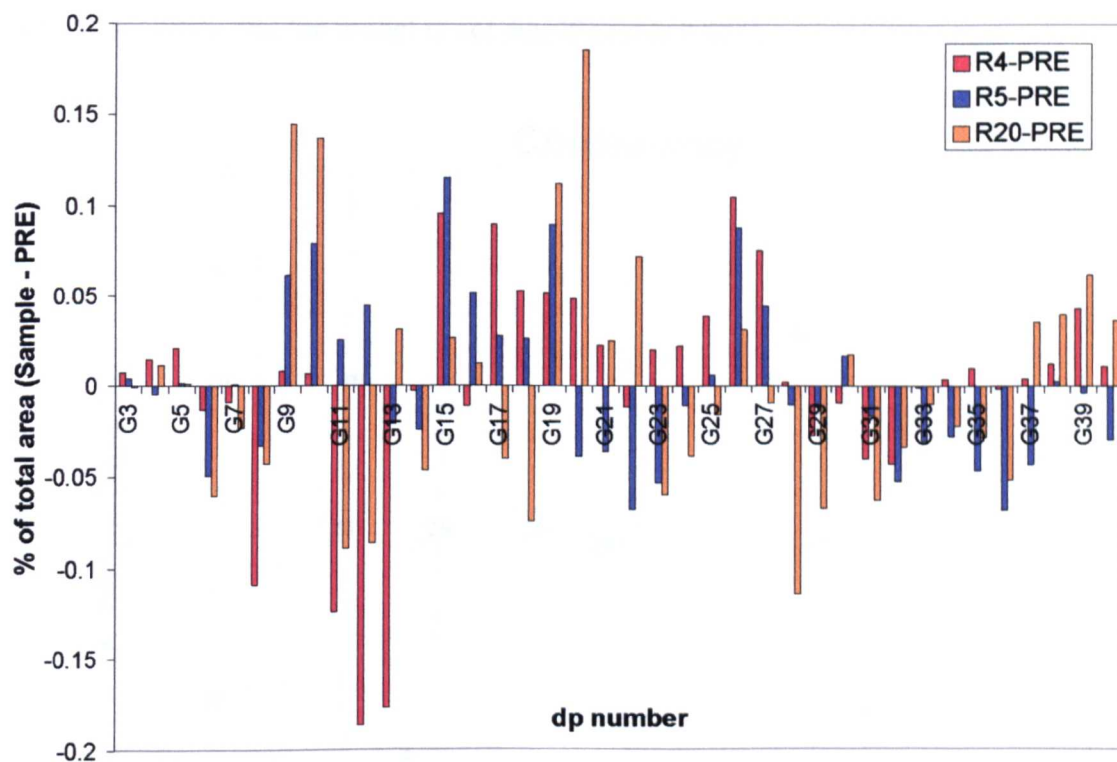


Figure 7.35: Amylopectin branch chain differential analysis of four pre- and post-bumped samples

7.4.5 Capillary rheometer

The capillary rheometer was used to study the rheology of the molten rice material. This methodology avoids the problematic starch solubilisation. The protocol is explained in section 4.5.7 of chapter 4: Materials and methods. The consistency factor, formally equivalent to the viscosity of the material was used as an indication of the molecular weight of the starch molecules: The lower the consistency factor, the lower the molecular weight.

The set A 13 post-bumped samples prepared following the central composite experimental design described in section 7.2 were analysed by capillary rheometry. The results were used to generate a model of the variations of the consistency factor k as a function of the mill gap and bumping temperature, as shown on figure 7.36. The software used to compute the model was Design Expert™ (version 6.0).

The equation for the model is:

$$\text{Consistency} = 23.06 + 9.63 \cdot 10^{-3} \times \text{Mill gap } (\mu\text{m})$$

The probability that the model is not significant is 0.83%.

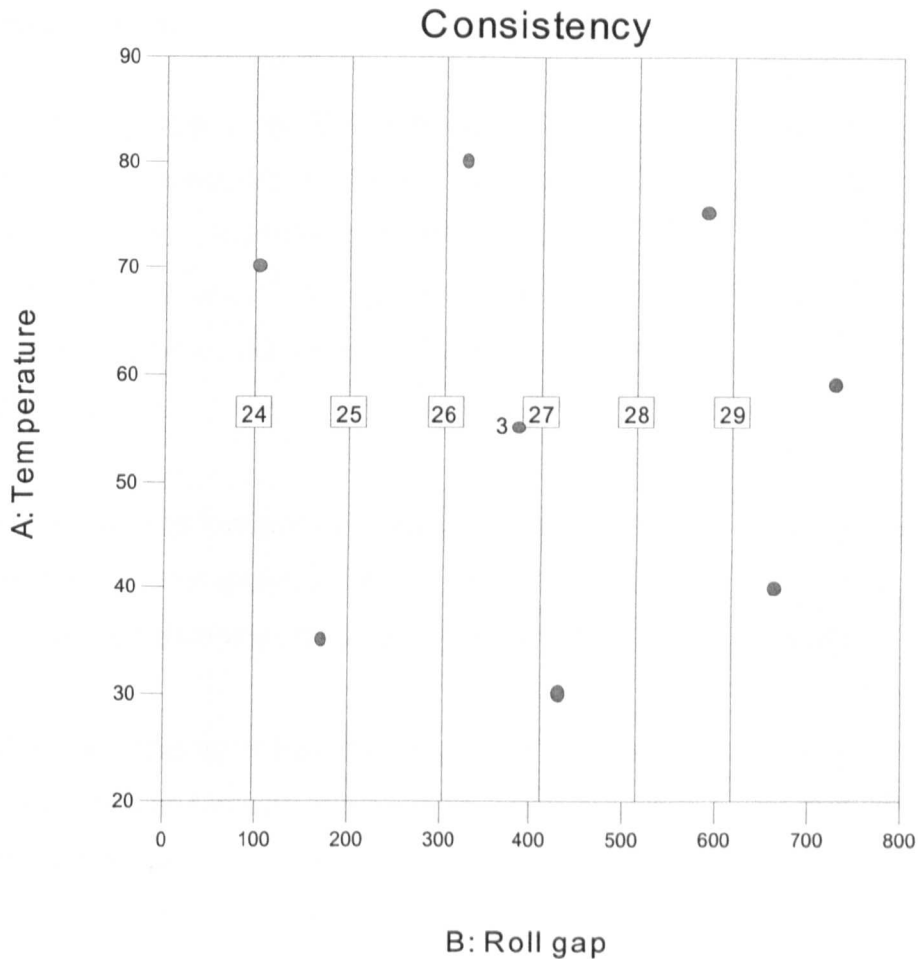


Figure 7.36: Model of the effect of the mill gap and bumping temperature on the molten post-bumped rice consistency factor. The dots indicate the parameters of the actual experiments (set A central composite experimental design) and the shading the level of accuracy of the model.

Figure 7.36 shows that the consistency factor decreased linearly with the mill gap, while the bumping temperature had no significant effect. It is likely that the effect of the temperature could not be detected by capillary rheometry because of the low sensitivity of the method. These observations were taken as a further indication that the post-bumped rice starch molecular weight decreases when the bumping severity increases, and that the mill gap has more influence on the post-bumped rice quality than the other bumping parameters.

During the puffing stage of the process, the bubbles of vaporised water inside the rice grains expand the material. The extent of the expansion depends on the molecular weight of the starch material. Thus the bumping, by reducing the rice starch molecular weight, plays a key role in improving the expansion of the puffed grains.

7.5 CONCLUSION

At the bumping step of the Rice Krispies™ process, the cooked rice grain can be thought of as a composite structure of amorphous, rubbery amylopectin material encased in a rigid, crystalline network of amylose-lipid complexes. The bumping step of the Rice Krispies™ process has a major effect on both the rubbery part and the crystalline part of the grain, and hence on the extent of the grain expansion during the puffing.

Firstly, the bumping loosens the network of crystalline amylose-lipid complexes that is formed in the rice grain during the cooking. This is thought to be a necessary condition for the grain to expand, during the puffing step of the process.

Secondly, the bumping reduces the molecular weight of the rice grain amylopectin molecules. The amylopectin branch chain analysis by HPLC (section 7.4.4) would indicate that the main C- or B-chains of amylopectin molecules are broken, rather than the outer A-chains. Consequently, the molten material during the puffing has a lower viscosity, which facilitates and improves the grain expansion.

The key factor in controlling the bumping seems to be the mill gap. The bumping temperature and rice variety have only a secondary effect on the quality of the post-bumped rice. It should be noted that the bumping temperature has an influence on the mill gap, because increasing the temperature dilates the rolls and reduces the mill gap.

To ensure a consistent post-bumped rice quality, the use of a small mill gap is recommended, so as to minimize the influence of the other parameters of the bumping. The RVA study of post-bumped samples distinguished four types of viscosity profiles, G1 to G4, and suggested that samples belonging to the profile type

G4 (most severely bumped samples) were the least influenced by secondary parameters such as bumping temperature and rice variety. Practically, type G4 samples were bumped with a mill gap below 400µm, as measured with a solder fed between the rolls.

The influence of the bumping on the proteins contained in the rice material was not investigated. Mujoo *et al.* (1998) found that disulfide bonds are formed between proteins during the processing of rice. Hamaker and Griffin (1993) showed that protein aggregates reinforce the cooked starch granules structure, and Batterman-Azcona and Hamaker (1998) found that these aggregates could be damaged by the bumping. Hence further studies on the bumping could involve the characterisation of protein aggregates in the pre-bumped and post-bumped material, and of their effect on the rice grain mechanical properties.

CHAPTER 8: STUDY OF THE TEMPERING STEP

8.1 INTRODUCTION

This chapter presents the results of a series of experiments aimed at understanding the phenomena that occur during the tempering step of the Rice Krispies™ process. To characterise the influence of the tempering step, all the samples studied were puffed and the rice grain expansion was measured.

The first experiment showed that the rice grains expand better when tempered (section 8.2).

Two hypotheses regarding what happens within the rice grains between the beginning and the end of the tempering were then formulated (section 8.3). The first one was that molecular relaxations, or physical ageing, take place in the glassy starch material. The second one expressed the possibility of re-equilibration of a temporary water gradient from the inside to the outside of the freshly dried grain.

Further experiments confirmed that both physical ageing and a temporary moisture gradient occur in the rice material during the tempering step (sections 8.4 and 8.5).

The hypothesis that the temporary moisture gradient had more influence on the expansion of the grains than the physical ageing was then introduced. The study was concluded with an experiment which confirmed this hypothesis (section 8.6).

8.2 EVIDENCE THAT TEMPERED RICE EXPANDS BETTER THAN NON-TEMPERED RICE

8.2.1 Protocol

Standard post-bumped rice (400g, 19% moisture content w.w.b) provided by the factory was dried to 11% moisture content w.w.b at 105°C. The weight of the rice was checked regularly until it reached the weight of 364g corresponding to the required moisture content. The drying lasted roughly 40 minutes.

The rice was then put to temper at room temperature for 8 hours. This sample was labelled 'DRIED'. Every hour 40g of the rice were taken and puffed, following the standard food hall puffing protocol.

Standard tempered rice, provided by the factory and labelled 'REFERENCE', was puffed at the same times, as a reference to control the variability of the experimental conditions.

Tempering time (h)	Names of puffed samples
0	'DRIED + 0h', 'REFERENCE + 0h'
1	'DRIED + 1h', 'REFERENCE + 1h'
2	'DRIED + 2h', 'REFERENCE + 2h'
3	'DRIED + 3h', 'REFERENCE + 3h'
4	'DRIED + 4h', 'REFERENCE + 4h'
5	'DRIED + 5h', 'REFERENCE + 5h'
6	'DRIED + 6h', 'REFERENCE + 6h'
7	'DRIED + 7h', 'REFERENCE + 7h'
8	'DRIED + 8h', 'REFERENCE + 8h'

Table 8.1: Summary of the puffed samples produced

Following the puffing, a digital picture of 50 grains of each sample was taken using an office scanner. The scanner was set to record 32-bit colour pictures at a resolution of 200dpi.

The pictures were then processed with image analysis software Paintshop Pro 6 and Scion to calculate the projected area of the grains on the scanner glass bed (section 4.6.1 of chapter 4: Materials and methods). The average areas were used as a measure of the degree of expansion of each sample. The standard deviations associated with these averages are in the range 5.05 - 8.28mm² (10 to 16% of the average grain areas), due to the fairly broad distribution of the rice grains sizes.

8.2.2 Variability of the scanner and image analysis method

Six pictures of the same 50 grains of the 'REFERENCE + 0h' sample were taken with the scanner. The average area for 50 grains from the six pictures was 49.87mm², and

the standard deviation between the areas was 1.02mm^2 . In the same way, six pictures of the same 50 grains of the 'DRIED + 0h' sample were taken. The average grain area calculated was 42.69mm^2 , and the standard deviation between the pictures was 0.43mm^2 . Figure 8.1 summarises these results.

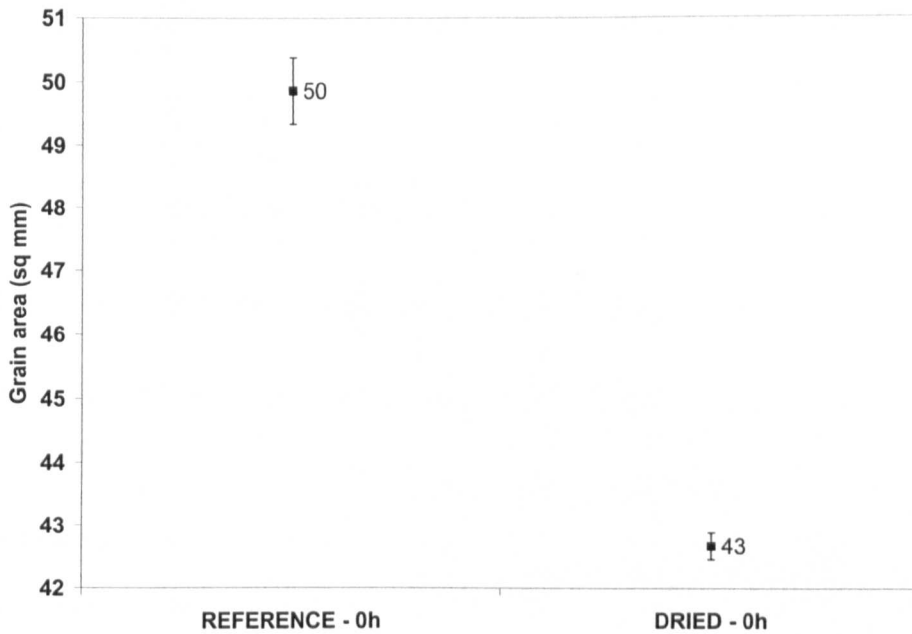


Figure 8.1: Evaluation of the variability in the measurement of the grain area, using 6 pictures of the same 50 puffed grains, for 2 different samples. The vertical lines indicate one standard deviation

8.2.3 Variability of the oven conditions

The 'REFERENCE' sample was puffed nine times at one-hour intervals. The nine average grain areas calculated using the digital pictures are shown in table 8.2. From these figures it appears that the oven conditions remained fairly constant, with perhaps an increase in temperature in the last 4 hours, as shown by the increase in the grain expansion.

Sample name	Average grain area (mm ²)
'REFERENCE + 0h'	49.51
'REFERENCE + 1h '	48.05
'REFERENCE + 2h '	49.05
'REFERENCE + 3h '	48.78
'REFERENCE + 4h '	48.29
'REFERENCE + 5h '	52.65
'REFERENCE + 6h '	50.10
'REFERENCE + 7h '	48.25
'REFERENCE + 8h '	53.26

Table 8.2: Evaluation of the variability of the puffing oven conditions. Evolution of the average grain area of the 'REFERENCE' sample over 8 hours

The average area of the nine measurements is 49.77mm^2 and the standard deviation between them is 1.92mm^2 .

8.2.4 Increase in the expansion of the freshly dried grains during tempering

The evolution of the average grain area of the 'DRIED' sample puffed after increasing tempering times is shown on figure 8.2.

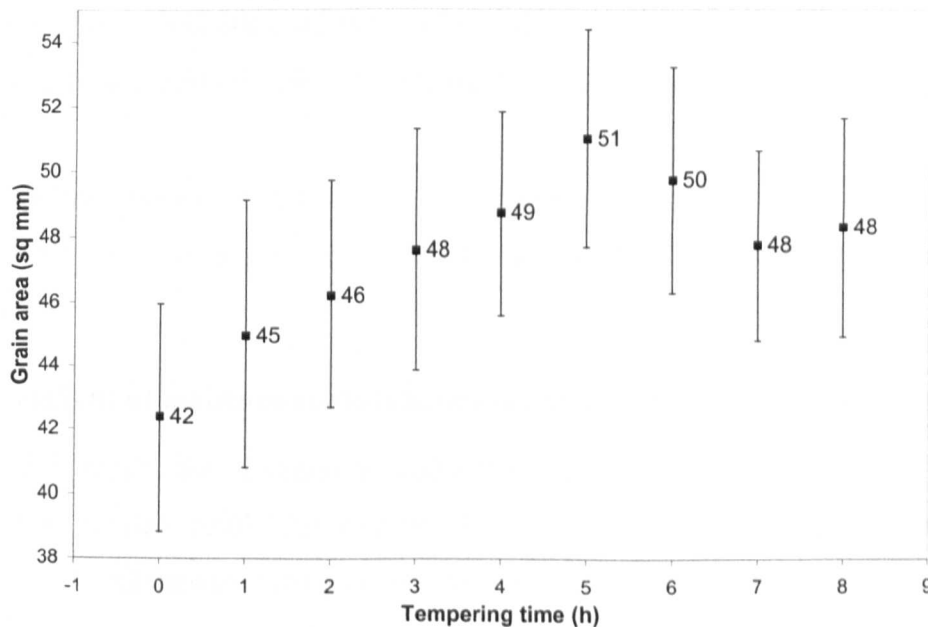


Figure 8.2: Evolution of the average grain area of the 'DRIED' sample over 8 hours of tempering. The vertical lines indicate two times the standard deviations of the 50 grains used to take the picture.

The expansion of the grains increased in the first four hours of tempering. Then it

reached a plateau in the same region as the 'REFERENCE' sample grain area (49.77mm^2). Grains puffed 24 hours after the beginning of the experiment (the following day) also had an average projected area of 48 to 50mm^2 . These results show that the rice grains undergo some changes during the first hours of tempering, resulting in a better expansion at the puffing stage of the process.

8.3 HYPOTHESES ON THE PHENOMENA OCCURRING DURING THE TEMPERING

8.3.1 Physical ageing

A polymer material stored below its glass transition is in a non-equilibrium state, which allows small molecular movements. The reorganisation of polymer molecules results in tighter packing. This phenomenon is called physical ageing. The amount of physical ageing is identifiable by DSC as a decrease in the enthalpy of the material. It can be likened to a physical state transition and therefore is completely reversible (cf. section 2.5.2 of chapter 2: Literature review).

Rice is composed mainly of starch, which is a natural polymer. The drying of post-bumped rice from 20 to 11% moisture content w.w.b takes the material through the glass transition from the rubbery into the glassy state (cf. section 6.3.2, figure 6.3 of chapter 6: Glass transition of the cooked rice). Thus it was suspected that some physical ageing might take place during the following tempering step.

To verify this hypothesis, experiments to measure the specific heat of powdered rice samples after various tempering times were conducted. The results are presented in section 8.4.

8.3.2 Gradient of moisture content inside the freshly dried rice grain

Figure 8.3 represents diagrammatically the hypothesis that a moisture content gradient is created inside the rice grain during the drying step that follows the bumping, and disappears during the tempering step by migration of water molecules.

On figure 8.3a, the post-bumped rice grain has an even distribution of its water content. During the drying, the hypothesis is that water is removed from the edges of the grain, while the inside remains mainly unaffected. Thus a gradient of moisture

content is created within the grain, whose edges become dryer than the inside, as represented on figure 8.3b. During the tempering, the gradient decreases as the water from the inside part of the grain migrates towards the edges, as shown on figure 8.3c. Finally (figure 8.3d), the distribution of water inside the grain becomes even again.

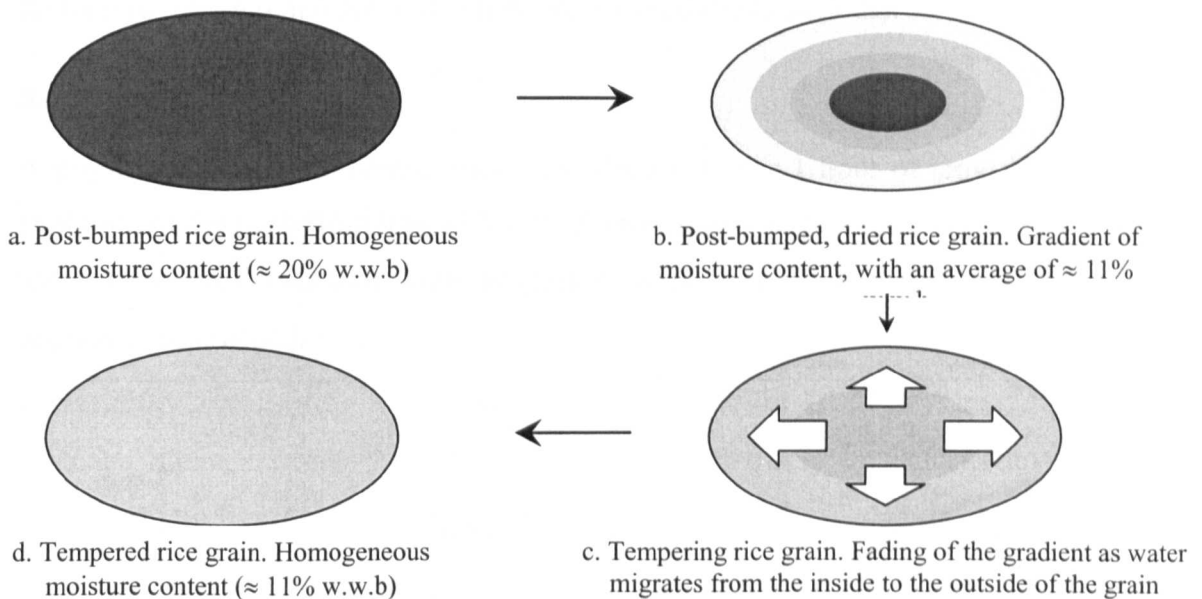


Figure 8.3: Gradient of moisture contents inside the post-bumped, freshly dried rice grain

The consequence of an uneven partitioning of water at the beginning of the tempering could be that the outer part of the rice grain has a moisture content below the optimal puffing level of 11% w.w.b, while the inner part of the grain has a higher moisture content. Thus the outer part could act as a ‘shell’ limiting the expansion of the grain. During the tempering the water migration from the inside to the outside of the grain would remove this shell effect, resulting in a better puffing.

To verify the existence of a gradient of moisture content in the freshly dried rice grains, the evolution of their water activity during the tempering was measured. This is discussed in section 8.5.

8.4 EVIDENCE OF PHYSICAL AGEING IN THE TEMPERING RICE

8.4.1 Protocol

Tempered rice provided by the factory was powdered and packed into stainless steel DSC pans. The capacity of the pans was 40 to 50mg of sample. The moisture content

of the tempered rice was 11% w.w.b. To remove the physical ageing history of the sample, the pan was heated in the DSC a first time from -40°C to 90°C at $10^{\circ}\text{C}\cdot\text{min}^{-1}$. Immediately after this first run, a second run was performed to record the profile of the refreshed sample. The pan was then left to temper at 20°C inside the DSC instrument. DSC profiles were recorded after 1, 2, 3, 4, 6, 8, 10 and 12 hours of tempering (cf. section 4.5.4.3 of chapter 4: Materials and methods).

8.4.2 Results

A physical ageing endothermic peak was identified after 1 hour of tempering. The evolution of the peak from 0 to 12 hours of tempering is indicated on figure 8.4. The area of the peak increased with tempering times until 12 hours when a plateau seemed to be reached.

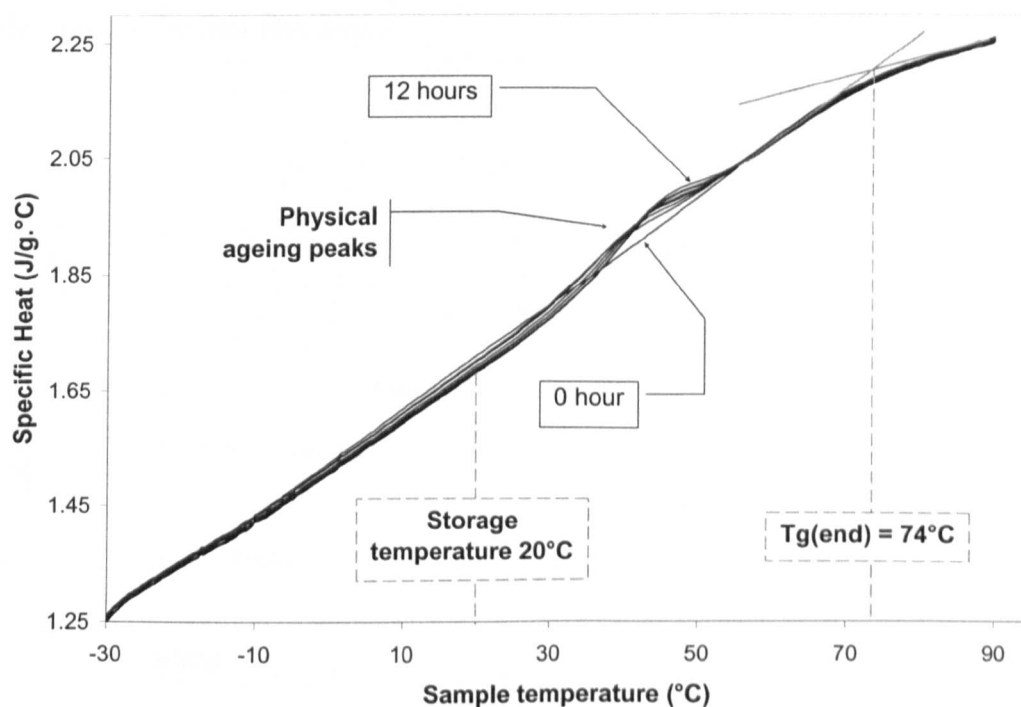


Figure 8.4: Physical ageing endothermic peak in 11% moisture content w.w.b cooked rice. Tempering times: 0, 1, 2, 4, 6, 8, 10, 12 hours

Figure 8.4 shows clearly the glass transition end temperature $T_g(\text{end})$ at 74°C , where the thermograms acquired at different ageing times converge into the rubbery state. This end point is in good agreement with the $\tan \delta$ glass transition temperature of 70°C determined by DMTA (section 6.3.2 of chapter 6: Glass transition of the cooked rice). It has been reported (Martinet, 2001) that the glass transition of starch

based systems measured by DSC is spread over a temperature range of several tens of degrees (up to 80 degrees C).

The physical ageing event is observed as expected at a temperature midway between the storage temperature of 20°C and the end of glass transition temperature of 74°C. Another characteristic of the enthalpy relaxation event associated with ageing in the glassy state is the shift of the peak position towards higher temperatures with increasing storage times. On figure 8.4, the peak onset temperature increased from 29.9°C after 1 hour of tempering up to 34.7°C after 12 hours of tempering.

The extent of physical ageing was characterised by the area of the peak, which corresponds to the enthalpy (ΔH) of the phenomenon (figure 8.5). A steady increase in ΔH was observed over the whole range of tempering times investigated, with a higher rate in the first four hours.

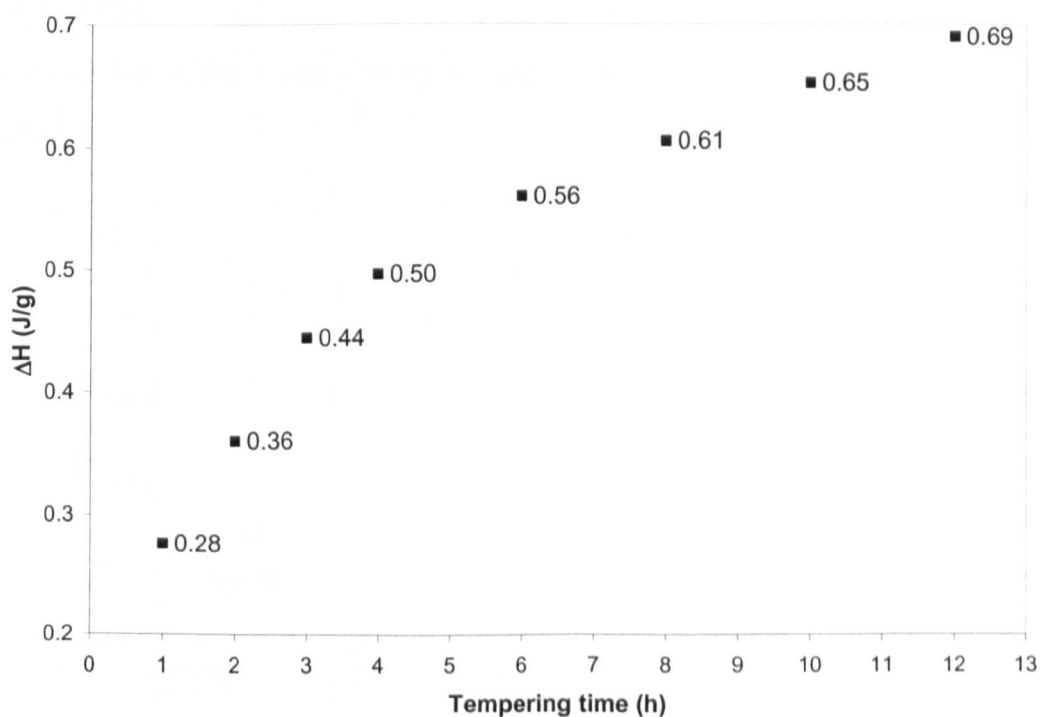


Figure 8.5: Evolution of the area of the physical ageing DSC peak of post-bumped, dried and powdered rice during the tempering

8.5 EVIDENCE OF A GRADIENT OF MOISTURE CONTENT IN THE FRESHLY DRIED GRAIN

8.5.1 Protocol

Post-bumped rice (20g, 19% moisture content w.w.b) provided by the factory was dried down to 11% moisture content w.w.b in a 105°C oven. The weight of the rice was checked regularly until it reached the weight of 18g corresponding to the required moisture content. The drying lasted about 20 minutes. The rice was then split into three samples:

- Sample A: 3g of rice were put to temper at 27°C in a Aw instrument (Decagon CX1) and the water activity (A_w) was recorded at regular intervals.
- Sample B: 8g of rice were put to temper in a tray open to ambient atmosphere in an air-conditioned room at 20°C.
- Sample C: 8g of rice were vacuum-sealed in an aluminium bag and put to temper in the same air-conditioned room at 20°C.

8.5.2 Results

The evolution of the water activity in sample A during the tempering is shown on figure 8.6.

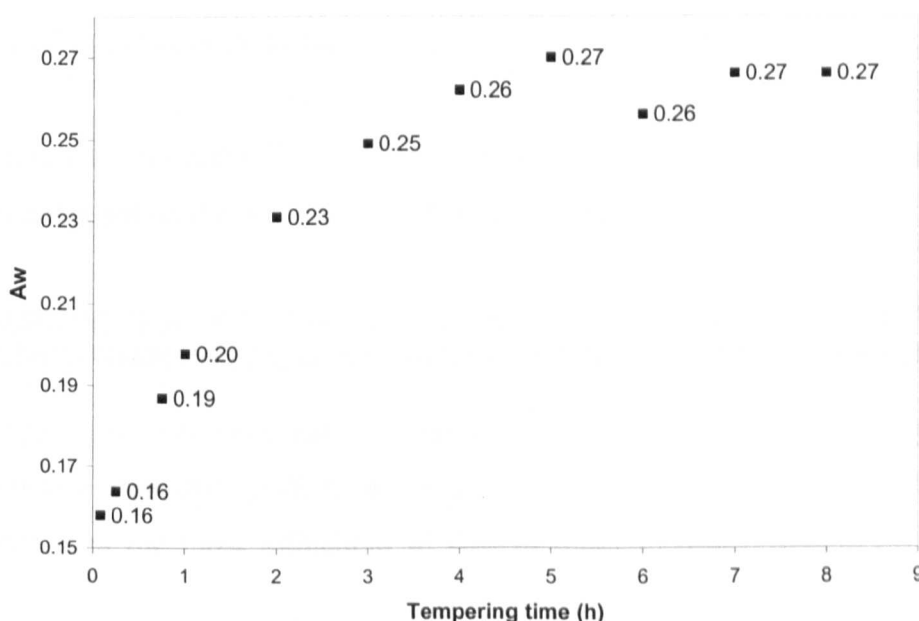


Figure 8.6: Evolution of the water activity (A_w) of post-bumped, dried rice during the tempering

The water activities of samples B and C measured after 8 hours of tempering are reported in table 8.3, together with the temperature at which the measurements were done.

Sample	Aw	Temperature (°C)
Sample B	0.237	25.9
Sample C	0.379	25.4

Table 8.3: Water activity of rice samples B and C after 8 hours of tempering

In the first 4 hours of tempering, the water activity of sample A increased from 0.16 up to a plateau at 0.27. This indicates that the moisture content of the outside part of the rice grains increased during the tempering. Two hypotheses can explain this increase:

- (a) The grains absorb moisture from the atmosphere.
- (b) Water migrates from the inside part of the grain to the outside, due the gradient created during the drying.

In sample C, vacuum sealing prevented moisture absorption from the atmosphere. Its water activity measured after 8 hours of tempering was nevertheless higher than the water activities of samples A and B measured at the same time: 0.38 versus 0.27 and 0.24 respectively. This confirms the hypothesis (b) of water migrating from the inside to the outside of the rice grain during the tempering, and thus confirms the presence of a gradient of moisture content in the freshly dried rice grain.

The comparison of sample C with samples A and B also shows that, if left exposed to ambient atmosphere, the rice loses some water during the tempering.

8.6 EVIDENCE THAT THE GRADIENT OF MOISTURE CONTENT HAS MORE INFLUENCE THAN PHYSICAL AGEING ON THE RICE GRAIN EXPANSION

After experiments showing that both physical ageing and water equilibration occur inside the rice grain during the tempering, a final experiment indicated that the latter phenomenon is the most influential in determining the quality of the puffed rice grains.

8.6.1 Protocol

Standard post-bumped rice provided by the factory was dried down to 11% moisture content w.w.b in a 105°C oven, following the protocol described in section 8.2.1.

The rice was then tempered for 24 hours in a vacuum-sealed aluminium bag, to allow for physical ageing and moisture content equilibration to take place. The sealed bag was then put in an 80°C oven for one hour in order to remove the physical ageing while preserving the homogeneous repartition of water inside the rice grains. The rice prepared in this way was labelled 'REFRESHED'.

The 'REFRESHED' rice was kept in the closed bag for a second tempering of 7 hours at room temperature (20°C). Every hour, beginning immediately after the rice was taken out of the 80°C oven, 40g of the rice were taken and puffed, following the standard food hall puffing protocol (cf. section 4.3.3 of chapter 4: Materials and methods).

Standard tempered rice, provided by the factory and labelled 'REFERENCE (2)', was puffed at the same times, as a reference to control the variability of the experimental conditions.

Following the puffing, digital pictures of each sample were taken as discussed in section 8.2.2.

8.6.2 Results

Figure 8.7 shows the evolution of the grain area during the first 7 hours of tempering for the 'REFRESHED' and 'REFERENCE (2)' samples. The evolution of the grain area of the 'DRIED' and 'REFRESHED (1)' samples presented in sections 8.2.3 and 8.2.4 (Table 8.2 and Figure 8.2) is also shown.

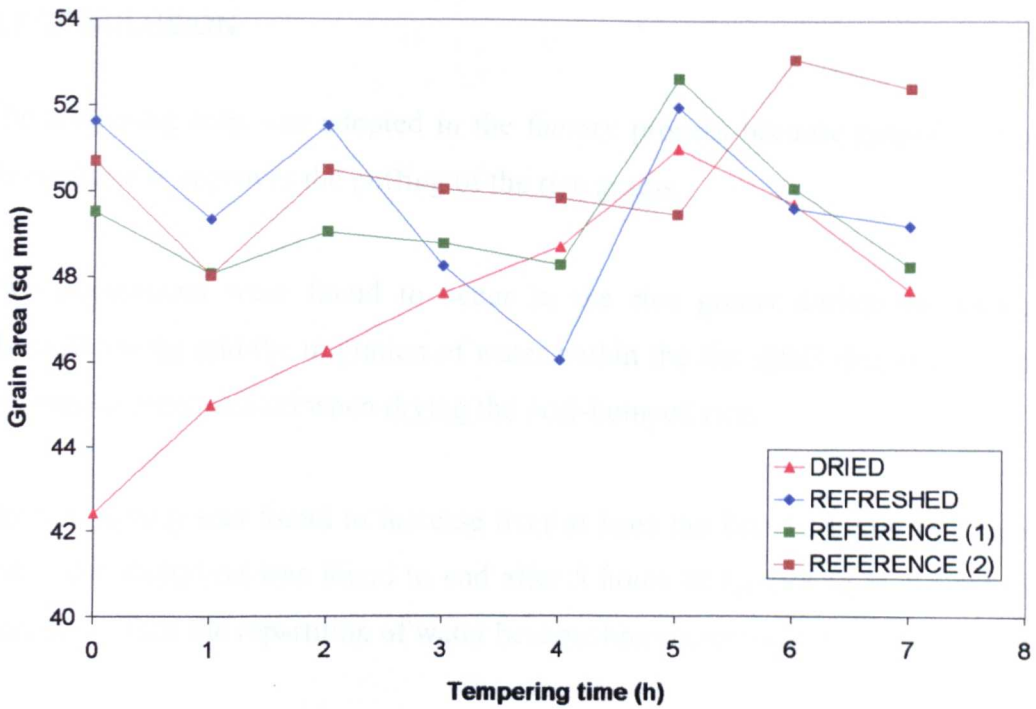


Figure 8.7: Evolution of the average grain areas of the 'DRIED', 'REFRESHED', 'REFERENCE (1)' and 'REFERENCE (2)' samples over 7 hours of tempering

The 'REFRESHED' sample was moisture equilibrated. Thus the only phenomenon that could take place during the tempering was physical ageing. The grain area of the 'REFRESHED' sample remained constant within the variability range indicated by the two 'REFERENCE' samples. This observation indicated that the physical ageing does not have a significant effect on the puffing.

The 'DRIED' sample was the only one which was not moisture equilibrated at the beginning of the experiment, and the only one whose expansion increased with tempering time. This result indicated that the equilibration of moisture contents inside the rice grain during the tempering has a role in improving the expansion of the grain at the puffing stage of the process.

8.7 CONCLUSION

The tempering step was adopted in the factory process because empirical findings showed that it improves the puffing of the rice grains.

Two phenomena were found to occur in the rice grains during the tempering: Physical ageing and the migration of water within the rice grain due to a gradient of moisture content created when drying the post-bumped rice.

Physical ageing was found to increase over at least the first 12 hours of tempering. The water migration was found to end after 5 hours of tempering in the laboratory conditions, then the repartition of water became homogenous through the rice grain.

Of the two phenomena, the water migration appeared to be the one responsible for the improvement of the rice grains expansion at the puffing stage of the process. A possible mechanism could be that before tempering, the drier outer part of the grain acts as a shell which limits the expansion, while after tempering, this shell is softened by the homogenous repartition of water.

From a technological point of view, because the equilibration of water repartition inside the rice grain is complete after 5 hours of tempering, it might be possible to reduce the tempering time currently set at 16 hours.

CHAPTER 9: EFFECT OF THE BUMPING PARAMETERS ON THE PUFFED GRAIN DEGREE OF EXPANSION

9.1 INTRODUCTION

The puffing, final step of the Rice Krispies™ process, consists in a quick toasting of the rice grains at 230°C, which results in the creation of steam bubbles inside the grains and the expansion of the material. All previous steps of the process have an influence on the extent of the expansion. In particular, the bumping is a key operation in determining the quality of the end product. Chapter 7 studied the molecular phenomena that occur during the bumping and how these are affected by some of the process parameters: The mill gap, bumping temperature and rice variety. This chapter examines how two of the bumping parameters, the mill gap and temperature, affect the degree of expansion of the puffed rice.

For this purpose, the samples described in chapter 7, section 7.2 were dried, tempered and puffed. Sections 9.2.2 and 9.2.3 examine the separate effects of the mill gap and bumping temperature on the puffed rice grains expansion. Section 9.2.4 uses the 13 samples prepared following the central composite experimental design shown on figure 7.1 (chapter 7) to model the joint effect of mill gap and bumping temperature. Section 9.2.5 uses the 20 samples prepared following the d-optimal experimental design presented on figure 7.2 (chapter 7) to investigate the correlation between grain expansion and the four groups and two sub-categories of samples identified by RVA (section 7.2.4, figure 7.8 of chapter 7: Bumping step of the Rice Krispies™ process).

Two parameters were used to characterise the puffed grain expansion: The bulk density (also called 'can weight' at the factory, where it is used as a standard quality control test) and the projected grain area onto the glass bed of an office scanner. Both methods are described in section 4.6.1 and 4.6.2 of chapter 4: Materials and methods.

9.2 INFLUENCE OF THE MILL GAP AND BUMPING TEMPERATURE ON THE EXPANSION OF THE PUFFED GRAINS

9.2.1 Description of the samples used

Set A, set B and set C of samples described in section 7.2 of chapter 7: Bumping step of the Rice KrispiesTM process have been puffed and used for this chapter. A few more samples (description (ii) below) have been studied as well.

(i) Six samples were bumped at the Manchester factory (set B). The material used was Selenio rice cooked on the same day at the factory. The temperature was kept constant at 45°C and the mill gap varied from wide to small to produce a range of samples from non-bumped to over-bumped. The type of mills did not allow a precise measurement of the mill gap. The samples were labelled F01 to F06, with F01 the non-bumped sample, F02 the widest mill gap sample and F06 the smallest mill gap sample. The samples were then dried, tempered and puffed both at the factory and at the university, following the protocols detailed in sections 3.3 of chapter 3: Evaluation of the industrial process and 4.3 of chapter 4: Materials and methods respectively.

(ii) Three samples were bumped at the Manchester factory. The material used was Selenio rice cooked on the same day at the factory. The mill gap was kept constant and three bumping temperature (temperature of the rice grains) levels were tested: 31°C, 39°C and 42°C. The samples were labelled accordingly and puffed at the university following the protocol described in section 4.3.3 of chapter 4: Materials and methods.

(iii) Thirteen samples (set A), labelled S01 to S13, were bumped at the university following a central composite experimental design with two factors: bumping temperature and mill gap (figure 7.1, chapter 7). The material used was cooked Selenio rice. Following the bumping, the samples were dried, tempered and puffed at the university, following the protocols described in sections 4.3.2 and 4.3.3 of chapter 4: Materials and methods.

(iv) Twenty samples (set C), labelled R01 to R20, were prepared at the Battle Creek WKKI pilot plant, following a d-optimal experimental design with three factors:

bumping temperature, mill gap and rice variety (figure 7.2 and table 7.2, chapter 7). Following the bumping, the samples were dried, tempered and puffed at the pilot plant, according to the protocol described in sections 3.3.5 and 3.3.6 of chapter 3: Evaluation of the industrial process.

9.2.2 Influence of the mill gap on the puffed rice grains expansion

Figure 9.1 shows that the puffed rice bulk density decreased as the mill gap decreased from samples F02 to F06. Both pilot plant and university puffing results are presented to show that the grain expansion achieved at the factory is better than at the university. The two series of results show the same trend, which validated the small-scale puffing process that was developed at the university. The non-bumped sample F01 did not expand at all, which resulted in a very large bulk density not shown on figure 9.1: 368g.L^{-1} for the pilot plant puffing and 1131g.L^{-1} for the university puffing. ANOVA analyses with a 5% confidence level indicated that samples puffed at the university were all statistically different (horizontal blue lines on figure 9.1) and that samples puffed at the pilot plant were all statistically different except F04 and F05 (horizontal red lines on figure 9.1).

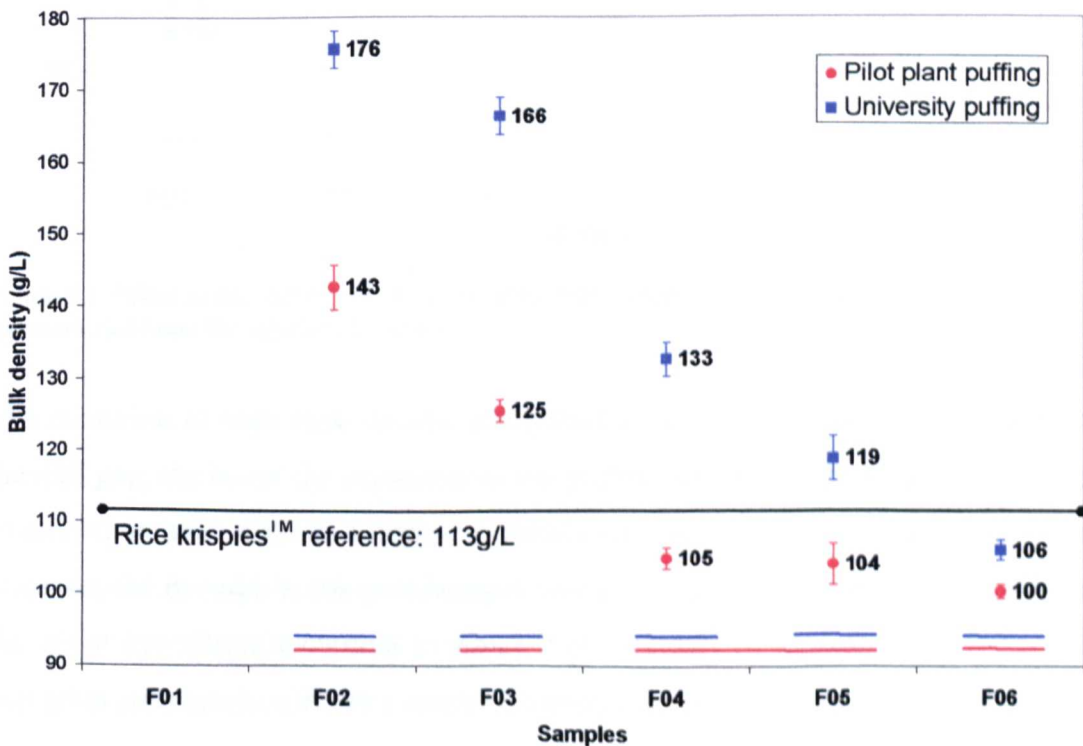


Figure 9.1: Effect of the mill gap on the bulk densities of six puffed samples (set B). The vertical lines represent two times the standard deviation

Figure 9.2 shows that the puffed rice projected grain area increased as the mill gap decreased from samples F01 to F06. Again, the comparison of pilot plant and university puffing results showed that the grain expansion achieved at the factory is better than at the university, but that both series of results showed the same trend. ANOVA analyses with a 5% confidence level indicated that samples puffed at the university were all statistically different and that samples F02 & F03 and samples F04 & F05 puffed at the pilot plant were not statistically different (horizontal red lines).

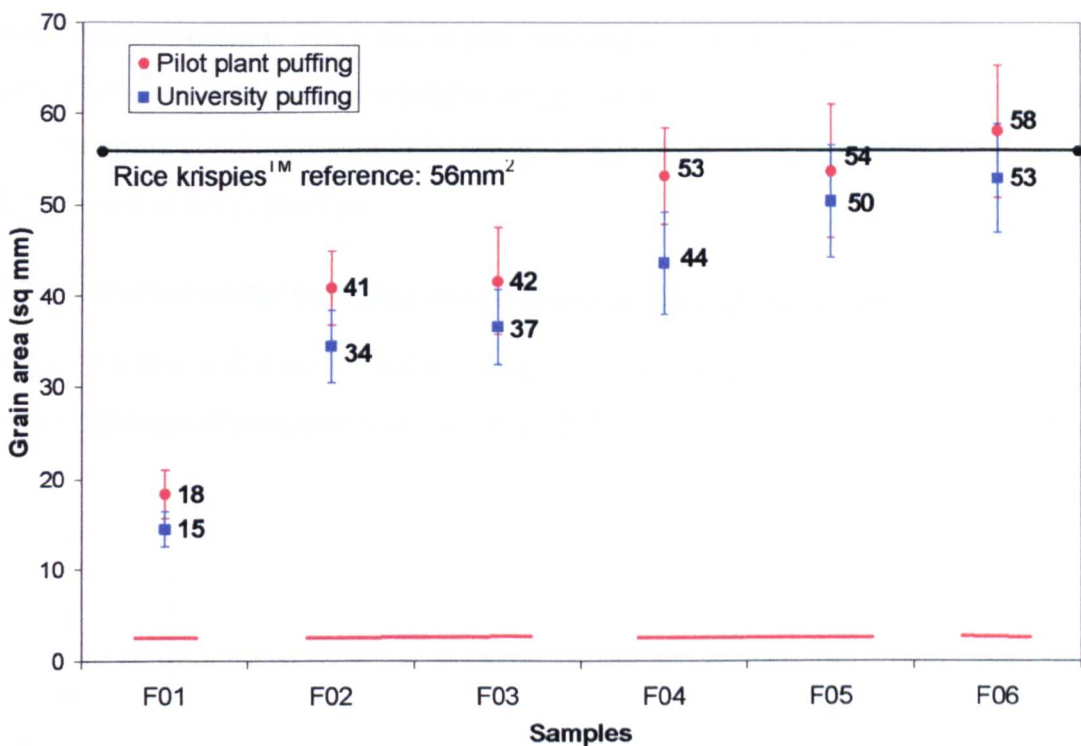


Figure 9.2: Effect of the mill gap on the grain areas of six puffed samples (set B). The vertical lines represent two times the standard deviation

The evolution of both bulk density and puffed grain area indicated that the smaller the mill gap, the better the expansion of the puffed rice, within the range of mill gaps examined in this section. Chapter 7 results showed that decreasing the mill gap increases the damage to the post-bumped rice grains structure. This tends to confirm the initial hypothesis according to which it is necessary to weaken the post-bumped rice grain structure to achieve a proper expansion of the rice at the puffing step of the process.

The bulk densities of pilot plant puffed samples F04 and F05 are the closest to that of

commercial rice krispies™, 113g.L^{-1} (figure 9.1). Similarly the grain areas of pilot plant puffed samples F04, F05 and F06 are the closest to the one of rice krispies™, 56mm^2 (figure 9.2). Therefore the mill gap for optimum puffing was thought to be in the range of those used to prepare samples F04, F05 and F06.

These three samples, F04, F05 and F06, belong to the same group G4 of samples identified with the shape of their RVA profiles in section 7.2.3 of chapter 7: The bumping step of the Rice Krispies™ process. The four RVA groups were relevant to detect differences in the post-bumped samples due to mill gap, rice variety and bumping temperature. They also appear relevant as a guidance to set up the bumping conditions in order to ensure a proper expansion of the rice grains at the puffing step: The bumping conditions should be set up so that the post-bumped material falls into the group 4 of RVA profiles.

9.2.3 Influence of the bumping temperature on the puffed rice grains expansion

Figure 9.3 shows that the puffed rice projected grain area decreased slightly when the bumping temperature increased from 31 to 42°C.

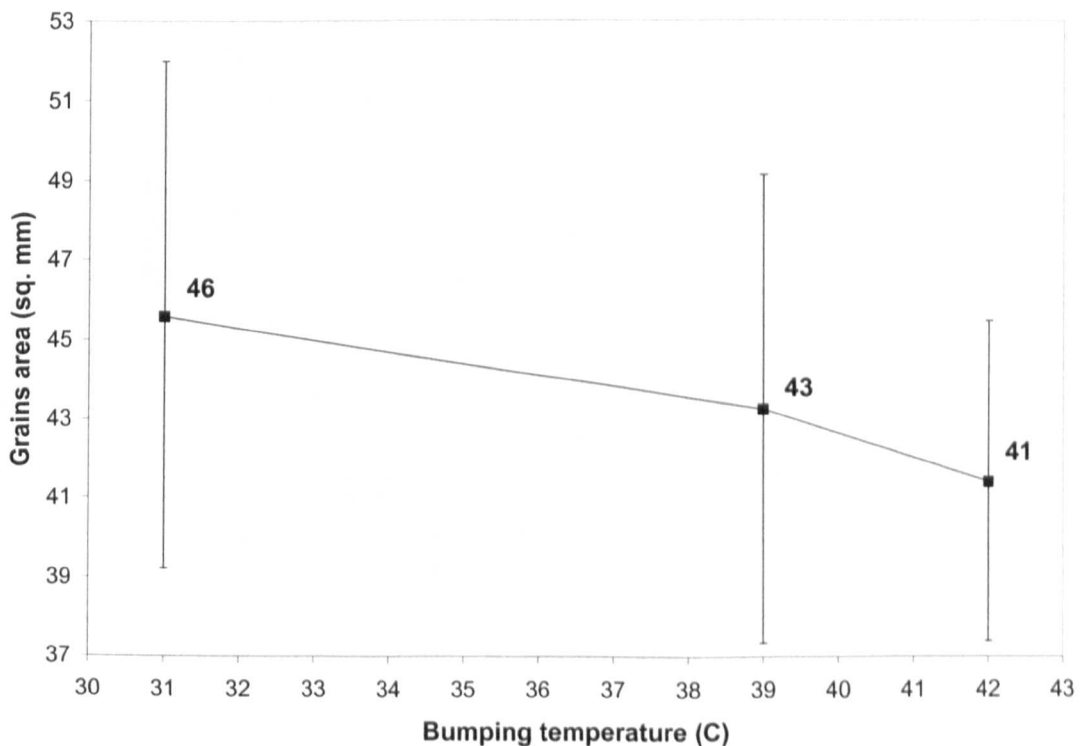


Figure 9.3: Effect of the bumping temperature on the grain areas of three puffed samples. The vertical lines represent two times the standard deviation

ANOVA analyses with a 5% confidence level showed that there is no significant difference between the 31°C and 39°C samples and between the 39°C and 42°C samples. A significant difference was found between 31°C and 42°C samples only. This confirmed the chapter 7 observation (section 7.2.4) that bumping temperature has a secondary effect compared to the mill gap in determining the structure of the post-bumped rice, and hence of the puffed rice.

9.2.4 Combined effect of mill gap and bumping temperature on the puffed rice grains expansion

This section uses the results from the set A 13 samples S01 to S13 central composite design described in section 7.2, analysed with Design Expert software.

Figure 9.4 shows that the puffed rice bulk density (called ‘can weight’ at the factory) decreased when mill gap and bumping temperature decreased, and that the mill gap effect was larger than the bumping temperature effect.

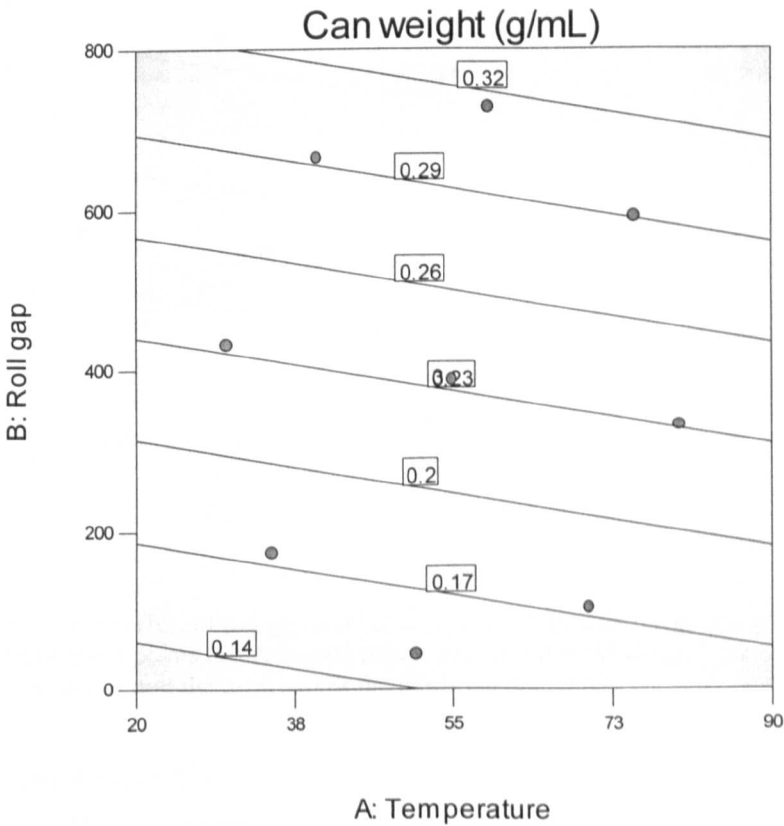


Figure 9.4: Model of the effect of roll gap and bumping temperature on the puffed rice bulk density. The dots indicate the experimental points (set A central composite experimental design), the shading the level of accuracy of the model, and the level curves the predicted bulk density.

The equation of the model is:

$$\begin{aligned} \text{Bulk density (g/mL)} = & + 0.15 \\ & + 4.51 \cdot 10^{-4} \times \text{Temperature (}^\circ\text{C)} \\ & + 2.36 \cdot 10^{-4} \times \text{Mill gap (}\mu\text{m)} \end{aligned}$$

The probability that the model is not significant is 0.01%.

Similarly, figure 9.5 shows that the puffed grain area increased when mill gap and bumping temperature decreased, and that the mill gap effect was larger than the bumping temperature effect.

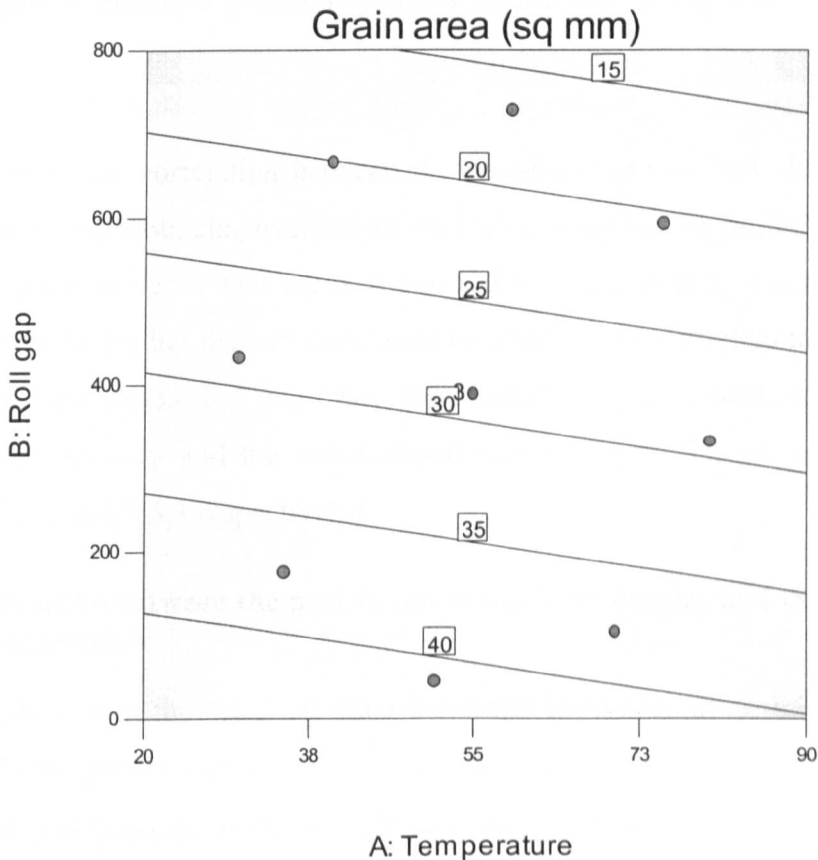


Figure 9.5: Model of the effect of roll gap and bumping temperature on the puffed grain area. The dots indicate the experimental points (set A central composite experimental design), the shading the level of accuracy of the model, and the level curves the predicted grain area.

The equation of the model is:

$$\begin{aligned} \text{Grain area (mm}^2\text{)} = & + 45.66 \\ & - 6.05 \cdot 10^{-2} \times \text{Temperature (}^\circ\text{C)} \\ & - 3.48 \cdot 10^{-2} \times \text{Mill gap (}\mu\text{m)} \end{aligned}$$

The probability that the model is not significant is 0.01%.

These models show that decreasing the mill gap and, to a smaller degree, the bumping temperature improves the rice grains expansion.

9.3 PREDICTION OF THE PUFFING QUALITY FROM THE POST-BUMPED RICE PARAMETERS

The quality of the material just after the bumping is routinely assessed at the factory by measuring its bulk density, following a protocol similar to the one described in section 4.6.2 of chapter 4: Materials and methods. The information is used to adjust the mill gap to ensure a proper expansion of the rice at the puffing step of the process.

In this section, the correlation between the post-bumped rice bulk density and the puffed grain expansion, characterised by its bulk density and its puffed grain area, is studied in order to verify that the post-bumped rice bulk density can effectively be used as a tool to predict the rice expansion (section 9.3.1). Correlations between the puffed grain expansion and two other characteristics of the post-bumped rice, the grain height recovery and the post-bumped rice RVA profile, are also examined (sections 9.3.2 and 9.3.3 respectively).

9.3.1 Correlation between the post-bumped rice bulk density and the puffed rice degree of expansion

Using the data from the set C 20 trials d-optimal experimental design described in section 7.2, the puffed material bulk density and the puffed grain area were plotted against the post-bumped material bulk density, as shown on figures 9.6 and 9.7 respectively. The samples were bumped and puffed at the Battle Creek pilot plant.

The results indicated that the lower the post-bumped rice bulk density, the better the expansion. However, the correlation was relatively poor with linear regression correlation coefficients equal to 0.57 and 0.59.

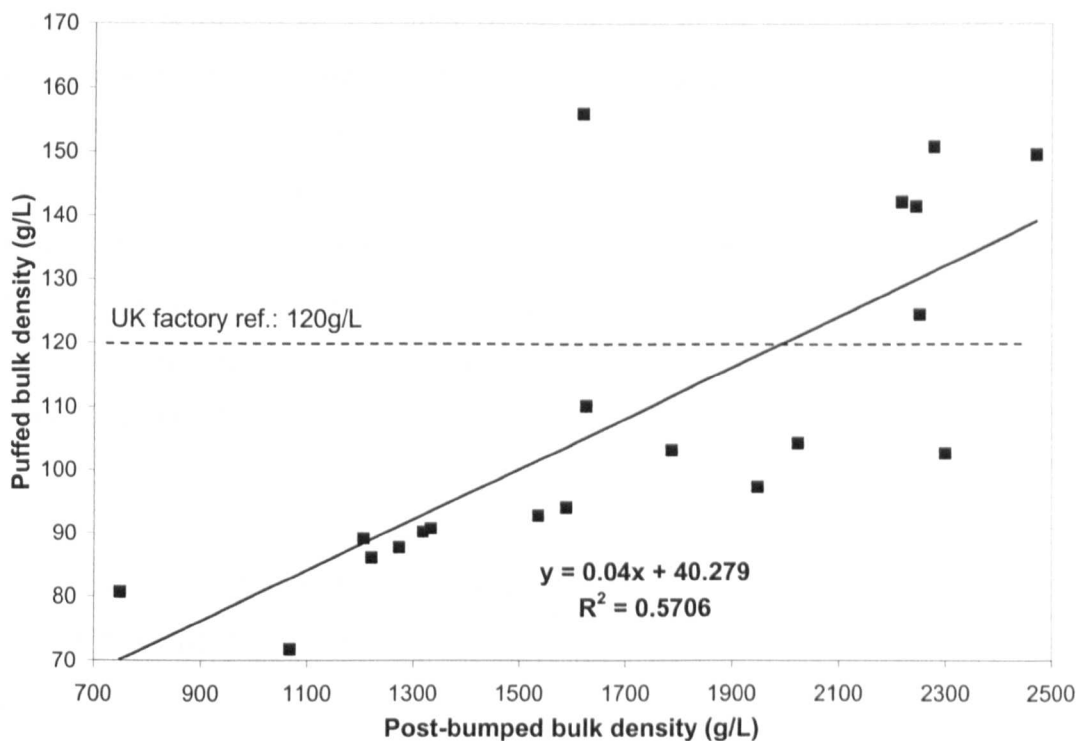


Figure 9.6: Correlation between the post-bumped rice bulk density and the puffed rice bulk density

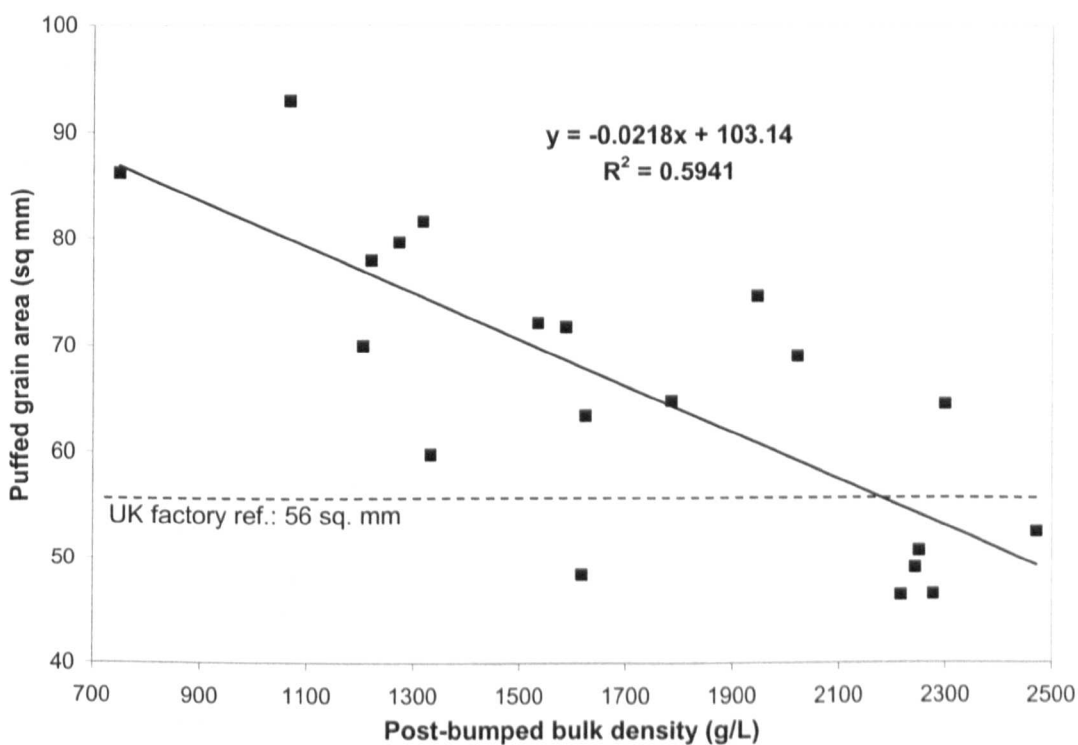


Figure 9.7: Correlation between the post-bumped rice bulk density and the puffed grain area

9.3.2 Correlation between the post-bumped rice grains height recovery and the puffed rice degree of expansion

The height recovery is the ratio between the post-bumped and the pre-bumped grains

heights, and is used as an indication of the damage to the grain structure during the bumping (the lower the height recovery, the more damage). Using the data from the set A 13 trials central composite experimental design described in section 7.2, the puffed material bulk density and the puffed grain area were plotted against the post-bumped rice height recovery, as shown on figures 9.8 and 9.9 respectively. The samples were bumped at the university, and puffed at the Manchester pilot plant. The height recovery measurement protocol is described in section 4.5.2 of chapter 4: Materials and methods.

The results indicated that the lower the height recovery, i.e. the more damaged the post-bumped rice grains, the better the expansion. A good correlation was found between the puffed grain area and the height recovery, with a correlation coefficient equal to 0.94.

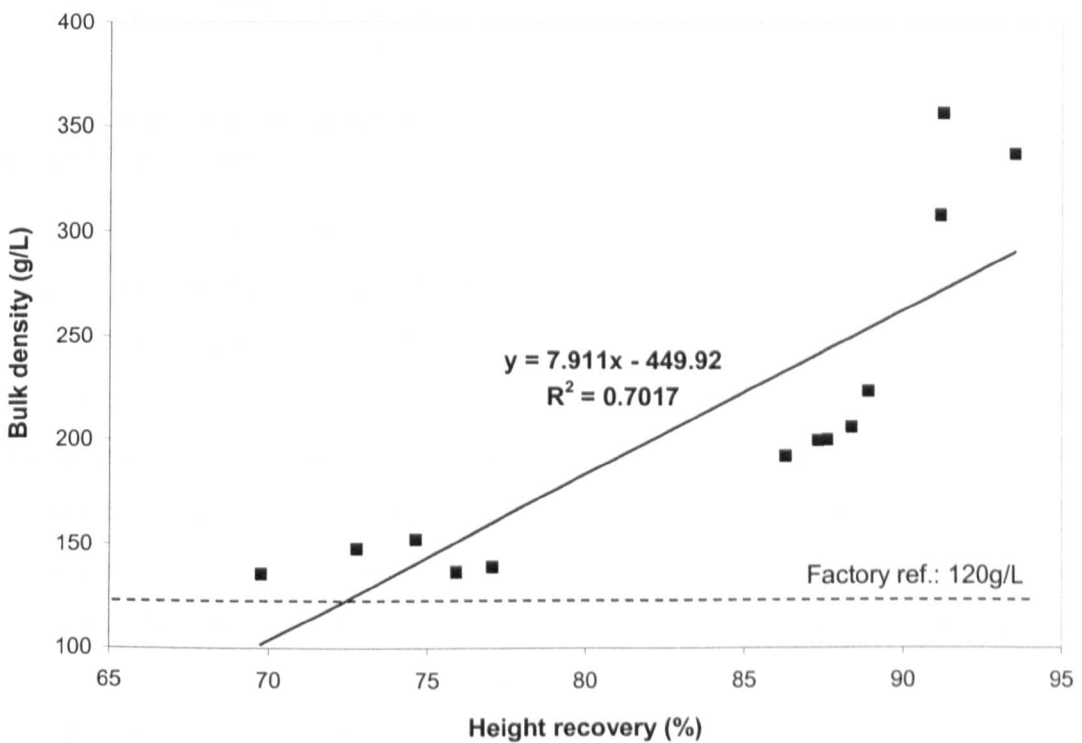


Figure 9.8: Correlation between the post-bumped rice grain height recovery and the bulk density of the puffed material

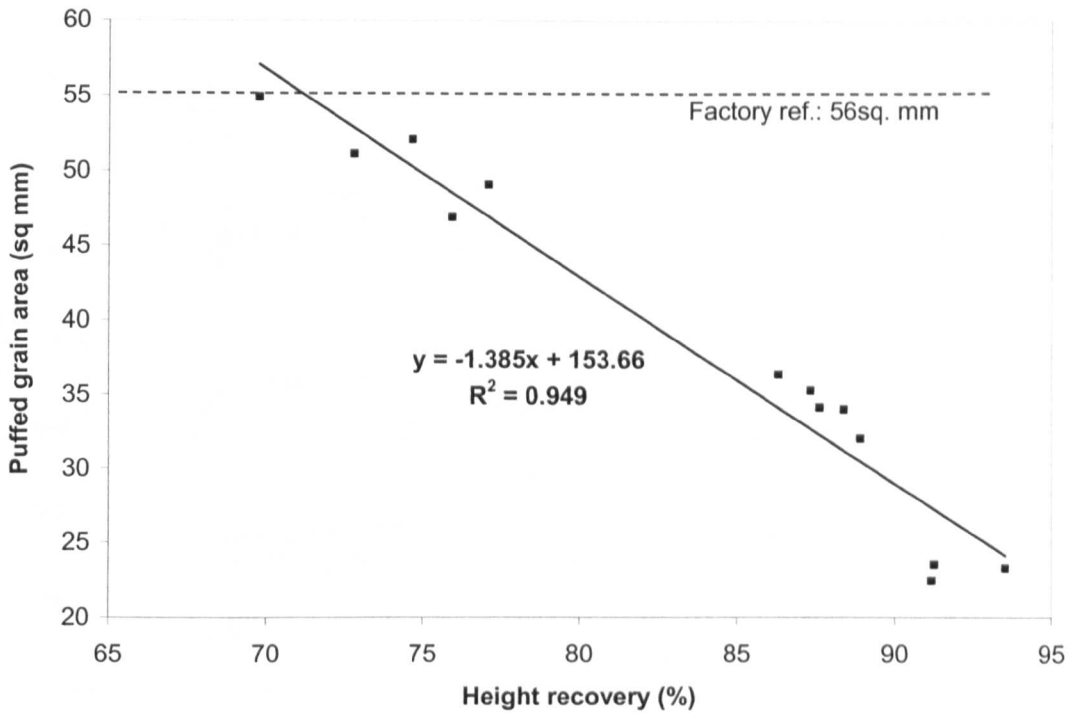


Figure 9.9: Correlation between the post-bumped rice grain height recovery and the puffed grain area

9.3.3 Correlation between the post-bumped rice RVA profile and the puffed rice degree of expansion

In sections 7.2.3 and 7.2.4 of chapter 7, four groups of post-bumped samples, G1 to G4, were identified according to the shape of the samples RVA profiles, and brought useful information on the bumping conditions and the post-bumped grains structure. The mill gap was the main factor determining these groups: G1 grouped non-bumped samples and samples bumped with large mill gaps, G2 and G3 grouped samples bumped with intermediate mill gaps, and G4 grouped samples bumped with the smallest mill gaps. The rice variety and bumping temperature had a secondary influence, which was visible with the samples bumped with larger mill gaps (groups G1, G2, G3). Similarly, two subcategories of group G4 were identified, G4' and G4+, which all had the G4 RVA profile general shape, but with some differences such as an unusually high cold paste viscosity (G4+) or an extra shoulder in viscosity at 1200 seconds (G4'). These subcategories G4+ and G4' corresponded to samples of the rice varieties Medium Grain (MGR) and Shot Grain (SGR) respectively bumped with relatively large mill gaps (among the largest in the range covered by group G4), which evidenced an effect of the rice variety when the mill gap was large enough not too mask other influences.

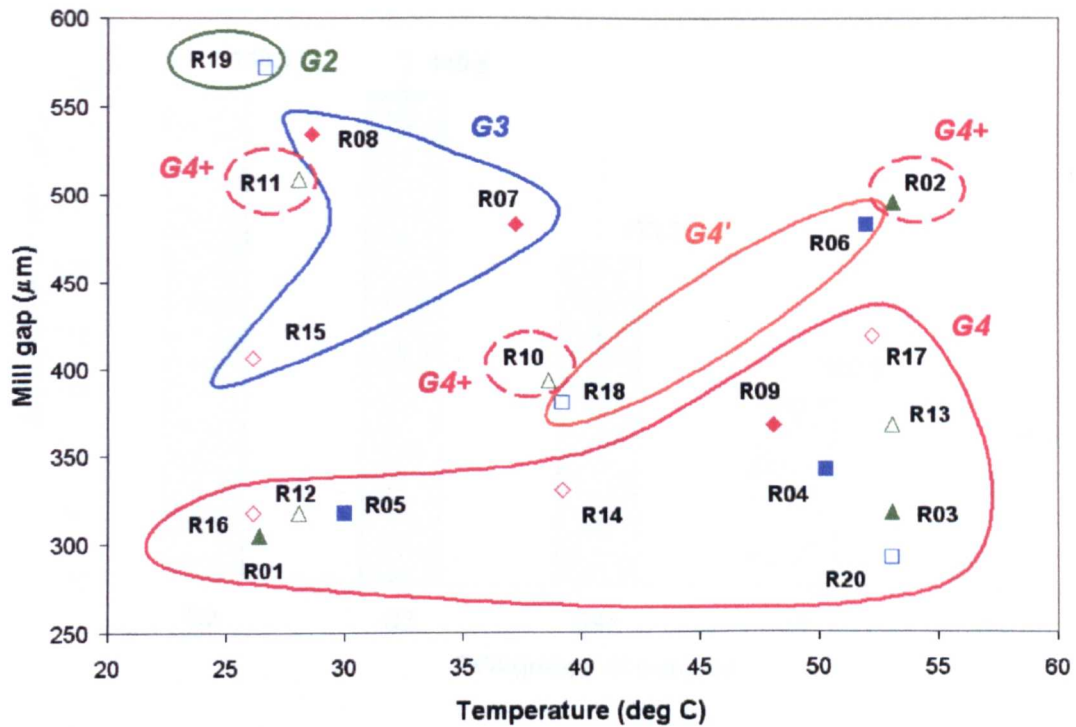


Figure 9.10: Diagram showing the correspondence between the four groups and two sub-categories of samples identified by RVA and the d-optimal experimental design conditions (▲△ Medium grain variety, ■□ Short grain variety, ◆◇ Selenio variety)

The effect of the puffing on the groups of samples, including the subcategories G4+ and G4', was assessed by measuring each group average bulk density of the expanded rice and puffed grain area. The samples used were those of the set C 20 trials d-optimal experimental design described in section 7.2 (table 7.2) of chapter 7: Bumping step of the Rice Krispies™ process. The groups and the repartition of the samples within each group are shown with the experimental conditions on figure 9.10. Data for group G1 is not available because no sample of this experimental design belonged to this group.

Figure 9.11 presents the average bulk density of the expanded rice for each of the four RVA groups and the two subcategories.

An ANOVA analysis with a 5% confidence level showed that groups G2 and G3 were not significantly different from each other, G4+ was significantly different from others, and G4' and G4 were not significantly different from each other.

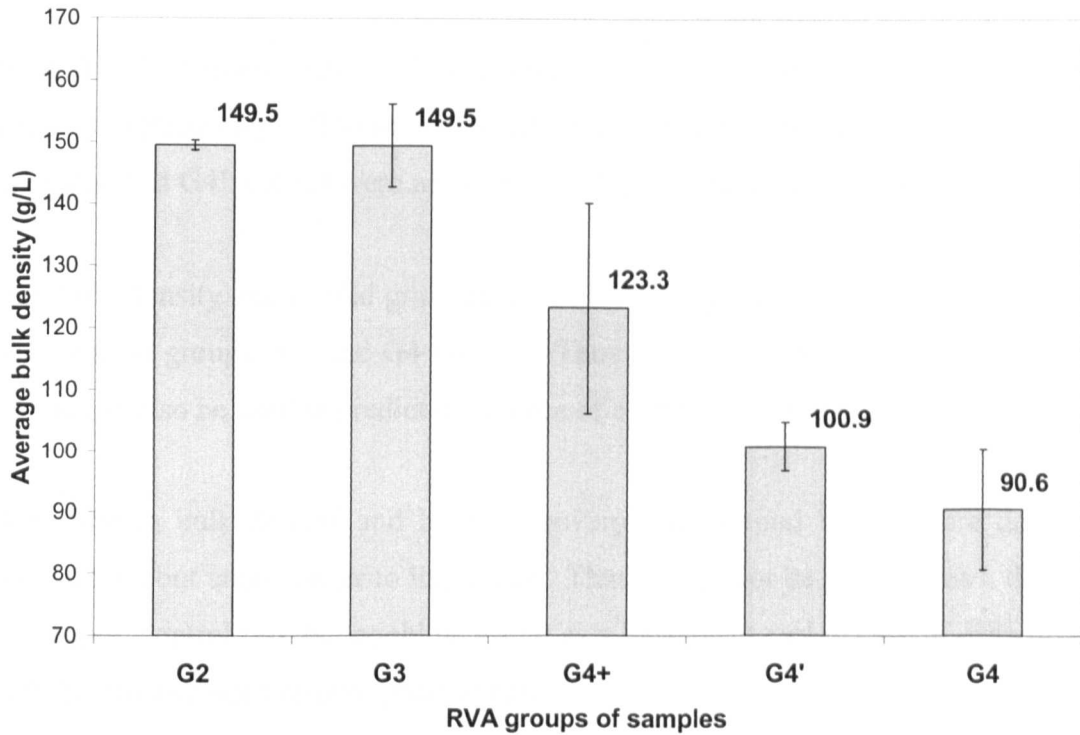


Figure 9.11: Average bulk densities of the RVA groups of samples identified with the Battle Creek d-optimal experimental design samples. The vertical lines represent two times the standard deviation.

Figure 9.12 presents the average puffed grain areas for each of the four RVA groups and the two subcategories.

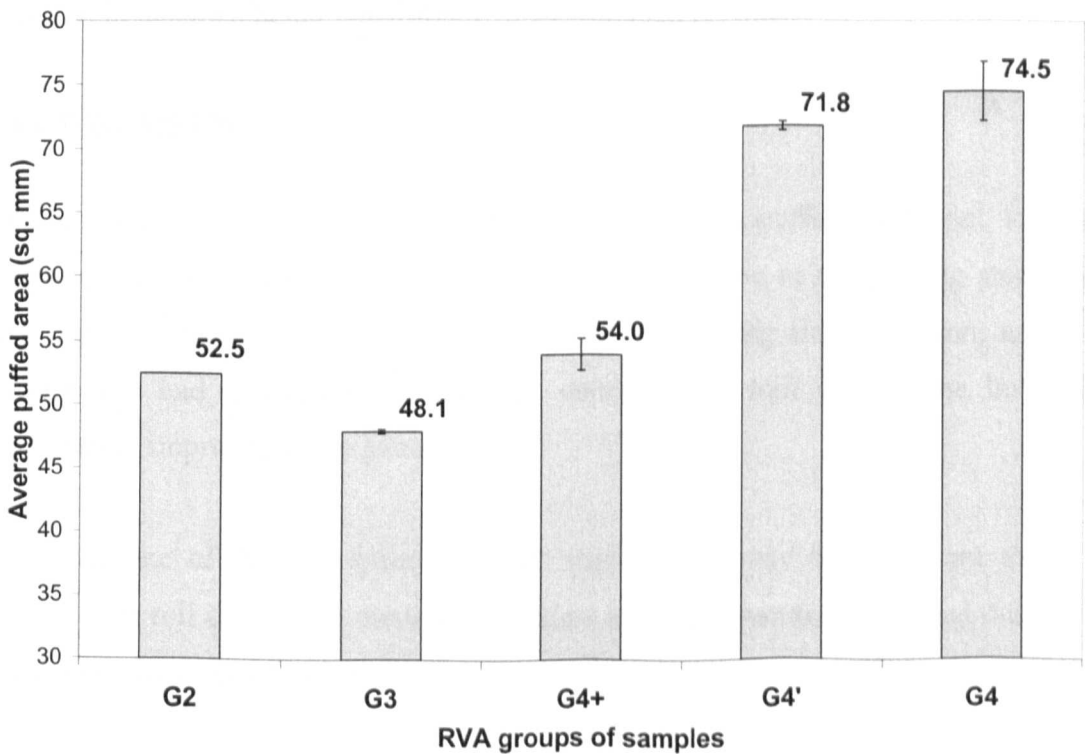


Figure 9.12: Average puffed grain areas of the RVA groups of samples identified with the Battle Creek d-optimal experimental design samples. The vertical lines represent two times the standard deviation

An ANOVA analysis with a 5% confidence level showed that groups G2 and G4+ were not significantly different from each other, G3 was significantly different from all others, and G4' and G4 were not significantly different from each other.

Both bulk density and puffed grain area indicated a significant increase in the grain expansion in groups G4' and G4 samples. Thus the post-bumped rice RVA profiles groups can also be used to predict the degree of expansion of the puffed material.

Compared to bulk density and height recovery, the method brings more detailed information, but takes longer to implement. Thus it may not be practical as a day-to-day quality control test, but could be useful as a diagnostic tool in case of difficulties with the process, such as poor grain expansion.

From an engineering point of view, the bumping should aim at producing G4 type samples to obtain a proper grain expansion. Another reason is that the grain internal structure and properties of G4 type samples are determined principally by the mill gap, which minimises the influence of the rice variety and the bumping temperature and should ensure a better consistency of the finished product.

9.4 CONCLUSION

The bumping of the cooked rice is necessary to obtain a puffable material, and the bumping conditions influence the extent of the expansion at the puffing step. The mill gap was found to be the main parameter controlling the expansion, and the temperature had a secondary effect. To decrease the mill gap or the bumping temperature improved the expansion.

The influence of the roll speed was not studied, but may be important too. To increase the roll speed may damage the grains internal structure more, and thus help improving the grains expansion.

Characterisations of the post-bumped material could be used to assess the product quality and predict the extent of the subsequent expansion.

The bulk density of the post-bumped material is a measurement already in use at the factory. It is a rapid and easy to implement method, however the correlation between this parameter and the puffed grains extent of expansion was poor.

A good correlation between the post-bumped rice grains height recovery and the puffed grains area was found. This method takes a bit longer to implement than the bulk density measurement.

RVA profiles brought the most information on the post-bumped material, and could also be used to predict the grains expansion. However, the method is time consuming and would be most useful only as a diagnostic tool in case of process difficulties and poor finished product quality.

CHAPTER 10: GENERAL DISCUSSION AND CONCLUSIONS

10.1 INTRODUCTION

From a technical point of view, the Rice Krispies™ process can be described as a series of unit operations that transform the raw rice material into expanded rice grains. The work presented in this thesis constitutes an attempt at describing the Rice Krispies™ process from a molecular point of view, by identifying the phenomena that take place inside the rice grains as they go through each unit operation. It is based on the several developments of cereal science in the last 20 years, such as the refinement of the amylopectin molecule model, the understanding of the sequence of gelatinisation phenomena, the study of the starch materials glass transition and of the role of amylose-lipid complexes, physical ageing and retrogradation in determining the texture of cooked cereal products.

Three operations of the Rice Krispies™ process, the bumping, tempering and puffing, were examined with more attention, because the conditions under which they are carried out can have a large influence on the quality of the finished product.

This chapter reviews the cooked rice material molecular phenomena that have been identified and studied in the course of the project, and their roles in determining the Rice Krispies™ structure.

10.2 GLASS TRANSITION AND RELATED PHENOMENA IN THE COOKED MATERIAL

10.2.1 Glass transition of the cooked rice

Rice is initially cooked with a flavour liquor and steam heating in pressure cookers. The flavour liquor contains low molecular weight sugars and other materials which influence the glass transition of the starch material. Because the exact composition of the flavour liquor was not known, the glass transition temperature of the cooked rice could not be predicted. Hence the cooked rice glass transition temperature was determined by dynamic mechanical thermal analysis (DMTA) for a range of

moisture contents (5 to 35% w.w.b). The glass transition line was based on sinusoidal measurements at a frequency of 1Hz.

The steps of the Rice Krispies™ process were mapped on the temperature / moisture content state diagram, as shown on figure 10.1.

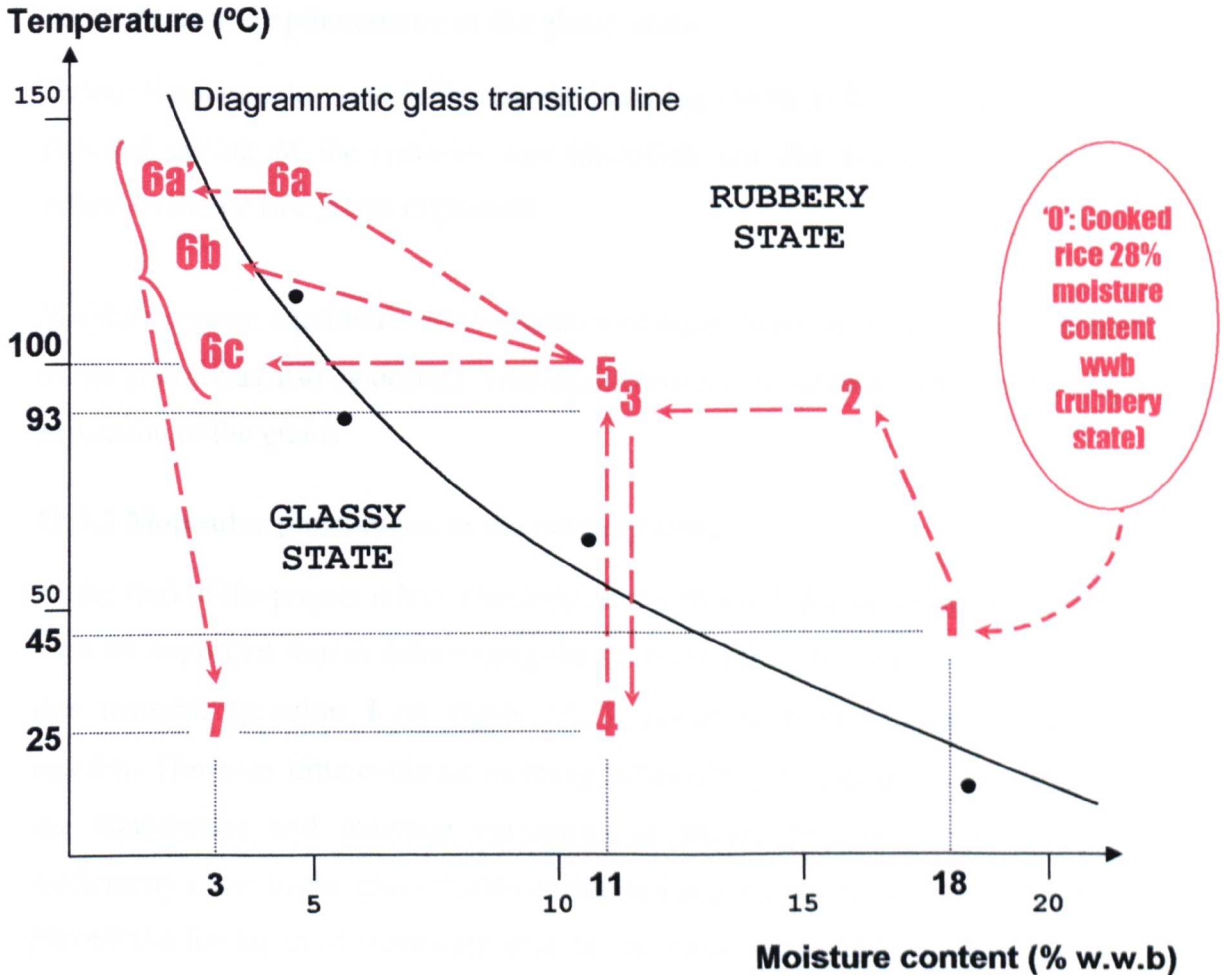


Figure 10.1: Path (1→7) followed on the theoretical glass transition diagram by the rice material during the bumping, tempering and puffing steps of the Rice Krispies™ process (• experimental points; the line is added as a guide to the eye)

On figure 10.1, the process operations are labelled as follow:

- **1**: Bumping step
- **1-2-3**: Post-bumping drying step (93°C). The drying is assumed to take place in two phases, because the heat transfer is likely to be faster than the water evaporation: Phase **1-2** represents the heating phase, and phase **2-3** represents drying at constant temperature.
- **3-4**: Cooling phase as the dried sample is taken out of the oven

- **4**: Tempering step
- **4-5-6**: Puffing step. Phase **4-5** represents the heating of the tempered sample, and phase **5-6** represents the expansion coupled with loss of moisture.
- **6-7**: Cooling phase as the puffed sample is taken out of the oven
- **7**: Finished product

10.2.2 Molecular phenomena in the glassy state

During the tempering step following the bumping (position **4** on figure 10.1), some physical ageing of the material was identified, but did not appear to have an influence on the rice grains expansion.

Moisture content equilibration by migration of water from the inner to the outer parts of the grains was also evidenced. This equilibration was necessary to ensure a proper expansion of the grains.

10.2.3 Molecular phenomena in the rubbery state

At the start of the project it had been suggested that amylopectin retrogradation could have an important role in determining the structure of the rice grains. In the cooked rice material (position **1** on figure 10.1), starch retrogradation is theoretically possible. However little evidence of retrogradation was found, and it is thought that the temperature and moisture conditions at which the rice is processed are sufficiently close to the glass transition line to keep the retrogradation rate low and prevent the formation of significant amounts of retrograded starch.

10.3 EFFECT OF THE BUMPING ON THE COOKED RICE GRAINS STRUCTURE

The bumping is a necessary step in the Rice Krispies™ process to ensure a good expansion of the rice grains.

10.3.1 Amylose-lipid complexes

The formation of a grain-wide amylose-lipid complexes network during the cooking of the rice material was observed. This network could reinforce the grain structure and limit the solubility of the amylose. One of the functions of the bumping could be to disrupt the network, so that a proper expansion of the material at the puffing step

is obtained. A model of the repartition and organisation of the amylose lipid-complexes within the cooked rice grains was proposed.

The study of amylose-lipid complexes in the Rice Krispies™ process constitutes a good practical example of the importance of the complexes in determining the texture and quality of a real cereal product.

10.3.2 Modification of the amylopectin molecular weight

The effect of the bumping on the amylopectin molecular weight was monitored with a series of techniques: Ultracentrifugation of dilute solutions of pre-bumped and post-bumped rice starch; relative viscosity measurements; complete isoamylase debranching of amylopectin followed by high pressure liquid chromatography (HPLC) separation of the branches by degree of polymerisation; viscosity measurement of the molten material by capillary rheometer.

Evidence that bumping reduces the amylopectin molecular weight was gathered. The reduction in molecular weight is thought to decrease the elastic modulus of the material, and hence to improve the rice grains expansion at the puffing step of the process. A small number of breakings in the amylopectin branched structure main chains could be enough to reduce significantly the average molecular weight and thus the material elastic modulus.

The study of the effect of the bumping on the amylopectin structure with the branch separation HPLC technique did not show any major changes in the chain lengths between the pre-bumped and post-bumped materials. Hence it is proposed that the decrease in molecular weight is due to few breaks in some long chains (B-chains) rather than many breaks in the shorter A-chains.

No change in the amylose molecular weight was observed. It is possible that the complexation with lipids helps protect the molecules. Also, the linear structure of amylose makes it less prone to breakage by physical deformation than the branched amylopectin.

10.3.3 Effect of mill gap and bumping temperature on the post-bumped rice grains

From the findings, the mill gap is the main parameter determining the extent of damage to the rice grain structure during the bumping, and the puffed grains degree of expansion. X-rays measurements showed that to reduce the mill gap results in more damaged amylose-lipid complexes. Viscosity measurements showed that a smaller mill gap also reduces the amylopectin molecular weight. The bulk density and puffed grain area characterisations of the finished product showed that reducing the mill gap improves the expansion of the material. The optimal mill gap, as measured with a solder fed between the rolls (cf. section 3.3.4 of chapter 3: Evaluation of the industrial process), was found to be approximately 300 μm . Reducing the mill much below this figure would result in too flat rice grains, or even flakes.

The same techniques showed that the bumping temperature has a secondary influence on the post-bumped rice structural damage and on the puffed rice expansion. To decrease the bumping temperature increases the structural damage and improves the puffing.

Three very different types of rolls were used to bump the cooked rice material: A texture analyser (linear compression speed 10mm.s⁻¹), a small roller drier (diameter 160mm, speed 25rpm), and a full-scale factory mill (diameter 510mm, speed 300rpm). All caused sufficient changes in the rice grains to allow them to expand. Thus it appeared that the material needs to be compressed beyond its elasticity limit to be puffable, but that the rate of compression is a less important factor in determining the expansion.

The importance of the mill gap was based on the studies reported in this thesis. However other parameters such as the bumping rolls diameter and speed, the rice grains size and composition, and the extent of rice cooking are likely to have an important influence as well in the determination of the end product expansion.

10.3.4 Correlation between the post-bumped rice characteristics and the puffed product expansion

The measurements of the post-bumped rice bulk density, height recovery and RVA profiles allowed to predict the extent of the puffed material expansion.

As the bumping severity increased, for example by reducing the mill gap, the post-bumped bulk density and the height recovery decreased, and the puffed grains expansion improved. The best correlation was found between the height recovery and the puffed grains areas.

RVA profiles carry the most information on the post-bumped material and could be classified into four main types (G1 to G4) and two subcategories. G1 and G4 correspond to the least and most severe bumping conditions. The best puffed rice expansion was obtained for samples with G4 type of RVA profiles. The RVA method is longer to implement than the bulk density and height recovery, and hence would be most useful as a diagnostic tool in case of process difficulties or poor finished product quality, rather than as a day-to-day quality control tool.

10.3.5 Practical conclusions for factory operations

This project has allowed a food understanding of the process unit operations. The results gathered suggest that the following could be critical control points:

10.3.5.1 Raw material formulation

- **Amylose content:** Results suggested that a high amylose content (>20% w.w.b) in the raw rice has a detrimental effect on the puffing. This is compatible with the proposed model where the disruption of the amylose-lipid complexes network at the bumping step is necessary for puffing. Therefore, based on these findings, low amylose varieties (14-18% w.w.b) would be preferable.
- **Lipid content:** No pattern was found in the effect of raw rice free lipid content on puffing, which is likely to be due to the low amounts of lipids required to form significant amounts of amylose-lipid complexes. Again, the model proposed would suggest that low levels of lipids (0.4-0.7% free lipids w.w.b) in the raw material are likely to produce a better puffing.

- The process was successfully mapped on a state diagram (glass transition temperature versus moisture content), and the glass transition was found to be an important process parameter. Hence the importance of monitoring the amount and formulation consistency of the flavour liquor added to the rice, because of the sugars and moisture that it contains, which can affect the cooked material glass transition.

10.3.5.2 Technical specifications

- Forces applied to the rice grains during the bumping: In the course of the project the mill gap has proven difficult to assess, and this point would deserve further attention. The use of a material more ductile than the solder or of a laser-based system could be considered to measure the mill gap and its variations over several days and months. Also, changing the operating temperature of the rolls alters their diameter by dilation or contraction. Thus the bumping temperature can affect the mill gap, which has a significant effect on the bumped material quality.

10.3.5.3 Process optimisation

- The moisture equilibration that takes place during the tempering was completed within 8 hours in laboratory conditions. Thus it may be possible to reduce the factory tempering time without adverse effects, although other factory operations restrictions may require to keep the current tempering time of 16 hours.

10.4 SUGGESTIONS FOR FUTURE STUDIES

The main contribution of the project was the gathering of evidence of what is happening during the processing of Rice KrispiesTM at a molecular level: Formation and dislocation of amylose-lipid complexes, amylopectin molecular weight reduction, glass transition, physical ageing, water movements and equilibration, and the determination of their relative importance in influencing the quality of the puffing. Several ideas for further studies arose during the project.

10.4.1 Amylose-lipid complexes

To understand better the role of amylose-lipid complexes in the rice grains structure and how and to what extent the bumping must dislocate the complexes to ensure a

proper puffing, a series of samples with various amounts of amylose-lipid complexes would need to be studied.

Thus, rice samples of one variety could be cooked with increasing amounts of added lipids, so as to have a range of samples with increasing amounts of amylose-lipid complexes to process in the usual factory conditions. A link between the amount of amylose-lipid complexes in the pre-bumped and post-bumped material and the puffed product expansion could then be investigated.

A further study on amylose-lipid complexes would involve the complete modelling of the structure of the complexes inside the rice grains, before and after bumping.

10.4.2 Amylopectin molecular weight study

Amylopectin constitutes approximately 70% of the rice grains, and therefore may have an important influence on the structure of the product. To understand in more details this influence, a study of the amylopectin fine structure, its effect on the texture of the cooked rice and how it is affected by the bumping could be considered.

One way to do this would be to bump a series of samples with various mill gaps so as to create different levels of damaged amylopectin, and to assess which of and to what extent the A-, B- and C-chains have been fractured by using the HPLC separation of debranched amylopectin and the analytical ultracentrifugation techniques. The same series of samples could then be taken through to the puffing step so as to investigate a link between the state of the amylopectin in the samples and their puffability.

10.4.3 Variety study

The composition of the raw rice material, in particular the amylose and lipid contents and the amylopectin molecular weight, has a role in determining the structure of the expanded product. The amylopectin fine structure, as well as the rice grain dimensions, may have an influence too.

In order to study the influence of the raw rice characteristics on the expansion of the puffed product, a wide range of rice varieties could be chosen and put through the Rice KrispiesTM process. Links between the raw rice characteristics and the end

product shape and degree of expansion could then be investigated, and ranges of acceptability for the raw material characteristics and composition could be defined as a quality control tool. Such a variety study could also be an occasion to build a database of RVA gelatinisation profiles that could be used to assess incoming rice crops rapidly.

BIBLIOGRAPHY

- Batterman-Azcona, S. J., and Hamaker, B. R. (1998).** Changes occurring in protein body structure and α -zein during cornflake processing, *Cereal Chemistry* 75, 217-221.
- Becker, A. (2001)** Starch conversion and particle properties determining the rapid visco-analyser (RVA) profile, PhD, University of Nottingham, Nottingham.
- Becker, A., Hill, S. E., and Mitchell, J. R. (2001).** Relevance of amylose-lipid complexes to the behaviour of thermally processed starches, *Starch-Starke* 53, 121-130.
- Blanshard, J. M. V. (1987).** Starch granule structure and function: A physicochemical approach. In *Starch: Properties and potential, Critical reports in applied chemistry*, T. Galliard, ed. (Chichester, UK, John Wiley and sons), pp. 16-54.
- Blennow, A., Engelsen, S. B., Munck, L., and Moller, B. L. (2000).** Starch molecular structure and phosphorylation investigated by a combined chromatographic and chemometric approach, *Carbohydrate polymers* 41, 163-174.
- Buléon, A., Colonna, P., Planchot, V., and Ball, S. (1998).** Starch granules: Structure and biosynthesis, *International journal of biological macromolecules* 23, 85-112.
- Caldwell, E. F., Fast, R. B., Getgood, S. J., Lauhoff, G. H., Shouldice, F. J., Taylor, D. D., and Thomson, W. J. (1990).** Unit operations and equipment - III. Tempering, flaking and toasting. In *Breakfast cereals and how they are made*, R. B. Fast, and F. C. Caldwell, eds. (American Association of Cereal Chemists, Inc.), pp. 109-134.
- Caldwell, E. F., Fast, R. B., Ievolella, J., Lauhoff, C., Levine, H., Miller, R. C., Slade, L., Strahm, B. S., and Whalen, P. J. (2000).** Cooking of ready-to-eat breakfast cereals, *Cereal Foods World* 45, 244-252.

- Carvalho, C.** (2000). Wheat extrudate DMTA temperature profile and glass transition (Nottingham).
- Champagne, E. T.** (1996). Rice starch composition and characteristics, *Cereal foods world* *41*, 833-838.
- Chen, C.-M., and Yeh, A.-I.** (2000). Expansion of rice pellets: Examination of glass transition and expansion temperature, *Journal of cereal science* *32*, 137-145.
- DellaValle, G., Vergnes, B., Colonna, P., and Patria, A.** (1997). Relations between rheological properties of molten starches and their expansion behaviour in extrusion, *Journal of Food Engineering* *31*, 277-295.
- Donovan, J. W.** (1979). Phase transitions of the starch-water system, *Biopolymers* *18*, 263-275.
- Dupuy, K.** (2001). Kellogg's Rice Krispies are made from water-maid rice - April 28, 1928 (www.abbeville-online.com).
- Fan, J. T., Mitchell, J. R., and Blanshard, J. M. V.** (1996a). The effect of sugars on the extrusion of maize grits .1. The role of the glass transition in determining product density and shape, *International Journal of Food Science and Technology* *31*, 55-65.
- Fan, J. T., Mitchell, J. R., and Blanshard, J. M. V.** (1996b). The effect of sugars on the extrusion of maize grits .2. Starch conversion, *International Journal of Food Science and Technology* *31*, 67-76.
- Farhat, I. A., Blanshard, J. M. V., and Mitchell, J. R.** (2000). The retrogradation of waxy maize starch extrudates: Effects of storage temperature and water content, *Biopolymers* *53*, 411-422.
- Fast, R. B., Lauhoff, G., Taylor, D., and Getgood, S.** (1990a). Flaking ready-to-eat breakfast cereals, *Cereal foods world* *35*, 295-298.
- Fast, R. B., Shouldice, F., Thomson, W., Taylor, D., and Getgood, S.** (1990b). Toasting and toasting ovens for breakfast cereals, *Cereal foods world* *35*, 299-310.

- Fast, R. B.** (1999). Origins of the US breakfast cereal industry, *Cereal Foods World* *44*, 394-397.
- Fast, R. B., and Caldwell, E. F.** (1990). Breakfast cereals and how they are made, 1st edn (St Paul, Minnesota, American association of cereal chemists).
- Georget, D. M. R., and Smith, A. C.** (1996). The effect of sugars on the mechanical properties of preprocessed cereals, *Journal of thermal analysis* *47*, 1377-1389.
- Godet, M. C., Tran, V., Delage, M. M., and Buléon, A.** (1993). Molecular modelling of the specific interactions involved in amylose complexation by fatty acids, *International journal of biological macromolecules* *15*, 11-16.
- Goodfellow, B. J., and Wilson, R. H.** (1990). A Fourier transform IR study of the gelation of amylose and amylopectin, *Biopolymers* *30*, 1183-1189.
- Hamaker, B. R., and Griffin, V. K.** (1990). Changing the viscoelastic properties of cooked rice through protein disruption, *Cereal Chemistry* *67*, 261-264.
- Hamaker, B. R., and Griffin, V. K.** (1993). Effect of disulfide bond-containing protein on rice starch gelatinization and pasting, *Cereal Chemistry* *70*, 377-380.
- ✓ **Han, X.-Z., and Hamaker, B. R.** (2001). Amylopectin fine structure and rice starch paste breakdown, *Journal of cereal science* *34*, 279-284.
- Han, Y.-L., and Hill, S. E.** (1999). Study of the cooking and bumping of rice (Nottingham, University of Nottingham).
- Harding, S. E.** (1997). The intrinsic viscosity of biological macromolecules. Progress in measurement, interpretation and application to structure in dilute solution, *Progress in biophysics and molecular biology* *68*, 207-262.
- Heinemann, C., Conde-Petit, B., Nuessli, J., and Escher, F.** (2001). Evidence of starch inclusion complexation with lactones, *Journal of Agricultural and Food Chemistry* *49*, 1370-1376.
- ✓ **Hoseney, R. C.** (1994). Starch. In *Principles of cereal science and technology*, The American Association Cereal Chemists (AACC) ed., pp. 29-63.

Juliano, B. O. (1983). Lipids in rice and rice processing. In *Lipids in cereal technology*, P. J. Barnes, ed. (London, Academic Press), pp. 305-330.

Juliano, B. O. (1985). Polysaccharides, proteins and lipids of rice. In *Rice chemistry and technology*, B. O. Juliano, ed. (St Paul, Minnesota, American Association of Cereal Chemists), pp. 59-174.

Juliano, B. O. (1992). Structure, chemistry and function of rice grain and its fractions, *Cereal Foods World* 37, 772-779.

✓ **Juliano, B. O., and Bechtel, D. B.** (1985). The rice grain and its gross composition. In *Rice chemistry and technology*, B. O. Juliano, ed. (St Paul, Minnesota, American Association of Cereal Chemists), pp. 17-57.

Juliano, B. O., and Sakurai, J. (1985). Miscellaneous rice products. In *Rice chemistry and technology*, B. O. Juliano, ed. (St Paul, Minnesota, American Association of Cereal Chemists), pp. 569-618.

Kalichevsky, M. T., Blanshard, J. M. V., and Marsh, R. D. L. (1993a). Applications of mechanical spectroscopy to the study of glassy biopolymers and related systems. In *The glassy state in foods*, J. M. V. Blanshard, and P. J. Lillford, eds. (Nottingham, Nottingham University Press), pp. 133-156.

Kalichevsky, M. T., Jaroszkiewicz, E. M., Ablett, S., Blanshard, J. M. V., and Lillford, P. J. (1992). The glass transition of amylopectin measured by DSC, DMTA and NMR, *Carbohydrate Polymers* 18, 77-88.

Kalichevsky, M. T., Jaroszkiewicz, E. M., and Blanshard, J. M. V. (1993b). A study of the glass transition of amylopectin sugar mixtures, *Polymer* 34, 346-358.

Levine, H., and Slade, L. (1992). Glass transition in foods. In *Physical chemistry of foods*, H. G. Schwartzberg, and R. W. Hartel, eds. (Marcel Dekker), pp. 83-221.

Levine, L. (1993). Musing on the mechanics of flaking rolls, *Cereal Foods World* 38, 873-874.

Levine, L. (1994). Engineering - Miscellaneous Topics On Breakfast Cereal Making, *Cereal Foods World* 39, 456-457.

Levine, L. (1996a). Model for the sheeting of dough between rolls operating at different speeds, *Cereal Foods World* *41*, 690-697.

Levine, L. (1996b). Some more discussion about cereal flaking and a little bit about dough sheeting, *Cereal Foods World* *41*, 466-&.

Levine, L., and Levine, S. (1997). A preliminary investigation of the deformation of cereal pellets by flaking rolls, *Cereal Foods World* *42*, 444-451.

Lourdin, D., Coignard, L., Bizot, H., and Colonna, P. (1997). Influence of equilibrium relative humidity and plasticizer concentration on the water content and glass transition of starch materials, *Polymer* *38*, 5401-5406.

Martinet, C. (2001) Ageing of starch and starch-sugar systems in the glassy state, PhD, University of Nottingham, Nottingham.

Matveev, Y. I., Grinberg, V. Y., and Tolstoguzov, V. B. (2000). The plasticizing effect of water on proteins, polysaccharides and their mixtures. Glassy state of biopolymers, food and seeds, *Food Hydrocolloids* *14*, 425-437.

Mitchell, J. R., Hill, S. E., Paterson, L., Vallès, B., Barclay, F., and Blanshard, J. M. V. (1997). The role of molecular weight in the conversion of starch. In *Starch - Structure and functionality*, P. J. Frazier, A. M. Donald, and P. Richmond, eds. (Cambridge, UK, The royal society of chemistry), pp. 68-76.

Morrison, W. R. (1995). Starch lipids and how they relate to starch granule structure and functionality, *Cereal Foods World* *40*, 437-445.

Morrison, W. R., and Gadan, H. J. (1987). The amylose and lipid contents of starch granules in developing wheat endosperm, *Journal of cereal science* *5*, 263-277.

Morrison, W. R., Law, R. V., and Snape, C. E. (1993a). Evidence for inclusion complexes of lipids with V-amylose in maize, rice and oat starches, *Journal of cereal science* *18*, 107-109.

Morrison, W. R., Tester, R. F., Snape, C. E., Law, R. V., and Gidley, M. J. (1993b). Swelling and gelatinization of cereal starches. IV: Some effects of lipid-

complexed amylose and free amylose in waxy and normal barley starches, *Cereal Chemistry* 70, 385-391.

Mujoo, R., Chandrashekar, A., and Ali, S. Z. (1998). Rice protein aggregation during the flaking process, *Journal of Cereal Science* 28, 187-195.

Murugesan, G., and Bhattacharya, K. R. (1989a). The Nature of Starch in Popped Rice, *Carbohydrate Polymers* 10, 215-225.

Murugesan, G., and Bhattacharya, K. R. (1989b). Rheological and Hydration Properties of Popped Rice, *Journal of Texture Studies* 20, 325-333.

Murugesan, G., and Bhattacharya, K. R. (1991a). Basis For Varietal Difference in Popping Expansion of Rice, *Journal of Cereal Science* 13, 71-83.

Murugesan, G., and Bhattacharya, K. R. (1991b). Effect of Some Pretreatments On Popping Expansion of Rice, *Journal of Cereal Science* 13, 85-92.

Nyquist, H. (1983). Saturated salt solutions for maintaining specified relative humidities, *Int J Pharm Tech & Prod Mfr* 4, 47-48.

Onyeador, M. (2002). X-ray analysis of cassava starch samples cooked with increasing amounts of glycerol-mono-stearate (GMS).

Peat, S., Thomas, G. J., and Whelan, W. J. (1952). Evidence of multiple branching in waxy maize starch, *Journal of Chemistry Society* 722, 4546-4548.

Peleg, M. (1996a). Mathematical characterization of the plasticizing and antiplasticizing effects of fructose on amylopectin, *Cereal Chemistry* 73, 712-715.

Peleg, M. (1996b). On modeling changes in food and biosolids at and around their glass transition temperature range, *Critical Reviews in Food Science and Nutrition* 36, 49-67.

Perdon, A., Siebenmorgen, T. J., and Mauromoustakos, A. (2000). Glassy state transition and rice drying: Development of a brown rice state diagram, *Cereal Chemistry* 77, 708-713.

Raphaelides, S., and Karkalas, J. (1988). Thermal dissociation of amylose-fatty acid complexes, *Carbohydrate research* 172, 65-82.

Robin, J. P., Mercier, C., Charbonniere, R., and Guilbot, A. (1974). Linearized starches. Gel filtration and enzymic studies of insoluble residue from prolonged acid treatment of potato starch, *Cereal Chemistry* 51, 389-406.

Sevenou, O., Hill, S. E., Pesheck, P., Enz, J., and Mitchell, J. R. (2002). From dough to bread: The end of a foam. Paper presented at: AACC annual meeting and exhibition (Montreal, Quebec, Canada).

Swales, J. (1999). Factors determining cereal product structure (Nottingham, University of Nottingham (Division of food sciences)), pp. 46.

Tako, M., and Hizukuri, S. (2000). Retrogradation mechanism of rice starch, *Cereal Chemistry* 77, 473-477.

Tolstoguzov, V. B. (2000). The importance of glassy biopolymer components in food, *Nahrung-Food* 44, 76-84.

Tongdang, T. (2001). Molecular structure of native and processed rice, PhD, University of Nottingham, Nottingham.

Watson, M. E., and Galliher, T. L. (2001). Comparison of Dumas and Kjeldahl methods with automatic analyzers on agricultural samples under routine rapid analysis conditions, *Communications in Soil Science and Plant Analysis* 32, 2007-2019.

Wiles, P.G., Gray, I.K., and Kissling, R.C. (1998). Routine analysis of proteins by Kjeldahl and Dumas methods: Review and interlaboratory study using dairy products, *Journal of AOAC International* 81, 620-632.